ISSN 1028-8546

Azərbaycan Milli Elmlər Akademiyası
Fizika-Riyaziyyat və Texnika Elmləri Bölməsi
Fizika İnstitutu

1

Fizika

Cild
IX
2003

Bakı ✵ Elm

THE PECULIARITIES OF ELECTRIC AND GALVANOMAGNETIC PROPERTIES OF $Fe_{1,2}Cr_{1,8}S_4$

L.M. VALIYEV, Sh.O. ORUJEVA, A.I. AKHMEDOV
Institute of Physics, Azerbaijan National Academy of Sciences,
Baku. Az - 1143, H. Javid av. 33

Electric and galvanomagnetic properties of ferrimagnetic compound $Fe_{1,2}Cr_{1,8}S_4$ were investigated. It is revealed, that magnetic resistance is negative with the sharp peak in the range of $T_c \cong 250K$ and it is shown, that the spontaneous Hall coefficient reduces exponentially with the temperature in the region of the magnetic ordering.

$FeCr_2S_4$ has the spinel structure and is the ferrimagnetic semiconductor with the Curie temperature ~180K [1,2]. The chromium ions in the octahedral sublattice are replaced partially by the enelyse ions in order to get magnetic semiconductors with the high Curie temperature and it was shown, that $Fe_{1,2}Cr_{1,8}S_4$ has also spinel structure and is ferrimagnetic with the Curie temperature $T_c \cong 250K$ [3,4]. However the information lack on the electric and in particular galvanomagnetic properties gives no chance to present the full picture of the semiconductive properties and its correlation with the magnetic structure. Therefore the temperature dependences of the electroconductivity, the Hall effect and magnetoresistance of the given content in the wide temperature of the magnetic phase transition, were investigated. The receipts and the samples analysis were conducted by the technology described earlier [4].

The electroconductivity was measured by the compensated method on the constant current, but galvanomagnetic properties in the magnetic field of the strength up to 12K.

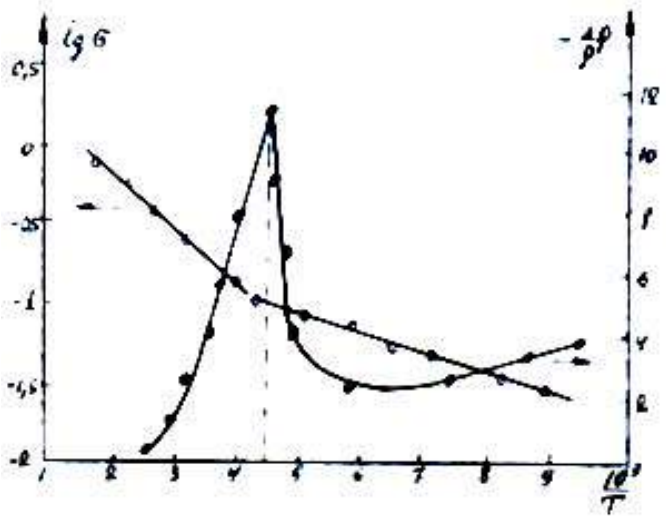

Fig.1. The dependence of $lg\sigma$ and $\frac{\Delta\rho}{\rho}$ on the temperature for $Fe_{1,2}Cr_{1,8}S_4$.

The dependence of $lg\sigma$ and $\frac{\Delta\rho}{\rho}$ on $\frac{10^3}{T}$ for this constant is presented on fig.1. As it is seen from the figure, the content has the semiconductive nature of the conductivity. So that in the range $100 \div 250^0$K the electroconductivity increases with the temperature growth with the activation energy ~ 0,02eV. The activation energy of the conductivity changes in the range of the magnetic ordering, and it becomes equal to ~0,07eV. Therefore the activation energy of the conductivity reduces by ~0,05eV at the transition in the magnetic ordering state. This result is in agreement with the theory, developed in the paper [5], in which the electroconductivity of the antiferromagnetic semiconductors was examined by means of *S-d* exchange model. It is concluded in these papers, that magnetic sublattice with the opposite orientation of spins, which in consequence of the exchange interaction with the conductivity electrons create the additional periodical potential, having more low symmetry, than that of crystals, occur at the transition into the magnetic-ordered state and the energy bands fission and the reduction of the activation energy, may occur, what we have confirmed experimentally.

The dependences of on $\frac{10^3}{T}$ are also presented on fig.1. It is seen, that the value of $\frac{\Delta\rho}{\rho}$ is negative, moreover it achieves the maximum (12%) in the region of the magnetic phase transition. Such anomalies of the magnetoresistance at the Curie point in the ferromagnetic semiconductors achieve quiet essential values, for example 80% for $FeCr_2S_4$ (T_c=130K) and even 10^4 times for EuSe (T_c=8K) [6].

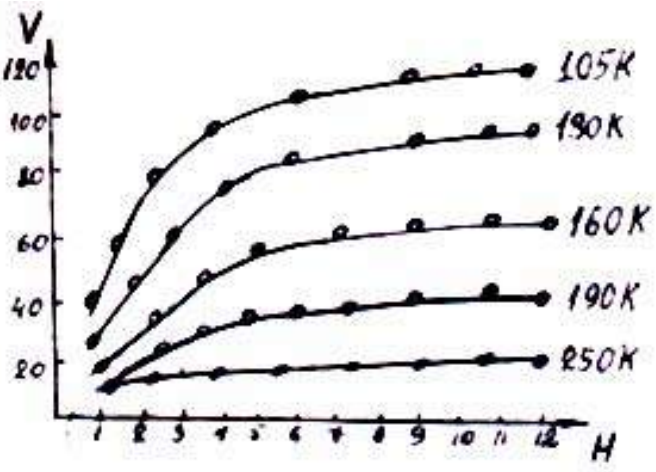

Fig.2. The field dependence of the Hall potential at various temperatures for $Fe_{1,2}Cr_{1,8}S_4$.

Such behavior of the magnetoresistance is connected both with the energy bands splitting and with the current carriers scattering on the disordered spins. Such relatively low value

of the jump of $\frac{\Delta\rho}{\rho}$ at the Curie point in $Fe_{1,2}Cr_{1,8}S_4$ in comparison with the ferromagnetic semiconductors with high agility values proves once more, that the jump value of $\frac{\Delta\rho}{\rho}$ is connected obviously with the value of the current carriers agility, what is discussed in the paper [6].

The field (0-12K) and temperature (90÷250K) dependences of Hall potential of $Fe_{1,2}Cr_{1,8}S_4$ are also investigated. The field dependences of the Hall potential at various temperatures of $Fe_{1,2}Cr_{1,8}S_4$ is presented on fig.2.

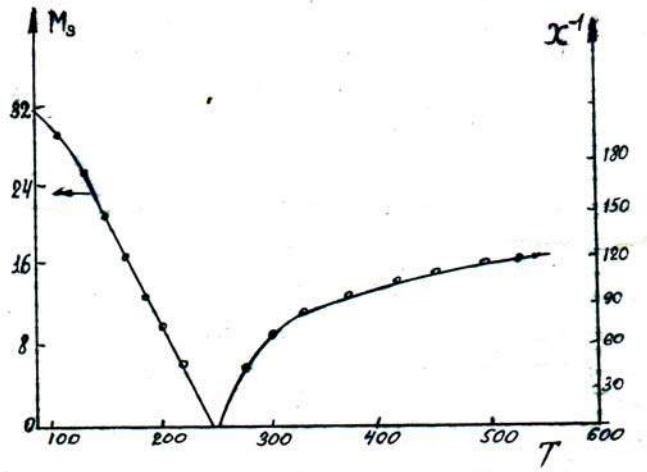

Fig.3. The temperature dependence of the spontaneous magnetization M_s and paramagnetic susceptibility χ_m^{-1} for $Fe_{1,2}Cr_{1,8}S_4$.

The Hall-e.m.f. in the magneto-ordered compounds (ferro and ferrimagnetics) is presented by the sum:

$$V_x = (R_0 H + R_1 M)\frac{J}{d}$$

where $R_0 H \frac{J}{d}$ is classical and $R_1 M \frac{J}{d}$ is anomalous potential, correspondingly. The anomalous Hall potential at $H \to 0$ turns out into the spontaneous Hall potential, which has the form:

$V_{XS} = R_S M_S \frac{J}{d}$, since $R_0 H \frac{J}{d} = 0$, where R_s is the spontaneous Hall coefficient, M_s is the spontaneous magnetization, d is the sample thickness, J is the sample current. V_{xs} and M_s are determined by the extrapolation of $V_x(H)$ and $M(H)$ from the region of the paroprocess on the $H=0$ axis and the coefficient R_s is calculated as a ration:

$$R_s = \frac{V_{xs} d}{M_s J}$$

The magnetization and paramagnetic susceptibility of $Fe_{1+x}Cr_{2-x}S_4$ ($0 \le x \le 0.5$) system are investigated by us before [4]. The values of the spontaneous magnetization in the temperature interval 90÷250K and the paramagnetic susceptibility of the compound $Fe_{1,2}Cr_{1,8}S_4$ calculated from these experiments are presented on fig.3.

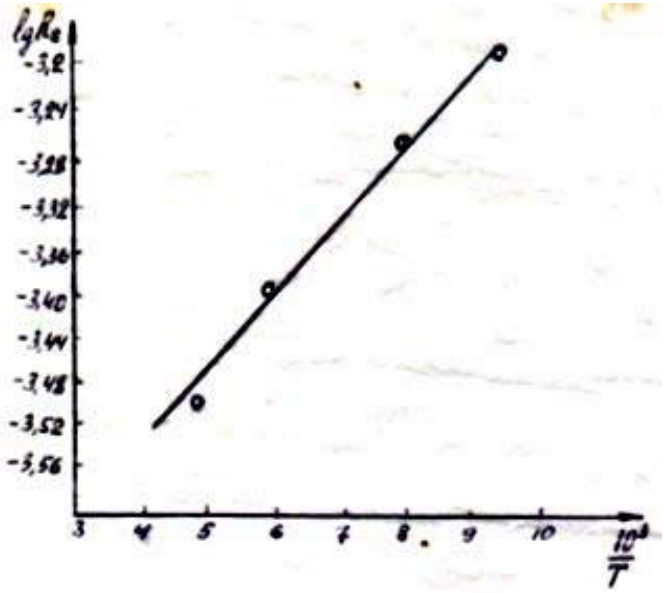

Fig.4. The dependence of the Hall coefficient lgR_s on the temperature for $Fe_{1,2}Cr_{1,8}S_4$.

The value are V_{xs} is calculated from the dependence of $V_x \sim H$ at various temperatures in the range $T < T_c$, in which values V_{xs} are determined by the value extrapolation V_x for $H \to 0$ in the process region.

The dependence of lgR_s on $\frac{10^3}{T}$ is presented on fig.4. As it is seen from the figure, the spontaneous Hall coefficient reduces exponentially with the temperature increase. Since the spontaneous Hall coefficient is the consequence of the spin-orbital interaction between the current carriers and the localized magnetic moments, it indicates on the fact that the magnetic heterogeneity of the given compound increases with the temperature increase.

[1] *P. Gibart, J.L. Dormann and J. Pelerin.* Phys. Stat. Sol.,1969, v.36, №1, pp. 187-194.

[2] *P. Gibart, M. Robbins and V.G. Lamberh.* J. Phys. Chem.Sol., 1973, v.34, №8, pp.1363.

[3] *M. Robbins, R. Wolf, A.S. Kartzic, R.C. Sherwood and M.A. Miksovsky.* J. Appl. Phys., 1970, 41, 1086.

[4] *R.Z. Sadikhov, L.M. Valiyev, N.B. Nabiyeva, Z.M. Namazov*. Phys. Stat. Sol (a), 1986, 94, k103.

[5] *E.A. Turov, Y.P. Irkhin*. FMM, T9 №4, pp.488-497.

[6] *P.F. Bongers, C. Haas, A.M.J.G. Van Run and G. Zamarsky*. J. Appl.Phys. 1969, vol. 40, № 3, p.958.

L.M. Vəliyev, Ş.O. Orucova, A.İ. Əhmədov

$Fe_{1,2}Cr_{1,8}S_4$-ÜN ELEKTRİK VƏ QALVANOMAQNİT XASSƏLƏRİNİN XÜSUSİYYƏTLƏRİ

$Fe_{1,2}Cr_{1,8}S_4$ birləşməsinin elektrik və qalvanomaqnit xassələri tədqiq edilmişdir. Maqnit müqavimətinin $T_c \approx 250$ K-də kəskin pikə malik olmaqla mənfi qiymət aldığı müşahidə edilmiş və spontan Holl əmsalının maqnit nizamlı oblastda temperaturla eksponensial azaldığı göstərilmişdir.

Л.М. Валиев, Ш.О. Оруджева, А.И. Ахмедов

ОСОБЕННОСТИ ЭЛЕКТРИЧЕСКИХ И ГАЛЬВАНОМАГНИТНЫХ СВОЙСТВ $Fe_{1,2}Cr_{1,8}S_4$

Исследованы электрические и гальваномагнитные свойства ферримагнитного соединения $Fe_{1,2}Cr_{1,8}S_4$. Обнаружено, что магнитное сопротивление отрицательно с резким пиком в области $T_c \approx 250$K и показано, что в области магнитного упорядочения спонтанный холловский коэффициент экспоненциально уменьшается с температурой.

Received: 28.11.02

SIMULATION OF THRESHOLD PROPERTIES OF FERROELECTRIC LIQUID CRYSTAL

H.F. ABBASOV, A.R. IMAMALIYEV
Baku State University,
Z. Chalilov str. 23, 370145

The one-dimensional model of thin planar ferroelectric liquid crystal cell has been considered. The dependences of threshold voltage both on some material parameters of ferroelectric liquid crystal (spontaneus polarization, anisotropy of dielectric permittivity, elastic constants) and on some external parameters (cell thickness, anchoring energies) have been obtained. The qualitative explanation of obtained results has been proposed.

One of the basic problems by utilizing of liquid crystal displays is to reduce the operating voltages as much as possible. The later can be essentially reduced in the case of ferroelectric liquid crystals (FLC) [1]. The first reason of so high sensitivity to an external electric field is the strong coupling of the electric field with spontaneous polarization. Except of spontaneous polarization, the threshold voltage of electrooptical effect is influenced by elastic constants, anisotropy of dielectric permittivity of FLC, surface conditions etc. In this paper the attempt was made to study influence of each of these factors on the FLC switching threshold on the basis of numerical calculations.

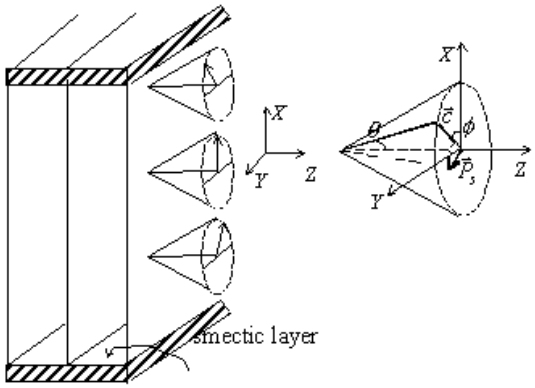

Fig.1. The cell geometry

The description of electrooptic properties of FLC-cell can be reduced to determination of the director field $\vec{n}(\vec{r},t)$. The later is given in the given point of space by two angles: the tilt angle θ and the azimuthal angle ϕ (fig. 1):

$$\vec{n} = \vec{n}(\sin\theta\cos\phi, \sin\theta\sin\phi, \cos\theta) \qquad (1)$$

The tilt angle depends mainly on temperature and the electric field essentially does not change its value. But the azimuthal angle varies spatially in absence of an electric field, and additionally in time under the field action. In thick samples, where the spirally twisted structure takes place, the angle ϕ varies both in a direction, perpendicular to layers, and in layers plane ($\phi = \phi(x, z)$), but in thin samples, only in a layer plane [2]. Therefore, for not too high fields the task of finding of a director field $\vec{n}(\vec{r},t)$ is reduced to the task of searching of azimuthal angle $\phi(x, t)$ distribution, what is determined by the competition of elastic and surface forces, and also by the electric field force.

It is not difficult to deduce the balance torque equation allowing us to determine the equilibrium configuration of the system $\phi(x)$ (the thickness is less than pitch of spiral structure: $d << L$):

$$G\theta^2 \frac{d^2\phi}{dx^2} + P_S E\cos\phi + \left(\frac{P_S^2}{2\chi_\perp \varepsilon_0} + \frac{\Delta\varepsilon\varepsilon_0\theta^2E^2}{2}\right)\sin 2\phi = 0 \qquad (2)$$

under boundary conditions

$$G\frac{d\phi}{dx}\Big|_{\pm d/2} = \left(W_1\cos\phi \pm W_2\sin 2\phi\right)_{\pm d/2} \qquad (3)$$

$$0 \le x \le d/2, \qquad -\pi/2 \le \phi \le \pi/2$$

The following notations are used: G is an elastic constant, P_s is a spontaneous polarization, E is an electric field strength, $\Delta\varepsilon = \varepsilon_{||} - \varepsilon_\perp$ is an anisotropy of dielectric permittivity, $\chi_\perp$ is transversal component of the dielectric susceptibility, ε_0=8.85pf/m is electric constant.

The first term in the right hand side of equation (3) expresses the polar interaction of molecules with the substrate surface. The polar interaction tends to orient the spontaneous polarization toward, or out of the surface. It is equivalent to a condition $\phi(d/2)=-\phi(-d/2)=\pi/2$ for our geometry. The second term is a dispersion part of the surface energy: the dispersion interaction is responsible for planar orientation of smectic A phase and required $\phi(d/2)=\phi(-d/2)=\pi/2$. The appropriate anchoring energies are denoted by W_1 and W_2. The signs «-» and «+» concern to top and bottom surfaces respectively.

For FLCs, used in electrooptical cells the typical values of P_s, G, θ, $\chi_\perp$ and $\Delta\varepsilon$ have the order of 10^{-4}cm^{-2}, 10^{-11}N, .0.4, 10, -3, respectively. Other external parameters W_1, W_2, d and E have the order of

$$10^{-4}\ J\cdot m^{-2},\ 10^{-5}\ J\cdot m^{-2},\ 5\cdot 10^{-6}\ m,\ 10^6\ \frac{V}{m},$$

respectively. Furthermore, we represent the polar part of anchoring energy as

$$W_1 = W_{10} + \alpha \cdot P_S \qquad (4)$$

where W_{10} is the permanent (independent of spontaneous polarization) component of polar anchoring energy, the second term is the contribution due to the spontaneous polarization. It is reasonable to take $W_1 \cong 10^{-5}\ J \cdot m^{-2}$ and $\alpha \cong 0.5\ V$.

The dynamics of the switching process can be described by the equation similar to (2):

$$\gamma\theta^2 \frac{\partial\phi}{\partial t} = G\theta^2 \frac{\partial^2\phi}{\partial x^2} + P_S E \cos\phi + \left(\frac{P_S^2}{2\chi_\perp \varepsilon_0} + \frac{\Delta\varepsilon\varepsilon_0\theta^2 E^2}{2}\right)\sin 2\phi \qquad (5)$$

under the same boundary conditions. γ_ϕ is a rotational viscosity that has the order $0.1\ Pa \cdot s$.

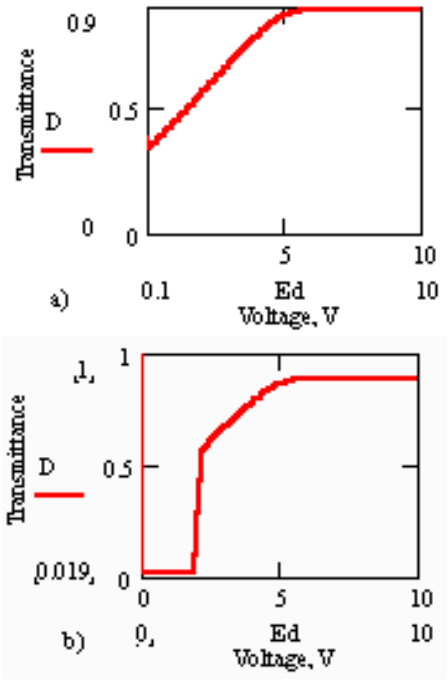

Fig. 2. Volt-contrast characteristics of FLC cell: a)the initial state is twist; b) the initial state is uniform

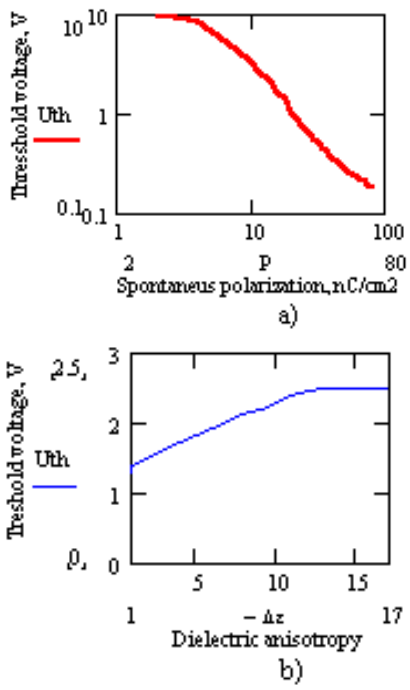

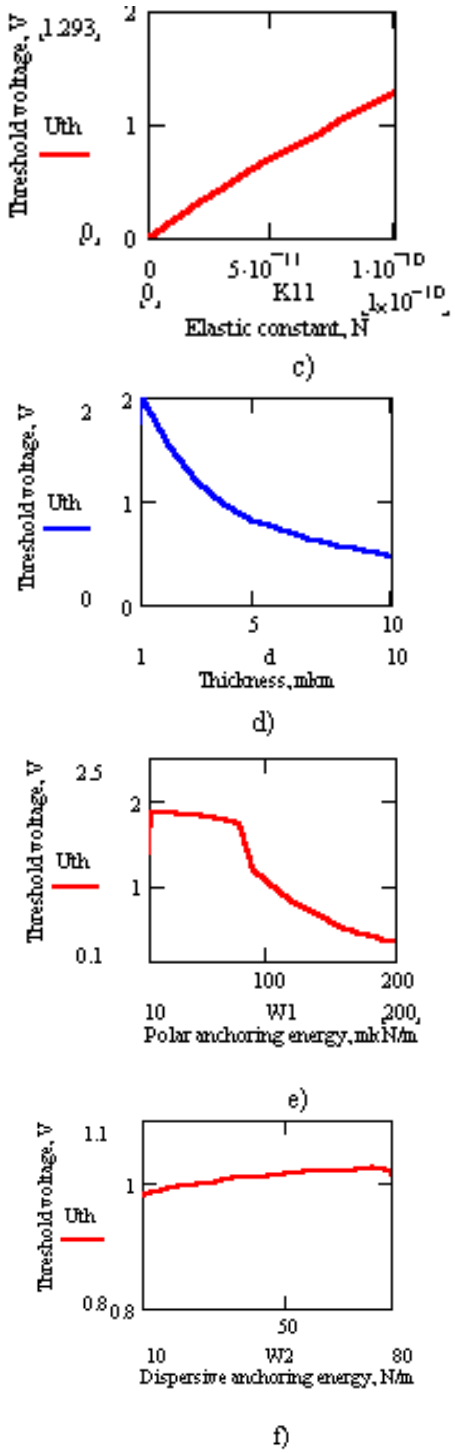

Fig 3. The dependence of threshold voltage on a) spontaneous polarization b)dielectric anisotropy; c)elastic constant; d)cell thickness; e)polar anchoring energy; f) azimuthal anchoring energy

The equation (5) is a nonlinear heat conduction equation with boundary conditions (2) of general form and can be solved by the sweep method [3].

To know the dependence $\phi(x,t)$, it is not difficult to find light transmittance of FLC cell in the crossed polarizers, for example, by Johnes' (2x2) retardation matrix method [4].To study the threshold characteristics of the FLC cell the slowly rising electric field (with the rate of order $1\frac{V}{s}$) has been applied. As seen from a fig. 2a, the transition from twist state to uniform state has not threshold character. But if as the initial state to take the uniform state $(\phi = -\pi/2)$, the transition to other uniform state $(\phi = \pi/2)$ has clearly expressed threshold character (fig. 2b).

The results of numerical calculations are shown in fig.3, as dependences of a threshold voltage on spontaneous polarization, dielectric anisotropy, cell thickness, elastic constant and anchoring energies.

As expected, the threshold voltage is proportional to spontaneous polarization (fig. 3a). A small deviation from this low in the range of weak spontaneous polarizations is related, on our opinion, to polar anchoring of molecules with a surface, which appears as a destabilizing factor. For upper surface there is an excess of free energy of density about $\frac{W_1}{d}$ that is comparable with field energy P_sE.

The dielectric permittivity also influences on the value of the threshold. As, the interaction of a field with negative dielectric anisotropy appears as the stabilizing factor (appropriate density of energy has the order $\frac{-\Delta\varepsilon\varepsilon_0 U^2}{2d^2}$), with increasing of $|\Delta\varepsilon|$ the threshold voltage slowly rises (fig. 3b).

The transition from one homogeneous state to another occurs by creation of intermediate twist state of energy density about $\frac{G}{d^2}$. Therefore the threshold voltage increases with rising of an elastic coefficient. This dependence has the form of direct proportionality with surprising accuracy (fig.3c).

The increasing of cell thickness leads at first to the diminishing of the threshold voltage, however, in further this tendency loosened (fig.3d). A reason of it also is weakening of polar anchoring energy density.

The destabilizing role of polar anchoring is expressed also in following: the threshold voltage diminishes with increase of polar anchoring energy W_1 (fig. 3e). The breaks observed in a graphics hint about qualitatively different ways of switching at different intervals of values W_1.

As the dispersion interaction of molecules with a surface acts as the stabilizing factor, the threshold voltage slowly rises with increase of dispersive part of anchoring energy W_2 (fig. 3f).

Note that the proposed model is one – dimensional where the switching by domain wall motion is not under consideration.

[1] *N.A. Clark, M.A. Handshy, S.T. Lagerwall*. Mol. Cryst. Liq. Cryst., 1983, v.93, p.213.

[2] *Y. Ouchi, H. Takezoe, A. Fukuda*. Jap. J.Appl. Phys., 1987, v.26, №1, p.1.

[3] *A.A. Samarskiy, A.B. Gulin*. Numerical methods, Nauka, 1987, 427 pp.

[4] *Yariv, P. Yeh.* Optical waves in crystals. John Wiley & Sons, 1993, 616 pp.

H.F. Abbasov, A.R. İmaməliyev

SEQNETOELEKTRİK MAYE KRİSTALIN ELEKTROOPTİK XASSƏLƏRİNİN MODELLƏŞDİRİLMƏSİ

Birölçülü hal üçün nazik planar seqnetoelektrik maye kristal nümunəsinin riyazi modeli qurulmuşdur. Astana gərginliyinin həm maye kristalın maddi parametrlərindən (spontan polyarizasiya, dielektrik nüfuzluğunun anizotropiyası, elastik sabit), həm də xarici parametrlərdən (yuvacığın qalınlığı, ilişmə enerjiləri) asılılığı müəyyən olunmuş və bu asılılıqların keyfiyyətcə izahı verilmişdir.

Х.Ф. Аббасов, А.Р. Имамалиев

МОДЕЛИРОВАНИЕ ЭЛЕКТРООПТИЧЕСКИХ СВОЙСТВ СЕГНЕТОЭЛЕКТРИЧЕСКОГО ЖИДКОГО КРИСТАЛЛА

В данной работе представлена одномерная модель тонкой планарной ячейки сегнетоэлектрического жидкого кристалла. Установлена зависимость порогового напряжения, как от материальных параметров жидкого кристалла (спонтанной поляризации, анизотропии диэлектрической проницаемости, упругой постоянной), так и от внешних параметров (толщины ячейки, энергий сцепления). Приведена качественная интерпретация полученных результатов.

Received: 26.02.03

THE STRUCTURAL TRANSFORMATIONS IN $Cu_{1.50}Ag_{0.5}Te$

Y.G. ASADOV, R.B. BAYKULOV
Institute of Physics, Azerbaijan National Academy of Sciences,
Baku. Az - 1143, H. Javid ave. 33

The structural phase transition in $Cu_{1.50}Ag_{0.5}Te$ were investigated by the high-temperature roentgenodiffractometric method, and it was shown, that at the room temperature $Cu_{1.50}Ag_{0.5}Te$ is two-phase and is composed of the rhombic phase with the lattice parameters a=7.319Å, b=22.236Å, c=36.458Å and the rhombic phase with the lattice parameters a=3.12Å, b=4.04Å, c=6.87Å. The both rhombic phases transfer into the two primitive cubic phases with the parameters a_1=7.0091Å и a_2=6.8787Å, respectively, by the temperature increase at 469K.

The Cu_2Te compound on the state diagram of the Cu-Te system corresponds to the compound 33,3 at % Te and melts at 1393 K[1]. In [2] it is shown, that Cu_2Te is crystallized in the hexagonal structure with lattice parameters: a_o=4.237Å, c_o=7.274Å, a space group P6mmm, the elementary cell contains Z=2, the density ρ_x=7.274 g/cm^3.

According to [3] for Cu_2Te the rhombic structure with the lattice parameters a=7.319Å$\approx\sqrt{3}\,a_o$, b=22.236Å$\approx 3c_o$, c=36.458Å$\approx 5c_o$, which is the superstructural hexagonal phase, is determined at the room temperature. In [3-9] it is shown by various authors and naturally by various methods, that in Cu_2Te five structural transformations at 448, 548, 593, 638 and 848K occur in the temperature range 290-1220K.

In [10] it is shown by the high-temperature roentgeno-diffractogramic method, that:

a) The second hexagonal phase with the lattice parameters a=8.4191Å, c=21.8733Å is yielded at 448 K from the Cu_2Te crystal, composed of the rhombic and hexagonal phase with the lattice parameters: a=7.319Å, b=22.236Å, c=36.458Å and a=4.1418Å, c=7.1833Å. The parameter c of the rhombic phase is sharply cut Δc=0.72Å with the phase formation, what gives reasons to make conclusion, that the second hexagonal phase is formed at the expense of the rhombic phase.
b) At 540 K the parameters a and b of the rhombic phase reduce by the jump, but the parameters a and c of the first hexagonal phase increase by the jump. The reason is the displacement of the cations and the cation vacancies.
c) At 590 K the rhombic and first hexagonal phases transfer into the second hexagonal phase and crystals Cu_2Te become one-phase at the temperature range 590-638 K.
d) At 638 K the diffraction reflections, belonged to the rhombic phase, are restored with the appearance of the reflection from the plane (111) of the high-temperature fcc phase.
e) At 848 K the rhombic and second hexagonal phases transfer into the fcc phase with the lattice parameters a=6.1140Å.

In [11] it is shown, that the crystals $Cu_{1.50}Zn_{0.50}Te$ at the room temperature, as Cu_2Te, are two-phase and composed of the hexagonal phase with the lattice parameters a=4.2478Å, c=7.2334Å and the rhombic phase with the lattice parameters of the corresponded lattice parameters Cu_2Te.

At 811±2 K the rhombic phase transfers into the hexagonal phase. In this process the parameters of the hexagonal phase do not suffer the jump. It testifies the fact, that at the transformation of the rhombic phase into the hexagonal, the latter is to be the primer. The hexagonal phase itself at 970±2 K transfers into the high-temperature fcc phase of the lattice parameter a=6.1187Å.

It follows from the above-presented, that in crystals Cu_2Te the partial substitution of Cu atoms by the Zn atoms, having the same charge and close ion radii, cut the number of the phase transformations from five in Cu_2Te up to two in $Cu_{1.50}Zn_{0.50}Te$.

The results of the high-temperature roentgenodiffractogram researches of the influence of the partial substitution of the cooper atoms by the silver atoms on the structure, mechanism and the temperature of the structural transformations in the crystal Cu_2Te are represented in the present paper. With this purpose, the method of the direct synthesis, i.e. the chemical interaction of the initial components, is used for the receipt of the homogeneous samples of the $Cu_{1.50}Ag_{0.5}Te$ compound. The initial components, taking part in the compound, have the following purities: cooper is electrolytic, silver and tellurium are of the special pure mark (SP). The synthesis conditions and the crystals growth by the Bridgemann's method are represented in [10].

The temperature roentgenographic researches was carried out on the diffractometer DRON-3M with the temperature attachment URVT-2000.

Experiments were carried out in the vacuum (10^{-2} Pa). The condition of the survey permission was made ~1º. The diffractograms are recorded persistently, the diffraction angles are determined by the method of the intensities peaks measurement. In experiments the error of the reflection angle determination did not exceed the value $\Delta\theta$=±0.02º.

From the crystal ingot $Cu_{1.50}Ag_{0.5}Te$ the thin plane of the size 2×4×4 mm was cut off and at the room temperature 18 diffraction reflections (table 1) are fixed from the indicated sample in the angle interval 20º≤2θ≤80º.

For the precious indexing of the diffraction data from $Cu_{1.50}Ag_{0.5}Te$ they were compared with the calculated values of the interplane distances d_i, and corresponding indices $h_ik_il_i$ of the reflection planes, calculated on the base of the parameters of the elementary cell Cu_2Te, CuAgTe and Ag_2Te. As it is seen from the table 1, the experimental values are satisfactorily coincided with the calculated parameters d_i of the lattice parameters of the rhombic phase Cu_2Te. From experimental d_i, as it is seen from the table 1, some d, i.e d=2.4715 (110); 2.0060 (112); 1.7177 (004); 1.5608 (200) and 1.4145 (114) are indexed on the base of the parameters of the rhombic phase CuAgTe. It follows hence, that the crystals $Cu_{1.50}Ag_{0.5}Te$ at the room temperature are two-phase, i.e crystallized in the rhombic structure Cu_2Te and CuAgTe, besides the relative number (quantity) of Cu_2Te is more than CuAgTe.

Table 1

The diffractogram's calculation of $Cu_{1.50}Ag_{0.50}Te$. $CuK_\alpha(\lambda_\alpha=1.5418$ Å), filter – N_i, Regime: 38 κV, 22 mA.

NN	θ	I/I_0	$d_{exp.}$(Å)	Cu_2Te		CuAgTe		Parameters of the elementary cell, Å	T_{exp} K
				$d_{cal.}$(Å)	hkl	d_{cal}(Å)	hkl		
1	2	3	4	5	6	7	8	9	10
1	15º41´	17	2.8534	2.8534	208				
2	16º30´	33	2.7144	2.7155	209				
3	16º52´	100	2.6574	2.6586	084			Rhombic	
4	17º30´	95	2.5636	2.5623	256			*a*=7.3193	
5	18º11´	15	2.4715	2.4707	090	2.4716	110	*b*=22.2435	
6	18º39´	42	2.4107	2.4181	302			*c*=36.3636	
7	20º11´	50	2.2345	2.2340	340				
8	21º27´	40	2.1081	2.1093	099				
9	21º45´	30	2.0807	2.0807	319				293
10	22º36´	42	2.0060	2.0059	348	2.0064	112	Rhombic	
11	22º48´	19	1.9893	1.9887	364			*a*=3.1216	
12	23º29´	18	1.9352	1.9349	370			*b*=4.0423	
13	24º14´	52	1.8788	1.8775	2103			*c*=6.8708	
14	25º02´	11	1.8224	1.8224	411				
15	26º40´	11	1.7177	1.7185	393	1.7177	004		
16	28º44´	9	1.6040	1.6032	3105				
17	29º36´	4	1.5608	1.5614	459	1.5608	200		
18	33º02´	12	1.4145	1.4145	541	1.4111	114		
1	15º39´	10	2.8584	2.8560	208				
2	16º29´	35	2.7173	2.7176	209				
3	16º51´	100	2.6601	2.6622	084			Rhombic	
4	17º28´	97	2.5688	2.5661	256			*a*=7.3367	
5	18º09´	20	2.4748	2.4748	090	2.4746	110	*b*=22.2732	
6	18º33´	50	2.4227	2.4239	302			*c*=36.4101	
7	20º07´	48	2.2410	2.2391	340				
8	21º25´	34	2.1109	2.1110	099				
9	21º43´	30	2.0835	2.0838	319				373
10	22º33´	36	2.0102	2.0089	348	2.0093	112	Rhombic	
11	22º46´	35	1.9920	1.9924	364			*a*=3.1280	
12	23º26´	23	1.9389	1.9390	370			*b*=4.0522	
13	24º12´	45	1.8807	1.8804	2103			*c*=6.8860	
14	24º59´	15	1.8255	1.8259	411				
15	26º36´	13	1.7215	1.7218	393	1.7215	004		
16	28º42´	10	1.6054	1.6060	3105				
17	29º32´	10	1.5640	1.5642	459	1.5640	200		
18	33º00´	10	1.4155	1.4178	541	1.4132	114		
1	15º38´	5	2.8605	2.8595	208				
2	16º28´	30	2.7202	2.7206	209				
3	16º49´	100	2.6647	2.6660	084			Rhombic	
4	17º27´	90	2.5714	2.5700	256			*a*=7.3477	
5	18º07´	15	2.4788	2.4788	090	2.4784	110	*b*=22.3092	
6	18º35´	50	2.4189	2.4275	302			*c*=36.4280	
7	20º06´	45	2.2429	2.2428	340				
8	21º24´	32	2.1126	2.1141	099				
9	21º42´	30	2.0852	2.0865	319				423
10	22º31´	35	2.0128	2.0117	348	2.0121	112	Rhombic	
11	22º45´	30	1.9935	1.9956	364			*a*=3.1312	
12	23º24´	20	1.9413	1.9418	370			*b*=4.0622	
13	24º10´	40	1.8830	1.8838	2103			*c*=6.8940	
14	24º57´	14	1.8276	1.8282	411				
15	26º34´	12	1.7235	1.7247	393	1.7235	400		
16	28º40´	10	1.6070	1.6087	3105				
17	29º30´	10	1.5656	1.5663	459	1.5656	200		
18	32º54´	10	1.4192	1.499	541	1.4149	114		

After the diffraction reflection record at the room temperature, without changing the angle interval and the crystals orientation the furnace was switched on and the record was carried out every 50 K. Before every record the corresponding temperature was kept constant during 40 min. Under this conditions, the essential changes did not occur in

the reflection number and their intensities up to 423 K. Only at 423 K the four couple diffraction reflections (fig.1), whose calculations are represented in the table 2, are fixed in the previous angle interval. As it is seen from the table 2 and fig.1 the low-temperature two-phase crystal $Cu_{1.50}Ag_{0.5}Te$ at 469±1 K transfers into the two primitive cubic phases with the lattice parameters: a_1=7.009*Å* и a_2=6.878*Å*, distinguished by the elementary cell parameters and the diffraction reflections intensities, where $I^1_{(220)} > I^2_{(220)}$, $I^1_{(222)} > I^2_{(222)}$, $I^1_{(320)} < I^2_{(320)}$ and $I^1_{(400)} < I^2_{(400)}$.

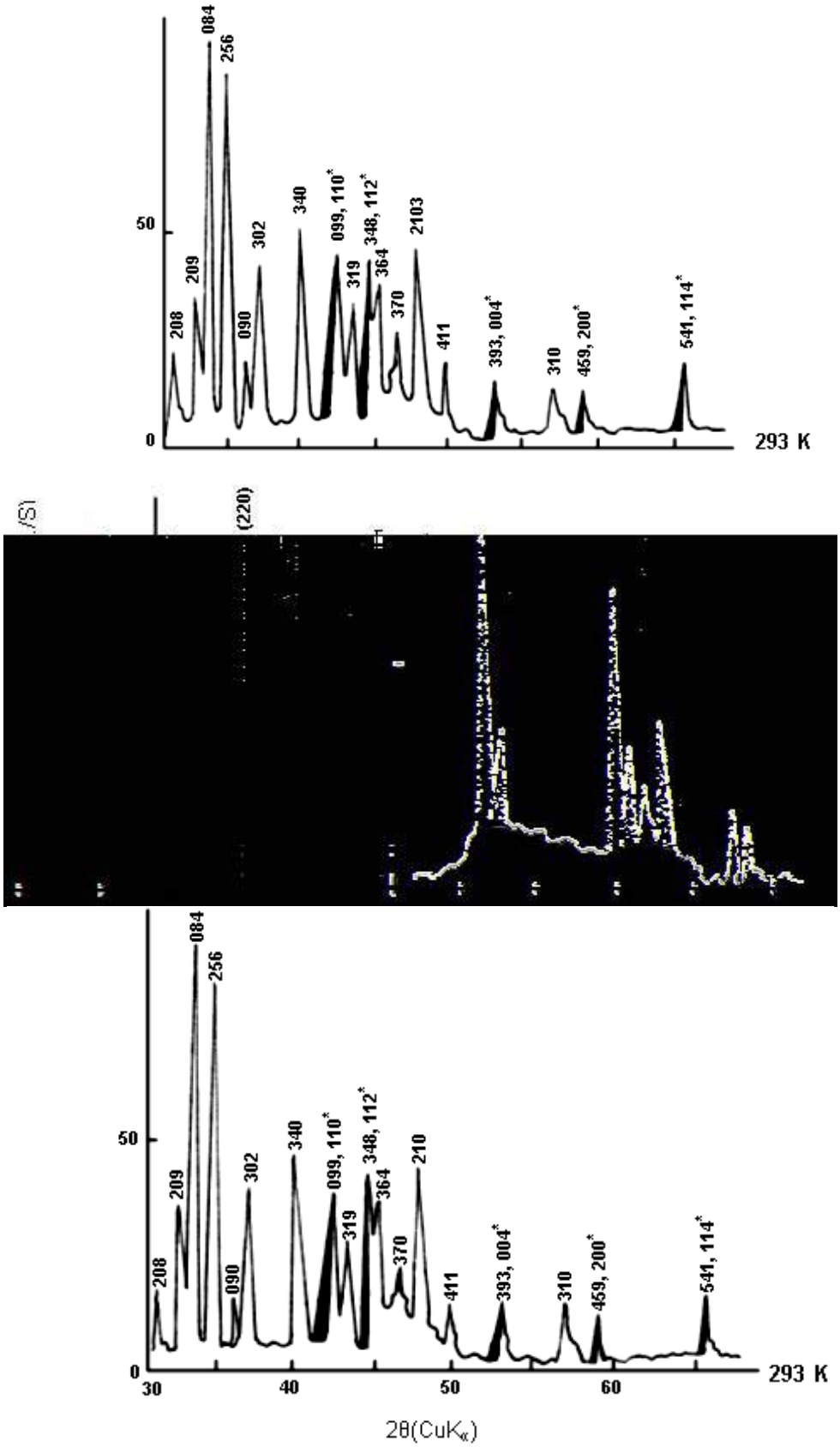

Fig.1. The crystal's diffractogram of $Cu_{1.50}Ag_{0.50}Te$ (the rhombic phase reflex is marked by the star)

Table 2

The diffractogram's calculation of $Cu_{1.50}Ag_{0.50}Te$.

N	θ	I/I_0	$d_{exp.}$(Å)	$(P)_1$		$(P)_2$		Parameters of the elementary cell , Å	$T_{exp.}$ K
				$d_{cal.}$(Å)	hkl	$d_{cal.}$(Å)	hkl		
1	18º07´	100	2.4788	2.4781	220	-	-		
2	18º29´	40	2.4319	-	-	2.4320	220	$(P)_1$	
3	22º24´	80	2.0228	2.0234	222	-	-	a=7.0091	
4	22º51´	30	1.9853	-	-	1.9857	222		
5	23º22´	40	1.9438	1.9436	320	-	-		473
6	23º50´	20	1.9082	-	-	1.9078	320	$(P)_2$	
7	26º06´	10	1.7524	1.7523	400	-	-	a=6.8787	
8	26º38´	5	1.7196	-	-	1.7197	400		
1	18º06´	100	2.4812	2.4801	220	-	-		
2	18º27´	38	2.4365	-	-	2.4362	220	$(P)_1$	
3	22º23´	83	2.0244	2.0249	222	-	-	a_1=7.0146	
4	22º48´	38	1.9824	-	-	1.9891	220		
5	23º21´	22	1.9452	1.9455	320	-	-		573
6	23º48´	45	1.9105	-	-	1.911	320	$(P)_2$	
7	26º05´	10	1.7536	1.7537	400	-	-	a_2=6.8906	
8	26º35´	10	1.7227	-	-	1.7226	400		

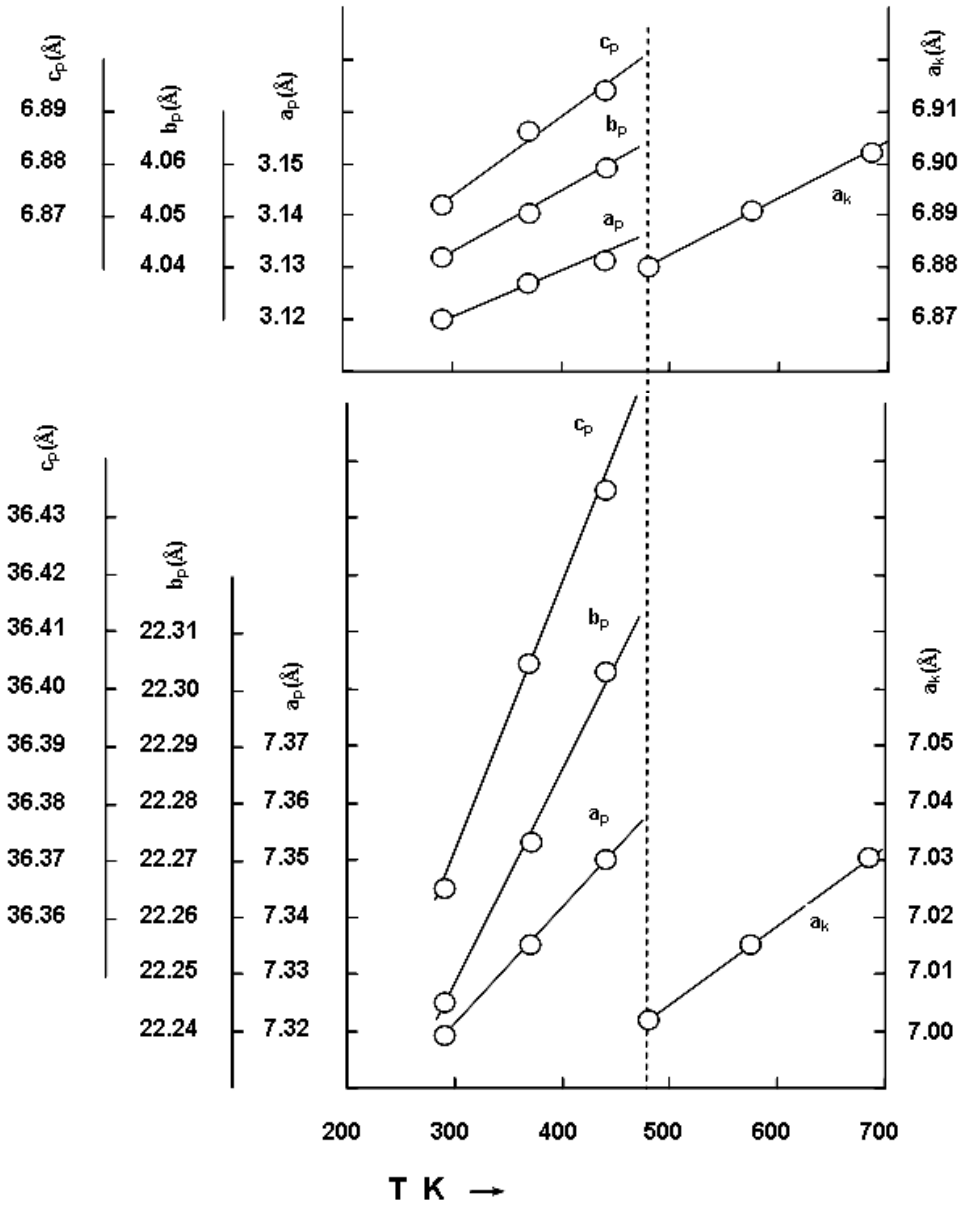

Fig.2. The temperature dependencies of the lattice parameters of both rhombic and cubic phases.

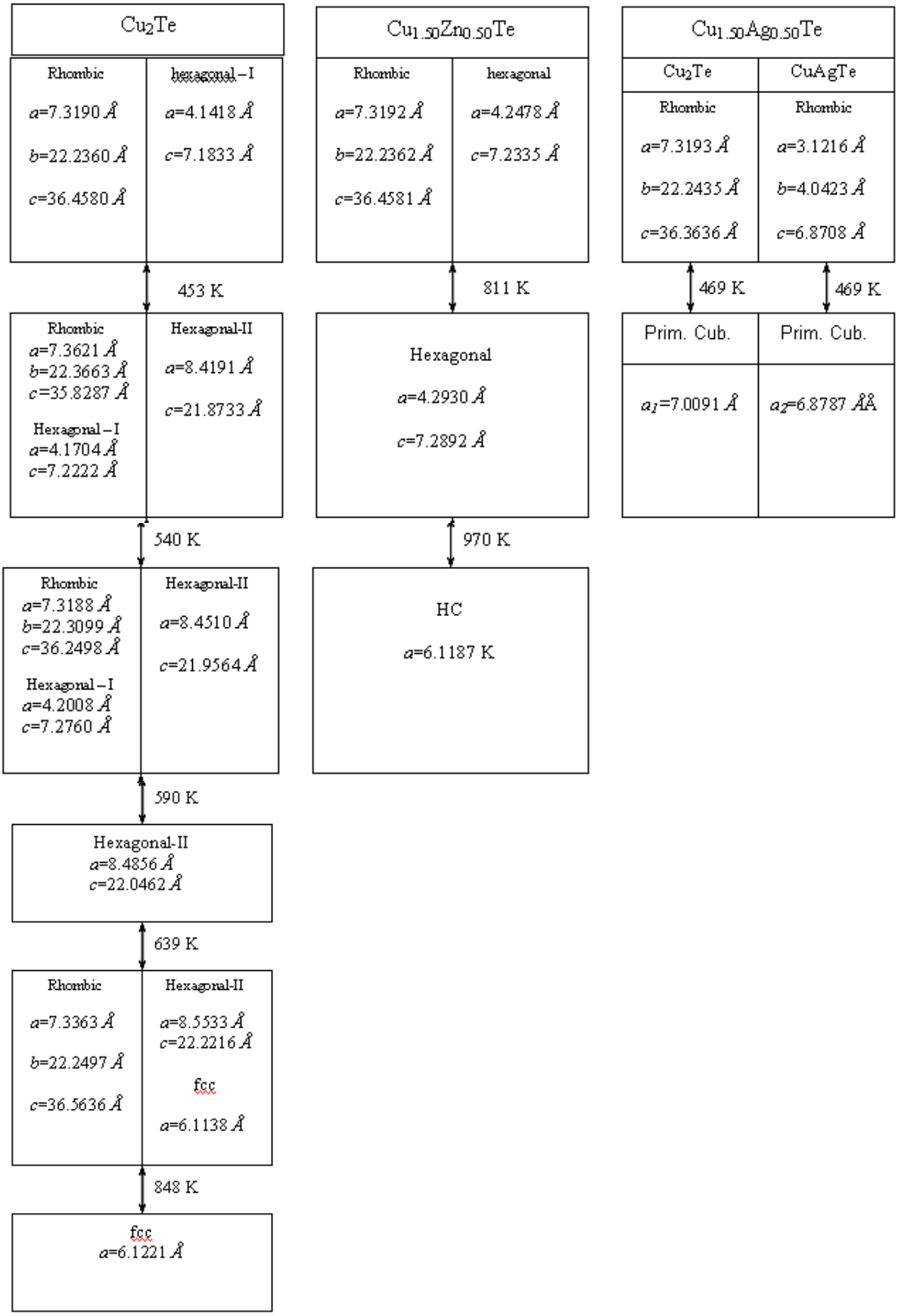

Fig.3. The scheme of the structural transformations in Cu_2Te, $Cu_{1.50}Zn_{0.50}Te$ and $Cu_{1.50}Ag_{0.50}Te$.

At the further heating the both primitive cubic phases kept their individuality, but at the reverse cooling below 469 K they transfer into the two ordered phases, one of which is identical by the lattice parameters to the low-temperature phase Cu_2Te, and another to CuAgTe. As it was noticed, the low-temperature rhombic phase Cu_2Te after the four intermediate phase transformations at 848 K transfers into the high-temperature fcc phase with the lattice parameters a=6.114Å. It is known about the second phase, i.e CuAgTe, that at the room temperature it is crystallized in the structural type of the rhombic CuTe with the lattice parameters a=3.12Å, b=4.05Å, c=6.875Å, ρ=8.20g/cm^3. However, the space groups with *Pmmm* on *Pmm2* (the suppression is absent) is changed with regard to the ordered substitution of the half of Cu atoms by Ag atoms.

In spite of the fact, that the compound $Cu_{1.50}Ag_{0.5}Te$ at the room temperature is two-phase and crystallized in the structural type Cu_2Te and CuAgTe, neither the transformation temperature nor the high-temperature modifications structures do not correspond.

The schemes for the comparison of the structural transformations in $Cu_{1.50}Ag_{0.5}Te$, Cu_2Te and $Cu_{1.50}Zn_{0.5}Te$ are represented on fig.2. These differences represented on the scheme are mainly connected with the spreading of two types of cations between the layers of tellurium atoms in the tetrahedral and octahedral vacuums.

The temperature dependencies of the lattice parameters $Cu_{1.50}Ag_{0.5}Te$ are represented on fig.3. As it is seen from fig.3, the parameters *a(T), b(T), c(T),* of both rhombic and *a(T)* of both cubic phases increase in a linear fashion. The coefficient of the line expansion, calculated from the temperature dependencies of the existing phases lattice parameters.

As it is seen from the table 3, the rhombic phase, crystallized by the structural type Cu_2Te, is strongly deformed in the direction [100], i.e. $\alpha_a>\alpha_b\approx\alpha_c$ but the rhombic phase, crystallized by the structural type CuAgTe, is deformed in the direction [010], i.e. $\alpha_a<\alpha_b>\alpha_c$. It is the main reason of the instability of the both rhombic phases, which at 469 K transfer into the high-temperature primitive cubic phase.

Table 3

The heat expansion of $Cu_{1.50}Ag_{0.50}Te$.

$T_{str.}$ K	Modification	$T_{exp.}$ K	The line expansion coefficient 10^{-6} degree^{-1}			
			α_a	α_b	α_c	$\bar{\alpha}=\frac{\sum\alpha_i}{3}$
469	Cu_2Te	293-373 293-423	29.7 29.8	16.7 22.7	16.0 13.6	20.8 22.0
	CuAgTe	293-373 293-423	25.6 23.7	30.6 37.9	27.7 26.0	28.0 29.2
	P_1 P_2	473-573 473-573	0.80 17.3			

[1] *Kien Van Con, H. Rodot*. Domaine d'existance et proprietes electriques des composes du systeme Cu-Te. Compt. Rend. Acad. Sci. (Paris), 1965, 260, p.1908-1914.

[2] *H. Novotny*. Z. Metallkunde, 1994, 37, p. 40-42.

[3] *A.L. Stevels*. Phase transitions in nickel and copper selenides and tellurides. Philips. Res. Repts., 1969, 24, p. 124.

[4] *M.U. Tsypin and A.A. Chipizhenko.* Izv. Ak. Nauk, SSSR, Ser. Neorgan, Mater., 1974, 10, p. 1210

[5] *P. Kubaschevski and L. Nolting.* Ber. Bunsenqes, Phys. Chem., 1973, 17, p. 70.

[6] *H. Gravemann. and H. Walbaura.* Z. Metallk., 1956, 47, p.433.

[7] *F. Guastavino, H. Luqueet and J. Bougnot*. Etude du diagramme de phase du sustem Cu-Te dans le damaine de la solution solide $Cu_{2-x}Te$ ($0<x<16$). Mater. Res. Bull., 1956, 8, p.935.

[8] *J. Bougnot, F. Guastavino, H. Laquet, D. Sodini.* Etude du domaine d'existtence de laphase d" du Tellure cuivreux appartir de la conductive electrique. Müter. Res. Bull., 1973, 5, p.763.

[9] *N. Vouroutzis and Monolikas*. Phys. Stat. Sol., (a), 1989, 111, p.491.

[10] *L.V.Rustamova, G.B.Gasimov,K.M.Jafarov,Y.G Asadov.* Neorganicheskiye materiali, 1991, vol. 26, №10, 2065.

[11] *Y.G. Asadov, S.Y. Asadova, A.I. Movlamverdiyeva, F.K. Isayev.* Neorganicheskiye materiali, 2002, volume 38, №11, c.1-6. (in Russian)

Y.G. Əsədov, R.B. Baykulov

$Cu_{1.50}Ag_{0.50}Te$ KRİSTALINDA QURULUŞ ÇEVRİLMƏSİ

Yüksək temperatur rentgendifraktometrik metodu ilə $Cu_{1.50}Ag_{0.50}Te$ kristalında quruluş çevrilməsi tədqiq edilmişdir və göstərilmişdir ki, otaq temperaturunda qəfəs parametrləri a=7.319 Å, b=22.236 Å, c=36.458 Å və a=3.12 Å, b=4.04 Å, c=6.87 Å olan iki rombik fazadan ibarət olub, 469 K-də qəfəs parametrləri a_1=7.0091 Å və a_2=6.8787 Å olan iki primitiv kub fazaya keçir.

THE STRUCTURAL TRANSFORMATIONS IN $Cu_{1.50}Ag_{0.5}Te$

Ю.Г. Асадов, Р.Б. Байкулов

СТРУКТУРНЫЕ ПРЕВРАЩЕНИЯ В $Cu_{1.50}Ag_{0.50}Te$

Высокотемпературным рентгендифрактометрическим методом исследовались структурные фазовые переходы в $Cu_{1.50}Ag_{0.50}Te$ и было показано, что при комнатной температуре $Cu_{1.50}Ag_{0.50}Te$ является двухфазным и состоит из ромбической фазы с параметрами решетки a=7.319Å, b=22.236Å, c=36.458Å и ромбической фазы с параметрами решетки a=3.12Å, b=4.04Å, c=6.87Å. С повышением температуры при 469 К обе ромбические фазы превращаются в две примитивные кубические фазы с параметрами a_1=7.0091Å и a_2=6.8787Å соответственно.

Received: 27.02.03

THE ELECTRIC AGEING OF THE POLYETHYLENE AND POLYPROPYLENE POLYMER MIXTURES IN THE REGION OF LOW ADMIXTURES OF ONE OF THE COMPONENTS

A.A. ALIYEV

The Institute of Radiation problems, Azerbaijan NAS,
370143, Baku, H. Javid ave. 31"a"

The influence (1-10 weight %) of polypropylene (PP) concentrations in polyethylene (PE) upon the durability to the electric ageing was studied. It is shown, that the injection of the low (1-2 weight %) PP concentrations into PE increase the PE durability to the erosion and oxidation, caused by the electric discharge effect and leads to the growth of the PE electric solidity.

INTRODUCTION

One of the reasons of the high-voltage insulation break is the development of the electric discharge in the place of the gas inclusion inside the insulation [1]. The second main reason of the insulation break under the long influence of the electric field is the appearance and development of the partial break channels in the parts with the sharp heterogeneity field, i.e. dendrites or triings, leading to the gradual loss of the material mass (erosion) and the local reduction of its thickness and at last to its full break.

In order to increase the high-voltage polymer insulation lifetime it is necessary to create the material, having the monolith structure (with the minimal number of the gas inclusion and heterogeneities), and having the resistance to the electric discharge effect.

Recently the polymer mixtures have attracted the researcher attention. The obtained materials have the complex of the new properties, which are absent at the initial polymers [2].

There are a number of works, devoted to the research of the PP-PE mixtures with the purpose of the PP shock strength increase, fragility temperature drop, but there is no information on the research of the PP-PE mixtures with the purpose of the application as a polymer insulation.

The properties of the polymer mixtures, components of which do not come into the chemical interaction with each other, essentially depend on its structure, which, in its turn, is determined by the concentration relationship between the components, with the increase of the component content in the matrix of another the mixture structure passes by the sequence the row of stages: the solution, the region of the interphase dissolution, the dispersed microheterogenous structure, the coagulation net, the inversion structure [3].

It might be supposed, that the mechanism of the polymer mixture damage under the influence of the external factors will also essentially depend on the concentration relationship between components.

THE EXPERIMENTAL PART

The work purpose is to investigate the electric ageing of the polypropylene (PP) and polyethylene (PE) mixtures films in the region of the low (up to 5-10) weight % of one of the components. The mixtures PP with PE were prepared from non-inhibited isotactic powders PP (the average weight mass $\overline{M}_\omega = 2.86 \cdot 10^5$, the average numerical molecular mass $\overline{M}_n = 6.23 \cdot 10^4$, $\overline{M}_\omega / \overline{M}_n = 4.6$, the crystallization degree $\chi = 64$) and PE $/\overline{M}_\omega = 4.15 \cdot 10^4$, $\overline{M}_n = 2.71 \cdot 10^4$, $\overline{M}_\omega / \overline{M}_n = 1.53$ $\chi = 49$) on the ball mill during 60 minutes with the following passing through the microextruder with the three regulated temperature bands-140, 160, 190°. The isotropic films were obtained by the extrudate pressing during 30 minutes at 200° and the pressure 200 atm. on the substrate from the polyimide film. The film thickness makes 100-120 mcm. The film were tempered in water at 30°C right after the pressing.

The influence of the electric discharge is realized in the asymmetric test cell, composed of the flat metal electrode, on which the tested sample of the polymer film was placed, with the air gap of the value 1.5 mm and the glass plate of the same thickness: the high electric voltage U=9 kV of the industrial frequency was applied to the metallized cover on the interface of the glass plate.

The sample weighing before and after the influence was made on the balance VLP-200 to a precision up to 0.05 mg. The oxidation is followed by the band of the carbonyl (C=0) groups at 1720 cm^{-1} by means of the UK-spectrophotometer. The electric strength E_{str} is determined on the current of the industrial frequency as the arithmetical average from the results of 10 independent relations measurements. U_{br} /h, where U_{br} is the break voltage, increasing with the velocity 2kV/s, h is the average thickness round the break place. The tangent of the corner of the dielectric losses $tg\delta$ and the dielectric constant ε of the films were measured by means of the bridge P-589.

RESULTS AND THEIR DISCISSION

The results of the polymer compositions PE-PP test are presented in the table 1. It is seen from the table 1, that the admixture of PP (0-5%) in PE causes the negligible changes of the electric characteristics of the following compositions.

The polyethylene and polypropylene are incompatible polymers. PE crystallizes in more stable orthorhombic lattice, while PP in the monoclinic shape. However, both components have the mutual influence on the crystallization process and the low-molecular structure formation [3-7].

The injection of the low (1-2 weight %) concentration PP in PE increases the PE resistance to the erosion and oxidation, caused by the electric discharge effect (fig.1 and 2).

Table 1.

The polymer compositions PE-PP characteristics

Sample	PE	PE+0.5%PP	PE+1%PP	PE+2 %PP	PE+5 %PP
Characteristics					
E_{str} кV/mm	118	116	120	118	116
$tg\delta \cdot 10^{-4}$	7	6	5	4	6
ε	2.2	2.4	2.8	2.9	2.7
Lg (ρ_v, ohm*m)	14.5	13.8	14.6	14.3	14.2

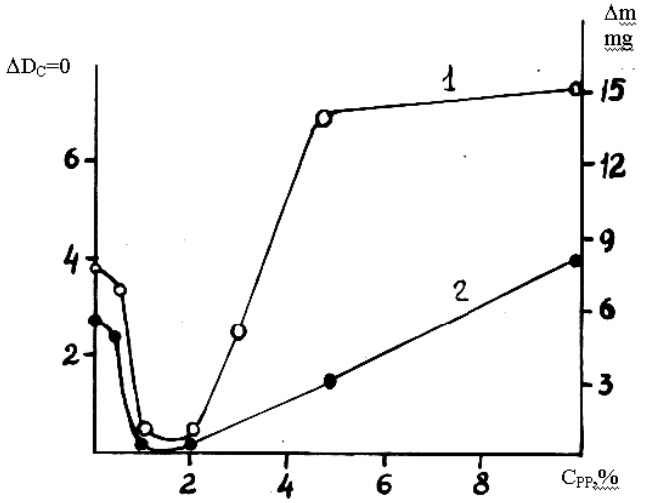

Fig. 1. The dependence of the mass losses Δm (1) and the oxidation degree (2) of the PE sample versus the PP content U_{agi}= *9 kV*, t_{agi}=20 hours.

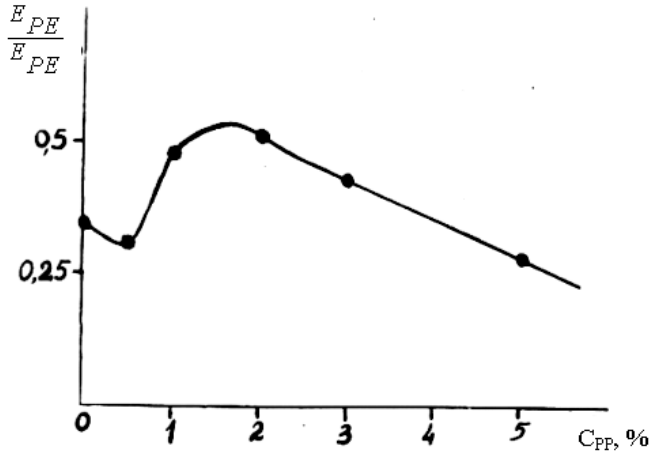

Fig. 2. The dependence of the electric strength E_{str} of the PE samples with the various PP content: U_{agi}= 9 kV, t_{agi}=10 hours.

It is known, that PP is less stable to the electric discharge influence, than PE, what is explained by the presence of the tertiary atoms of the carbons in the macromolecules. Actually, for 20 hours of the electric ageing in our conditions the mass decrease at the individual PP has made about 20 mg; but at the individual PE it is only 8mg.

It is seemed, that the injection of PE in PP should increase its resistance to the electric discharge influence and vice verse, however, it is not observed in the region of the low admixtures. The external nature of the mass and oxidation loss in the region 0.5-1 weight % PE in PP and in the region 1-2 % PP in PE may be explained by means of the interphase layer presentations.

According to [8,9] the external nature of the changes of the polymer mixtures properties in the region of the very low admixtures of one of the components (modifier) is explained by the spilling of the polymer solution at the determined modifier content, its emission in the dispersed phase and the formation of the interphase layer with the specific properties. The modifier may form the reinforced cage or fill the structural defects of the polymer matrix, i.e provide more small and one-phase structure or vice verse, expand the matrix structure and increase its defects.

Therefore, the reduction of the free volume occurs at the injection of the low admixture of PP in PE, the interphase layer becomes more dense, and the resistance to the electric ageing becomes maximal (table 2)

Table 2

The polymer compositions characteristics after the electric ageing

Sample-characteristics	PE	PE+0.5%PP	PE+1%PP	PE+2%PP	PE+5%PP
E_{str} кV/mm	43.0	38.0	60.0	64.0	32.0
$tg\delta \cdot 10^{-4}$	95.0	80.0	26.0	32.0	78.0
ε	3.2	3.8	4.7	4.8	4.2
lg, ρ_v, ohm*m	9.32	9.47	11.6	10.6	9.4
Δm, mH	7.5	6.6	0.87	0.93	14.8
ΔD_c=0	3.75	3.56	0.03	0.02	1.48

At the moment of the interphase spilling a number of the modifier particles of the small sizes are formed and the value of the interphase layer is maximal. The particles sizes increase with the further growth of the modifier content and their concentration falls [10] and the interphase layer reduces.

Actually, in our case the sharp oxidation reduction and the mass loss under the influence of the partial discharges, and also the electric strength growth are observed after the concentration of PP 1 weight % in PE.

[1] *A.N. Tzikin, S.N. Katkov*. Elektricheskoye stareniye polimernoy izolyatzii. L: Ximiya, 1968.
[2] *A.A. Popov, A.V. Russak, M.P. Gladilin, G.E. Zaykov.* Visokomolekulyarniye soyedineniya: A, 1986, v.28, №5, pp.1083-1087.
[3] *O.F. Noel, I.F. Carley*. Polymer Eagng Sci. 1975, v.15, p.117.
[4] *R.B. Robertson, D.R. Raul*. .J. Appl. Polymer Sci., 1973, v. 17., № 8., p. 2579.
[5] *J.W. Ten.* J., Appl. Polymer Sci., 1983, v. 28, №28, №2,. p. 605.
[6] *G. Ragosta, R. Greco, E. Martuscelli*. Polymer, 1982, v.23, №3, p. 466.
[7] *A.J. Lovinger, M.L. Williams.* J. Applied Polymer Sci., 1980, v. 25, №8, p. 1703.
[8] *Y.S. Lipatov, Y.V. Lebedev.* Phis.-khim. Mekhanika i liophilnost dispersnikh system. Resp. Mejved. Sb., Kiev, Naukova dumka, 1982, №14, p.3-13.
[9] *V.N. Kuznetzov, V.D.Klinov, L.V.Kandirin, L.V. Vergilin*. Phis-khim. mekanika i liophilnost disperstnikh sistem/ Resp. Mejved. Sb., Kiev, Naukova dumka, 1982, №14, p.14-20.
[10] *M.A. Novikov*. Visokomolekulyarniye soyedineniya, 1978, 20B, №3, p.224-226.
[11] *M.A. Bagirov, V.P. Malin, S.A. Abassov.* Vozdeystviye elektricheskikh razryadov na polimerniye dielektriki, Baku "ELM", 1975, p.167.
[12] *A.A. Aliyev, M.A. Bagirov, N.D. Huseynov, V.P. Malin, A.A. Popov.* Avtorskoye svidetelstvo №1515203, A1, 1989.
[13] *M.A. Bagirov, V.P. Malin, A.A. Aliyev, A.M. Gorbunov, N.D. Huseynova.* Elektroizolyatzionniye smesi polietile-polipropilen s malim soderjaniyem odnogo iz komponentov. Sb. trudov Az PI im. Ch. Ildirima, Baku, 1989, p.3-8.

A.Ə. Əliyev

POLİETİLEN VƏ POLİPROPİLEN POLİMER QARIŞIQLARIN KOMPONENTLƏRİNDƏN BİRİNİN KİÇİK AŞQARLAR SAHƏSİNDƏ ELEKTRİK «QOCALMASI»

Polietilenə polipropilenin müxtəlif konsentrasiyaları daxil edilməklə (1-10 çəki%) elektrik «qocalmasına» qarşı dayanıqlığı öyrənilmişdir. Həmçinin, polietilenə kiçik konsentrasiyalı (1-2% çəki ilə) polipropilenin əlavə edilməsi ilə polietilendə elektrik boşalmalar nəticəsində yaranan eroziya və oksidləşməyə qarşı dayanıqlığın və elektrik möhkəmliyin artması göstərilmişdir.

А.А. Алиев

ЭЛЕКТРИЧЕСКОЕ «СТАРЕНИЕ» ПОЛИМЕРНЫХ СМЕСЕЙ ПОЛИЭТИЛЕНА И ПОЛИПРОПИЛЕНА В ОБЛАСТИ МАЛЫХ ДОБАВОК ОДНОГО ИЗ КОМПОНЕНТОВ

Изучено влияние (1-10 вес %) концентраций ПП в ПЭ на стойкость к электрическому старению. Показано, что введение малых (1-2 вес %) концентраций ПП в ПЭ повышает стойкость ПЭ к эрозии и окислению, вызванному действием электрических разрядов и приводит к возрастанию электрической прочности ПЭ.

Received: 24.02.03

THE RESEARCH OF THE INFLUENCE OF THE ELECTRIC DISCHARGE ON THE GAS MEDIUM SF_6

K.B. GURBANOV
Institute of Physics, Azerbaijan National Academy of Sciences,
Baku. Az - 1143, H. Javid st. 33

In the article the physicochemical processes, proceeding in the system under the influence of the electric discharge (SF_6 is the dielectric discharge), are investigated. Taking into consideration the content changes in the SF_6 gas medium, the results, confirming the strong influence of the gas medium and electric discharge on the materials, are presented.

Gas, named electric gas (elegas) SF_6, having high electric strength, has found wide use in the high-voltage technique as an insulator [1,2,3]. In spite of the fact, that the elegas, consisting of two chemically active atoms and being passive in the form of the SF_6 molecule, creates the medium, conserving its simplicity for a long time, and provides the stable work of the high-voltage equipment.

The mechanism of the elegas molecule formation and the connection nature of the new sulphur atoms and six floor atoms have not been studied. Until last years the elegas molecule formation and the idea on the creation of the six covalent connection between sulphur atoms and six floor atoms were submitted as a common hypothesis. The results of the research, conducted in the last years, have called the hypothesis and the mechanism of the SF_6 molecule formation in questions [4]: the idea of the electron charge transformation from sulphur atoms into floor atoms has been put forward. Thus, in the SF_6 molecule the presence of the covalent and ion connection is taken into consideration. According to the two mechanisms, the SF_6 molecule, having the high symmetry, is formed at the expense of the location of sulphur atoms in the center and floor atoms at the octahedral corners. As in the molecule structure the distance between the sulphur and floor atoms is low, the numerical value $1{,}57 \cdot 10^{-10}$ has been determined.

The high symmetry and compression, observed in the elegas molecule, provide the resistance to the physic-chemical influence.

As the elegas is subject to the electric discharge influence, a number of changes occur in the SF_6 molecule and it may have the negative effect on the elegas medium. From this point of view SF_6, subjected to the electric influence, has the scientific-technical value in the research of the gas medium [3].

The influence of the torch (flare) electric discharge has been used in experiments. The electrode system, forming the torch electric discharge, enters the close volume and the discharge regime is chosen by the application of the variable voltage on the electrodes. In the case of the value of the applied high voltage is U=25 kV, the value of the electric current is 35 mcA.

After the receipt of the vacuum in the system 10^{-6} Pa experiments were conducted by the introduction of the SF_6 gas in the system before the atmospheric pressure. In the close system applying the influence of the electric discharge on the SF_6 gas the changes in the gas medium have been registered by the mass-spectrometer.

The spectrogram, registered by the SF_6 gas in the system, is represented on fig.1.

As it is seen from the fig.1, the spectrogram consists of the SF_6 molecule and the residual gas of the atmosphere air. In spite of the presence of a low number of the water evaporation, oxygen, carbon, nitrogen atoms and molecules, SF_6 shows its neutrality.

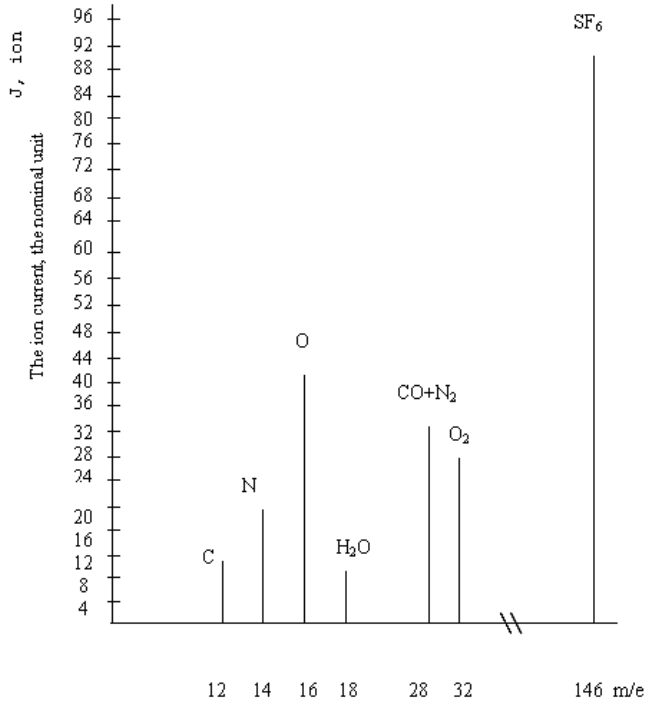

Fig.1. The mass-spectrogram, registered in the gas medium SF_6

In the above-presented regimes the spectrogram, registered by the influence of the torch electric discharge on the SF_6 gas, is represented on fig.2.

As it is seen from fig.2, the SF_6 gas (SF_6, SF_5, SF_4, SF_3, SF_2, SF, S, F) and another ions have been formed under the influence of the electric discharge. It should be noticed, that unlike SF_6 molecule the formed ions, being chemically active, have the strong influence on the gas atoms and molecules and contacting surface. Therefore, as it is seen from the mass-spectrogram, C_2F_5, C_2F_{10}, SOF_3, S_2N_3, SO_2F_2, SOF_4, SOF, SO_2, So and another molecules have been formed like the above-presented gas SF_6.

On the spot of the drawn by the needle lines the traces of the depth 100-150 mc are observed on the surface of the ceramic plates and glass, whose surface is fully covered by the dielectric lacquer and placed on the surface of the flat electrode. The results shows, that the medium, formed under the effect of the electric discharge on the SF_6 gas and having

the destructive power on the indicated materials, has a strong influence.

At the formation of the traces on the glass and another materials surface it has been determined by the application of the discharge power and the influence dependence, that both factors increases the traces depth on the surface and it is possible to cut the glass plate, placed on the flat electrode surface and having the thickness 150 mc, from the desired place during the fixed time and to open holes of the low diameter on its surface.

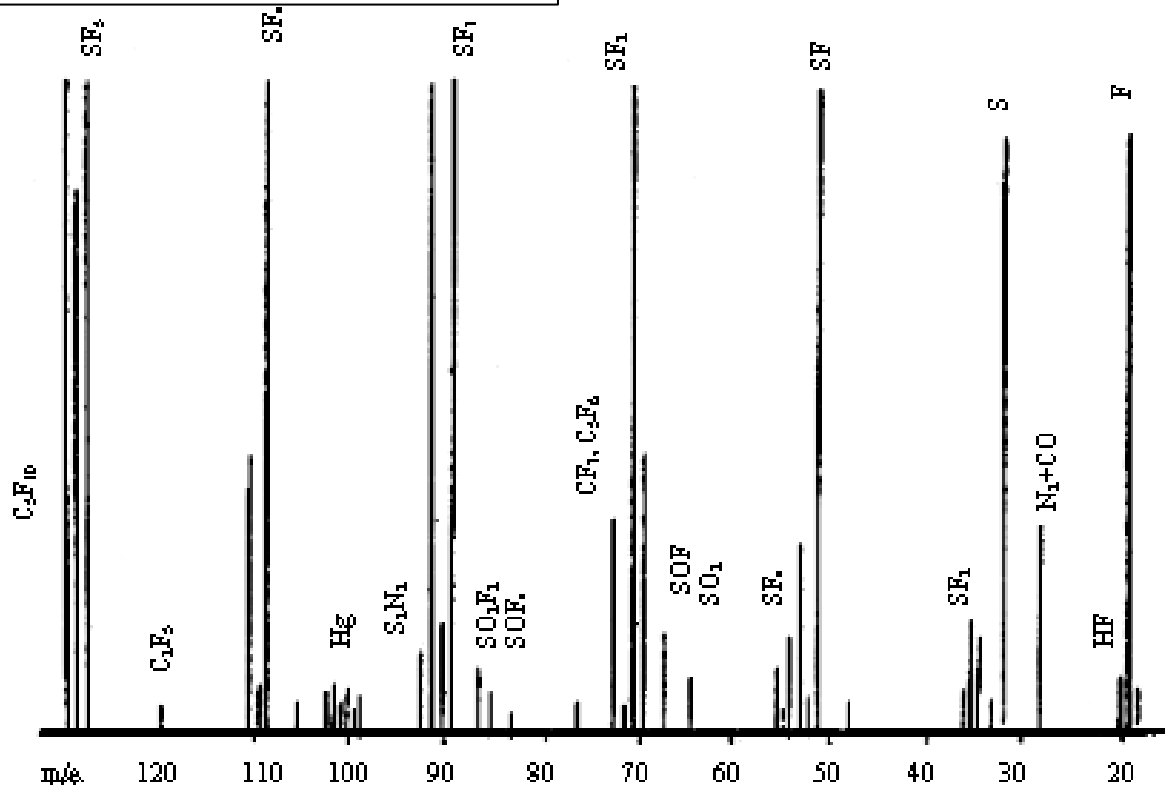

Fig.2. The mass-spectrogram, registered by the influence of the electric discharge on the gas medium SF_6.

With the purpose of the change of the adhesion, polishing and another properties of some dielectric materials, the indicated properties of the SF_6 gas, subjected to the influence of the electric discharge, are used as a non-mechanical, non-chemical and superior method.

It should be noticed at the same time, that the use of the SF_6 gas as an insulator in the high-voltage equipment production may lead to some difficulties and may have the negative influence on the stable work of the equipment. Taking this into consideration the strict demands should be applied to the simplicity of the SF_6 gas content, used in the high-voltage equipment, to the chosen materials for the production of the technical equipment and to the gas medium content. It is known from the research results, that each of the above-indicated factors has the significant value and the research results, conducted in three directions, have been submitted useful from the point of view of the expansion of the SF_6 gas application sphere. Applying the influence of the electric discharge on the elegas, the new achievements, obtained by the research of the chemical reaction in the gas, have been widely used in the production of the technical devices and materials.

The research results, having the scientific-technical use, have also the significant value in the determination of the research directions, the modern technological processes, the technical facilities production and the possibility of the scientific base application.

Thus, it is known from the research, that as a result of the gas reaction realization in the gas medium, placed on the discharge interval and influenced by the electric discharge, a row of the momentary, considerable changes are observed in the initial gas medium. In the system versus the initial gas content the various new gas atoms and their compounds, realized by means of the gas reaction, may be formed under the influence of the electric discharge on the material surface and volume, and from the point of view of various aspects it has the significant value in the content research. It is known, that polymer-dielectrics, applied as isolation materials, in the technique and technological processes are subject to the influence of the electric discharge and strong electric region. During the application the changes, observed in the chemical and electro-physical properties of dielectrics, may disable these materials, applied as insulator. In these processes side by side with the another factors the medium, surrounded by the dielectrics, and changes, occurring in this medium under the effect of the electric discharge, have the decisive influence.

[1] *N.N. Tihodeyev*. The transmission of the electric energy-Leningrad-Energoatomizd, 1984.
[2] *Ch.M. Juvarl, Y.V. Gotin, R.N. Mehdizade*.The corona discharge in the electronegative gas-"ELM", 1988.
[3] *V.M. Smirnov*.The negative ions-M: "Atomizdat", 1978
[4] *I.M. Bortnik*.-Elegas-M: "Nauka", 1982.

K.B. Qurbanov

QAZBOŞALMASININ SF_6 QAZ MÜHİTİNƏ TƏSİRİNİN TƏDQİQİ

Məqalədə elektrik qazboşalmalarının təsiri nəticəsində «SF_6 – qazboşalması təsiri» sistemində müşahidə olunan fiziki proseslər tədqiq edilmişdir. SF_6 qaz mühitində tərkib dəyişmələri qeydə alınaraq, SF_6 qaz mühitinin, qazboşalmalarının təsiri şəraitində, materiallara güclü təsir vasitəsi olmasını təsdiqləyən nəticələr təqdim olunur.

К.Б. Гурбанов

ИССЛЕДОВАНИЕ ВОЗДЕЙСТВИЯ ЭЛЕКТРИЧЕСКОГО РАЗРЯДА НА ГАЗОВУЮ СРЕДУ SF_6

В статье представлены результаты исследований физико-химических процессов, происходящих в системе «SF_6 – воздействие электрического разряда». Выявлены изменения газовой среды SF_6 в условиях воздействия факельного электрического разряда. Установлены факты, подтверждающие химическую активность ионов элегаза, образованных вследствие воздействия электрического разряда.

Received: 26.02.03

THE MODERN EVOLUTIONARY STATUS OF THE BINARY WOLF-RAYET TYPE STARS

J.N. RUSTAMOV

Shamakha Astrophysical Observatory named after N.Tusi, Azerbaijan National Academy of Sciences
F.Agaev str., 9, Baku 370143, Azerbaijan

The various modern evolutionary models for the binary Wolf-Rayet stars are considered. The evolutionary connection between various groups of binary *WR* stars is investigated. Proposed that *WR* stars with the *OVI* lines (*WR-OVI* stars) may be binary systems with compact components and *WN+WC* stars may be evolutionary transition objects between *WN* and *WC* stars.

1. Statement of the problem

After accumulation observational facts for the stars we must constrain physically reliable evolutionary models for these objects. Various models have been proposed for the understanding formation and evolution of Galactic Wolf-Rayet (*WR*) stars of population I, depending on the initial mass, chemical composition and binarity. In this paper we considered the models evolution of binary *WR* stars which are sufficiently verified with the observations and theoretical investigations. The evolutionary connection between various groups of binary *WR* stars is investigated.

In fact we know:

a) binary WR stars: *WR* stars with *O* components, *WR* stars with compact components – neutron stars or black holes, *WR* stars with mixing subtypes – *WN+WC* stars;

b) single *WR* stars.

Therefore we must explain origin and evolution of binary and single *WR* stars and evolutionary connection between different group of *WR* stars.

2. Formation and evolution of binary *WR* stars

In this section the evolutionary properties of close binary system and formation binary *WR* stars in this system are considered. It is known that a large part of the stars of the galactic disk are binaries. It is also known that progenitors of WR stars are massive *O* stars locating in the galactic disk. According to [1] 36% of the *O* stars are binaries. During the evolution the components of the close binary system can fill their Roche volumes, and lose mass in order to keep the star within the allowed surface. *WR* phenomena are observed namely when sufficiently mass loss takes place. The mass overflow via Roche surface and mass loss by stellar wind makes binary systems more convenient for the formation *WR* properties. Formation and evolution of *WR* stars in binary systems have been investigated in [2, 3, 4]. According to this investigations evolution massive close binary systems take place following way:

$$O_1 + O_2 \rightarrow WR_1 + O_2 \rightarrow c + O_2 \rightarrow c + WR_2 \qquad (1)$$

The evolution of the stars in binary systems is different from the evolution of a single star with the same mass and chemical composition. It is known that progenitors of the binary *WR* systems are massive close binary O_1+O_2 systems with a circular orbit. The O_1+O_2 system is called massive if at least one of its components will explode as *SN* and becomes to neutron star or a black hole. The O_1+O_2 system is called close binary if the period of this system is small enough that during evolution one or both components will fill the Roche lobe (Roche surface) – the critical equipotential surface of the star**.** The equipotential surfaces of components are crosses at first Lagrangian point *L1*, which is the point of gravitational balance between two components. Effective gravity is zero in point *L1* and matter can flow from one component towards the other. Process in which the star fills its Roche lobe and starts losing mass trough *L1* is called Roche lobe overflow - *RLOF*. The component losing mass due to *RLOF* is a mass loser, and the component that accepts matter is a mass accretor.

According to (1) in massive close binary system O_1+O_2 initially higher mass component (O_1) evolves more rapidly and system becomes to WR_1+O_2 and further WR_1 star in this system explodes as supernova (*SN*) and WR_1+O_2 system converts into $c+O_2$ where c is compact star (*c*- neutron star or black hole). The probability that the binary system remains bound is high, since the less massive star explodes [5]. From the evolutionary model (1) we may conclude that if the *SN* explosion does not disrupt the system the *WR* phase can appear twice, the first as *WR+O* system, the second as *WR+c* system. Another infer from (1) is that the number of *WR+c* systems might be expected to be similar to that of *WR+O* systems. Establishment the binary nature of *WR+c* stars from the spectral and photometric observations is very difficult because small amplitude of light and radial velocity (*RV*) variations. For the verifying theories on the formation of *WR* stars is important to determine what fraction of the *WR* stars are truly single. With the aid of model (1) we also can explain formation of $c+O_2$ system (*O* stars with compact components). *WR+c* and *c+O* type binary systems are called runaway stars because their location at high distances from the galactic disc.

As long as the radii of components of binary system O_1+O_2 are smaller than their Roche radius the system is detached system – only weak interactions can occur, i.e. interactions by tides, radiation, stellar winds, magnetic forces. For a given binary system, the Roche radius determined by the masses of the components and orbital period can be calculated. When one of the components (beginning more massive component) of the binary system during its evolution expands so that it fills its Roche surface (the stellar radius exceeds the Roche radius), mass transfer through the vicinity of the inner Lagrangian point (*L1*) starts. The binary system becomes too semi-detached. In semi detached systems the primary (more massive component) can lose of its initial mass sufficiently that is important for the formation of *WR* stars.

If the mass ratio of the components is near to 1 the two components can evolve simultaneously, while one component fills its Roche surface and loses matter, the another component can also expand and fill its Roche surface. In this case a contact binary is formed. The system can rotate as a solid body. The common surface can reach the outer Lagrangian point (L2), and mass loss through the vicinity of this point can occur. From this discussion it is obvious that the binary systems with the mass ratios less than 1 are convenient for the formation of the binary *WR* stars**.** Namely these systems become semi- detached and losses sufficiently mass that is necessary for the formation of *WR* stars.

Evolution of the stars in a massive close binary systems is strongly depends from the mass loss via *RLOF*. More massive component of the binary system is called primary. When the primary fills its Roche lobe, mass transfer starts. The gas on the surface of the primary will flow through the first Lagrangian point *L1* to the component. Depending on an initial period and masses in binary system, primary star can fill its Roche lobe:

1. core hydrogen burning phase - case *A*,
2. shell hydrogen burning phase - case *B* (the most frequent case),
3. shell helium burning phase - case *C*

When the Roche surface overflow phase ends, the remnant of the primary becomes to helium star. It is assumed that the accreting secondary evolves like a normal main sequence star. As a consequence of the rapid mass transfer the secondary can also expand and fill its Roche lobe. In this case contact system is formed, and the two stars have a common envelope. Namely in the case mass loss starts during core hydrogen burning the contact system forms. In the case mass transfer starts during shell hydrogen burning, it is easier to avoid contact phase. Therefore the binary systems where stellar radius increases during shell hydrogen burning or core helium burning are more convenient for the formation of binary *WR* stars.

Most model computations for the evolution of close binary stars were made under conservative assumptions, i.e. it is proposed that the total mass and the orbital angular momentum of the system are conserved during the mass transfer phase [6,7]. The conservative evolutionary computations lead only to a rough correspondence between observed and calculated parameters because factual loosing total mass and angular momentum by system. It is not very difficult to take into account mass and angular momentum losses from the system. Only a fraction β of the mass lost by the primary is accreted by the secondary, and also that a fraction γ of the total angular momentum is taken away by the matter leaving the system. This type of investigations is important for the obtaining real results which may be verifying by the observations.

_WR_ stars with _O_ components: _WR+O_ stars

The presence the absorption lines in the spectrum of some *WR* stars, the light and *RV* variations led astronomers to suggest *O* components for these stars. In 1939 for the first time was discovered the *WR* spectroscopic binary *V*444 *Cyg* [8]. For the being time we know many binary *WR+O* stars. According to modern evolutionary theories of close binary systems progenitors these systems are massive O_1+O_2 systems (see evolutionary model (1)). As noted above more massive component in binary system O_1+O_2 due to mass loss via *RLOF* and by stellar wind becomes to *WR* star.

In the seventies it was observationally confirmed that the absorption lines could originate in the *WR* star as well [9]. According to authors [10, 11] many of the *WR* stars with absorption lines are single. Therefore the *WR* stars can be called binaries only if light and *RV* variations was discovered. Since the discovery of *WR* stars, the problem of duplicity among *WR* stars has been a major one. Several years ago all *WR* stars were believed to be components of close binary systems. Therefore one of the important question concerning *WR* stars was whether all of them are members of close binary systems or single *WR* stars are also exist. Discovery the binary nature of *WR* stars is actual due to two reasons: first, for the understanding the role of the component in the formation of a *WR* star; second, the difficulty to determine the binary nature of the *WR* stars due to the widths of the spectral lines and low amplitude of the light and *RV* variations. After the discovery of *WR* binaries with compact components, we may estimate the real number binary *WR* stars. According to [12] 25% of *WR* stars are *WR+O* binaries. According to evolutionary model (1) the number *WR+O* system must be same with the number of *WR+c* ones. Therefore after to take into account the number of *WR* stars with compact components the percentage of binary *WR*'s increases up to 50%.

The study of *WR+O* binaries is important for the determination masses of WR stars. By measuring the velocities of both components in a *WR+O* system, we can determine the minimum masses and mass ratio of the two stars; if we can get some information about orbital inclination, we may calculate the masses of the *WR* stars. The determination of masses of *WR* stars in binary systems is complicated by two factors: a) uncertainties in the value of orbital inclination b) the errors in the determination velocity semi-amplitude. However, the mass ratio of the component of binary system may be determined correctly.

Observational properties some *WR+O* systems are investigated in [13]. The *WR* binaries in which the absorption spectrum of the *O* component is present and moves in the opposite sense than the *WR* emission lines denotes as *SB*2. In a some cases, the *WR* star is sufficiently brighter than its component that the spectra of *O* component is not present in the visible region, although the mass function of these systems implies with the presence of the massive component. Such *WR* binary systems denotes as *SB*1. Most of the *WR* binaries with massive components are *SB*2.

The masses of *WR* stars span a very large range: the mass of WR component of *CX Cep* is 11 M_O and the mass of *WR* component of *HDE* 311843 is 40 M_O. According to [14] the minimum masses of *WR* stars were strongly correlated with the mass ratios; stars with smaller masses were found in systems with smaller M_{WR}/M_O values. It is interesting that there are not correlation between *WN* and *WC* types and masses, though the mass ratios of *WR* binaries are correlated with types [15]. It is also interesting that the *WC* stars are not, in general, less massive than the *WN* stars. The reason may be that either not all *WN* stars become *WC* stars, or low mass *WC* stars are shorter lived than massive ones [16].

Another interesting problem is to determine the minimum mass that an *O* star must lose in order to be identified as a *WR* star. By extrapolation the current masses of the *WR* type components we may approximately determine the beginning mass of the *O* star. For the *WR+O* systems mass ratios approximately less than 0.6. Since the initial mass ratio of

O+O systems are nearly unity. From this we may infer that the *WR* components in binaries have lost at least 40% of their initial mass.

According to scenario Conti [17], a single *O* star will turn into a single *WR* star by stellar wind mass loss, while a binary *O+O* system will turn into a binary *WR+O* system by wind mass loss and mass loss via Roche surface. In this case are interesting: a) relative importance of wind mass loss and mass loss via Roshe surface b) what fraction of mass is accreted by the component?

It is interesting to compare the orbital eccentricities of the *O+O* and *WR+O* systems. All the *WR* stars with massive components have circular orbits except γ Vel (e=0.40), *HD*190918 (e= 0.43) and *HD* 92740 ($e \approx 0.6$). The longest period *WR+O* system with a circular orbit is *CV* Ser ($P \approx 30$ days). Most of the *O* stars with periods below 30 days have circular orbits. All the long period systems have non-circular orbits. In short period systems tidal interactions will circularize an orbit. If mass transfer has played a dominant role we might expect for the longer period systems to have circular orbits as well, since this is a consequence of mass transfer [18].

In some cases *WR* stars are member of eclipsing binary systems: *V*444 *Cyg*, *CX Cep*, *CQ Cep*, and *CV Ser*. Investigation of light curves of this eclipsing *WR+O* binary systems give us important information about physical characteristics of the *WR* stars that is necessary for understanding of their nature and evolution.

***WR+WR* binaries:**

Besides the *WR+O* systems there are some binary systems in which both members are *WR* stars (*WN+WC* stars). These stars have spectroscopic properties intermediate between *WN* and *WC* stars. It is known that the spectra of the most *WN* stars do not contain carbon, only lines of *CIV*$\lambda\lambda$5801 in the optical region and *CIV*$\lambda\lambda$1550 in the *UV* is observed. However strongest *CIII* lines (*CIII*λ4650 and *CIII*λ5696) are not generally observed in *WN* stars. If these lines are seen, the star is given subtype *WN+WC*, as if two stars were present. Although this does not mean that two separate stars are present. For the establishment the binary nature such systems *RV* and light variation investigations were need. Our photometric observations revealed light variation one of the *WN+WC* stars *AS*422=*MR*111 with the period 20^d [19].

The theory of the evolution of close binary stars predicts that *WN+WC* binaries might exist. The existence of such transition nitrogen-carbon stars indicate also an evolutionary connection between *WN* and *WC* stars. When *CNO* cycle approaches to the end and helium burning will begin and the carbon should manifest itself in the composition of the star. To produce *WR+WR* system the O star in a *WR+O* system must evolve into a *WR* during the lifetime of the other *WR* star. It is known that the lifetime of a *WR* stars is typically 10% of its *O* star life. Therefore the number of *WN+WC* systems must be small.

Investigation *WN+WC* system is very important for the understanding nature of *WR* phenomenon.

***WR* stars with compact components: *WR+c* stars**

The discovery of *OB* binary *X*– ray sources was important for understanding of massive binary star evolution with mass exchange and mass loss. One of the important conclusion from this was the prediction of the second *WR* binary phase (*WR+c*) in the evolution of massive binaries in which the component of the *WR* star is a neutron star of mass 1-2 M_O, or in some cases even more massive black hole [20].

The first observational fact that *WR+c* stars do exist to become clear from a study of the distribution (*z* distribution) perpendicular to the galactic plane of galactic *WR* stars for which distances was known. It was supposed that the *SN* explosion in a binary system has 'kicked' these stars out of the galactic plane and that they could be binary systems with the neutron-star component. Therefore *WR+c* stars must situate far from the galactic plane. It is found that single line *WR* stars (the *WR* stars presumed as single) tend to lie further from the galactic plane in the mean than double-line (presumed *WR+OB* binary) stars, which behave like normal population I of the galaxy. For a limited number within 6 kpc and v<12mag for which the duplicity was reliable determined, found $|z|$ =133 pc for single-line and 79 pc for double-line *WR* stars (*z* is distant from the galactic plane) [21]. From this concluded that, among the single-line stars, there exist a significant number *WR+c* stars. Among the *O* stars also there are runaway stars i.e. stars situated far from the galactic plane. This fact interpreted analogously runaway *WR* stars.

The next reasonable step would be photometric and spectral observations (for the revealing possible radial velocity, line profile, light variations) of individual *WR* stars for the establishment their duplicity. The spectral and photometric detection the duplicity of *WR+c* stars is very difficult because the radial velocity and light variations are very low. Spectral detection of duplicity more comfortable for the narrow line *WNL* (*WN*6-8) stars. A necessary minimum requirement is a reliable measure of the *RV* semi-amplitude of the *WR* component, which leads to an estimate of the mass of the compact component, after assuming a mass for the WR stars and the orbital inclination. If the masses of the secondary is in the range ~ 1-2 M_O, it could be a neutron star; if more than ~3 M_O a black hole component. Additional observational prove would come from the investigation phase dependent line profile variations.

he spectral and photometric searching for the duplicity among the *WR* stars with high probability of finding WR + c systems; e.g. single-line *WR* stars with high $|z|$ in the galaxy, surrounded by a ring nebula (ejected during the during rapid mass transfer from the pre-*WR* star to the component) lead to detection of *WR+c* stars. Presumably, many more *WR+c* stars remain to be detected.

The low mass-function for the *WR+c* stars indicate for the compact components mass ~0.5-2M_O in most cases, compatible with the presence of neutron star (*NS*) component. We thus assume 1.6 M_O, an appropriate mean value for *NS* in *X* ray binaries [22], in order to derive the *WR* star masses.

HD 197406 is more probably *WR+Black* Hole. The distance from the galactic plane for the *HD* 197406 is 799 pc because this star is called the extreme runaway. Obtained that the mass of compact component in *HD* 197406 is ~14 M_O . The light curve of this star shows a shallow dip of ~ 0.04mag.

Beside orbital motion, there are other physical processes which could produce the observed low-amplitude, periodic *RV* and light variations. One of them is pulsation of the star. It is known that massive He burning stars as identified with the late *WN*(*WN*6-8) and *WC* stars have radial pulsation periods in the range of 30 min [23].This period much shorter

than any periods observed in *WR+c* systems. Another reason of observed periodic variations may be also rotation. Rotation of the star associated with the surface inhomogeneities (may be associated with the magnetic field) might give periodic variations. However following observational facts make more probably that observed periodic variation is due to presence compact component of the *WR* star:

1. location at high z distance from the galactic plane
2. the presence ring nebulae around star

WR stars with the enhanced lines of *OVI*: *WR–OVI* stars

Another interesting group of stars is Pop. I *WR* stars whose optical spectra display the emission doublet *OVIλλ*3811, 3834. These stars are called *WR – OVI* stars [24]. According to our investigations at least some of these stars may be close binary systems with the probable compact components. We revealed following observational facts in favor this assumption:

a) similar *z* distribution of *WR* stars with *OVIλλ*3811, 3834 lines and *WR* stars with the probable compact components
b) rapid spectral variability of some spectral lines in the spectra of the *WR-OVI* stars; such a rapid spectral variability is characteristic for the *WR + c* stars [25]
c) considerable scattering in the dependence 'emission line widths – ionization potential' and uncertainty of spectral subtypes as estimated from the different criteria. These effects may be due to compact objects which are components of the *WR–OVI* stars [26].
d) the observation of the ring nebulae around some *WR–OVI* stars. Such ring nebulae are observed also around *WR+c* stars [27].
e) the discovery of the periodic variability of the light and radial velocity of the *WR–OVI* star *HD* 16523 [24]

3. The probable evolutionary connections between different group of binary *WR* stars

It is known that *WR* stars have been divided into three spectral types: the *WN*, *WC* and *WO*. It is suggested that the separation of *WR* stars to types is connected with the different chemical composition and related to stellar evolution [24]. We know *WN+O*, *WC+O*, *WO+O* systems. Progenitors of these systems are massive close binary O_1+O_2 systems. Therefore the evolutionary model (1) may be written in following form:

$$\begin{array}{ccccccccc} & & WN+O_2 & & & & & & c+WN \\ & & \downarrow & & & & & & \\ O_1+O_2 & \rightarrow & Of/WN+O_2 & \rightarrow & WC+O_2 & \rightarrow & c+O_2 & \rightarrow & c+Of/WN \rightarrow c+WC \\ & & \downarrow & & & & & & c+WO \\ & & WO+O_2 & & & & & & \end{array} \qquad (2)$$

As noted above the evolution of the stars in a massive close binary systems is strongly depends from the mass loss via *RLOF*. For a given binary system, the Roche radius depends from the masses of the component and orbital period**.** Therefore *RLOF* also depends from the mass ratio of the component. We suggest that formation *WN+O*, *WC+O* or *WO+O* systems from O_1+O_2 system depend from mass ratio in binary O_1+O_2. As noted above the mass ratios of *WR* binaries are correlated with types *WN* and *WC*. This observational fact is favor to our suggestion. According to [24] there is such evolutionary connection between *WN*, *WC* and *WO* types:

$$WN \rightarrow WC \rightarrow WO \qquad (3)$$

There is analogous evolutionary connection between *WN+O*, *WC+O* and *WO+O* binaries. In evolutionary model (2) we show arrows between these systems indicating probable evolutionary connection.

We suggest that transition from O_1+O_2 to $WR+O_2$ system also depends from that at what stage takes phase *RLOF* in binary system O_1+O_2. If *RLOF* takes place at core hydrogen burning phase (case *A*) formation of *WN+O* system more probable. If *RLOF* takes place at shell helium burning phase then (case *C*) the formation of *WC+O* and *WO+O* systems more probable.

It is known that there are evolutionary transition objects (*Of/WN*) between *O* and *WN* stars. Therefore must be evolutionary transition binary $Of/WN+O_2$ systems (quasi WR binaries) between O_1+O_2 and $WR+O_2$ type binaries. We also proposed that there are evolutionary transitional *c+Of/WN* objects between *c+O* and *c+WR* stars.

The evolutionary model (2) prorosed by us for the first time and is more detailed than model (1).

4. Main conclusions:

1. Progenitors of binary *WR* systems are massive close binary O_1+O_2 stars.
2. The masses of *WR* stars span a larger range than do their *O* type components. The average mass of a *WR* star is about $20M_O$.
3. The masses of *WC* stars are not less than those of *WN* stars.
4. The mass ratios of *WR+O* binaries are correlated with the types *WN* and *WC*.
5. *WR* stars in binaries have lost at least 40% their mass in becoming *WR* stars.
6. The short period *WR+O* systems have circular orbits, identical to what is know for the O_1+O_2 systems.
7. Some *WR-OVI* stars may have compact components.
8. *WN+WC* stars may be in the intermediate position of the evolution from *WN* to *WC* stars.

[1] *P.S. Conti, P. Massey, D. Ebbets, V.S. Niemela.* Astrophys. J. 1980, .№ 238, p.184.

[2] *B. Paczynsky*. In: Wolf-Rayet and High Temperature stars. ed. M.K.V. Bappu and J. Sahade 1973. P. 143.

[3] C.d*e Loore.* in: effects of Mass Loss in Stellar Evolution, IAU Colloq., 59, Ed. Chiosi C.and Stalio R. 1981, p.405.
[4] *D.Vanbeveren, J.P.de Greve, E.L. van Dessel, C. de Loore.* Astron. Astrophys., 1979, №.73, p.19.
[5] *C. de Loore, J.P. de Greve, J.P. de Cuyper.* Astrophys. Space Sci., 1975, №. 36, p. 219.
[6] *B. Paczynski*. Ann. Review Astron. Astrophys., 1971. № 9. p.183.
[7] *H.C. Thomas*. Ann. Review Astron. Astrophys. 1977. № 15, p.127.
[8] *O.C. Wilson.* Publ. Astron. Soc. Pacific. 1939, №51, p.55.
[9] *P.S. Conti*. Mem. Soc.Roy. Sci. Liege. 6^{e} Ser., 1976, № 9, p. 193.
[10] *P. Massey, P.S.Conti*. Astrophys. J. 1980, №242, p.638.
[11] *D. Vanbeveren, P.S. Conti*. Astron. Astrophys., 1980, №88, p. 230.
[12] *P. Massey.* Astrophys., J. 1980, № 236, p. 526.
[13] *P.Massey, P.S. Conti* 1977, №218, p. 431.
[14] *L.F. Smith.* In: Wolf-Rayet stars. ed. K.B.Gebbie and R.N.Thomas (NBS Spesial Publ. 307). p. 23.
[15] *A.F.J. Moffat.* in: IAU Coll., 1981, №.59.
[16] *P. Massey, V.S.Niemela.* Astrophys. J. 1981, 245, p.195.
[17] *P.S.Conti.* Mem. Soc. Roy. Sci. Liege 6^{e} Ser.1976,. №9, p. 193.
[18] *B. Paczynski.* Ann. Rev. Astr. Astrophys. 1971. №9, p. 183.
[19] *J.N. Rustamov, A.M. Cherepashchuk.* Astron. Zh. 1989, № 66, p.67.
[20] *E.P.J. van den Heuvel.* in: IAU Symp.,№73, 1976, p. 35.
[21] *B.Hidayat, K.Supelli, K.A. van der Hucht.* In: IAU Symp. №99 WR stars Observations, Physics, Evolution 1982, p.27.
[22] *D. Crampton, J.B. Hutchings, J.B.Cowley.* Astrophys.J. 1978, №225, L 163.
[23] *R.Stothers, N.R.Simon.* Astrophys.J. 1970, №160, p.1019.
[24] *A.M.Cherepashchuk, J.N.Rustamov.* Astrophysics and Space Sci. 1990. №167, p.281.
[25] J.*N.Rustamov*. Circular ShAO. 1998, №109, p. 12.
[26] *J.N.Rustamov*, Fizika, 2002, №2, p.56.
[27] *R.R.Treffers, Y.H.Chu*. Astrophys.J. 1982, №249, p.586.

C.N. Rüstəmov

QOŞA VOLF-RAYE TİPLİ ULDUZLARIN MÜASİR TƏKAMÜL STATUSU

Qoşa Volf-Raye ulduzların müasir təkamül modellərinə baxılmışdır. Müxtəlif qrupa daxil olan qoşa WR ulduzları arasında təkamül əlaqələri tədqiq olunmuşdur. OVI xətləri olan *WR* ulduzların (*WR - OVI* ulduzlarının) kompakt komponentləri olan qoşa sistemlər ola bilməsi fikri irəli sürülmüşdür. Ola bilsin ki, *WN + WC* ulduzları təkamülcə *WN* və *WC* ulduzları arasında keçid obyektləridir.

Д.Н. Рустамов

СОВРЕМЕННЫЙ ЭВОЛЮЦИОННЫЙ СТАТУС ДВОЙНЫХ ЗВЕЗД ТИПА ВОЛЬФА-РАЙЕ

Рассмотрены различные современные эволюционные модели для звезд Вольфа-Райе. Были исследованы эволюционные связи между различными группами двойных звезд *WR*. Предположено, что звезды Вольфа-Райе с линиями *OVI* (звезды *WR - OVI)* могут являться двойными системами с компактными компонентами. Звезды *WN + WC* могут являться эволюционно переходными объектами между *WN* и *WC* звездами.

Received: 04.03.03

THE POTENTIAL RELIEF CLOSE TO THE ISOLATED DISLOCATION IN Si

S.G. RZAYEV, Z.M. ZAKHRABEKOVA
The Institute of Physics Azerbaijan National Academy of Sciences
Baku. Az - 1143, H. Javid ave. 33

By the investigation of the Frenkel-Pull effect in the silicon, containing the one electrically active edge dislocation, it has been established that it creates the deep centers of Coulomb type. The relief of the potential energy of an isolated charge dislocation interaction with the charge carriers has been determined.

INTRODUCTION

The actual task of semiconductors physics is to reveal the mechanism and peculiarities of the defects influence on the electron process in semiconductor devices. This issue acquires the special actuality in microelectronics, as the small sizes of the active elements of the integrated circuits lead to the fact, that the defects occupy the considerable part of their working volume, in consequence of what the degree of the defects influence on their parameters increases.

Among the known defects edge dislocations are worthy of the special observation, due to their considerable influence on the electron processes in semiconductors.

As the analysis of numerous papers [1-6], devoted to the research of the dislocation electron activity shows that it was carried out in samples, containing the uncontrollable number of the dislocations. The complexity of their interaction picture both between each other and with the charge carriers and with the point defects makes the analysis of the obtained results more difficult. In consequence of these measured values have the high statistical spread, and the results are speculative and sometimes contradictory.

Therefore the study of the electric properties of an isolated dislocation has a considerable scientific and practical interest. The valuable information on the electric properties of an isolated dislocation may be obtained by research of the dependence of the height change of the potential barrier's bulk charge (BC) about the dislocation and dislocation conductivity on the electric field. These properties of the dislocation versus the direction and the electric field strength become apparent in a variable extent. In [7] we investigated in details conductivity along dislocation. However the unambiguous information on the relief and properties of the potential barriers, created by an isolated dislocation, which plays the determining role in the generation-recombination properties of the dislocation, is absent in the literature. Such factors as the dislocation interaction with the charge carriers and the impurity atoms, and also the electric and elastic disturbance of the adjacent regions of the lattice have the influence on the potential relief of BC. The simultaneous account of these factors and the construction of the theoretical model of the potential relief about the dislocation are very complicated. Therefore the experimental determination of such relief may give the valuable information on the real behavior of the BC potential barrier and the electric activity of the dislocation.

The present paper is devoted to the research of the height change of the BC potential barrier close to an isolated edge charge dislocation under the influence of the perpendicular external electric field with the purpose of the determination of the potential energy relief. The relief of the potential energy of the carrier's interaction (the shape of the potential barrier) with the dislocation has been determined from the research of the Frenkel-Pull effect (FPE) [8].

METHODS AND THE EXPERIMENT

The method of the thermostimulated currents (TSC), whose peculiarities are applicable to the investigated samples, represented in [7], is direct and experimentally convenient for the determination of the dependence of the potential barrier change on the electric field.

The research was carried out on the silicon epitaxy-planar n^+-p junctions of the integrated circuits. The basic region of the junction consists of the boron alloyed ($\approx 5\cdot 10^{16} cm^{-3}$) part of the epitaxy film of 111-surface with ~2.1μm thickness. The collector region consists of the n^+- buried layer, formed in p-substrate by the As diffusion ($\approx 10^{20} cm^{-3}$) and adjacent to it the vertical layer, created in the epitaxy film of the phosphorus diffusion ($\approx 5\cdot 10^{18} cm^{-3}$), which comes out on the film surface. The small area of the structure ($\sim 10^{-6} cm^2$) allows selecting samples, containing in the p-basic region an electrically active dislocation.

The complex of the independent methods [9-13]: the analysis of the J-V and C-V characteristics, the analysis of the thermostimulated currents (TSC), DLTS methods of the transmission and scanning electron microscopy (SEM), regime of the secondary electrons and the induced current, and methods of chemically selective and by-layered etching have been applied to reveal and study the electrically active dislocation (EAD). The type of the deep centers and their dislocation place in the p-n junction are determined by these methods, the region of the cylindrical bulk charge and the EAD core are revealed. The selected method makes possible to reveal and carry out the research of the electric activity of an individual dislocation at the absence of the electrically active defects. The statistic spread of the measured values is excluded, and the experiment is carried out in the controllable conditions. The microphotography of the investigated p-n structures, obtained by SEM in the combined regime of the secondary electrons and the induced current, is represented on fig.1a. Only one generation-recombination region, localized between basic and collector contacts in the form of the hollow light cylinder, (the region on the photo has elliptic shape because of the fact, that the electron beam of SEM falls on the sample surface under the oblique angle) has been revealed on the microphotography, i.e. only one electrically active defects has been revealed. The white spots over the basic region represent the contamination in the isolated SiO_2-layer, which disappears after the etching of this layer. The dark core of the defects (the cavity of cylinder) testifies the fact, that it is charged positive and intensive absorbs

electrons, in consequence of what it looks dark and the light region, surrounding the core, is charged negative, in consequence of what the intensity of the reflected from this region electrons is high, therefore it looks light on the microphotography.

a)

b)

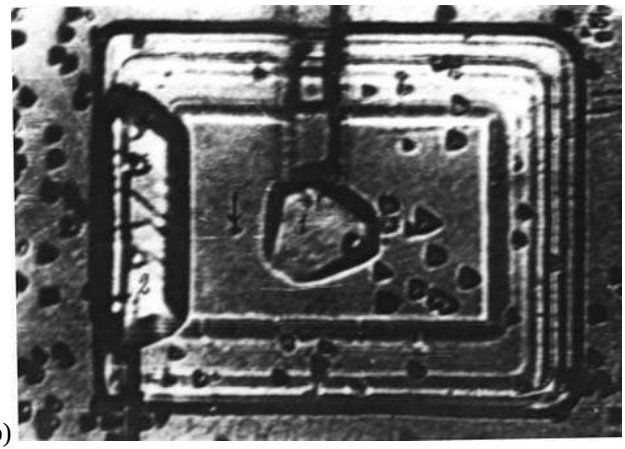

Fig.1. The microphotography of the p-n junction with the one electrically active defect (it is shown by the pointer):
a) in the combined regime of the secondary electrons and induced current of SEM. *E*=20 kV, ˣ1400. 1 and 2 are the metallic contacts, respectively to the base and collector. The dark region corresponds to SCL.
b) after the selective chemical etching-1 and 2 are windows under the basic and collector contacts.

The method of the chemical selective etching is applied for the determination of the defect nature. The microphotography of the investigated *p-n* structure after the etching, on which the dislocation etching pits are seen, is represented on fig.1b. The symmetry shape of the dislocation etching pits testifies the fact that the asymmetry etching pits [14, 15] correspond to 30 and 60˚ dislocations. As it is seen from the microphotography comparison (a and b), the secondary (without the impurity atmosphere) dislocation is revealed between the basic and collector contacts under the electrically active defect, the low value of the etching pit in comparison with another etching pit testifies this fact

Such difference in the size of the etching pits is explained by the dislocation genesis. Large etching pits correspond to the grown dislocations, which are germinated from the substrate in the film and are acquire in the process of the film growing by the impurity atmosphere. It is quickly dissolved by the selective etching [16], what causes the extra sizes of the etching pits. The secondary dislocations, occurring at the final stage of the technological process of the device production, have not time for acquisition the impurity atmosphere, therefore the etching pits, corresponding to them have the small sizes.

Thus, it is seen from the microphotography comparison (a and b- fig.1), that the electric activity show only the secondary dislocation (without the impurity atmosphere), its nuclear is charged positive. The latter testifies the donor type of the deep centers, created by the dislocation nuclear.

RESULTS AND THEIR DISCUSSION

Curves of the thermostimulated currents (TSC), obtained at the p-n junction only from the one electrically active edge dislocation in the basic region, at the various values of the reverse bias are represented on fig.2. As it was shown above, the absence in the basic region of the investigated p-n junction of another electrically active defects has been established by means of SEM.

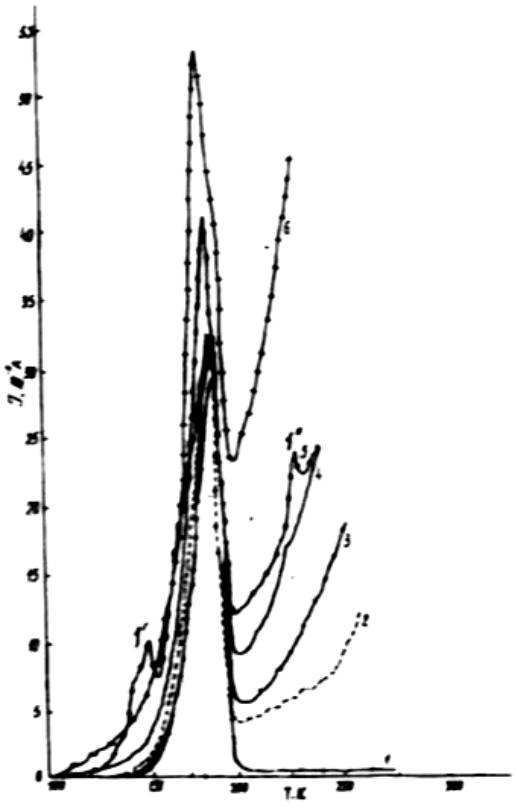

Fig.2. The thermostimulated currents at the various values of the reverse bias U_R on the *p-n* junction: U_R=(0, 2, 3, 4, 5, 6) B is for curves 1-6. The corresponding values of the electric field close to the dislocation are (0,6; 1; 1,24; 1,35; 1,5; 1,6)·10^5V·/cm. The velocity of the sample heating is b=0,35 K·s^{-1}.

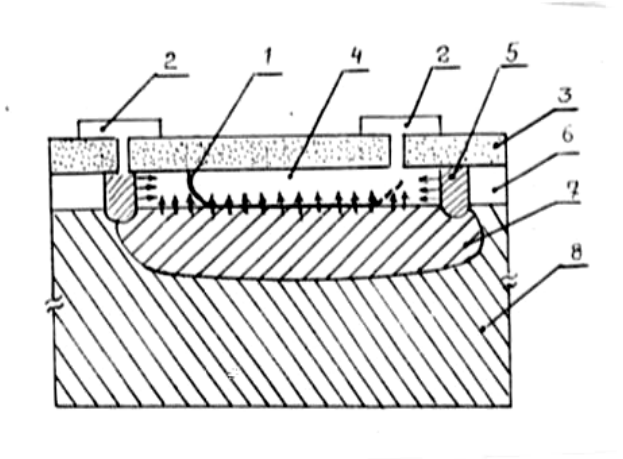

Fig.2a. The *p-n* junction cross-section with the one electrically active dislocation: 1 is the dislocation, 2 is the Al, 3 is SiO_2, 4 is the base, 5 is the collector, 6 is p-Si (the epitaxy layer), 7 is n^+-buried layer, 8 is p-Si- the substrate, 9 is the space charge layer and the field direction is shown by pointers.

These dislocations generate from the surface sources (the scratches, cut, microcracks) in the form of the half-loop and all of them (as a result of the low thickness of the film ~2 microns) approach the space charge layer (SCL) at the result of the slipping from the source under the influence of the voltage, occurring in films because of their nonuniform cooling. As it is shown in [17], in the heavy doped n^+-region the activation energy of the dislocation motion is more on 0,4eV, than in p-region. Therefore the n^+-region will prevent the dislocation motion, as a result the dislocation half-loop, approaching the n^+-heavy layer, i.e. the metallurgic interface of the p-n junction, will "spread" on the plane of the p-n junction, at the result the main part of the secondary dislocation will be localized in the space charge layer. It is confirmed by the by-layered etching of the film. As the field of the space charge layer is directed perpendicular to the plane of the p-n junction, and then it will be also directed perpendicular to the dislocation, placed in this plane. The section scheme of the investigated p-n junction and the place of the electrically active (secondary) dislocation localization (1) in the space charge layer are represented on fig.2a. It should be noticed, that in consequence of the fact, that the donor impurity concentration in the collector is two orders more, than that of the acceptor impurity in the base, SCL of the p-n junction will be wholly concentrated in p-base [11, 12]. The external reverse bias, applied to the p-n junction, increases the field of the space charge layer and increases its width. Because of the free carriers absence in SCL, the dislocation will cause all kinetic phenomena. As rising to the surface the dislocation hall-loop part, which takes its negligible part, is localized between basic and collector contacts (2), then the external field, applied to these contacts, will also be directed perpendicular to the dislocation part. Another rising to the surface dislocation half-loop part penetrates possibly the region of the SCL vertical part of the collector-base junction and therefore it is not presented on fig.1. Therefore, the external field, applied to the basic region, will be directed perpendicular to the dislocation. As it was established before [9, 11, 12], the peaks on the curves of TSC are caused by the thermal emission of the carriers, captured at levels, created by the dislocation. As it is seen from fig.2, by the field increase the TSC peak shifts at the temperature scale to the low value part and its height increases. As the peak on the curve of the thermostimulated current is directly caused by the emission of carriers, captured at the dislocation deep centers, then its shift at the temperature scale with the change of the external electric field at the given velocity of the sample heating indicates to the change of the height of the potential barrier, which carriers get over at the emission, i.e. .the Frenkel-Pull effect is observed (FPE). The value of the potential barrier decay $\Delta\varphi$ has been determined as the difference of the activation energy values, calculated by the peaks position at the temperature scale at various values of the electric field (fig.3)

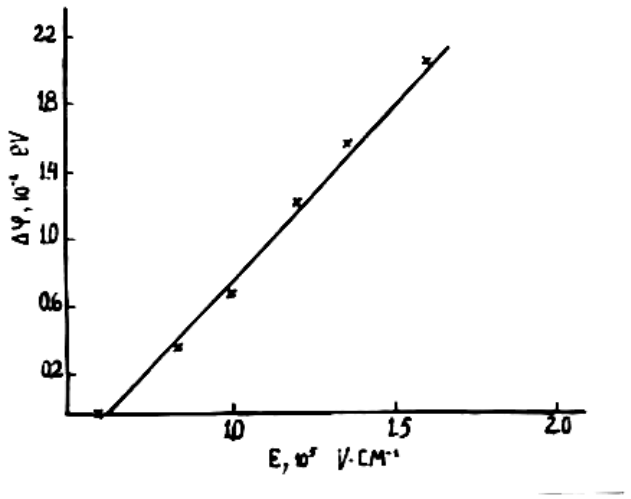

Fig.3. The dependence of the decay of the potential barrier height on the electric field.

It has been established by methods, represented in [9-11, 14], that the deep centers, created by the dislocation, are donor. By processing the experimental curves of TSC by means of the formula [10] the main parameters of the deep centers are determined:

$$ln\left(\frac{T_m^4}{b}\right) = ln\frac{\varphi}{kB} + \frac{\varphi}{kT_m} \qquad (1)$$

where T_m is the temperature corresponding to the maximum of TSC, b is the velocity of the sample heating, k is Boltzmann constant, φ is the activation energy (the height of the potential barrier), B is the emission coefficient. The activation energy determined of $ln\left(T_m^4 / b\right)$ on $1/T_m$ dependence makes φ=0.38eV and the emission coefficient, calculated by the cross point of the same straight line with the ordinate axis is $B=5.33\cdot10^3 c^{-1}\cdot K^{-2}$. Moreover, on the TSC line (fig.2) beside the main peak 1, on right and left, at the reverse bias on the *p-n* junction $V_R=5B$, two peaks$1'$ and $1''$, which coincide with the dislocation levels DH_1 and DH_3, obtained in [18] and also with the peaks A,B,C on the *DLTS* line, represented in [6]. These data testifies the authentic of the obtained results.

As it is seen from fig.3, the dependence $\varphi(E)$ is linear. By the extrapolation of the dependence to the zero value of the field, we will obtain for φ_0 the value 0,39eV, which coincides with the dislocation energy DH_2 in *p*-Si, obtained in [18].

The experimentally obtained dependence $\Delta\varphi(E)$ allows carrying out the identification of the deep centers type and

the form of their screening. According to the criterion, represented in [19.20], the line dependence $\Delta\varphi(E)$ testifies the Coulomb type of the dislocation centers and statistic nature of their screening, just as the dependence $\Delta\varphi \approx E^{1/3}$ occurs in the case of the dynamic screening. Thus, it follows from fig.3, that the dislocations in Si create the deep centers of the Coulomb type.

From experimentally determined dependence $\Delta\varphi(E)$, it is possible to construct the dependence of the potential barrier height on the distance to the dislocation nuclear $\Delta\varphi(X)$, i.e. to determine the form of the potential barrier irrespective of the type of the capture centers.

The dependence, represented in [21], has been applied for the determination of the potential barrier form (the relief of the potential energy).

$$\Delta\varphi(X) = E\varphi'(E) + \Delta\varphi(E) \qquad (2)$$

where $\Delta\varphi'(E)$ is the derivative of the $\Delta\varphi(E)$ function, which is determined by the graphic differentiation of the experimental dependence $\Delta\varphi(E)$ from fig.3.

The curve of the potential energy of the carrier's interaction with the one isolated edge dislocation (the form of the potential barrier) is represented on fig.4. Having φ(E), it is possible to determine the distance to the maximum of the potential barrier: $X_m = \Delta\varphi(E)/q$ (where q is the electron charge).

CONCLUSION

1. It is shown, that the charge edge dislocation in the silicon creates the deep centers of the Coulomb type.
2. The dependence of the change of the potential barrier height close to the charge edge dislocation in the silicon on the external perpendicular field has been determined and it is shown, that this dependence is linear by its nature.
3. The potential relief of the interaction energy of an isolated charge dislocation with the charge carriers has been determined.

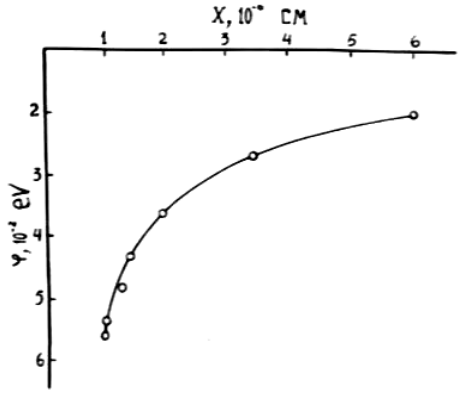

Fig.4. The relief of the potential energy close to the dislocation in the silicon. *X i*s the distance from the dislocation core.

[1] *W.T. Read*. Phyl. Mag., 1955, 46, 111.
[2] *G. Matare*. Elektronika defektov v poluprovodhikakh. Mir. M.1974.
[3] *L.A. Kazakevich, P.F. Lugakov, I.M. Phillippov*. FTP №4, 1989, p.722-725.
[4] *O. Madelung*. FTT, M. Nauka, 1985.
[5] *V.B. Shikin, Y.V. Shikina*. UFN, 1995, №8, p.887-917.
[6] *P. Omling, E.R. Weber, L.Montelius, H. Alexander, I.Michel*. J- Phys. Rev B, 1985, V.32, №10, p. 6571-6581.
[7] *S.G. Rzayev, E.P. Nakhmedov*. FTT, 1993, v.4, p.1083-1042.
[8] *Y.I. Frenkel*. JETF, 1938, 8, v.12, p.1292.
[9] *S.G. Rzayev*. Neorg. Mater., 1998, №12,p.1415-1419.
[10] *M.G. Buehler*. Sol. St. Electron, 1972, v.15, p.69-79.
[11] *A.G. Abdullayev, S.G. Rzayev*. Microelectronika, 1894, v.13, p.260-263.
[12] *S.G. Rzayev*. 1986, v.3 (118), p.21-25.
[13] *D.V. Lang*. J.Appl.Phys., 1974, v.45, p.3014-3032.
[14] *V.N. Yerofeyev, V.I. Nikitenko, V.I. Polovitzkiy*. Kristallografiya, 1971, v.1, p.190-196.
[15] *A. George, C. Escaragwage*. Phys. Stat. Sol. (b), 1972, v. 53, p. 483-496.
[16] *K. Sangval*. Travleniye kristallov. M.Mir, 1990.
[17] *V.I. Nikitenko, V.N. Yerofeyev, N.M. Nadgornaya*. "Issledovaniye podvijnosti dislokatziyi v kremnii" Collection "Dinamika dislokaziyi" Kharkov-1968, p.84-98.
[18] *V.V. Kveder, Yn.A. Osipyan, W. Schroter, G. Zoth*. Phys. St Sol. (a) 1982, v.72, p.701-713.
[19] *R.M.Hill*. Phyl.Mag. , 1971, v.23, p.59.
[20] *A.I. Gubanov*. JTF, 1954, v.24, p.308.
[21] *N.G. Volkov, E.K. Lyapidevskiy*. FTT, 1972, v.14, №5, p.1337-1340.

S.Q. Rzayev, Z.M. Zöhrabbəyova

SİLİSİUMDA TƏKLƏNMİŞ DİSLOKASİYANIN ƏTRAFINDAKI POTENSİAL RELYEF

Tərkibində bir elektrik aktiv qıraq dislokasiya olan silisium kristalında Frenkel-Pul effektinin tədqiqatı nəticəsində müəyyən edilmişdir ki, onun aktivliyinin səbəbi özəyində olan atomların doymamış rabitələridir. Göstərilmişdir ki, dislokasiya kulon tipli dərin mərkəzlər törədir. Təklənmiş yüklü dislokasiyanın yükdaşıyıcılarla qarşılıqlı təsirinin potensial enerjisinin relyefi müəyyənləşdirilmişdir.

С.Г. Рзаев, З.М. Захрабекова

ПОТЕНЦИАЛЬНЫЙ РЕЛЬЕФ ВБЛИЗИ ИЗОЛИРОВАННОЙ ДИСЛОКАЦИИ В Si

Исследуя эффект Френкеля-Пула в кремнии, содержащем одну электрически активную краевую дислокацию, установлено, что она создает глубокие центры кулоновского типа. Определен потенциальный рельеф энергии взаимодействия одной изолированной заряженной дислокации с носителями заряда.

Received: 19.03.03

OPTICAL PROPERTIES OF $LiNbO_3$

TALAT R. MEHDIYEV
Institute of Physics, Azerbaijan National Academy of Sciences,
Baku. Az - 1143, H. Javid ave., 33

The analysis of experimental results of some optical researches which have been carried out on pure and alloyed 0,03% Fe crystals of lithium niobate is resulted. The publication is continuation of ref. [20].

Before discussing the results of calculations in [20], we shall pay attention to the following experiments.

Thin plates of crystals $LiNbO_3$ and Fe(0.03 %): $LiNbO_3$, annealed during one hour at temperature near 500K, are positioned in the vacuum lightproof camera, in which they are anchored on a thin thread above a semitransparent metal plate. Oscillations of a crystal are checked on a diversion of an optical beam from the light pocket mirror anchored on a thread (the mass of a crystal is many times greater than mass of pocket mirror). The control of distance changes between a crystal and a plate, at appearance of a charge on a surface of a crystal, is carried out with the help of the interference microscope with the accuracy up to 0.5 micron. The temperature, during recording of a diffraction grating, is determined by measuring of an optical trajectory in dark area of a crystal.

In all cases, radiation from laser He-Ne (λ=6328Å, power of 30 Watt/cm^2) is created by the standard methodics for crystals $LiNbO_3$. Recordings of diffractograms from a crystal, in a time dependence of an exposure, have fixed changes of diffraction strips forms in the area of a light stain (fig. 1a, б), and also distribution of Δn on amplitude and section in one (fig.2.). It is necessary to note, that intensity distribution on the area of a light stain was created uniform one practically no more than 0,03%. Maximal values Δn are observed, when radiation from the laser is directed perpendicularly to an axis "C" of a crystal. The further experiments have shown that distribution Δn during lightning appreciably differs from distribution after removal of lightning. During investigations of relaxation time Δn, the quick and slow components are observed.

The observable effect is the result of appearance of an electric field in a crystal (strength about 10^5V/cm), causing Δn change and the appearance of a charge on a crystals surface depending on temperature, intensity and a wave length of laser radiation.

It is necessary to note, that there is no new effects in the obtained results, because in 1966 in paper [2] the observation of the effect of photoinduced change of the index of refraction and after that [3] on a possibility of the use this effect for the recording phase holograms with high efficiency [4-9]. Results of similar observations, but in an electric field (by electrical compass method) also have been published in paper [1]. The fact is known, that the spatial charge is formed in ferroelectrics - photoconductors, on boundaries of uniformly lightning area. Change of spontaneous polarization of crystal P_s in a place of lightning causes the appearance of depolarization electric field E which can save it self long-lived time at the low conductance of a crystal (in case of the mobility for $LiNbO_3$ is approximately equal to 10^{-4}cm$^2\cdot$s$^{-1}\cdot$V^{-1} [13]). This electric field strength is the magnitude of interatomic interactions degree and, therefore, leads to deformations of electronic configurations not only the impurity centers, but also in atoms constituting this crystal structure. This consequence is a result of observable changes of P_s and Δn. The change P_s on the other hand, causes the appearance of a depolarization electric field. Due to a photoconduction this field is screened, i.e. the electric field inside the light stain area will have zero value at long enough time of lightning. At this moment the quantity Δn can be calculated, as it has been done in paper [10].

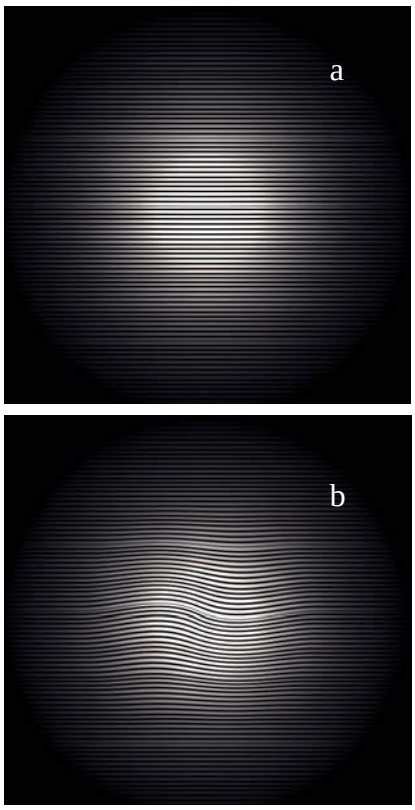

Fig.1. a. The diffraction pattern, when effect on crystal it is not observed yet;
b. Contortions of the diffraction strips in area light stain

In calculations by cluster method of electronic structure $LiNbO_3$ it has been received the data on spontaneous polarization P_s (0,77cm^{-2}) [11], taking place in the consent with the experimental results 0,71cm^{-2} [12]. Ionization or excitation of an impurity increases its polarizability in two times and so the ferroelectric impurity is polarized by a macroscopic field so the dipole moment of an impurity changes also. The deformation lattice near the impurity causes of the dipole moment change of the impurity centre [17].

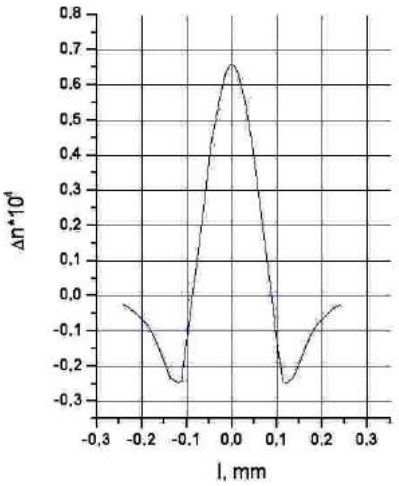

Fig.2. Distribution Δn in the area of a light stain

In [10] the expression of distribution function $P(r)$ is obtained taking into consideration [18]. From this we have the following expression

$$\Delta P_s \approx \frac{\alpha^* f P_s N}{4\pi}(f+1),$$

where f is the Lorentz factor; $E=f P_s$ is a macroscopic field; α^* is a polarizability of an impurity; $\alpha f P_s$ is change of the dipole moment of an impurity. For the case $a_B<r_c$ (shallow impurities) f is equal to zero. Thus, quantity of change ΔP_s and consequently Δn, are obtained by deep levels. The macroscopic field leads to zero at the homogeneous lightning of the short-circuited crystal. In this case the change of n is caused by change of the polarizability α of the impurity centers. The value $\Delta\alpha_0$ depends on the optical polarization of the same impurity atoms and the deformation area of the crystal. After stopping of the lightning, because of relaxation process of excited states of impurities, P_s returns to an initial equilibrium value. However, Δn does not return to an initial value. That means that the inducted field with very large relaxation time appears in the earlier lightning area (fig.3).

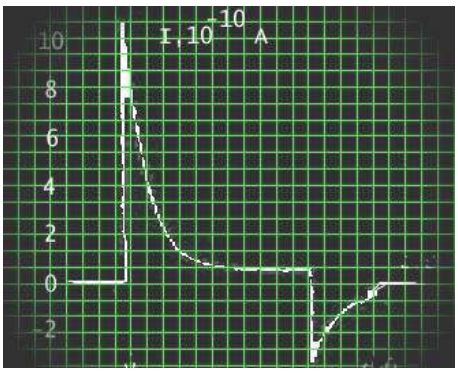

Fig.3 Changes of a photoelectric of a short circuit in crystal Fe: $LiNbO_3$.

Time of scan of a signal is 250s. The first emission of a signal corresponds to insert of light, second - to lockout.

The electric field at the non-homogeneous lightning (so it is possible for itself to present a problem on distribution of light on o a crystal taking into consideration of lightning and non-lightning areas) is determined by concentration of free electrons. It is necessary to take into account that concentration of free electrons is, less, than the trapped electrons one. Thus, the photoinduced field E is defined by the charge distribution on traps and as follows from the above mentioned, leads to the unreturning of Δn to the initial value after stopping of lightning. On the other hand, the photoinduced field can be obtained using the equivalent circuit:

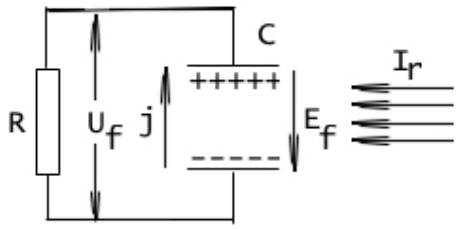

where R is the loading resistor, R_c in internal resistance of a crystal ($R_c<<R$), U_f is a voltage drop on the loading resistor, I_r is the intensity light, impinging on a crystal, j is spatial component of a current $\vec{j}$, directed to normal to an face surface of the plane-parallel plate thickness d, E_f is photoinduced field strange in the capacitor C. The induced field strange is determined by charge density ρ on the capacitor plates which have arisen as a result of lightning of a crystal by light, more over $\frac{d\rho}{dt} = j - \sigma E$, σ is an admittance. As $E = \frac{4\pi\rho}{\varepsilon_l}$, where ε_l - longitudinal component of dielectric constant, then we, taking into account the time of the dielectric relaxation $t_d = \frac{\varepsilon_l}{4\pi\sigma}$, obtain $\frac{dE}{dt} + \frac{E}{t_d} = -\frac{4\pi j}{\varepsilon_l}$. It follows that $E_f = -\frac{j}{\sigma}$ and $E(t) = E_f\left(1 - exp\left(-\frac{t}{t_d}\right)\right)$. At $t>> t_d$, $j = -\sigma E_f$. Here it is possible to present σ as the total of the some two contributions: σ_f - a photoconductivity and σ_d - eigen conductivity, more over σ_f is not a small value in comparison with σ_d. Defining j as αGJ, where α is an absorption constant; G is Glass coefficient and $\sigma_f = \alpha K_f J$ where K_f is a conductivity coefficient, we have:

$$E_f = -\frac{G}{K_f\left(\frac{\sigma_d}{\sigma_f} + 1\right)}$$

and, if $\sigma_f >> \sigma_d$, then E_f is defined only by a material plate parameters, i.e. by the relation $\left(-\frac{G}{K_f}\right)$. For Fe:$LiNbO_3$ the values of Glass's constants are given by the relation in [19]:

$$G_{33}^L \approx G_{31}^L = 2-4; G_{22}^L \approx 0.1-0.3;$$
$$G_{12}^c \approx 0.1-0.5 >> G_{15}^L$$

At $t << t_d$ and the minor current j, the charge separation will be only because of photovoltaic field. In the case of niobate lithium, it is necessary to take into account also, that there is a dependence of cross spatial orientation of a polar axis of the crystal $\vec{C}$ and the current $\vec{j}$. The quantity of a photorefraction field, estimated in the experiment on $LiNbO_3$, is equal to 850 V/cm. Also the storage charge is equal to $4\cdot10^{-12}$ Q, and field of a spatial charge - 1800 V/cm. For Fe:$LiNbO_3$ value of photorefraction field is equal to $\approx1.5\cdot10^4$V/cm.

The solution of distribution problem of a spatial charge and the field near the boundary of homogeneously lighted area at the presence and absence of the external electric field is well-known [1]. The size of area of a spatial charge at presence of the external field E_o is defined by following expression:

$$l = \frac{2kT}{eE_0}\left(\sqrt{1+\left(\frac{2kT}{eE_0 l_D}\right)^2}-1\right)$$

where l_D is a screening distance of Debye which at presence of the concentration traps N, is defined by the expression $l_D = \sqrt{\frac{\varepsilon kT}{4\pi e^2 N}}$. Under conditions $E_0 > \frac{kT}{el_D}$ the character size of area of the spatial charge will be expressed from. $l = \frac{\varepsilon E_0}{4\pi eN}$. For $E_o\approx10^4$V/cm and $N\approx10^{18}$cm^3 the character size of area is approximately equal 10^{-7}cm that it is less, than the character size of area of the non-homogeneous lightning, which is equal to the wave length or more. It allows to use a quasi-neutrality condition analyzing photorefraction effect at which it can be proposed that local electron concentration is defined by the light intensity in the given point (it usually means that Δn connects with an intensity distribution weakly at the enough strong lightning and is defined only by value of an external field). The diffusion field appears usually at the external field absence at the non-homogeneous lightning, for example at recording holograms on $LiNbO_3$ in [15]. Its value is expressed by $\frac{kT}{eL}$, where L is a character length of light intensity change, for example the character wave is defined by the sinusoid wave length for the sinusoidal spatial distribution of light intensity. It is confirmed by the experimental results on hologram recording in which it is shown, that the first Fourier-component value of a diffusion field is equal to $\frac{2\pi kT}{\lambda}$ (but only it is of interest at calculations of the hologram diffraction efficiency). This value is equal to $1.5\cdot10^3$V/cm at room temperature and $\lambda\approx10^{-4}$cm.

In ref. [14] it is informed about investigations of temperature and spectral dependences of photovoltaic current in ferroelectrics, in $LiNbO_3$ particularly. It has been shown, that a photoconductivity and photovoltaic effect in $LiNbO_3$ are connected to interband or impurity to band transitions. The appearance of the photovoltaic current can be consequence of volumetric photovoltaic effect in the homogeneous and homogeneously lighted $LiNbO_3$ [19.] In this case the current direction is defined by the axes direction of spontaneous polarization, even in the absence of the electric field. At ionization of the impurity centre in a polar crystal, as it is shown in ref. [16], the free made electrons have a privaled velocity direction on spontaneous polarization direction or against one, i.e. the probability of the appearance of electrons as a result of ionization, which has the velocity direction parallel to P_s, differs from the probability of the appearance of the electron having an opposite direction of velocity. It is connected with the distortion of wave functions in an unsymmetrical field of the impurity centre. The application of this model has difficulties because of small carriers mobility in $LiNbO_3$ (conductivity must have the jump character), and the recombination time essentially exceeds 10^{-8} s, but quite agrees to Fe: $LiNbO_3$ in which the supplier of electrons is the impurity atom Fe^{2+} in a conduction band.

Thus, the expression for a current, determining the volumetric photovoltaic effect $j=\sigma E+K\alpha\Phi$ where K is the proportional coefficient of spontaneous polarization P_s, α is an absorption constant of light, is applicated completely in the case of Fe: $LiNbO_3$ and if we use the results of ref. [20], then j will explain the fact and character of changes of an absorption constant completely. On the other hand, the presence of 90°-phase shift between lattices at hologram recording on $LiNbO_3$ [15] is a necessary condition of realization of the diffusion mechanism of recording.

[1]. *V.I.Belinicher, I.F.Kanayev, V.K.Malinovskii, B.I.Sturman* Izv. AN SSSR, ser..fizicheskaya, 1977, 41, №4, p.733-739.

[2]. *A.Ashkin, G.D.Boyd et al*. Appl. Phys. Letts.1966, 9,72.

[3]. *F.S.Chen* J.Appl. Phys. 1969, 41, 3275.

[4]. *J.J. Amodei* RCA Rev., 1971,32,185.

[5]. *D.L.Staebler, J.J.Amodei* J.Appl.Phys., 1972, 43, 1042.

[6]. *M.F.Deygen, S.G.Odulov et. all.* FTT, 1974, 16, 1895.

[7]. *V.L.Vinitskii, N.V.Kuhtarev* ФТТ, 1974, 16, 3714.

[8]. *D. Von der Linde, A.M.Glass, K.F.Rodgers* Appl. Phys. Letts. 1974,25,155.

[9]. *D. Von der Linde, A.M.Glass, K.F.Rodgers* Appl. Phys. Letts. 1975,26,22.

[10]. *A.P.Levanuk, V.V.Osipov* Izv. AN SSSR, ser. fizicheskaya, 1977, 41, №4, p.753-770.

[11]. *L.Hafid, F.M.Michel-Calendini*, J.Phys. C: Solid State Phys., 1986, 19, 2907-2917.

[12]. *M.E.Lines, A.M. Glass*, in book "Principles and Applications of Ferroelectrics and Related Materials", ed. Marshal and Wilkinson, 1979, Oxford:Clarendon Press.

[13]. *A.V.Rujnikov*, Avtoreferat dissertatsii, LGPI, Leningrad, 1976.

[14]. *V.M.Fridkin, B.N.Popov, P.V.Ionov* Izv. AN SSSR ser. fizicheskaya, 1977, 41, №4, p.771-774.

[15]. *V.B.Markin, S.G.Odulov, M.S.Soskin* Izv. AN SSSR, ser. fizicheskaya, 1977,41, №4, p.822-829.

[16]. *A.M.Glass, D. Von der Linde and et.al.*, J.Electron. Mat., 1975, 4, 915.

[17]. *A.P.Levanyuk, V.V.Osipov,A.S.Sigov* Ferroelectrics, 1976, 14, 643.

[18]. *A.P.Levanuk, V.V.Osipov*. FTT, 1975,17,3595.
[19]. *B.I.Sturman, V.M.Fridkin* "The photovoltaic and photorefractive effects in noncentrosymmetric materials" 1992, Gordon&Breach Science Publishers S.A.., Amsterdam.
[20]. *Talat R..Mehdiyev* Fizika, 2002,8,n.4, p.50-56.

Tələt R. Mehdiyev

$LiNbO_3$ –NİN OPTİK XASSƏLƏRİ

Təmiz və 0.03%-li Fe-la aşqarlanmış neobat litium kristalları üzərində aparılmış bəzi optik tədqiqatların eksperimental nəticələrinin analizi verilmişdir. Bu məqalə [20] – nin davamıdır.

Талат Р. Мехтиев

ОПТИЧЕСКИЕ СВОЙСТВА $LiNbO_3$.

Приведен анализ экспериментальных результатов некоторых оптических исследований, проведенных на кристаллах ниобата лития чистого и легированного 0,03% Fe. Данная публикация является продолжением статьи [20].

Received: 25.03.03

THE INFLUENCE OF IMPURITIES ON KINETICS OF ANNEALING OF $Ge_{1-X}Si_X$ RADIOACTIVE DEFECTS

Sh.M. ABBASOV
Institute of Physics, Azerbaijan National Academy of Sciences,
Baku. Az - 1143, H. Javid ave. 33

In the present work there have been presented the results of our previously carried out investigations of electrophysical properties of solid solutions of *n*-$Ge_{1-x}Si_x$ [1, 2] and conductivity compensation of an electronic $Ge_{1-x}Si_x$ under irradiation has been studied. The irradiation was conducted at 77 K and at room temperature by electrons with energy of 4.5 MeV and by γ-quanta of ^{60}Co.

The results of study of Hall effect and conductivity and the influence on them of isochronous annealing of $Ge_{1-x}Si_x$ monocrystals grown by Chokhralsky method and alloyed Sb ($5\cdot10^{-14}$-$1\cdot10^{15}$cm^{-3}) have been presented. Atomic content of Si was 0.05-0.15%. The annealing was carried out at 300-420 K, exposure time at each temperature was 15 min.

The levels E_c-0.13eV, E_c-0.2eV in a lower part of the forbidden zone belong to the most electrically active acceptors in a spectrum of arising in *n*-$Ge_{1-x}Si_x$ radioactive defects. The annealing temperatures 350, 420 K correspond to the acceptor states. The structure of defects to which the acceptor states belong was discussed in [2].

In the present work we'll only emphasize that the acceptors energetic characteristics and their radioactive constants depend on Si content and in formation of a defect corresponding to the acceptor state *E*, an atom of *V* group element takes part. The similar process of defect formation occurs also in Ge.

The concentrations of donors and acceptors were calculated with the use of the temperature dependence of electrons concentration by a law of active masses. The results obtained by means of two calculation methods [3, 4] which in use to the irradiated Ge have been analyzed in [5], coincide. The calculation was made in approximation of equality of electron effective masses and long-orbit splitting of basis donor state in Ge and $Ge_{1-x}Si_x$, therefore the quantitative comparison with the data for Ge had been presented only for $Ge_{1-x}Si_x$ with Si 0.05% at.

In the case of *n*-$Ge_{1-x}Si_x$ due to the increase of acceptors during irradiation the compensation of conductivity increases up to the change a type of conductivity.

The kinetics of the electrons concentrations change in germanium and solid solutions with Si 5% at and Si 10% at with conductivity of *n*-type is presented in fig. 1. In Ge samples at relative integral flow corresponding to the sharp pass of Hall coefficient through the minimum the $n\rightarrow p$ conversion of conductivity type occurs.

At Φ/N_0 respective doses in samples of solid solution with Si 5% at and Si 10% at the $n\rightarrow p$ conversion of conductivity type (defined by Lissajous figure) also takes place. However, these transitions are not accompanied by passing Hall coefficient through the minimum and in the indicated sections the samples are in a compensated state.

It has been established that as the silicon content in a solid solution increases, a dose necessary for the $n\rightarrow p$ conversion, decreases. It follows from this that the more silicon in the samples of solid solution of *n*-$Ge_{1-x}Si_x$ irradiated by the same respective doses of electrons, the greater the concentration of holes after conversion of conductivity type which for the samples with Si content 0; 5; 10% at amount to $6.5\cdot10^{11}$cm^{-3}, $2\cdot10^{12}$cm^{-3}, $1.4\cdot10^{13}$cm^{-3}, respectively. In fig. 2 the doses dependences of N_D (1) and N_A (2) for *n*-$Ge_{1-x}Si_x$ with Si 0.05% at are presented. As for donor states, it was observed experimentally both decrease and increase of donor concentration with Φ dose. In fig.3 the temperature dependences of Hall mobility of the electrons for the same sample are given.

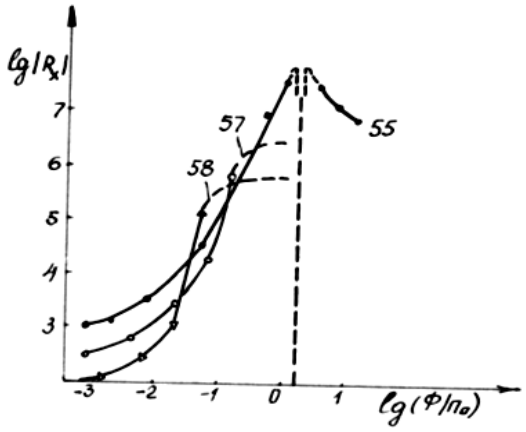

Fig. 1. Dependence of Hall coefficient on relative integral dose for different samples of *n*-type $Ge_{1-x}Si_x$.
55 – Ge samples alloyed Sb, 57 and 58 - the samples of $Ge_{1-x}Si_x$ solid solution with 5% and 100% of Si respectively.

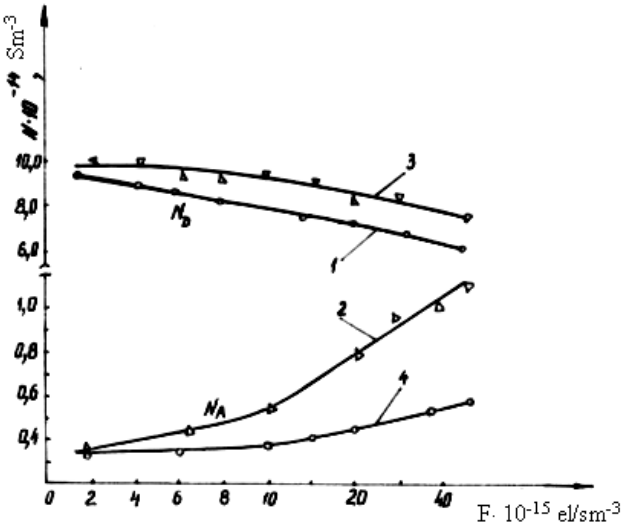

Fig. 2. Dose dependence of N_D (1) and N_A (2) for *n*-$Ge_{1-x}Si_x$ with 0.05% Si at.

The Hall mobilities of current carriers have been estimated on experimental temperature dependences of Hall

coefficient and electrical conductivity. In order to discuss experimental results, the temperature dependences of Hall mobility are presented prior irradiation and after the proper annealing. It has been established that mobility of *p*-type samples with Si 0; 5; 10; 15% at within the temperature range 80-300K is significally higher than prior irradiation.

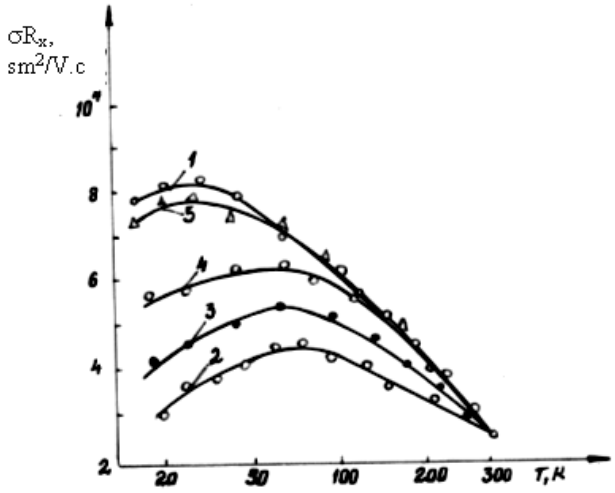

Fig. 3. Temperature dependences of Hall mobility of electrons $Ge_{1-x}Si_x$ with x=0.05.

The annealing of the irradiated samples at 300 K slightly decreases the value of Hall mobility except the germanium sample of *p*-type in which the mobility increases a little.

The annealing at T=420K leads to the increase of Hall mobility as compared with the mobility values prior irradiation. In a sample with Si 15% at the mobility is almost reduced to the initial value. For comparison of the experimental results in different samples, in fig. 4 there have been given the dependences of relative Hall mobilities (M/M_0) on Si% at measured at temperature 80 K, where M_0 is a value of mobility the prior irradiation. The mobility in all samples measured at once after irradiation, increased on an average by a factor of 2 (curve 1). The annealing at 300K almost reduces the initial mobility except germanium (curve 2) in which the mobility still increased by 3.7 times, the further annealing at 420K increased inversely the value of Hall mobility (curve 3) except a sample of solid solution of $Ge_{1-x}Si_x$ with Si 15 % at.

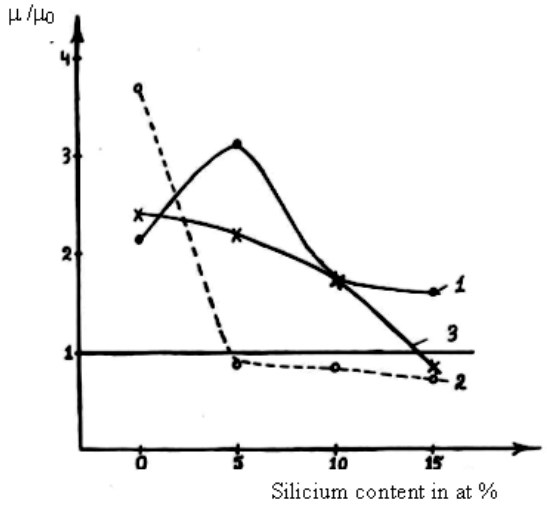

Fig.4. Dependence of relative Hall mobilities (M/M_0) on Si in % for *p*-$Ge_{1-x}Si_x$.

The analysis of temperature dependences of Hall coefficient and mobility of charge carriers in irradiated and annealed samples of Ge and $Ge_{1-x}S_x$ permits to draw the following conclusions:

1. Decrease of N_D during irradiation observed experimentally along with the other dose dependences of N_D is not connected to electrically inactive defects in a model [6]. The stability of such defects as the acceptor states E_c=0.2eV is limited within the temperature range 350-420K.

2. The number of the radioactive levels and their ionization energies depend on Si content in solid solutions.

3. One can change markedly the values of Hall mobility depending on the temperature of irradiation, annealing and Si content in solid solution. Indeed, as it is seen from fig. 3 (curve 3), the mobility in samples of solid solution with Si 0-10 % at, irradiated at 100K and annealed at 420K, increases on an average by a factor of two, as compared with the initial mobility. This seems to be connected to a change of charge state of the non-homogeneities regions.

[1] *Sh.M. Abbasov, G.T. Agaverdiyeva, Sh.I. AbbasovI.* Influence of low-temperature irradiation on lifetime of majority carriers in solid solutions of $Ge_{1-x}Si_x$. EURASIA CONFERENCE ON NUCLEAR SCIENCE AND ITS APPLICATION IEC-2000, 23-27 October, Izmir, Turkey p. 501.

[2] *N.A. Ukhin, A.K. Abiyev, Sh.M. Abbasov, G.M. Gasumov*. FTP, 1984. v. 18, is. 6, p. 981-985.

[3] *D. Blekmor*. Statistics of electrons in semiconductors. M. Mir, 1964. 392 p.

[4] *V.V. Emtsev, T.V. Mashovets, S.M. Rivkin*. The role of group V impurities in the formation of defects in germanium under γ-irradiation in: Proc. Intern conf. radiate damage semiconductors. Rcading 1973, London; Bristol: Inst Phys. 1973,ser 16.p.17-25.

[5] *A.F. Lehar, I.E. Whitehouse.* Solid State Communs, 1975. 17, №12, p. 1609-1612.

[6] *T.V. Mashovets, V.V. Emtsev.* Point defects in germanium. In; Proc of intern. conf. on lattice defects in semiconductors, Freiburg 1975, London, Bristol: Inst. Phys 1975. ser 23, p. 1603-1607.

Ş.M. Abbasov

$Ge_{1-x}Si_x$ BƏRK MƏHLULUNDA YARANAN RADİASİYA DEFEKTLƏRİNİN KİNETİK TABLAMASINDA AŞQARLARIN ROLU

Bu işdə bizim tərəfdən əvvəllər öyrənilmiş n - $Ge_{1-x}Si_x$ bərk məhlulunun elektrofiziki xassələrinə elektron şüalarının təsirinin davamı olaraq, n - $Ge_{1-x}Si_x$ bərk məhluluna γ və elektron şüalarının təsiri ilə kompensasiya olunma və yaranan radiasiya

defektlərinin kinetik tablamasında aşqarların rolu öyrənilmişdir. Bunun üçün şüalanma mənbəyi kimi ^{60}So - γ qurğusundan və enerjisi 4,5 MeV olan elektron sürətləndiricisindən istifadə olunmuşdur. Şüalanma temperaturu 77K÷300K-dir.

Ш.М. Аббасов

ВЛИЯНИЕ ПРИМЕСЕЙ НА КИНЕТИКУ ОТЖИГА РАДИАЦИОННЫХ ДЕФЕКТОВ Ge_{1-x} Si_x

В настоящей работе приведены результаты начатых нами ранее исследований электрофизических свойств твердых растворов *n*-Ge_{1-x} Si_x [1,2] и изучена компенсация проводимости электронного Ge_{1-x} Si_x при облучении. Облучение осуществлялось при 77К и при комнатной температуре электронами с энергией 4,5 МэВ и γ - квантами ^{60}Co.

Received: 26.03.03

-+

EFFECTS OF WEAK NEUTRAL CURRENTS IN THE SEMI-INCLUSIVE $l^{\mp}N \to l^{\mp}hX$ REACTIONS

S.K. ABDULLAYEV, A.I. MUKHTAROV, M.Sh. GODJAYEV
Baku State University
Z. Khalilov st., 23, Baku, 370143

The investigation of electroweak asymmetries in the deep-inelastic scattering of polarized lepton on polarized nucleons is carried out in framework of the standard theory and in the quark-parton model. The expressions for left-right, polarization, charge-polarization and charge asymmetries are obtained.

1. The standard model (SM) of the electroweak interactions of the elementary particles [1] has achieved a great success in the description of series of the experiments, which have been carried out in the various laboratories of the world. In particular, one of its exact checking has been alone on the e^-e^+ – colliders LEP, SLC and TRISTAN, as the result of which the agreement with the experimental data has been obtained. Alongside with e^-e^+ - annihilation the deep-inelastic scattering processes of the polarized leptons on the polarized nucleons play the important role in the check of standard theory and they are intensive investigated experimentally at the present time [2-6].

In the present paper the effects of weak neutral currents (SNT) in the semi-inclusive reactions are considered

$$\ell^{\mp} + N \to (\gamma^*; Z^0) \to \ell^{\mp} + h + X, \qquad (1)$$

in which the lepton and the picked out inclusive adron *h* are registered on the coincidence and *X* is the system of non-detectering adorns.

The especial attention is paid to p-add polarization effects. The polarization fenomena are more sensitive to the reaction mechanism and allow to recognize the contributes of SNT easily. The investigation of the polarization particle correlations give the possibility to check the series of OCD predictions, to calculate the spin structure functions of adrons, to define the momentum distribution of the quarks and gluon inside of the polarized nucleons. The study of the polarization phenomena has got the special actuality last years, because of the obtaining of the high-energy beams of the polarized leptons and the creation of the polarized proton –antiproton beams and targets.

The Feynman diagrams for lepton creation of the inclusive adron *h* are presented in the fig.1.

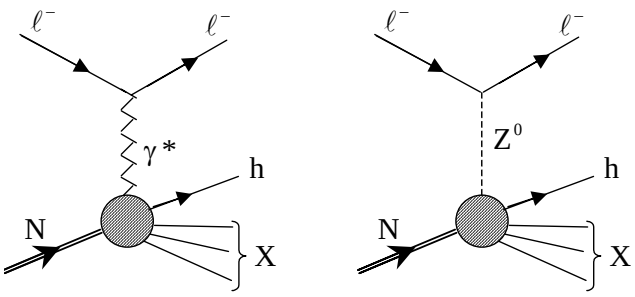

Fig. 1. Deep-inelastic leptocreation of adron h: $\ell^{\mp}N \to \ell^{\mp}hX$.

2. At first we consider the parton subprocess

$$\ell^- + q \to (\gamma^*; Z^0) \to \ell^- + q, \qquad (2)$$

and discuss the series of its qualitative properties at high energies. It is easy to be convinced, that in the process (2) of the exchange of proton and Z^0- bozon the spiralities of lepton and quark must be kept separately. That is why the process (2) is characterized by four independent spiral amplitudes F_{LL},F_{RR},F_{RL} and F_{LR} (the first and the second indexes show the spiralities of lepton and quark correspondingly), that describe the following reactions:

$$\ell_L^- + q_L \to \ell_L^- + q_L, \quad \ell_R^- + q_R \to \ell_R^- + q_R,$$
$$\ell_L^- + q_R \to \ell_L^- + q_R, \quad \ell_R^- + q_L \to \ell_R^- + q_L.$$

In the SM framework the spiral amplitudes are defined by expressions:

$$F_{\alpha\beta} = \frac{Q_e Q_q}{t} + \frac{g_\alpha^\ell g_\beta^q}{t - M_Z^2} \quad (\alpha, \beta = L; R)$$

where $t = q^2$ is the square of the transfer momentum, M_Z is the mass of Z^0- bozon, g_L^ℓ and g_R^ℓ (g_L^q and g_R^q) –are the chiral bond constants of lepton (quark) with Z^0- bozon, the values of which are equal to:

$$g_L^\ell = \frac{-1/2 + x_w}{\sqrt{x_w(1 - x_w)}},$$

$$g_R^\ell = \sqrt{\frac{x_w}{1 - x_w}}, \qquad (4)$$

$$g_L^q = \frac{(T_3 - Q_q x_w)}{\sqrt{x_w(1 - x_w)}},$$

$$g_R^q = -Q_q \sqrt{\frac{x_w}{1 - x_w}}$$

where $x_w = \sin^2\theta_w$ is the Weinberg's parameter; Q_q is the electric charge, T_3 is the third projection of the weak isospine of quark q .Let us give the cross-section of the subprocess (2) at the determined values of the spiralities of initial and final particles.

$$\frac{d\sigma}{dy}(\ell^-_\alpha q_\alpha \to \ell^-_\alpha q_\alpha) = 4\pi\alpha^2 s F^2_{\alpha\alpha},\ (\alpha = L\ or\ \ R),$$
$$\frac{d\sigma}{dy}(\ell^-_\alpha q_\beta \to \ell^-_\alpha q_\beta) = 4\pi\alpha^2 s(1-y)^2 F^2_{\alpha\beta},\ (\alpha = L\ or\ R;\ \ \beta = R\ or\ L), \tag{5}$$

where s is the square of the total energy of the system $\ell^- q$ in c.m.s the variable y is connected with the lepton scattering angle $\tilde{\theta}$ in c.m.s by the following relation

$$y = -\frac{t}{s} = \frac{1}{2}(1-\cos\tilde{\theta}).$$

The differential cross-section of the parton subprocess (2) is given by the following expression

$$\frac{d\sigma}{dy}(\ell^- q \to \ell^- q) = \pi\alpha^2 s\{(1-\lambda)(1-h_q)F^2_{LL} + (1+\lambda)(1+h_q)F^2_{RR} + \\ + [(1-\lambda)(1+h_q)F^2_{LR} + (1+\lambda)(1-h_q)F^2_{RL}](1-y)^2\} \tag{6}$$

where λ and hq are spiralities of lepton and quark.

3. Let us consider the distribution function of quark (anti-quark) in the polarized nucleon $f^{N(h_N)}_{q(h_q)}(x)$ $\left(f^{N(h_N)}_{\bar{q}(h_{\bar{q}})}(x)\right)$, which describes the probability of quark q (antiquark $\bar{q}$) revealing in the nucleon with the momentum part x, having the spirality h_q ($h_{\bar{q}}$). This function satisfies the following equations:

$$f^{N(-h_N)}_{q(-h_q)}(x) = f^{N(h_N)}_{q(h_q)}(x),$$
$$f^{N(+1)}_{q(+1)}(x) + f^{N(+1)}_{q(-1)}(x) = f_q(x), \tag{7}$$

where $f_q(x)$ presents itself as the usual distribution function of quark q in nucleon. According to QCD the quark distribution functions in nucleon depend on the square of the transfer momentum q^2: $f_q(x, q^2)$ also.

In SM frameworks the differential cross-section of hall-inclusive reaction $\ell^- N \to \ell^- hX$ must be written in the following form:

$$\frac{d\sigma^{(-)}}{dxdydz} = \sum_{q,\ h_q} f^{N(h_N)}_{q(h_q)}(x, q^2) D^h_q(z) \frac{d\sigma(\ell^- q \to \ell^- q)}{dy} + \sum_{\bar{q},\ h_{\bar{q}}} f^{N(h_N)}_{\bar{q}(h_{\bar{q}})}(x, q^2) D^h_{\bar{q}}(z) \frac{d\sigma(\ell^- \bar{q} \to \ell^- \bar{q})}{dy} =$$

$$= 2\pi\alpha^2 sx \sum_q \{ f_q(x, q^2) D^h_q(z)[(1-\lambda)(F^2_{LL} + (1-y)^2 F^2_{LR}) + (1+\lambda)(F^2_{RR} + (1-y)^2 F^2_{RL})] +$$
$$+ f_{\bar{q}}(x, q^2) D^h_{\bar{q}}(z)[(1-\lambda)(F^2_{LR} + (1-y)^2 F^2_{LL}) + (1+\lambda)(F^2_{RL} + (1-y)^2 F^2_{RR})] - \tag{8}$$
$$- h_N \Delta f_q(x, q^2) D^h_q(z)[(1-\lambda)(F^2_{LL} - (1-y)^2 F^2_{LR}) - (1+\lambda)(F^2_{RR} - (1-y)^2 F^2_{RL})] -$$
$$- h_N \Delta f_{\bar{q}}(x, q^2) D^h_{\bar{q}}(z)[(1-\lambda)(F^2_{LR} - (1-y)^2 F^2_{LL}) - (1+\lambda)(F^2_{RL} - (1-y)^2 F^2_{RR})]\}$$

Where

$$\Delta f_q(x, q^2) = f^{N(+1)}_{q(+1)}(x, q^2) - f^{N(+1)}_{q(-1)}(x, q^2),$$

$$s = (P+k)^2;\ x = -q^2/2(P\cdot q);\ y = (P\cdot q)/(P\cdot k),\ z = (P\cdot p_h)/(P\cdot q),$$

h_N is the nucleon spirality; k, P and p_h are 4 momentums of an initial lepton, nucleon and final adron h; q-k-k' is 4-vector of the momentum transfer; $D^h_q(z)$ ($D^h_{\bar{q}}(z)$) is the fragmentation function of quark (antiquark) in adron h.

The differential cross-section of process $\ell^+ N \to \ell^+ hX$ must be obtained from (8) with the help of neutral substitutions $F_{R\beta} \leftrightarrow F_{L\beta}$ (β=R; L):

$$\frac{d\sigma^{(+)}}{dxdydz}=2\pi\alpha^2 sx\sum_q\{\, f_q(x,q^2)D_q^h(z)[(1-\lambda)(F_{RL}^2+(1-y)^2F_{RR}^2)+(1+\lambda)(F_{LR}^2+(1-y)^2F_{LL}^2)]+$$

$$+\, f_{\bar q}(x,q^2)D_{\bar q}^h(z)[(1-\lambda)(F_{RR}^2+(1-y)^2F_{RL}^2)+(1+\lambda)(F_{LL}^2+(1-y)^2F_{LR}^2)]-$$

$$-h_N\Delta f_q(x,q^2)D_q^h(z)[(1-\lambda)(F_{RL}^2-(1-y)^2F_{RR}^2)-(1+\lambda)(F_{LR}^2-(1-y)^2F_{LL}^2)]- \qquad (9)$$

$$-h_N\Delta f_{\bar q}(x,q^2)D_{\bar q}^h(z)[(1-\lambda)(F_{RR}^2-(1-y)^2F_{RL}^2)-(1+\lambda)(F_{LL}^2-(1-y)^2F_{LR}^2)]\}$$

The W.N.C displays can be observed by the means of revealing of character *P* - and *S* - odd effects. Such effects are:

1. left -right asymmetries

$$A^{(\mp)}(\ell_L^{\mp}-\ell_R^{\mp})=[\,\sigma_L^{(\mp)}-\sigma_R^{(\mp)}\,]/[\,\sigma_L^{(\mp)}+\sigma_R^{(\mp)}\,], \quad (10)$$

$$A^{(\mp)}(\ell_L^{\mp}-\ell_R^{\pm})=[\,\sigma_L^{(\mp)}-\sigma_R^{(\pm)}\,]/[\,\sigma_L^{(\mp)}+\sigma_R^{(\pm)}\,]; \quad (11)$$

2. polarization asymmetries

$$A_p^{(\mp)}=[\,\sigma_{RR}^{(\mp)}-\sigma_{LL}^{(\mp)}\,]/[\,\sigma_{RR}^{(\mp)}+\sigma_{LL}^{(\mp)}\,], \qquad (12)$$

$$A_a^{(\mp)}=[\,\sigma_{RL}^{(\mp)}-\sigma_{LR}^{(\mp)}\,]/[\,\sigma_{RL}^{(\mp)}+\sigma_{LR}^{(\mp)}\,]. \qquad (13)$$

3. charge-polarization asymmetries

$$B_p^{(\mp)}=[\,\sigma_{RR}^{(\mp)}-\sigma_{LL}^{(\pm)}\,]/[\,\sigma_{RR}^{(\mp)}+\sigma_{LL}^{(\pm)}\,], \qquad (14)$$

$$B_a^{(\mp)}=[\,\sigma_{RL}^{(\mp)}-\sigma_{LR}^{(\pm)}\,]/[\,\sigma_{RL}^{(\mp)}+\sigma_{LR}^{(\pm)}\,]. \qquad (15)$$

4. Charge asymmetries

$$C_{\alpha\beta}=[\,\sigma_{\alpha\beta}^{(-)}-\sigma_{\alpha\beta}^{(+)}\,]/[\,\sigma_{\alpha\beta}^{(-)}+\sigma_{\alpha\beta}^{(+)}\,],\ (\alpha,\beta=R;\ L) \qquad (16)$$

.

Here $\sigma_L^{(-)}=\dfrac{d\sigma_L^{(-)}}{dxdydz}$ and $\sigma_R^{(-)}=\dfrac{d\sigma_R^{(-)}}{dxdydz}$;

($\sigma_L^{(+)}$ and $\sigma_R^{(+)}$)-differential cross-sections semi-inclusive GNR of the left- and right-polarized lepton (antilepton) on nucleons, $\sigma_{RR}^{(\mp)}$, $\sigma_{LL}^{(\mp)}$, $\sigma_{RL}^{(\mp)}$ and $\sigma_{LR}^{(\mp)}$ are cross-sections of process (1) at the spiralities of collising particles $\lambda=1$, $h_N=1$; $\lambda=-1$, $h_N=-1$; $\lambda=-1$, $h_N=-1$ and $\lambda=-1$, $h_N=1$.

The electroweak asymmetries (10)-(16) are expressed by the spiral amplitudes $F_{\alpha\beta}$, as it takes place in the electron-position annihilation processes [7-9]. For example, the left-right asymmetry $A(\ell_L^- - \ell_R^+)$ is defined by the following expression

$$A(\ell_L^- - \ell_R^+)=\frac{1-(1-y)^2}{1+(1-y)^2}\,\frac{\sum_q(F_{LL}^2-F_{LR}^2)[\,f_q(x,q^2)D_q^h(z)-f_{\bar q}(x,q^2)D_{\bar q}^h(z)]}{\sum_q(F_{LL}^2+F_{LR}^2)[\,f_q(x,q^2)D_q^h(z)+f_{\bar q}(x,q^2)D_{\bar q}^h(z)]}. \qquad (17)$$

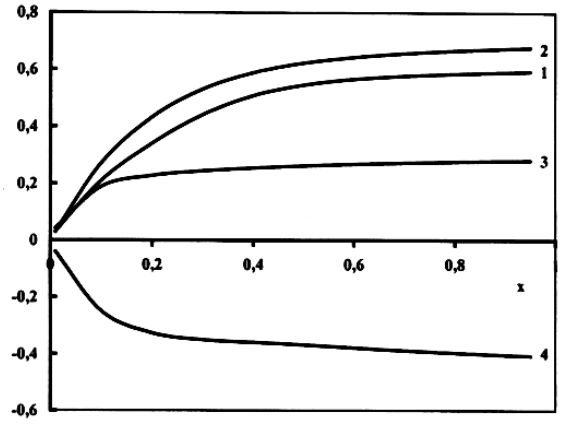

*Fig. 2.*Dependence of the left-right asymmetries $A(e_L^- - e_R^+)$, $A(e_R^- - e_L^+)$, $A^{(-)}(e_L^- - e_R^-)$, $A^{(+)}(e_L^+ - e_R^+)$ y=0,7.

4. The expressions of observed values have the phenomenological parameters that are quark and antiquark distribution functions in the polarized nucleons, values of which are defined by the experiment. In references [10-14] there are the assembages of quark distribution functions in adrons. For numerical estimates of the electroweak asymmetries we used the distribution functions of the valence and sea polarized quarks (antiquark) in nucleons given in [14].

We presented the numerical calculations of electroweak asymmetries (10)-(16) in the case of π - mezon electrocreation $e^{\mp}p\to e^{\mp}\pi X$ at $\sqrt{s}=300$ Gev (*ep*-collider HERA), x_w=0.232. The quark fragmentation function in π mezon is parametrized in the form $D_q^{\pi}(z)=N\dfrac{(1-z)^n}{z}$, where *N* and *n* are constant. It is supposed that strange quark and antiquark part in the fragmentation process in π - mezons is a small one. In dependences of left-right asymmetries $A(e_L^- - e_R^+)$, $A(e_R^- - e_L^+)$, $A^{(-)}(e_L^- - e_R^-)$,

$A^{(+)}(e_L^+ - e_R^+)$ and the charge asymmetries C_{RR}, C_{LL}, C_{RL}, C_{LR} on a variable x at the fixed value y=0,7 is given on the figures 2 and 3. As it is seen, the left-right asymmetries $A(e_L^- - e_R^+)$, $A(e_R^- - e_L^+)$, $A^{(-)}(e_L^- - e_R^-)$ and the charge asymmetries C_{RR}, C_{LL} increase monotonously with increase of X, and the asymmetries $A^{(+)}(e_L^+ - e_R^+)$, C_{RL} and C_{LR} decrease monotonously.

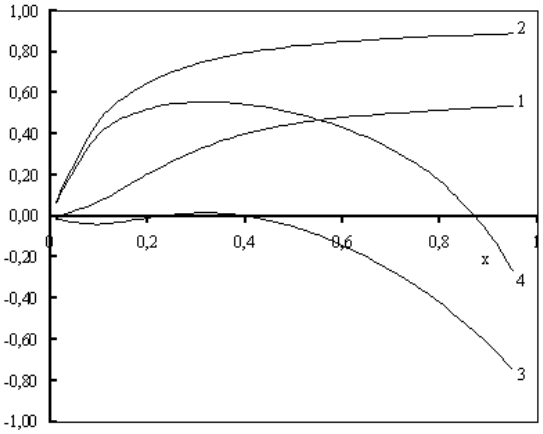

Fig. 3. Dependence of charging asymmetries C_{RR}, C_{LL}, C_{RL}, C_{LR} (curves 1, 2, 3 and 4 accordingly) from variable x at y=0,7.

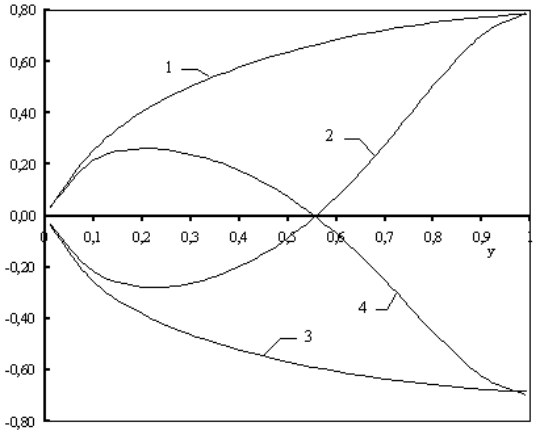

Fig.4. Dependence of charge-polarizing asymmetries $B_p^{(-)}$, $B_a^{(-)}$, $B_p^{(+)}$ and $B_a^{(+)}$ (curves 1, 2, 3 and 4 correspondingly) on variable y at x=0,5.

The analogous behaviour of asymmetries is observed for its y-dependences at fixed x (see fig. 4), where the dependence of charge-polarization asymmetries $B_p^{(\mp)}$ and $B_a^{(\mp)}$ on y at x=0.5 is presented.

[1] *S. Weinberg*. Phys. Rev. Lett. 1967, 19, 1264.
A. *Salam.* Elementary Particle Theory, Stockholm, 1968, p. 367.
[2] *Lampe, E. Reya*. Phys. Reports. 2000, 332**,** 1.
[3] *K. Askerstaff et al*. Phys. Lett. B404, 1997, 383.
[4] *K. Abe et al*. Phys. Rev. Lett. 1995, **75**, 25.
[5] *P.L. Antony et al*. Phys. Rev. Lett. D54, 1996, 6620.
[6] *K. Abe et al.* Phys. Rev. Lett. 1997, 79, 26.
[7] *S.K. Abdullayev*. Ya.F, 1995, 58, 695.
[8] *S.K. Abdullayev*. Ya.F, 1995, 58, 1460.
[9] *S.K. Abdullayev, A.I. Mukhtarov*. E.Ch.A.Ya., 1995, 26, 1264.
[10] *H.Y. Cheng, S.N. Lai*. Phys. Rev., D41, 1990, 91.
[11] *A.D. Martin, W.I. Striling, R.G. Roberts*. Phys. Rev., D50, 1994, 6734.
[12] *A.D. Martin, W.I. Striling.* Phys. Rev., D51, 1995, 4756.

S.K. Abdullayev, A.İ. Muxtarov, M.Ş. Qocayev

YARIMİNKLYUZİV $l^{\mp}N \to l^{\mp}hX$ PROSESLƏRİNDƏ ZƏİF NEYTRAL CƏRƏYAN EFFEKTLƏRİ

Standart və kvant-parton modelləri çərçivəsində polyarizə olunmuş elektronların polyarizə olunmuş nuklonlardan dərin qeyri-elastiki səpilmə proseslərində elektrozəif asimmetriyalar tədqiq edilmişdir. Sağ-sol, polyarizasiya, yük və yük-polyarizasiya asimmetriyaları üçün ifadələr alınmışdır.

С.К. Абдуллаев, А.И. Мухтаров, М.Ш. Годжаев

ЭФФЕКТЫ СЛАБЫХ НЕЙТРАЛЬНЫХ ТОКОВ В ПОЛУИНКЛЮЗИВНЫХ $l^{\mp}N \to l^{\mp}hX$ РЕАКЦИЯХ

В рамках стандартной теории и кварк-партонной модели проведено исследование электрослабых асимметрий в глубоконеупругом рассеянии поляризованных лептонов на поляризованных нуклонах. Получены выражения для лево-правых, поляризованных, зарядово-поляризационных и зарядовых асимметрий.

Received: 27.03.03

İKİ PYEZOELEMENTLİ PYEZOELEKTROMEXANOTRON HƏRƏKƏT ÇEVİRİCİSİNİN YARADILMASININ XÜSUSİYYƏTLƏRİ

N.E. HÜSEYNOV
Azərbaycan Texniki Universiteti
370073, H.Cavid küçəsi, 25

Bu işdə təklif olunan iki pyezoelementli PEMHÇ-nin xarakteristikalarının eksperimental tədqiqinin nəticələri verilmişdir.

Disk formasında pyezoelementlərdən istifadə etməklə hazırlanmış iki pyezoelementli pyezoelektromexanotron hərəkət çeviricisinin (PEMHÇ) işinin keyfiyyətini analiz etmək və parametrlərini uyğunlaşdırmaq üçün onların dinamik xarakteristikalarının öyrənilməsi vacib məsələlərdən biridir [1]. Dinamik xarakteristikalar PEMHÇ-nin konstruksiyasından, pyezoelementin forma və ölçülərindən asılı olaraq dəyişir.

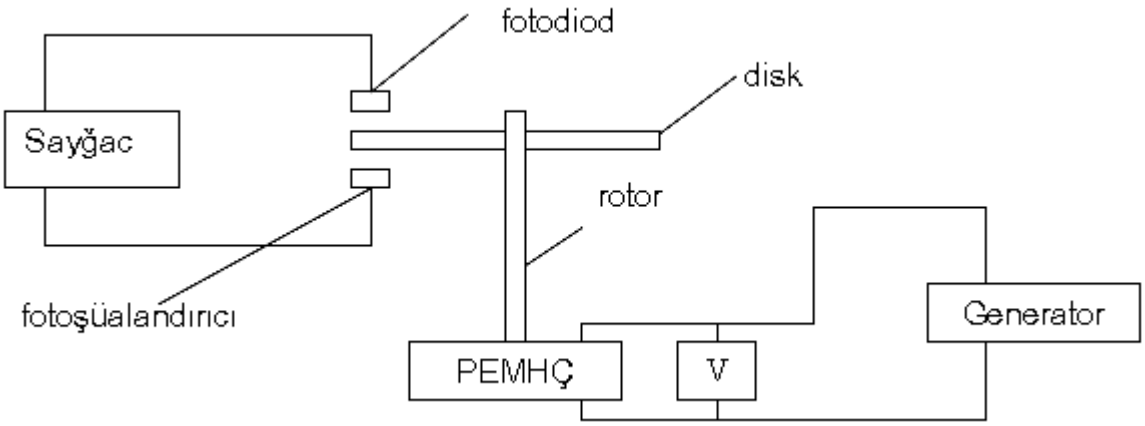

Şəkil 1. PEMHÇ-nin dinamik xarakteristikalarını tədqiq edən qurğunun struktur sxemi.

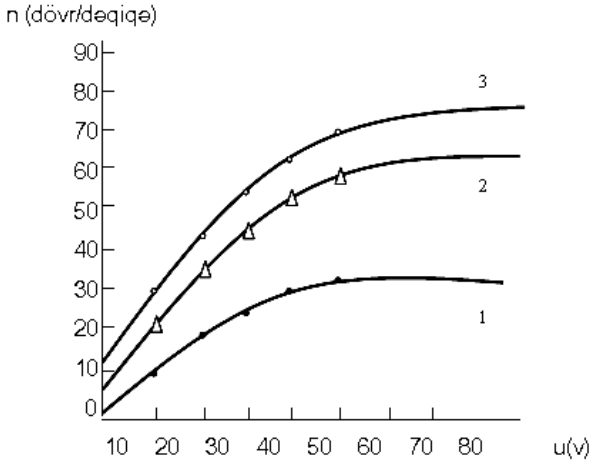

Şəkil 2. Rezonans tezliyində (f_r) müxtəlif mexaniki keyfiyyətliliyə malik pyezoelementlərdən hazırlanmış PEHMÇ-nin dinamik xarakteristikaları ($n=f(u)$). 1.Qm=200(*STQ*-24m); 2.Q_m=500(*STQ*-24); 3.Q=600(*STQ*-35).

Tədqiqat dəqiqliyini artırmaq üçün əvvəlcə müxtəlif mexaniki keyfiyyətlilik (Q) əmsallarına malik sirkonat-titan-qurğuşun (*STQ*) ailəsindən olan və eyni ölçülü pyezoelementlərdən təşkil edilmiş disk (dairəvi) formasında bir pyezoelementli PEMHÇ-nin dinamiki xarakteristikalarını, məsələn, onun rotorunun dövrlər sayının (n) pyezoelementə verilən gərginlikdən asılılığını öyrənək. Bunun üçün şəkil 1-də göstərilən qurğudan istifadə olunmuşdur. Qurğunun iş prinsipi aşağıdakı kimidir. Generatordan tezliyi PEMHÇ-nin rezonans tezliyinə bərabər gərginlik verilir. PEMHÇ-nin rotoruna bir nöqtədən deşiyi olan disk bərkidilmişdir. Diskdəki deşiyə uyğun nöqtədə diskin bir tərəfindən fotoşüalandırıcı, digər tərəfindən isə fotoqəbuledici diod deşiyin oxu üzərində qarşı-qarşıya quraşdırılmışdır. PEMHÇ-ə generatordan müəyyən amplitudlu gərginlik verildikdə PEMHÇ-nin rotoru fırlanmağa başlayır. Rotora bərkidilmiş disk fırlandıqda, deşik olan hissə fotodiodun qarşısından keçdikdə sayğac bir impuls qəbul edir, bu isə rotorun bir dövr etməsi deməkdir. Nəticədə böyük dəqiqliklə PEMHÇ-nin rotorunun bir saniyədəki dövrlər sayı qeyd olunur. Müxtəlif mexaniki keyfiyyətliliyə malik pyezoelementlər üzərində qurulmuş bir elementli PEMHÇ-nin rotorunun dövrlər sayının (n) pyezoelementə verilmiş gərginlikdən (u) asılılığı şəkil 2-də göstərilmişdir. Şəkildən görünür ki, pyezoelementə verilən gərginlik (u) artdıqca n əvvəlcə artır və sonra isə stabilləşir.

Şəkil 3-də verilmiş sabit gərginlikdə ($u=const$) və rezonans tezliyində $n=f(u)$ asılılığın stabil hissəsi üçün n-nin Q-dən dəyişməsi verilmişdir. Göründüyü kimi mexaniki keyfiyyətliliyi yüksək olan pyezoelementdən ibarət PEMHÇ-nin dinamiki xarakteristikaları daha yuksəkdir. Mexaniki keyfiyyətlilik yüksəldikcə n-nin artması qeyri-xəttidir.

İndi isə iki pyezoelementli PEMHÇ-nin xarakteristikalarının tədqiqinə nəzər yetirək. Bu halda aşağıdakı

şərtlər daxilində tədqiqat aparılmışdır: 1)pyezoelementlərin rezonans tezliyi bir-birindən fərqlidir ($f_{r1} \neq f_{r2}$), amma onların mexaniki keyfiyyət əmsalları bərabərdir ($Q_{m1}=Q_{m2}$); 2)pyezoelementlərin rezonans tezlikləri bərabər ($f_{r1} = f_{r2}$), amma onların mexaniki keyfiyyət əmsalları müxtəlifdir ($Q_{m1}\neq Q_{m2}$). Birinci halda iki pyezoelementli PEMHÇ-i üçün iki ədəd generator tələb olunur. İki pyezoelementli PEMHÇ-nin iki ədəd generatordan istifadə etməklə çıxarılmış dinamiki xarakteristikası şəkil 4-də göstərilmişdir. Hər iki pyezoelementin qidalanması üçün generatordan 80V qədər gərginlik verilmişdir. Şəkildən göründüyü kimi 2-ci əyri 1-ci əyriyə nisbətən daha yaxşı dinamiki parametrlərə uyğundur və rotorun dövrlər sayı u=50V-a kimi xətti artır.

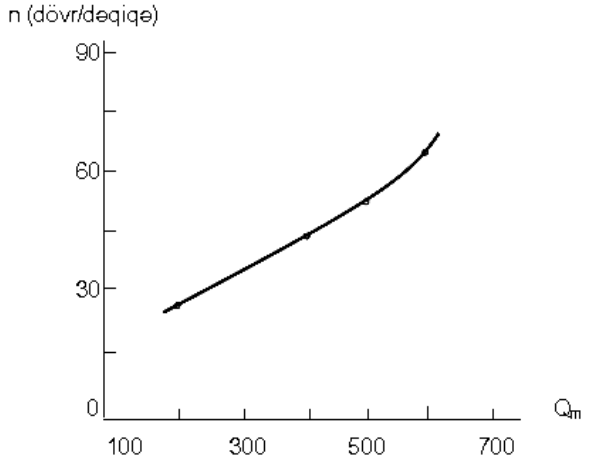

Şəkil 3. PEMHÇ-nin rotorunun dövrlər sayının (n) pyezoelementin mexaniki keyfiyyətlilik əmsalından (Q) asılılığı ($n=f(Q)$). u=50V.

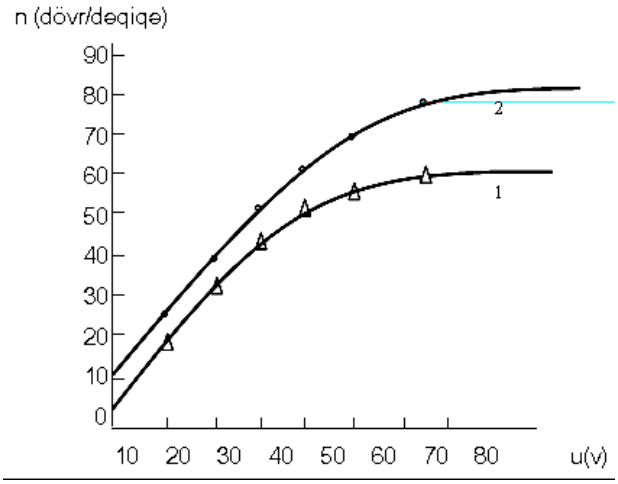

Şəkil 4. İki pyezoelementli PEMHÇ-nin rotorunun dövrlər sayının (n) pyezoelementlərə tətbiq olunmuş gərginlikdən asılılığı ($n=f(u)$). 1. Birinci elementə f_{r1}-də verilmiş gərginlik 70 V-a qədər dəyişdirilir. Q_{m1}=200; 2.elementlər ardıcıl birləşdirilir və $f_{r1}>f_{r2}$; $Q_{m1}=Q_{m2}$=200; $l_1< l_2$; elementlərə verilmiş gərgin lik 70V-a qədər artırılıb.

Məlumdur ki, sütun şəkilli çeviricilər üçün mexaniki rezonansın şərti və rezonans tezliyi (f_r) uyğun olaraq belə təyin olunur [2,3].

$$l = \frac{C^E}{4f_r} \quad \text{və} \quad f_r = \frac{C^E}{4l}, \qquad (1)$$

Burada l – sütun şəkilli pyezoelementin uzunluğu, C – elastik moduldur. (1)-dən görünür ki, pyezoelementin elastik modulu və mexaniki keyfiyyətliliyi eyni olduqda, yəni $C_1 = C_2$ və $Q_{1r}=Q_{2r}$, f_r – artdıqca elementin uzunluğu (l) azalır və bu da əks pyezoelektrik rejimində pyezoelementin ümumi deformasiyasının (Δl) azalmasına və PEMHÇ-nin rotorunun fırlanma sürətinin kiçilməsinə səbəb olar. Digər tərəfdən məlumdur ki, pyezoelementlərin mexaniki keyfiyyətliliyi (Q_m) artdıqca onun rezonans tezliyi (f_r) azalır [2,3,4], yəni

$$Q = \frac{1}{2\pi f_r c_k R_k} \quad . \qquad (2)$$

Burada C_k – pyezoelementin deformasiya etmək qabiliyyətidir; R_k – rezonans müqavimətidir.

(2) - dən görünür ki, mexaniki keyfiyyətliliyi böyük olan pyezoelementlərin rezonans tezliyindəki elektrik müqaviməti kiçik olur, bu da pyezoelementin verilmiş elektrik gərginliyində (tərs pyezoelektrik rejimində) böyük mexaniki enerjiyə malik olmasını göstərir. Pyezoelektrik keramik materialların domen strukturuna malik olması mexaniki rəqslər zamanı onlarda güclü enerji itkilərinə səbəb olur və mexaniki keyfiyyətlilik (Q_m) azalır. Ona görə də pyezoelementlər arasında qurulmuş pyezorezonatorlar adətən xətti elastik sistem rejimində (yəni Huk qanunu çərçivəsində) işləməlidir.Əgər PEMHÇ-ə pyezorezonator kimi baxsaq, onda onun rotorunun fırlanma sürətinin verilmiş gərginlikdən asılılığın ($n=f(u)$) qeyri-xəttliliyini pyezoelementdəki enerji itkilərilə əlaqələndirmək olar. Ona görə də $n=f(u)$ asılılığın düzxəttli hissəsinin genişliyi PEMHÇ üçün böyük əhəmiyyət kəsb edir və rotorun fırlanma sürətini böyük miqyasda tənzim etməyə imkan verir.

Yuxarıda qeyd etdik ki, PEMHÇ-də pyezoelementlərin uzunluğu f_r ilə, n isə Q ilə sıx əlaqədədirlər. Uzunluğun kiçik götürülməsi rezonans zamanı pyezoelementin rəqs amplitudunun (Δl) azalması ilə nəticələndiyi üçün f_r elə seçirlər ki, Δl kəskin azalmasın. Lakin pyezoelementin uzunluğunun böyük götürülməsi də texnoloji (polyarizasiya) və elektrik parametrləri (böyük tutum müqaviməti və kiçik elektrik tutumu) baxımında pisləşmə ilə nəticələnir. Ona görə də şəkil 1-də göstərilən PEMHÇ pyezorezonatoru iki elementli seksiyadan ibarətdir. Pyezoelementlərin birləşdirilməsindən asılı olaraq pyezorezonatorun mexaniki keyfiyyətliliyini dəyişmək olar. Məsələn, ardıcıl birləşdirilmiş pyezoelementlərdən ibarət pyezorezonatorun ümumi mexaniki keyfiyyətliliyi ($Q_{üm.}$)

$$\frac{1}{Q_{üm.}} = \frac{1}{Q_{m1}} + \frac{1}{Q_{m2}}$$

kimi təyin oluna bilər. Bizim halda: Q_{m1}=500 və Q_{m2}=600 pyezoelementlərdən ibarət pyezorezonator üçün

$$Q_{üm.} = \frac{Q_{m1} \cdot Q_{m2}}{Q_{m1} + Q_{m2}} \approx 300$$

olacaqdır. Eksperimentlər göstərir ki, pyezoelementlərin *Q, l* və f_r parametrlərini tənzim etməklə PEMHÇ-dəki pyezorezonatorun rejimini elə seçmək olar ki, *n=f(u)* asılılığın düzxəttli oblastı daha çox genişlənsin (şəkil 5).

Şəkildən görünür ki, Q_{m1}=500 olan pyezorezonatorun *n=f(u)* xarakteristikasının düzxəttli oblastı təqribən 42V (əyri 1), Q_{m2}=600 olan pyezorezonatorun *n=f(u)* xarakteristikasının düzxəttli hissəsi 50V (əyri 2) və bu pyezoelement ardıcıl birləşdirilməsi nəticəsində alınan PEMHÇ-nin *n=f(u)* xarakteristikasının isə düzxəttli hissəsi 70V-a qədərdir. Şəkildən görünür ki, ardıcıl birləşmiş iki pyezoelementli PEMHÇ-nin müəyyən gərginliklərdə rotorun dövrlər sayı da yüksəkdir. Beləliklə, pyezorezonatorlardan ibarət PEMHÇ-nin dinamiki xarakteristikasını onun təşkil olunduğu pyezoelementlərin f_r, *Q* və həndəsi ölçülərini dəyişməklə tənzim etmək olar.

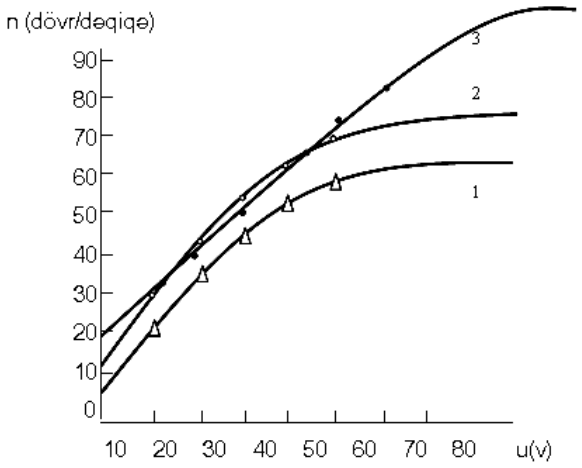

Şəkil 5. *n=f(u)* asılılığı. 1.Q_{m1}=500; 2. Q_{m2}=600; 3. elementlər ardıcıl birləşdirilir; $f_{r1}=f_{r2}$. Pyezoelementlərə verilmiş gərginlik 70V-a qədər artırılıb.

[1] *A.A. Erofeev*. Piyezoelektronnıye ustroystva avtomatiki. L.Maşinostroyeniye, 1982, 211s.

[2] *B.S. Aronov*. Elektromexaniçeskiye preobrazovateli iz piyezoelektriçeskoy keramiki. L. Enerqoatomizdat, 1990.

[3] Ultrazvukovıye preobrazovateli. pod red.*E.Kikuçi*, M.Mir, 1972, 424s.

[4] Piyezokeramiçeskiye preobrazovateli: Spravoçnik pod red. *S.İ.Puqaçeva*, L.Sudostroyeniye, 1984, 256s.

N.E. Huseynov

THE PECULIARITIES OF CREATION OF TWOPIEZOELEMENT PIEZOELEKTROMECHANOTRON ACTION TRANSISTOR

Here is presented results of investigation on expantion of the linear area of dependence of the number of turns on voltage *n=f(u)* of twopiezoelement piezoelektromechanotron action transistor.

Н.Э. Гусейнов

ОСОБЕННОСТИ СОЗДАНИЯ ДВУХПЬЕЗОЭЛЕМЕНТНОГО ПЬЕЗОЭЛЕКТРОМЕХАНОТРОННОГО ПРЕОБРАЗОВАТЕЛЯ

Представляются результаты исследования по расширению линейного участка зависимости числа оборотов ротора от напряжения (*n=f(u)*) двухпьезоэлементного пьезоэлектромеханотронного преобразователя движения.

Received: 27.03.03

THE STRUCTURE OF THE SHORT-RANGE ORDER OF THE AMORPHOUS $TlInSe_2$

D.I. ISMAILOV, E.A. ALAKBAROVA, F.I. ALIYEV
Institute of Physics, Azerbaijan National Academy of Sciences,
Baku. Az - 1143, H. Javid av. 33

The short-range order in thin amorphous $TlInSe_2$ films has been investigated. The curves of radial distribution of atoms in the amorphous $TlInSe_2$ films are constructed on the base of the integral analysis of the fast electrons scattering intensity and the parameters of the short-range order: the radii of the coordination spheres and numbers of the nearest neighbor have been determined.

According to data [1,2] in the Tl-In-Se system the triple $TlInSe_2$ compound having the effective photo and strain sensitive semiconductive properties, has been revealed. Electron diffraction research [3] of the phase content of the $TlInSe_2$ films, obtained by the simultaneous and consequent vacuum settling of Tl, In, Se at room temperature, shows the formation of the $TlInSe_2$ compound with the structure of TlSe type, the Tl-In-Se films are amorphous irrespective to the order of the components settling.

Fig. 1. Electron diffraction photograph from amorphous $TlInSe_2$ films.

The purpose of the present paper is to determine the short-range order parameters of amorphous $TlInSe_2$, obtained from the vapor phase. The amorphous $TlInSe_2$ films of the thickness ~200Å have been obtained by the evaporation in the vacuum from the tugsten furnace on the NaCl substrate and celluloid at room temperature, the settling velocity was ~20Å/Sec. The obtained amorphous films are characterized by the diffraction figures (fig.1), on which the diffusion lines corresponding to $S=4\pi\cdot\sin\theta/\lambda=2{,}00$Å; 3,39Å and 5,04Å are well seen. These data coincide with the data, obtained before [3]. The subsequent crystallization of these films at ~170ºC leads to the $TlInSe_2$ crystal formation with the known parameters of the tetragonal lattice $a=8{,}075$Å, $c=6{,}847$Å [4].

The curve of the experimental intensity has been obtained on the PC, conjugated to the electronograph *ER*-102. The curve of the radial distribution of atoms (*CRDA*) of amorphous $TlInSe_2$, is presented on fig.2. The curve contains three, obviously expressed maximums at $r_1=2{,}70$Å, $r_2=3{,}68$Å and $r_3=4{,}25$Å. The areas under the corresponding maximums are equal to $\Delta=28{,}4$, $\Delta=31{,}2$ and $\Delta=67{,}6$, respectively.

The distance $r_1=2{,}70$Å may be interpreted as average from the distance between In-Se and Tl-Se atoms, the tetrahedral covalent radii are, according to [6], equal to 1,47Å for thallium, 1,17Å for selenium and 1,44Å for indium. The calculation of the area value under the first peak gives the value Δ=25,9, what coincides with the corresponding experimental data of the interatomic distance in $TlInSe_2$.

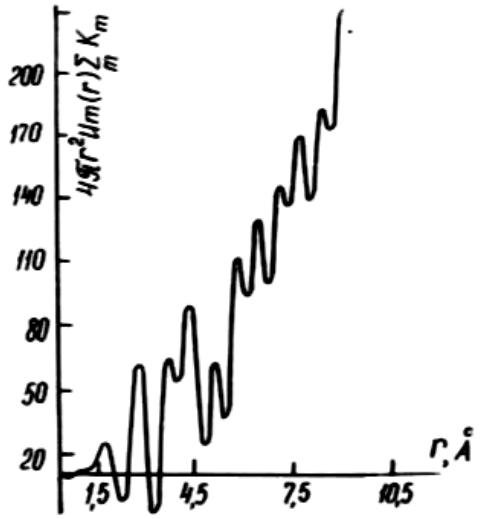

Fig. 2. The curve of the radial distribution of atoms in amorphous $TlInSe_2$ films.

The second coordination sphere with $r_2=3{,}68$Å may be interpreted as average of the distances In-Se and Tl-Se. There are Tl-Se distances approximately equal to r_2 in the crystal lattice of $TlInSe_2$. These distances are more than the sum of the octahedral covalent radii of Tl(In) and selenium atoms, as the sum in the case of Tl-Se is equal to 1,73Å+1,40Å=3,13Å and In-Se1,53Å+1,40Å=2,93Å. The calculation of the area value under the second peak of $TlInSe_2$, *CRDA* gives the value Δ-39,0. It is possible to explain by the fact, that obviously, in the second coordination sphere the Tl-Se distance is more possible, than that of In-Se. The distance $r_3=4{,}25$Å corresponds to the distance between same-named atoms Se-Se, Tl-Tl, In-In.

There are the same distances in the crystal lattice $TlInSe_2$, in consequence of what unlike the double structural and crystallochemical analog of the $A^2B^4C^5_2$ semiconductors, in which atoms of the IV group have undeformed tetrahedral anions [6], in compounds $A^3B^3C^6_2$, whose representative is $TlInSe_2$, analogous tetrahedrons of which are deformed. Beside the tetrahedrons deformation the specific deformation of octahedrons is observed in amorphous films $TlInSe_2$.

Possibly, it is connected to the fact, that in amorphous films $TlInSe_2$ the connection between particles is provided not only by the electrostatistic attraction of the opposite ions, but by the combination with the intermediate valence.

It has been shown by the research of the amorphous phases of the compound Ti-Se and Tl-S, that in amorphous phases of the compounds with the TlSe structure $n_{Se,\ Se}$=6, and $n_{Tl,\ Tl}$=4. It is possible to assume, that $n_{In,\ In}$ is equal to 4. Then the calculation of the area value under the corresponding peak gives the value Δ=67,3, what almost coincides with Δ_3=67,6.

Thus, it is possible to make a conclusion:

- The short-range order in the amorphous and crystal phases of $TlInSe_2$ are close and the structural elements of the crystal phase are conserved in amorphous films.

[1] *G.D. Huseynov, G.B. Abdullayev, E.M. Gojayev, et.al.* Constitutional diagram and physical properties of TlSe-InSe pseudo-binary system. Mater. Res. Bull. 1972, v.7, №12, p.1497-1503.

[2] *M.B. Babanli, A.N. Mamedov, A.A. Kuliyev.* Jurnal "Fiz. Khimiya" 1976, v.50, №7, p. 1888-1889.

[3] *D.I.Ismayilov,F.I. Aliyev, R.M.Sultanov, R.B.Shafi-zade.* Neorganicheskiye materiali, 1999, v.27, №3, p. 474-476

[4] *D. Muller, G. Eulenberger, H. Hahn*. Z. Anorg. allgem.chem., 1973, Bd 398, S. 207-220

[5] *B.K. Vainshtein, V.M. Fridkin, V.L. Inderbom.* Sovremennaya kristallographiya M. Nauka, 1979, v.2, p. 359

[6] *N.A. Goryunova, Y.A. Valov*. Poluprovodniki $A^{II}B^{IV}C_2^{V}$. M. Sov.radio.1974, p.376.

[7] *D.I. Ismayilov, M.F. Aliyeva*. Fizika, 1996, v.2, №2, p.43-45.

C.İ. İsmayılov, E.Ə. Ələkbərova, F.İ. Əliyev

AMORF $TlInSe_2$ TƏBƏQƏLƏRİNDƏ YAXIN NİZAM QURULUŞU

$TlInSe_2$ nazik amorf təbəqələrinin yaxın nizam quruluşu tədqiq edilmişdir. Sürətli elektronların səpilmə intensivliklərinin inteqral analizi əsasında atomların radial paylanma əyriləri qurularaq yaxın nizam parametrləri koordinasiya sferalarının radiusları və yaxın qonşuluqdakı atomların sayı - koordinasiya ədədləri təyin olunmuşdur.

Д.И. Исмаилов, Э.А. Алекберова, Ф.И. Алиев

СТРУКТУРА БЛИЖНЕГО ПОРЯДКА АМОРФНЫХ ПЛЕНОК $TlInSe_2$

Исследован ближний порядок в тонких аморфных пленках состава $TlInSe_2$. На основе интегрального анализа интенсивности рассеяния быстрых электронов построены кривые радиального распределения атомов в аморфных пленках соединения $TlInSe_2$ и определены параметры ближнего порядка: радиусы координационных сфер и числа ближайщих соседей.

Received: 28.03.03

MEMORY EFFECT IN FERROELECTRIC - SEMICONDUCTOR WITH IN COMMENSURATE PHASE OF $TlGaSe_2$

V.P. ALIYEV, S.S. BABAYEV, T.G. MAMMADOV, MIR-HASAN YU. SEYIDOV, M.M. SHIRINOV

Institute of Physics, Azerbaijan National Academy of Sciences,
Baku. Az - 1143, H. Javid av. 33

R.A. SULEYMANOV

Baku State University
Z. Khalilov st., 23, Baku, 370143

The paper is devoted to the research of the non-equilibrium properties of the incommensurate (INC) phase of the improper ferroelectric-semiconductor $TlGaSe_2$. The influence of the prehistory of the heat treating of the crystal, i. e. annealing at the fixed, stabilized temperature in the region of INC- phase on the dielectric constant (ε) behavior of the sample in the vicinity of the phase transition (PT) – INC phase – the commensurate (C) ferroelectric phase studied. The peculiar case of the memory effect realization leading to the temperature range change of the INC-phase existence is observed for the first time in $TlGaSe_2$.

INTRODUCTION

The layered crystal $TlGaSe_2$ belongs to the ferroelectrics-semiconductors group and attracts attention by its unusual dielectric [1], elastic [2, 3], thermodynamic [4-6], optical [7, 8] and other properties near the structural PT. In the paraelectric phase $TlGaSe_2$ is a monoclinic crystal with the space group (SG) of the symmetry C_{2h}^6 [9]. The X-ray investigations [10] have revealed the formation of the several polytypes of the monoclinic modification (C_2^2, C_s^4, C_{2h}^2) of $TlGaSe_2$. To the present time it has been experimentally shown, that the $TlGaSe_2$ polytype with SG in the paraphase C_{2h}^6 suffers the consequence of the structural PT with temperature decrease at the atmosphere pressure [11]. At T_i~116K the second order PT realizes from the high-temperature paraelectric phase into INC-phase, and the first order PT from the INC-phase into the improper ferroelectric C-phase, T_c≈106K, accompanied by the quadrupling of the crystallographic axis $\vec{c}$. In the polar phase the spontaneous polarization vector is placed on the layer plane. The modulated structure of the INC-phase is caused by the soft mode condensation near the Brillouin zone edge with the wave vector $\vec{k}_i = (\delta, \delta, 0.25)$, where δ is the incommensurable parameter. In spite of numerous attempts the symmetry of the low-temperature polar phase and the temperature dependence of δ in the INC-phase region have not been established up to the present time.

It was shown in [7, 8, 12-15], that the temperature behavior of some physical parameters of $TlGaSe_2$ demonstrates the strong sensitivity to the thermocyclization due to which the physical properties of $TlGaSe_2$ are ambiguous and depend on the sample prehistory. The impurity and defect states in $TlGaSe_2$ and their influence on PT and physical properties of this crystal have not yet been revealed.

In the present work we describe for the first time the anomalous memory effect in $TlGaSe_2$ demonstrated itself on the curve $\varepsilon(T)$ in the C-phase near T_c as a result of the annealing of the sample at the fixed temperature in the INC-phase region.

SAMPLES AND EXPERIMENT METHODS

The $TlGaSe_2$ sample in the form of the plane-parallel plate of the sizes *3,3x4x4 mm*^{3}, cut out from the monocrystal ingot grown by the modified Bridgeman-Stockberger method was used. Electrical contacts were provided by application of Ag-paste to the working surfaces of the crystal. Measurements of $\varepsilon(T)$ have been conducted in a quasi-static regime with the temperature change velocity 0,5 K/min far from and 0,1 K/min near T_c by the application of the alternating current bridge at the frequency 50 KHz. The sample has been in the thermostatic chamber of the cryostat during the measurement. The temperature has been measured by the platinum thermometer. The stabilization precision of the temperature has not been worse than $\pm$ *0,01K*.

The following measurement procedure has been applied. At first the sample has been cooled up to the liquid nitrogen temperature and kept at this temperature during 30 min. This condition provides the disappearance of the initial non-equilibrium states in the C-phase. Then in the smooth temperature change regime the sample has been heated up to the given temperature in the region of the INC-phase and kept (annealed) at this temperature during an hour and cooled again up to the liquid nitrogen temperature. The $\varepsilon(T)$ curve has been recorded during the subsequent sample heating up to the thermostabilization temperature. The subsequent $\varepsilon(T)$ measurement cycles have been conducted by the analogous temperature conditions of the experiment. Before the change of the annealing temperature of the sample, the latter has been heated up to the room temperature, then cooled and kept during an hour at the liquid nitrogen temperature.

EXPERIMENTAL RESULTS AND THEIR DISCUSSION

The temperature dependence of ε in $TlGaSe_2$ in wide temperature range, including the structural PT points, has been measured at the sample heating after its cooling from the room temperature is shown in fig.1,a. As it is seen from fig. 1a, the curve $\varepsilon(T)$ is characterized by anomalies in the form of precise maxima at the PT point from the paraelectric

phase to the INC- phase at T_i=114,9K and near PT point from INC-phase to the C - phase at T_c=106,5K. It follows from the measurements, that the $\varepsilon(T)$ dependence in the high-temperature paraelectric phase follows the Curie-Weis law. The Curie constant value and PT temperature values are in good agreement with the existing data [16-18]. The distinct anomaly on the $\varepsilon(T)$ curve from the C-phase side at T=102 K has been revealed in $TlGaSe_2$ sample of the given technological quality (see fig.1a). It has been shown on the example of the layered $TlInS_2$ crystal, isostructural to $TlGaSe_2$, that the similar anomaly is also observed on the $\varepsilon(T)$ dependence below T_c and is connected with the coexistence in the registered temperature range of the polar regions of the C-phase and non-disintegrated parts of the INC-phase modulation wave [19]. It is possible to suppose, that the anomaly below T_c in the $\varepsilon(T)$ curve in $TlGaSe_2$ has the same nature as in $TlInS_2$.

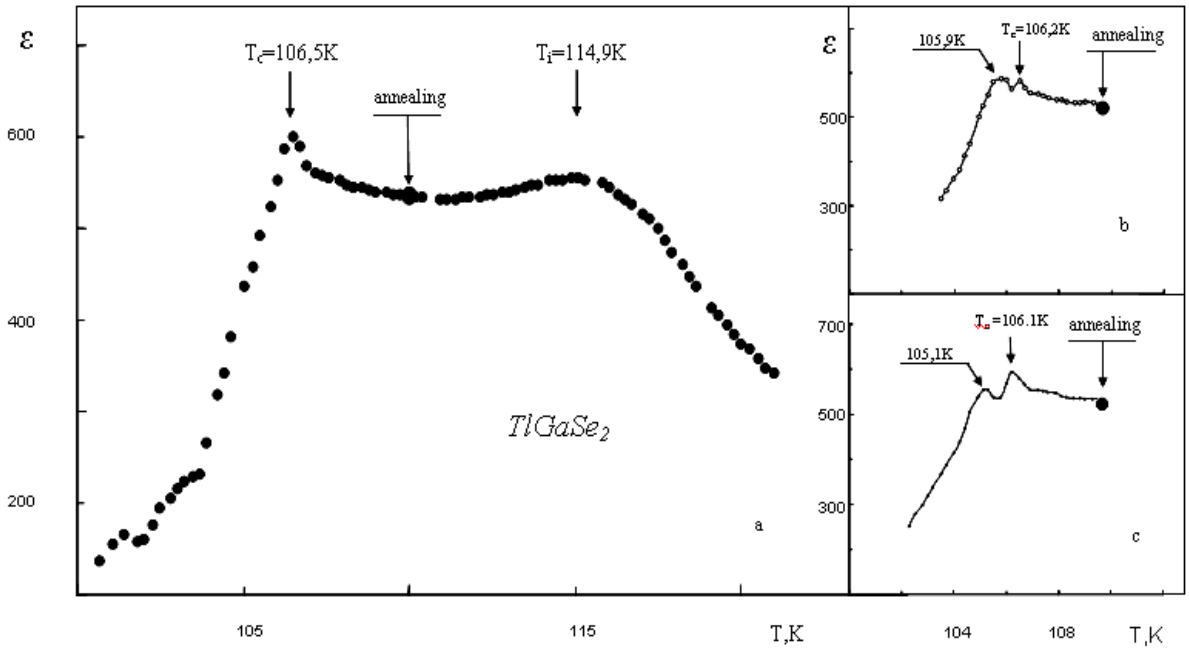

Fig.1. The temperature dependence ε of the layered crystal $TlGaSe_2$, measured at the heating mode after: a) previous cooling of the crystal from the room temperature, b) the four hours annealing of the crystal inside the INC-phase at T_{an} =110K, c) the five hours annealing of the sample inside the INC-phase at T_{an} =110K.

The $\varepsilon(T)$ dependences for $TlGaSe_2$ crystals, obtained at heating process after the crystal annealing in the fourth and fifth times in the INC-phase at T_{an}=110K during an hour are presented in figs. 1b and 1c, respectively. The fact of the extra anomaly appearance on the $\varepsilon(T)$, beginning with the fourth measurement cycle, in the form of the low maximum at T=105,9 K is clearly seen. At the same time temperature stabilization of the sample at T_{an} leads to the shifting of the PT temperature from INC phase to the C phase to the lower temperature side. This shifting for the fourth cycle of annealing is about 0,3K. The fifth annealing cycle does not practically change the T_c, but leads to the shifting of the second maxima from 105,9K to 105,1K.

As it is known [20-23], the annealing of the crystal during the long time within the incommensurate phase leads to the formation of the long-live metastable states, connected with the defects density wave (DDW) which is formed in the crystal, as a resuet of the spatial redistribution of impurities and structural defects in the periodic field of the INC phase. Since the relaxation time of the mobile defects, determined by their diffusion mobility, considerably exceeds the time, required for the measurement of $\varepsilon(T)$ from the ferroelectric phase to T_{an}, it is possible to assume the conservation of DDW (and consequently solitons in the potential relief, created by the impurities and mobile defects) out of the INC-phase region. As it is shown in [24, 25] this peculiarity of INC phase leads to the shifting of the T_c in $TlInS_2$ crystals to the low temperature region.

To explain the appearance of the second peak in $\varepsilon(T)$ dependence of $TlGaSe_2$ after annealing at T_{an} within INC phase one can suppose, that the structure of the real $TlGaSe_2$ crystal is essentially heterogeneous. The fracture of the investigated sample by cleaving has revealed the presence of two qualitatively distinct by its dielectric properties macroscopic parts: $TlGaSe_2$ –I and $TlGaSe_2$ –II. The $\varepsilon(T)$ curves for $TlGaSe_2$ –I (fig. 2a) and $TlGaSe_2$ –II (fig. 2b), obtained at sample heating after its cooling from the room temperature, are presented in fig. 2.

As it is seen from fig.2a, the dependence $\varepsilon(T)$ of the smaller by the size sample $TlGaSe_2$ –I (3,3x1,6x4 mm^3) is qualitatively similar to the initial crystal $\varepsilon(T)$ with T_i=112,8K and T_c=106K. The temperature dependence $\varepsilon(T)$ for the larger by its size sample $TlGaSe_2$ –II (3,3x2,3x4 mm^3) distinguishes essentially from $\varepsilon(T)$ for $TlGaSe_2$–I. As it is seen from fig. 2b, the anomaly, connected with PT to INC – phase occurs at T_i=111,8K and becomes strongly diffused. The temperature T_c, determined from the given experiment for the sample $TlGaSe_2$ –II makes 106,2 K. The fact of the sudden rise of the ε for the sample $TlGaSe_2$ –II beginning from T=107K is connected with the significant growth of the electroconductivity of the indicated part of the sample. It should be noticed, that the multiple annealing of the samples $TlGaSe_2$ –I and $TlGaSe_2$ –II during an hour inside the INC-

phase has not been accompanied by the extra anomaly appearance on the curve $\varepsilon(T)$. At the same time the thermal annealing of the samples within the INC phase leads to low temperature shifting of T_c in $TlGaSe_2$ –II by 1,9K, and 0,4K in $TlGaSe_2$ –I.

Taking into consideration the possible formation of different polytypes of $TlGaSe_2$, it is possible to assume, that

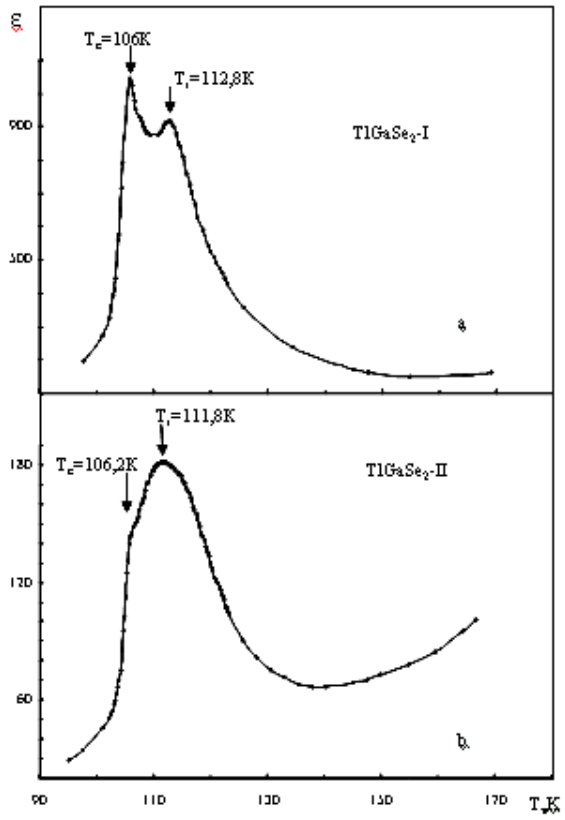

Fig. 2. The temperature dependence ε of the sample parts $TlGaSe_2$, obtained by the consequent spalling: a- $TlGaSe_2$-I; b- $TlGaSe_2$-II. The measurements have been conducted in the heating mode after the previous cooling of both samples from the room temperature.

$TlGaSe_2$ –I and $TlGaSe_2$ –II belong to the various polytypes. However, in this case, $TlGaSe_2$ polytype, whose symmetry of the high-temperature phase is distinguished from C_{2h}^6, should be supposed. The structural research data present in reference [9] testifies the presence of the INC-phase only in polytypes $TlGaSe_2$ with the symmetry of the high-temperature paraphase C_{2h}^6. In papers [18, 26-28] attempts, made to reveal the INC-phase in other modifications of $TlGaSe_2$ by the methods of the neuron diffraction and X-rays, have not been successful.

We suppose, that the concentration of impurities and mobile defects, essentially distinct in the various parts of the sample, has existed in the initial real crystal $TlGaSe_2$ and the part of the initial sample, i.e. $TlGaSe_2$ -II, is characterized by the higher concentration of impurities and structural defects in comparison with $TlGaSe_2$ -I. Therefore, in the initial sample $TlGaSe_2$ the phase transition from the INC-phase to the commensurate ferroelectric phase after a long stay of the sample inside the INC-phase will be realized in two neighboring temperature points, in accordance with the different values of shifting of T_c in different parts of the sample.

CONCLUSION

Thus, in the present paper the results of the qualitatively new case of the memory effect realization- influence of the sample prehistory on the temperature behavior of ε, presented by the extra anomaly appearance in $\varepsilon(T)$ in the neighborhood of INC-C PT point have been for the first time represented in the $TlGaSe_2$ crystal. It is suggested, that in the various parts of the crystal the “frozen” states of defects and impurities with the various concentration, occur after the annealing of the sample in the INC-phase due to the irregular distribution of the impurities and defects existed in the initial sample. Therefore, PT to the commensurate ferroelectric phase in the different parts of the initial sample $TlGaSe_2$, subjected to the thermal annealing in the INC-phase, occurs at various, but close temperatures.

[1] *K.R. Allahverdiyev, N.D. Ahmedzade, T.G. Mammadov, T.S. Mammadov, M-H. Yu. Seyidov*. FNT, 2000, 26, 1, 76.

[2] *Y.V. Ilisavskiy, V.M. Sternin, R.A. Suleymanov, F.M.Salaev, M-H .Yu. Seyidov*. FTT, 1991, 33, 1, 104.

[3] *R.A. Suleymanov, M.-H. Yu. Seyidov, F.M. Salaev*. FTT, 1991, 33, 6, 1797.

[4] *N.A. Abdullayev, K.R. Allahverdiyev, G.L. Belenkiy, T.G. Mammadov, R.A. Suleymanov, Y.N. Sharifov.* DAN Az. SSR, 1985, 41, 12, 21.

[5] *N.A. Abdullayev, T.G. Mammadov, R.A. Suleymanov.* FNT, 2001, 27, 8, 676.

[6] *E.S. Krupnikov, F.Y. Aliyev*. FTT, 1988, 30, 10, 3158.

[7] *K.R. Allakhverdiev, M.A. Aldzanov, T.G. Mammadov, E.Yu. Salaev*. Sol. St.Com., 1986, 58, 5, 295.

[8] *K.R. Allakhverdiev, S.S. Huseynov, T.G. Mammadov, M.M. Tagiyev, M.M.Shirinov*. Izv. AN. SSR. Neorg. Mat., 1986, 25, 11, 1858.

[9] *D. Muller, H. Hahn.* Z. Anorg. allg. chem., 1978, 438, 258.

[10] *S.G. Abdullayev, V.A. Aliyev*. DAN Az.SSR, 1980, 36, 8, 34.

[11] *D.F. McMorrow, R.A. Cowley, P.D. Hatton, J.Banys.* J. Phys: Condens. Matter, 1990, 2, 3699.

[12] *Y. P. Gololobov, S.A. Shilo, I.A. Yurchenko.* UFJ 35, 1990, 11, 1721.

[13] *Y. P. Gololobov, V.M. Perga, I.N. Salivonov, E.E. Shigol*. FTT, 1992, 34, 1, 115.

[14] *N.A. Borovoy, Y. P. Gololobov.* FTT, 1997, 39, 9, 1652.

[15] *Y. P. Gololobov, S.A. Shilo, I.A. Yurchenko*. FTT, 1991, 33, 9, 2781.

[16] *A.K. Abiyev, N.A. Bahishov, A.E. Bahishov, M.S. Gajiyev*. Izv. Vuzov Fizika, 1989, 12, 84.

[17] *R.M. Sardarly, O.A. Samedov, I.Sh. Sadykov, E.I. Mardukhaeva, T.A. Gabibov*. Sol. St. Com., 1991, **77**, 6, 453.

[18] *H.D. Hochheimer, E. Gmelin, W. Bauhofer, Ch. von. Shnering– Schwarz, H.G. von. Shnering, J. Ihringer, W. Appel*. Z. Phys. B. – Condens. Matter., 1988, 73, *2*, 257.

[19] *R.A. Suleymanov, M-H .Yu. Seyidov, F.M.Salaev and F.K.Mikailov* , FTT, 1993, 35**,** *2*, 348.

[20] *J.P. Janet, P. Lederer*. J. Phys. Lett (Paris), 1983, 44, 257.

[21] *L. Folcia, M.J. Tello and J.M. Perez-Mato, J.A. Zubillaga.* Solid State Comm.,1986, 66, 25.
[22] *C.L. Folcia, M.J. Tello and J.M. Perez-Mato*. Physical Review B, 1987, 36, 13, 7181.
[23] *C.L. Folcia, J.M. Perez-Mato and M.J. Tello.* Physical Review B, 1988, 38, *7*, 5055.
[24] *S. Ƶzdemir, R.A. Suleymanov, E. Civan and T. Firat.* Solid State Commun., 1996, 98.
[25] *S. Ƶzdemir, R.A. Suleymanov, K.R. Allakhverdiev, F.A. Mikailov and E. Civan*. Solid State Commun., 1995, 96, 757.
[26] *S.B Bahrushev, B.E. Kvyatkovskiy, N.M. Okuneva, K.R. allahverdiyev, R.M. Sardarli*. Preprint 886, FTI im, A.F. Ioffe, S.-Petersburg, 1984, 12.
[27] *V.A. Aliyev Kristallografiya.* 1990, 35, 2, 506.
[28] *O. Plyush, A.U. Shelet*. Kristallografita, 1999, 44, 5, 873.
[29] *B.S. Kulbishev, S.M. Zaytzev, A.Ch. Malsagov*. Izv. AN. SSR. Neorg. Mater., 1987, 23, 3, 511.

V.P.Alıyev, S.S. Babayev, T.Q. Məmmədov, Mir-Həsən Y.Seyidov, R.A. Süleymanov, M.M. Şirinov

$TlGaSe_2$ KRİSTALININ NİSBƏTLİ SEQNETOELEKTRİK FAZASINDA TERMİK YADDAŞ EFFEKTİ

Məqalədə qeyri-məxsusi seqnetoelektrik $TlGaSe_2$ kristalının nisbətsiz fazasının (NF) qeyri-tarazlıq xassələri tədqiq olunur. Göstərilmişdir ki, kristalın nisbətsiz fazada stabilləşdirilmiş, müəyyən temperaturda saxlanması NF-dan nisbətli seqnetoelektrik fazaya keçidi ətrafında ilk dəfə olaraq NF-nın temperatur intervalının dəyişməsi və seqnetofazada T_c yaxınlığında $\varepsilon(T)$ asılılığında əlavə anomaliyanın əmələ gəlməsi kimi yaddaş effekti müşahidə olunur.

В.П.Алыев, С.С. Бабаев, Т.Г. Мамедов, Мир-Гасан Ю. Сеидов, Р.А. Сулейманов, М.М. Ширинов

ЭФФЕКТ ТЕРМИЧЕСКОЙ ПАМЯТИ В СОРАЗМЕРНОЙ СЕГНЕТОЭЛЕКТРИЧЕСКОЙ ФАЗЕ КРИСТАЛЛА $TlGaSe_2$.

Работа посвящена исследованию неравновесных свойств несоразмерной (НС) фазы несобственного сегнетоэлектрика полупроводника $TlGaSe_2$, а именно, изучению влияния предыстории – температурной выдержки кристалла во времени (отжиг) при определенной, стабилизированной температуре в области НС – фазы – на поведение диэлектрической проницаемости (ε) образца в окрестности фазового перехода (ФП) НС – соразмерная (С) сегнетоэлектрическая фаза. Впервые зарегистрирован своеобразный случай реализации эффекта памяти, сводящийся к изменению температурного интервала существования НС – фазы и к появлению дополнительной аномалии на кривой $\varepsilon(T)$ в сегнетофазе в окрестности T_c.

Received: 06.04.03

THE STUDY OF MAGNETIC-PHAZE STATE OF (Ni, SB, CR, K)/Y·Al_2O_3 CATALYSTS AND ELECTRON PROPERTIES OF PROMOTORS IN PROPAN DEHYDROGENATION REACTION

S.A. JAMALOVA
Institute of petrochemical processes of NAS of Azerbaijan
Baku, N. Rafiyev str., 30

The results of investigation on establishment of the changes in the catalysts magnetic properties depending on the conditions of their synthesis, incineration temperature and duration have been presented in the article for comparison of these properties with the catalysts activity in propane dehydrogenation reaction. The interaction of Ni^{2+} ions with a carrier is established.

The paper deals with the study of (Ni, Sb, Cr, K)/y·Al_2O_3 magnetic-phase state of catalysts and electron properties of promotors with purpose to find out their interaction with the carrier (y·Al_2O_3) in propan dehydrogenation reaction.

From the point if view of catalysts the special meaning has the character of metal oxides and ion distributions on the surface and in the volume of the carrier in the dependence on preparing conditions, thermotreatment of catalysts and the influence of reaction medium on the temperature of magnetic phase transfer in the Neel's point.

To solve these tasks it is necessary to apply magnetic and thermal methods (thermal capacity and temperature conductivity), allowing to study the structures of catalysts. The catalysts samples, taken for analysis are distinguished by the conditions of their preparing.

The catalysts were prepared under conditions of the atmospheric pressure and low atmospheric pressure (P=10-15mm·Hg).

The incineration time was variated from 1.5h to 5h. The incineration temperature was changed from 400°C to 650°C. For investigation of the influence of the dehydrogenation medium on the magnetic characteristics of catalyst, the propan dehydrogenation reaction at the temperature 580-620°C and propan valume velocity of feed 150-300h^{-1} is carried out on these catalysts.

The essential change of porouso-structural catalyst characteristics preparing in the conditions of lowed atmospheric pressure was established by the author earlier and in addition, the influence of these changes on the thermal conductivity and temperature conductivity (K) [1] was established also.

The magnetic permittivity (χ) of catalyst is investigated by Faraday method on the installation with photoelectric compensation [2] in the magnetic field strength interval 1000-7000 Gauss (Gs). The value χ of all investigated catalysts didn't depend on the field strength that shows on the absence of ferromagnetic impurities in the catalyst (metallic nickel). For calculation of χ and magnetic momentum (μ), the correction on the diamagnetism Al_2O_3, Sb_2O_3, K_2O and ions Ni^{2+}, Cr^{3+} was introduced.

The temperature change of magnetic phase transfer in the Neel's point (T_N) in the dependence on incineration temperature of samples was investigated by heat capacity method on the installation for measurements of thermal material coefficients by the impulse – light method [3,4].

The solution of the problem of the thermal distribution inside of the thermal isolated sample, boundered by two parallel is the base of this method.

The increase of the interaction between ions Ni^{2+} in the incinerated samples is confirmed by the increase of Neel's temperature and as a result the change of magnetic interaction energy is observed [5].

It is established by the author earlier, that the increase of incineration temperature of the catalyst up to 600°C increases the exchange interaction between ions Ni^{2+} and rises the catalyst activity [6].

The Bete-Payerlsa-Weissa (BPW) method was used for estimate of the change interaction.

The magnetic interaction energy of non-compensated spins of neighbouring ions at the room temperature is less, than value $kT(E_{magn}<kT)$, where k is Boltzmann constant, therefore the spins oriented almost antyparallelly and antiferromagnetism is observed. However, the energy, which equal to kT_2 is enough one to excite some fluctuations of summary magnetic moment of unpaired spin system. If the temperature is hire that Neel's temperature, then the magnetic interaction energy becomes more, than $kT(E_{magn}>kT)$ and therefore the ferromagnetism is destroyed and the system becomes paramagnetic one.

The changes of the magnetic permittivity (χ), the magnetic moment (μ), the Neel's temperature (T_N) and catalytic activity (Ni-Cr-Sb-K)/Al_2O_3 of the catalysts of the propan dehydrogenation, prepared in the conditions of lowed atmospheric pressure in dependence on the incineration temperature change ($T_{inc.}$) are presented in the fig 1.

With the increase of the incineration temperature from 400 to 650°C, T_N shifts to the high temperatures and increases from 220 to 270°C. The symbat change of T_N and A (activity) in the dependence on $T_{inc.}$ is observed.

The shift of T_N to the high temperature, when $T_{inc.}$ increases, shows that the antiferromagnetic interaction degree between metal ions increases. From another side, the formation process of catalyst structure can take place with the formation of new magnetic phases of types: $NiAl_2O_4$ and $NiSb_2O_6$.

As it follows from fig.1, the $T_{N.}$ and C_3H_6 yield increase with the increase of $T_{inc.}$. The symbat change and activity are caused by the active centers, which are the analogical phases, being in non-antiferromagnetic state. The forming antiferromagnetic phases at the temperature more, than 300-400°C destroy with the increase of incineration temperature. They become paramagnetic at the temperature higher, than T_N. In the internal $T_{inc.}$=580-600°C where the reaction goes, the catalyst will be in the paramagnetic state.

The Neel's temperature states constant and activity decreases at the temperature higher, than 650°C. Probably, it

is caused by the formation of catalyst structure and new antiferromagnetic phases leading to the decrease of paramagnetic centers concentration..

In the fig.1 the dependence of magnetic moment (μ) of catalyst on the incineration temperature is shown. As it follows from fig.1, the increase of the μ with the increase $T_{inc.}$ from 400 to 650°C is observed. In the incineration temperature interval $T_{inc.}$=750°C the essential decrease of the paramagnetic centers concentration is observed. However, in this interval T_N states constant. It shows that with the order of catalyst structure the T_N states unchangeable and the activity decreases.

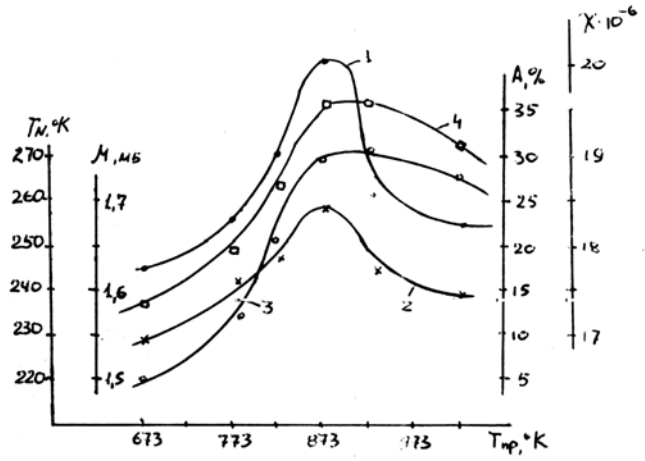

Fig.1. The dependence of magnetic characteristics (χ,μ) of (Ni-Cr-Sb-K)/γ·Al_2O_3 catalyst and Neel's temperature (T_N) on the catalyst incineration temperature ($T_{inc.}$°K)
1. magnetic permittivity (χ);
2. magnetic moment (μ, mB);
3. Neel's temperature (T_N°K);
4. catalyst activity (%mass.).

The decrease catalyst activity connects with the decrease of active catalyst surface in consequence of baking of catalyst poros in this case.

Thus, resuming the above mentioned, we can do the conclusion that the changes of activity and Neel's temperature allow to propose, that active centers in the propan dehydroqenation reaction are caused by the paramagnetic centers, which form at the increase of incineration temperature of catalyst higher, than $T_{N.}$

In the fig.2 the dependences of the magnetic permittivity and catalyst activity (Ni-Cr-Sb-K)/Al_2O_3 on the incineration time are shown. At the increase of the incineration time the magnetic permittivity increases and after 3,5 hours reaches the maximal value. The increase of the paramagnetic permittivity is caused by the increase of paramagnetic centers concentration. Later the decrease of χ value is observed (fig.2, curve 1.2). The identical picture is observed also for the dependence of the activity on the incineration time (fig.2, curve 3). Thus, the comparative date of permittivity and activity show, that catalyst activity is caused by the increase of the paramagnetic centers concentration. At this cause probably, the symbat change of activity and permittivity is observed.

The investigation of magnetic properties NiO-Al_2O_3 of catalyst gives the important information about the ions Ni^{2+} interactions and their localization in a lattice Al_2O_3.

The obtained results of magnetic moments are very interested. We propose, that Ni in the catalyst is as in the microcrystals NiO form, as ion Ni^{2+} form, introduced in a lattice Al_2O_3. As well known, that the theoretical value μ of the ion Ni^{2+} is equal to 3.4 mB in the octahedron empties, but the experimental one is equal to 3.0-3.2mB. The hydrate of protoxide of Ni has the layer structure, in which the every ion is in the octahedron, having six OH-groups.

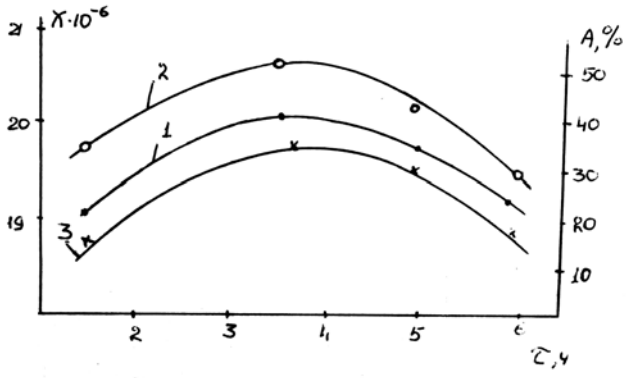

Fig.2. The dependence of magnetic permittivity and activity of (Ni-Cr-Sb-K)/γ·Al_2O_3 catalysts of propan gehydrogenation reaction on the incineration time of catalyst. 1. magnetic permittivity of fresh catalyst;
2. magnetic permittivity of waste catalyst;
3. catalyst activity (%mass.).

The results of the defining of magnetic permittivity (χ), calculated on 1 gr., and the magnetic moment (μ) for (Ni-Cr-Sb-K)/Al_2O_3 catalysts are given in the table 1.

The magnetic permittivity value (χ_{Ni}) of the catalyst, obtained under the usual conditions before the reaction (sample №1) is equal to $55\cdot10^{-6}$SGSE, but the magnetic moment value, calculated on the ion Ni^{2+} is equal to μ=2.81mB, that well agree with μ of ion Ni^{2+} for the pure spin value (2.83mB).

For the catalyst, prepared at the low atmospheric pressure (sample №2) the μ is equal to 3.1mB, that is accordance with μ for Ni^{2+}, being in the octahedron positions (μ=3-3.2mB).

The weak enough interaction between ions Ni^{2+} states constant in the non-incinerated samples of catalyst.

The magnetic properties of the systems (Ni-Cr-Sb-K)/γ·Al_2O_3, prepared at the low atmospheric pressure and incinerated from 400°C to 650°C, differ abruptly from the magnetic properties of catalysts, prepared under the usual conditions (sample №1). The differences are caused by the presence of antiferromagnetic microcrystals NiO. For the catalysts before and after the work in the propan dehydrogenation reaction, the χ_{Ni} and μ change from $16\text{-}22\cdot10^{-6}$ SGSE to 1.53-2.83mB correspondingly. The magnetic moments of samples before and after reaction, and incinerated up to 680C during 5 hours also are essentially less, than the magnetic moment value (μ) of the ion Ni^{2+}/μ=2,83 mB).

The obtained results show, that in the catalyst the big part of NiO is in the form of the large enough crystals of antiferromagnetic phase NiO with strong interaction between Ni ions, that explains the low values of χ_{Ni} and μ.

Table 1.

Magnetic characteristics of (Ni-Cr-Sb-K)/Al_2O_3 catalysts

Sample №	Catalyst composition, %	Treatment conditions (T_c.=650°C)				Makeweight m, mg	f	$A_{av}=\frac{f}{m}$	$\chi\cdot10^{-6}$	μ, mB
		Incineration time	Pressure, mmHg	fresh	waste					
1	NiO – 3 Sb_2O_3 - 3 Cr_2O_3 – 7.5 K_2O – 2.5	5	760	fresh	-	6.6	12.21	1.85	55	2.81
2	- « -	5	15	fresh	-	5.21	13.96	2.68	68	3.11
3	NiO – 6 Sb_2O_3 - 8 Cr_2O_3 – 8 K_2O – 3.0	5	760	fresh	-	2.655	2.86	1.076	21	4.71
4	- « -	5	760	-	waste	6.515	5.798	0.89	16.46	1.53
5	- « -	5	15	fresh	-	5.75	6.38	1.109	21.4	1.79
6	- « -	1.5	15	fresh	-	3.76	3.61	0.96	19.75	1.67
7					waste	8.8	9.06	1.03	21.13	1.73
8	- « -	3.5	15	fresh	-	4.32	4.31	0.997	20.03	1.704
9		3.0		-	waste	6.3	6.34	1.006	20.65	2.23
10	- « -	5.0	15	fresh	-	11.6	12.59	1.085	19.9	1.68
11				-	waste	1.165	1.14	0.98	20.14	2.2

[1] *S.A. Jamalova, O.N. Novruzov, A.A. Gasimov, V.A. Quseinova, M.M. Seidrzayeva.* Fizika, Izvestiya AN Azerb., 1998, №1, p. 40-43.

[2] *A.T. Pilipenko, L.I. Savrinskiy, A.I. Zubenko.* "Koordinatsionnaya khimiya", 1981, v.7, №1, p.25-33.

[3] *D.A. Jogolev, V.B. Volkov.* "Naukovo dumka", Kiev, 1976.

[4] *D.W. Klark, P.S. Hush, J.R. Jandle*. J. Chem. Plys, 1972, v.57, p.3503.

[5] *J.A. Pople, G.A. Segal*. J. Chem. Phys, 1987, v.47, p.158.

[6] *S.A. Jamalova, A.A. Gasimov, O.N. Novruzov, S.A. Zeinalova, Kh.A. Amrakhova.* Fizika, Izvestiya AN Azerb., 1999, №3, p. 72-74.

S.Ə. Camalova

PROPANIN DEHİDROGENLƏŞMƏ REAKSİYASINDA (Ni-Cr-Sb-K)/γ-Al_2O_3 KATALİZATORUNUN MAQNİT FAZA HALININ VƏ PROMOTORLARIN ELEKTRON XASSƏLƏRİNİN ÖYRƏNİLMƏSİ

Məqalədə katalizatorların maqnit xassələrində baş verən dəyişikliklərin onların sintez şəraitdən, közərtmə temperaturundan və müddətindən asılılığını müəyyən etmək üçün, həmçinin, bu xüsusiyyətlərin propanın dehidrogenləşmə reaksiyasında katalizatorların aktivliyi ilə müqayisə məqsədi ilə, çökdürücü ilə Ni^{2+} ionları arasında qarşılıqlı təsir dərəcəsinin müəyyən edilməsi aparılan tədqiqatların nəticəsi əks olunur.

С.А. Джамалова

ИЗУЧЕНИЕ МАГНИТНО-ФАЗОВОГО СОСТОЯНИЯ (Ni-Cr-Sb-K)/ γ-Al_2O_3 КАТАЛИЗАТОРОВ И ЭЛЕКТРОННЫХ СВОЙСТВ ПРОМОТОРОВ В РЕАКЦИИ ДЕГИДРИРОВАНИЯ ПРОПАНА

В статье представлены результаты исследования по выявлению изменений, происходящих в магнитных свойствах катализаторов в зависимости от условий их синтеза, температуры прокалки и ее продолжительности и сопоставление этих свойств с активностью катализаторов в реакции дегидрирования пропана.

Установлена степень взаимодействия ионов Ni^{2+} с носителем.

Received: 05.04.03

MGR INVESTIGATIONS IN $Ga_{0,8}Fe_{0,02}S_6$ CRYSTALS

GEIS SULTANOV, MAZAHIR ALDJANOV, ELMIRA KERIMOVA
Institute of Physics, Azerbaijan Academy of Science,
Baku. Az - 1143, H. Javid st. 33

The magnetic and Mossbauer investigation of GaS:Fe crystals have been carried out. In the temperature region 80÷300 K magnetic susceptibility is found to be weakly dependent on temperature. The value of quadrupole splitting determined from the room-temperature Mossbauer spectrum is equal to ΔE_Q=2.95 ±0.03 mm/s. In GaS:Fe iron is assumed to substitute for gallium and to exist in low-spin divalent state This assumption is confirmed by a good agreement between the experimental and theoretical values of ΔE_Q obtained from the calculation of the $[GaFe^{2+}S_6]^{8-}$ impurity complex electronic structure by the Hukkel's method.

Keywords: Magnetic, susceptibility, quantum, splitting, spectrum.

Introduction

According to crystallographic data [1] GaS has hexagonal structure with space group of $P6_3/mmC$ and lattice parameters: a=3.587Å and c=15.492Å . Because of Ga and S atoms location the crystalline structure of GaS can be presented as alternation of dense packed layers...S-Ga-Ga-S... moreover each atom of Ga us tetraedrically connected with three atoms of S and one atom of Ga, thus R(Ga-S)=2.33Å , R(Ga-Ga)=2.447Å (fig.l) and are clouse to the value of sum of and covalent radiuses (R cov Ga=1.23Å and R cov S=1.04E) that indicates to covalent character of chemical bond.

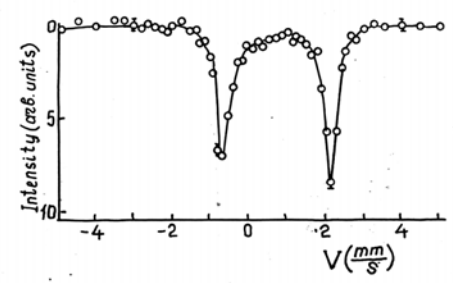

Fig.1. Mössbauer spectra of GaS:Fe at room temperature.

The fact that each Ga atom is connected with three S atoms and one Ga atom indicates to the fact that chemical bond of Ga atoms must be anisotropy. In fact, such anisotropy of chemical bond is sharply displayed in many physical properties of this crystal [2-4].

That's why the investigation of chemical bond anysotropy in GaS is in interested. Method of nuclear gammaresonance (NGR) is one of method widely used in investigation of chemical bond and its anysotropy. Such parameters of NGR as a result of quadrupole splitting and effect possibility, strongly depends on anysotropy of chemical bond. The pollycrystallic $Ga_{0.98}Fe_{0.02}S$ sample have been used during investigations.

Experimental results

Mössbauer spectrum of GaS:Fe has a from of well allowed quadrupole dublet with quadrupole splitting ΔE_Q=2.95±0.03 mm/s (fig.l). The temperature dependence in range of 80-300K of magnetic susceptibility of GaS:Fe crystal is represented on. Experimental values of $\chi(T)$ weakly depend on temperature. The interpretation of quadrupole splitting value in Mossbauer spectra of ion compositions are usually carried out within the theory of lygand field (see for example [5]). But in many cases such method is found to be too roudh. That's why numerical quantocemical methods of Mossbauer parameters calculation have been developed for the last year.

We carried out quantochemical calculation of electron structure of impure complexes by widened Hynkel method [6]. Table data have been taken from [7]. Calculation of Mossbauer parameters have been carried out on program used in [8].

Calculation and discussion of results

Quadrupole splitting for ^{57}Fe nucleuses with spin of state J=1/2 and excited one J=3/2 is determined by expression [5]

$$\Delta E = \tfrac{1}{2} e^2 g Q \left(1 + \eta^{2/3}\right)^{1/2} \qquad (1)$$

where $eg = V_{zz} + \left(\partial^2 V / \partial Z^2\right)_0$ -z-component of electric field gradient tenzor on nucleus, $\eta = \left(V_{xx} - V_{yy}\right)/V_{zz}$ -asymmetry parameter, eQ-nuclear quadrupole moment, moreover for nucleuses Q=0.21 barn [4.5].

According to [5], and η values can be determined from following formula:

$$\left(V_{zz}\right)_{val} = e\left\{\tfrac{4}{7}(1-R)_{3d} <1/r^3>_{3d} \left[N_{x^2-y^2} + N_{z^2} + N_{xy} - \tfrac{1}{2}\left(N_{xz} - N_{yz}\right)\right] + \tfrac{4}{5}(1-R)_{4p} <1/r^3>_{4p} \left[-N_{px} + \left(N_{px} - N_{py}\right)\right]\right\} \qquad (3)$$

$$\left(\eta V_{zz}\right)_{val} = e\left[\tfrac{6}{7}(1-R)_{3d} <1/r^3>_{3d} \left(N_{yz} - N_{xz}\right) + \tfrac{6}{7}(1-R)_{4p} <1/r^3>_{4p} \left(N_{py} - N_{px}\right)\right] \qquad (4)$$

Where "val" and "lat" indexes concern to the introduction of Fe valence electrons and lygand one. As it follow, for example, from [9, 10], valence introductions of five $3d$-and three p-orbitals are equal to

$$\left(V_{zz}\right)_{val} = (1-\gamma_\infty)\sum \frac{e_i\left(3z_i^2 - r_i^2\right)}{r_i^5}$$
$$\left(\eta V_{zz}\right)_{val} = (1-\gamma_\infty)\sum \frac{3x_i\left(x_i^2 - y_i^2\right)}{r_i^5} \qquad (5)$$

where $(1-R)_d$ and $(1-R)_{4p}$-Shternheymer factors for *3d* and *4p* electrons, $<1/r^3>3d$ and $<1/r^3>4p$ –average values of reverse cubes of radiuses of *3d*- and *4p*-membrans, N_α- populations of α orbitals.

According to [10, 5], $(1-R)_{3d}$=0,68, and $<1/r^3>3d$ values depend on valent state of Fe ion; forming (calculating) 4.78 a.e. for Fe^{3+} and 4.44 a.e. for Fe^{2+}.

Introductions of *4p* electrons to quadrupole splitting are usually not large huge and approximate correlation can be used in their estimation [11]:

$$(1-R)_{4p} <1/r^3>4p = 1/3\ (1-R)_{3d} <1/r^3>3d$$

Lattice introductions are calculated on following formulas [4]:

$$(V_{zz})_{val} = (1-\gamma_\infty)\sum \frac{e_i(3z_i^2 - r_i^2)}{r_i^5}$$

$$(\eta V_{zz})_{val} = (1-\gamma_\infty)\sum \frac{3x_i(x_i^2 - y_i^2)}{r_i^5}$$

Where x_i, y_i, z_i-decart coordinates of lygands in axles system, connected with metal, -metal r_i-lygand distance, e_i-lygand charges. Besides, it's usually assumed that $(1-\gamma_\infty)$=12 [5,6].

To determine unknown values in (1)-(5) we applied to widen Hynkel method.

As its known, standard numerical method of quantum chemistry allows to calculate electron structure final system only. That's why to obtain a sensible results we need right part of crystal, the calculation will be made for.

From GaS crystalline structure, examined above, one can see that minimum cluster, reproducing (showing) crystallochemical peculiarities of whole lattice have to be chosen like eight atoms Ga_2S_6 grouping which is represented on fig.2.

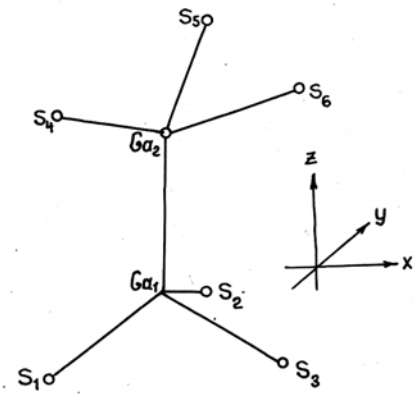

Fig.2 . Structure of Ga_2S_6 cluster.

Decart coordinates of atoms calculated from known crystallographic data are given in table 1.

Table 1.

Decart coordinates of atoms of $[Ga_2S_6]^8$ cluster.

Atom	*x*, Å	*y*, Å	*z*, Å
Ga_1	0	0	0
Ga_2	0	0	2.448
S_1	0	-2.071	-1.075
S_2	-1.793	1.035	-1.075
S_3	1.793	1.035	-1.075
S_4	0	-2.071	3.523
S_5	-1.793	1.035	3.523
S_6	1.793	1.035	3.523

Right cluster charge, obtained in neutral crystal can be determined by following method. As one atom lygand *S* atom has oxidation degree equal to -2. Then, due *GaS* to crystal electro neutrality, atom should be given oxidation degree equal to +2. Thus, we deal with $[Ga_2S_6]^{1-}$ cluster. It is important to stress that oxidation degree equal to +2 doesn't contradict to well known fact that *Ga* is three valent, quite the opposite, it's proved by *GaS* structure peculiarities. In fact, oxidation degree equal to +2 means that only 2 valent of atom are saturated as a result of interaction with S atom. In this case the saturation of third valent is possible because of Ga-Ga covalent bond formation only, which is vally taken place.

In connection with this fact we made a calculation of $[GaFe^{2+}Se\ ]^{8-}$ and $[GaFe^{3+}S_6]^{7-}$ clusters containing Fe atoms in 2 more stable oxidations degrees by means of widen Hynkel method. In connection with the magnetic measurements results, Fe atoms are considered to be low-spin. Clusters structure replies are shown on fig.2 with substitution Ga_2 to Fe.

The composition and energies of some bordering MO of $[GaFe^2S_6]^{2-}$ cluster are given. $[GaFe^{3+}Se_6]^{7-}$ cluster is different for the reason it has not one electron. It follow that upper of both clusters maintain considerable introduction Fe of atom AO. That's why their Mossbauer parameters must be too different, which principally gives a possibility to determine valent state of Fe atoms in GaS:Fe. Besides one can see that comparatively large splitting and high degree of electron decolization is typical for B3MO and low vacant MO. It proved that the conclusion about low spin state of *Fe* atoms is correct. Finally, unlike the $[Ga_2S_6]$ clusters, $[GaFeSe_6]$ clusters do not maintain metal. Metal bond: the lowest orbital, in which AO of S, P_z and dZ^2 types are represented completely is $\varphi_{30}\Delta E_Q$ orbital.

Calculated popularization of Fe atoms AO and charges of all cluster's atoms are given in table 2.

Table 2

Calculated popularization of *Fe* atoms AO and charges of all cluster's atoms.

Clusters	Charges of atoms			Populations								
	e(*S*)	*e*(Ga)	*e*(Fe)	4*S*	$4P_y$	$4P_z$	$4P_x$	d_{xy}	d_{yz}	d^2_{xy}	d_{xz}	$d_{x^2-y^2}$
$[GaFe^{2+}S_6]^{8+}$	-1.52 -1.38	1.28	-0.64	0.40	0.14	0.04	0.14	1.42	1.65	1.75	1.65	1.42
$[GaFe^{3+}Se_6]^{7-}$	-1.52 -1.24	1.28	0.02	0.40	0.08	0.04	0.08	1.26	1.55	1.75	1.55	

Upper number corresponds to GaS_3 group; under number-to Fe_2S_3 group.

As it is expected, S atoms carry negative charges, moreover charges in GaS groups are larger that in FeS_3, groups. It indicates to large electropositiveness of Ga in comparison with Fe, which also has a reflection in correlation of Ga and Fe charges. Orbitals population of *Fe* atoms changes enough (visibly) in the process to transition from $[GaFe^{2+}Se]^{1-}$ clusters to $[GaFe^{3+}Se_6]^{1-}$ one that should be displayed in theoretical values of quadrupole splitting. ΔE_Q values calculated on (1.!)-(!.5) formulas for both type of cluster in the processes of consistent increasing of mentioned introduction are given it table 3. One can see that anysotropy of electron density splitting on Fe atom gives only a half of full value of ΔE_Q.

Table 3

Theoretical values of ΔE_Q*(mm/s)* for $[GaFe^{2+}S_6]^{8-}$ and $[GaFe^{3+}Se_6]^{7-}$ clusters.

Clusters	Group				
	Fe	Ga-Fe	S_3Ga-Fe	S_3Ga-FeS_3	S_3Ga-eS^*_3
$[GaFe^{2+}S_6]^{8-}$	2.2	2.71	2.45	2.9	2.82
$[GaFe^{3+}Se_6]^{7-}$	3.18	3.79	3.56	4.01	3.9

In the beginning this results is seemed to be a little unexpected, but it becomes quite clear, if large positive charge o atoms and large value of field gradient created by single charge are taken into consideration.

Three *S* atoms complete formally the coordination sphere of Fe atoms to tetrahedr. How-ever ΔE_Q does not decrease, but increases, that is interpreted by differences of Ga and S charges mark. Introduction of S atoms in is not large in general. It allow to considering obtained estimation of to be reliable enough, even when S atoms is located in clusters border, hence error in estimation of their charge can be large. As GaS atoms are the nearest to *S* atoms in *GaS* crystal, then negative charge in atoms is probably overestimated.

Considering ΔE_Q values given in last three columns one can see that the model of $[GaFe^{3+}Se_6]^{7-}$ cluster is not satisfactory independently of *e(S)* estimation, as theoretical values of E_Q are different from experimental ΔE_Q=2.66 mm/s by 2. Quite opposite, $[GaFe^{2+}S_6]^{8-}$ cluster is corresponds to experiment very well. That's why we can confidentially make a conclusion that impure center in crystals GaS:Fe has structure of $[GaFe^{2+}S_6]^{8-}$.

[1] *Kuhn. Chey A.* Acta Cryst. (1976), B.32. 983.

[2] *K.K.Mamedov, M.A.Aldjanov, I.Q.Kerimov, M.I. Mextiyev.* FTT, 1977, 20, №1, 41.

[3] *G.D.Guseinov, A.L.Rasulov, E.M.Kerimova, M.Z.Ismailov*. Phys. Letters, 1966, 22, 562.

[4] *M.A. Aldjanov, M.D. Najafzade, Z.Y. Seidov*. FTT, 1999, 41, №01, 24.

[5] Chemical application of Mössbauer spectroscopy. M. "Mir", 1970, 502.

[6] *S.P. İonov, B.N. Qaribov*. J.Phys. Chem, 1980, 54, №11, 2721.

[7] *S.Alvares*. Table of Iterated Ionization Potetials for Extended Huckel Calculations, Itaca University, 1984.

[8] *V.I. Khlestkov, B.N. Burkin, R.E. Qeribov*. 1985, №2, 146.

[9] *M.Weissbluth, J.E. Maling,* I.Chem. Phys., 1976, 47, №10, 4166.

[10] *M.Weissbluth,* Coopevativity and electronic properties, Berlin, Springer, 1974, 212.

[11] *A.Tranvein*. Mössbauer spectroscopy on heme protein, Struct. and Bond, 1974, №20, 101.

Q.D. Sultanov, M.A. Alcanov, E.M. Kərimova

$Ga_{0.8}Fe_{0.02}S_6$ KRİSTALINDA MESSBAUER SPEKTRİNİN TƏDQİQİ

GaS:$^{+57}$Fe kristalında aparılan maqnit və Messbauer tədqiqatları 80÷300 K temperatur oblastında maqnit qavrayıcılığının temperaturdan zəif asılılığını müəyyənləşdirdi.

Otaq temperaturunda Messbauer spektrindən təyin olunmuş kvadrupol parçalanmanın qiyməti *E*=2,95mm/san. *E*-nin təcrübi qiyməti ilə $GaFe^{2+}S_6$ aşqar kompleksinin elektron quruluşunun MK-hesablanması əsasında alınmış nəzəri qiyməti arasındakı uyğunluqla təsdiqlənir.

Г.Д. Султанов, М.А. Алджанов, Э.М. Керимова

ИССЛЕДОВАНИЕ МЕССБАУЭРОВСКИХ СПЕКТРОВ КРИСТАЛЛОВ $Ga_{0,8}Fe_{0,02}S_6$

Проведены магнитные и мессбауэровские исследования кристаллов GaS:Fe. Установлена слабая температурная зависимость магнитной восприимчивости в области температур 80÷300K. Величина квадрупольного расщепления, определенная из мессбауэровского спектра при комнатной температуре, равна *E*=2,95мм/сек. Сделанное предположение дает хорошее согласие между экспериментальным и теоретическим значением величины *E*, полученным на основе результатов МК- расчета электронного строения примесного комплекса $GaFe^{2+}S_6$.

Received: 09.04.03

CHARACTERISTIC PECULIARITIES OF p-PbTe/n-$Pb_{0,99}Tm_{0,01}Te$ p-n TRANSITIONS

Ch.I. ABILOV
Azerbaijan Technical University,
Baku, 370073, H.Javid ave., 25.
Y. BABUR
Harran University, 63 300, Sanlyurfa, Turkey

On the basis of $Pb_{0,99}Tm_{0,01}Te$ single crystals and PbTe epitaxial layers the photoreceivers which are sensitive at 5-12 μm wavelength band have been fabricated. Spectral, volt-ampere and volt-farad characteristics have been studied on multielement scales of photosensitive structures. It was established that at 77 K product of differential resistivity at null dislocation and active area. R_0A is equal to 10 ohm·cm^2 (R_0A=10 ohm·cm^2). It has also determined that a main mechanism of current traverse is generation - recombination of charge carriers. The concentration gradient of electroactivity centers in field of volumetric charge band is about ~ $0{,}54\cdot10^{21}$ cm^{-4}, and therefore the generated p-n transitions are abrupt.

1. Introduction.

PbTe and solid solutions on its basis have wide application in semiconducting optoelectronics for creation of photoreceivers and injection layers operating at 3-5 μm and 8-14 μm wavelength band. Possibility of fabrication of devices operating at such a spectra of range is conditioned by alteration of the size of prohibited zone width, by way of regulating the stechiometric compound, which affaires simple to implement within the limit of homogeneity surfaces. Consequently, solid solutions of $Pb_{1-x}Tm_xTe$ can be exceedingly suitable for creation of photosensitive structures with practically valuable parameters. The present information contains results of investigations of some photoelectrical, volt-ampere and volt-farad characteristics of infrared emission receivers created by way of epitaxial build up of -PbTe thin layers into n-$Pb_{1-x}Tm_xTe$ single crystals.

2. Experimental.

Single crystals of *n*-$Pb_{1-x}Tm_xTe$ solid solutions have been grown by directed crystallization method and were used as a substrate for preparation of photosensitive structures. Mechanical processing was initially carried out, and after cutting of single crystals in a (100) plane direction aimed to removal of disturbed layers, their surfaces were treated with chemical etching in 6 % Br_2 solution in HBr. Then Electro-chemical polishing of the surface was provided in Norman etching (H_2O:KOH:glyserine and ethyl spirt=15ml:20g 35ml:20 g), with further removal of etching residues by deep flushing in dionized water flow. With the help of a "hot wall" method by using of two-phase lead and tellurium mixture (in stechiometri ratio), PbTe films were grown on these backings. To decrease concentration of self defects (eigen defects) in condensed films and to enable the courtral over charge carriers concentration in PbTe films, an additional source of tellurium vapor was used [1] in the process of growth. Thickness of grown pate epitaxial layer was within the margin of 5 to 10 μm. Scales of photosensitive elements were formed with the help of photolithography`, but prior to laying it onto the surface of films, metallic contact indium layer was applied by thermal evaporation in vacuum of prepared meza-structures formed 0,2 mm^2 and that of bonding pad was 0,05 mm^2. Gold wires of diameter. ~30 μm were joined to bonding pads by using of low-temperature solder ($T_{\pi A}$≈333K) consisting of 50% Br+25%Pb+12,5%Sn+12,5%Cd.

Volt-ampere and spectral characteristics of prepared p-n transitions in temperature interval of 77-300 K were studied as in [2]. Prepared structures were observed to have rectifying characteristics even at ~300 K.

3. Results and Discussion.

Fig.1 demonstrates volt-ampere characteristics (VACh) of p-PbTe/n-$Pb_{1-x}Tm_xTe$ diode structures at 77K. VACh forward-bias region is qualitatively described by a function $I=I_s exp(eV/\beta kT)$. Based on temperature dependence calculations β coefficient of which is equal to 2. It testifies to predominance of recombination constituent of electric current. Substantial distinction of $I\sim f$ (U) dependence is existence at U>150 mV in reverse-bias region of a section corresponding to tunnel break-through of *p-n* transition. Mentioned section gradually disappears by increasing the temperature. It is well known that in *p-n* transitions at 300 K is diffusional. It is well known that in *p-n* transitions of materials close in their contents to the materials preferred with the help of a device described in present work, considerable number of electroactive centers are refereed to exist, and increase of their concentration gradients affects on decrease of width of volumetric charge bend, and the concentration value of charge carriers on the boundary of volumetric charge carriers on the boundary of volumetric charge band may also increase in this case [3].

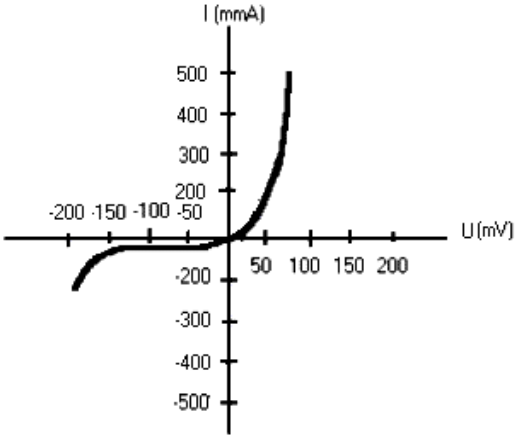

Fig.1. Volt-ampere characteristics of p-n structures p-PbTe/n-$Pb_{0,99}Tm_{0,01}Te$ pieced at 77 K.

In produced solid state structures of *p*-PbTe/*n*-$Pb_{1-x}Tm_xTe$ the growth of R_0A value against the degrease of temperature is bound up with diffusional constituent of the current, thus testifying to existence of above mentioned mechanism in them. At zero bias, the produced structures had $R_0=7,5\ k\Omega$ (at 300K) and $R_0=5k\Omega$ (at 77K). Determination the concentration gradient of electroactivity centers in field of volumetric charge band (a) was provided with the help of [4]

$$a = \frac{p+n}{W} \quad (cm^{-4}).$$

Where *p* and *n* are concentrations of charge carriers in *p* and *n* bands of p-n transitions and *W* is the width of volumetric charge band. According to voltage-capacitance characteristics of created structure *W*=0,003cm, and $n=0{,}43\cdot10^{18}cm^{-3}$ [5].

Hall finding [5] have established that $p=1{,}2\cdot10^{18}cm^{-3}$ in $Pb_{0,99}Tm_{0,01}Te$ single crystal. Consequently, $a=0{,}54\cdot10^{21}cm^{-4}$ derived value of volumetric charge concentration evidences to the formed p-n transition to be sharp.

Fig.2. shows the spectral characteristic of produced IR photoreceivers. Maximum of spectral characteristic is in agreement with wave length equal to 5,7 μm. Volt-watt sensitivity value of S_ζ was calculated with $S_\zeta=V(\lambda)/P(\lambda)$, (*V/W*) formulae, where $V(\zeta)$ is a photo-electromotive force (e.m.f.) on ж wave length for separate meza-structures $V(\zeta)=(70\text{-}94)\ \mu V$, $P(\zeta)$ is a power of radiation with χ wave length, incident on specimen, at 77K, the value of S_ζ for separate meza-structures amounted from 121 to 162 *V/W*. Photocurrent was defined as per measured value of photo-e.d.f (V_s) and the value of meza-structure resistance at zero shift of (R_0) :

$$I_{photo}=V_s(\zeta)/R_0\ .$$

At 300K the value of $I_{photo}=12{,}5\mu A$, and at 77K the value of $I_{photo}=18{,}8\ nA$.

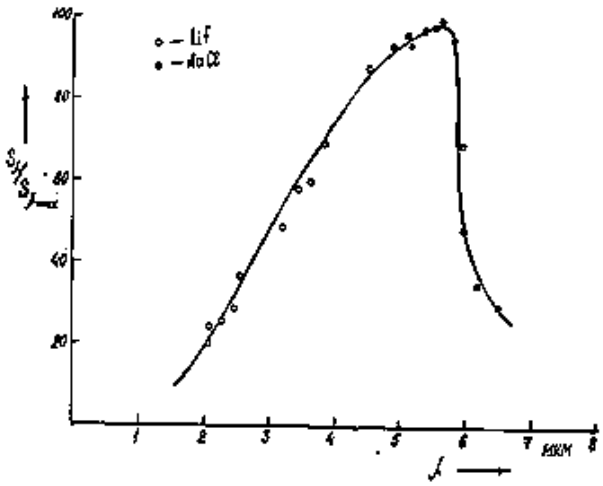

Fig.2. Spectral characteristic of photoreceiver on *p*-PbTe/*n*-$Pb_{0,99}Tm_{0,01}Te$ structure basis (○-prism from LiF; •-prism from NaCl).

[1] *S.L. Miloslavov, I.V. Saunin, D.A. Yaskov.* News of Academy of Science USSR, Neorganicheskie Materiali, 1983, v. 19, №1, p. 55-58.

[2] *I.V. Vikulin, V.I. Stafeyev.* Physics of semiconducting instruments. M., "Sovetskoye Radio", 1980, 212 p.

[3] *D.I. Ivanov, I.V. Saunin, D.A.Yaskov.* Journal of Phys. State Sol., 1984, v. 18, №5, pp.818-820.

[4] *M.R. Jonson, R.A. Chapman, I.S. Wrobel.* Infrared Phys., 1975, vol. 15, №4, pp. 317-319.

[5] *Ch.I. Abilov.* Abstract of dissertation of the doctor of technical sciences, 1994, Institute of Inorganic and Physical Chemistry Acad. of Sciences Azerb. Republ., 39 p.

Ç.İ. Əbilov, Y. Babur

p-PbTe/*n*-$Pb_{0,99}Tm_{0,01}Te$ *p-n* KEÇİDLƏRİNİN XARAKTERİSTİKALARININ XÜSUSİYYƏTLƏRİ

$Pb_{0,99}Tm_{0,01}Te$ monokristalları və PbTe epitaksial təbəqələri əsasında 5-12mkm dalğa uzunluqlarında həssas olan fotoqəbuledicilər hazırlanmışdır. Çoxsaylı elementlərin düzülüşündən ibarət olan fotohəssas quruluşlarda voltamper, spektral və voltfarad xarakteristikaları tədqiq edilmişdir. Müəyyən olunmuşdur ki, 77K temperaturunda tarazlıq halında differensial müqavimətin aktiv sahəyə hasili R_0A=10 Om·sm^2. Cərəyanın axma mexanizmi yükdaşıyıcıların generasiya-rekombinasiyası ilə aydınlaşır. Həcmi yüklər oblastında elektroaktiv mərkəzlərin konsentrasiya qradiyenti ~$0{,}54\cdot10^{21}$ sm^{-4} olduğundan, yaradılan p-n keçid kəskindir.

Ч.И. Абилов, Ю. Бабур

ОСОБЕННОСТИ ХАРАКТЕРИСТИК *p-n* ПЕРЕХОДОВ *p*-PbTe/*n*-$Pb_{0,99}Tm_{0,01}Te$

Изготовлены фотоприемники на основе монокристаллов $Pb_{0.99}Tm_{0.01}Te$ и эпитаксиальных слоев PbTe, чувствительных в диапазоне длин волн 5-12 мкм. На многоэлементных линейках фоточувствительных структур исследованы спектральные, вольтамперные и вольтфарадные характеристики. Установлено, что при 77 К произведение дифференциального сопротивления при нулевом смещении на активную площадь R_0A=10 Ом·см^2. Определено, что основным механизмом протекания тока является генерация-рекомбинация носителей заряда. Градиент концентрации электрически активных центров в области объемного заряда порядка ~$0{,}54\cdot10^{21}$ см$^{-4}$ и поэтому сформированные p-n переходы являются резкими.

Received: 14.04.03

QADOLİNİUM ELEMENTİNİN İŞTİRAKI İLƏ SnSe ƏSASINDA OLAN BƏRK MƏHLULLARIN QALVANOMAQNİT XASSƏLƏRİ

M.S. MURQUZOVA, M.İ. MURQUZOV, Ş.S. İSMAYILOV
Azərbaycan Tibb Universiteti
370022, Bakı, Bakıxanov küç., 23

İşdə $(SnSe)_{1-x}$-$(GdSe)_x$ (0,25≤x≤2,0 mol %) sistem ərintilərinin T=77÷420K temperatur intervalında Holl əmsalı (R_x), elektrik müqaviməti (ρ) və maqnit müqaviməti tədqiq edilmişdir. Müəyyən olunmuşdur ki, T=285÷310K temperaturlar intervalında göstərilən parametrlər anomal dəyişir. Müqavimətin temperatur asılılığı $T<T_a$ (T_a=285÷310K) intervalında metallik, $T>T_a$ intervalında isə yarımkeçiricilik xassəsi göstərir. Bu xassələrin dəyişməsinin ümumi qanunauyğunluğu araşdırılmışdır.

Sn-Gd-Se sistem ərintilərinin fiziki-kimyəvi xassələri [1-3] müəlliflər tərəfindən öyrənilmişdir. Gd metalının iştirakı ilə SnSe əsasında alınmış ərinti zəif deformasiya olunmuş ortorombik quruluşda kristallaşır [3,4]. Maddələrin fiziki təbiəti və kinetik xassələri tam öyrənilməmişdir [4] və onların ətraflı öyrənilməsi elmi və praktik maraq kəsb edir. Ferromaqnit təbiətli Gd metalının iştirakı ilə olan ərintilərdə müxtəlif növ maraqlı fiziki xassələr müşahidə olunur [5,6]. Digər tərəfdən deffekt və laylı quruluşa, ağır elementə malik olan ərintilər mürəkkəb zona quruluşuna malikdirlər. SnSe birləşməsi və onun əsasında alınmış bərk məhlul bu tip yarımkeçiricilərdəndir. Bu xüsusiyyətləri əsas götürərək $(SnSe)_{1-x}$-$(GdSe)_x$ sistemindən x=0,25; 0,5; 1,0 və 2,0mol % GdSe tərkibli maddələr sintez olunmuş [1,2] və onların T=77÷420^{0}K temperatur intervalında göstərilən parametrləri tədqiq edilmişdir.

Elektrik müqaviməti ρ və Holl gərginliyinin ölçülməsi kompensasiya metodu ilə sabit cərəyan dövrəsində aparılmışdır və buraxılan xətalar 6,2% təşkil etmişdir.

$\rho_x = \frac{U_x d}{J} = f(H)$ ifadəsinə əsaslanaraq maqnit sahəsindən asılılığından R_n- normal və R_a- anomal Holl əmsalları hesablanmışdır:

$$\rho_x = R_n H + \rho_x^a + \rho_x^p \qquad (1)$$

Burada U_x - Holl gərginliyi, J - nümunədən keçən cərəyanın qiyməti, d - nümunənin qalınlığı (H - maqnit sahəsi istiqamətində), ρ_x - Holl müqaviməti, ρ_x^p - paraproseslə bağlı Holl müqavimətini xarakterizə edir. Bizim hesablamalarda ρ_x^p-in qiyməti təxminən 10^{-5} tərtibində olduğu üçün onu nəzərə almamaq olar. Ona görə də (1) ifadəsini

$$\rho_x = R_n + \rho_x^a = R_n + R_a \qquad (1a)$$

şəkildə yazmaq olar [6]. Nümunələrdə termo e.h.q. (α)-nın işarəsinin dəyişməsinə əsasən maddələrin keçiriciliyinin p-tip olduğu müəyyən edilmişdir.

Təcrübələr göstərir ki, maddələrin elektrik keçiriciliyi T=77÷285K temperatur intervalında metallik və T>310K temperaturlarda isə yarımkeçiricilərə məxsus qanunla dəyişir (şəkil 1). T=285÷310K temperatur intervalında isə maksimumdan keçərək azalır. 2-ci şəkildə normal Holl əmsalının R_n temperatur asılılığı verilmişdir. Şəkildən göründüyü kimi R_n-in dəyişməsi nümunələrdə xüsusi müqavimətin (ρ) dəyişməsinə uyğundur (şəkil 2) və T=285÷310^{0}K temperatur intervalında ρ-nun qiymətində olduğu kimi maksimumluq müşahidə olunur.

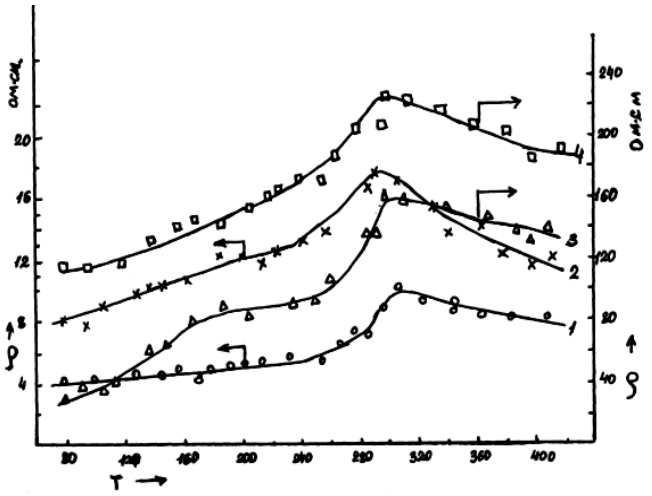

Şəkil 1. $(SnSe)_{1-x}(GdSe)_x$ sistem məhlullarında müqavimətin temperaturdan asılılığı: 1 - 0- x=0,25 mol %
2 - x- x=0,50 mol %
3 - Δ- x=1,00 mol %
4 - □- x=2,00 mol %

Daha maraqlı bir faktor isə maqnit müqavimətinin $\left(\frac{\Delta\rho_\perp}{\rho_0}\right)$ temperatur asılılığında müşahidə olunur. Belə ki, $\frac{\Delta\rho_\perp}{\rho_0}$ $T<T_a$ intervalında (T_a=285÷310^{0}K) işarəsi müsbət və $T>T_a$-da isə mənfidir (şəkil 3). Bu temperatur intervalı isə metallik keçiricilikdən yarımkeçiricilik xassəsinə keçid temperaturuna uyğundur. $\rho=f(T)$ və $R_n=f(T)$ asılılığı qrafiklərindən göründüyü kimi temperaturun verilmiş qiymətində tərkiblərdə Gd metalının miqdarı artdıqca onun müqaviməti və Holl əmsalı mütənasib artır. Bu isə tərkiblərdə Gd atomunun konsentrasiyasının artmasına uyğundur. Tədqiqatlar göstərir ki, alınan tərkiblər məhlullarda Sn atomunun bir qisminin Gd atomu ilə əvəz olunması ilə kristallaşır [4,5]. Gd üç valentli metal atomu olduğundan alınmış tərkiblər qismən hər bir qodalinium atomundan bir elektron hesabına kompensasiya olunmuş maddələr olur.

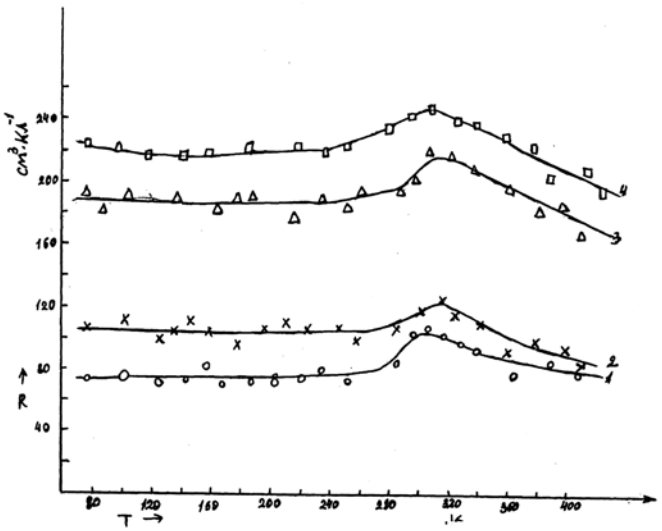

Şəkil 2. $(SnSe)_{1-x}(GdSe)_x$ sistem məhlullarında Holl əmsalının temperaturdan asılılığı: 1-x=0,25 mol %
2-x=0,50 mol %
3-x=1,00 mol %
4-x=2,00 mol %

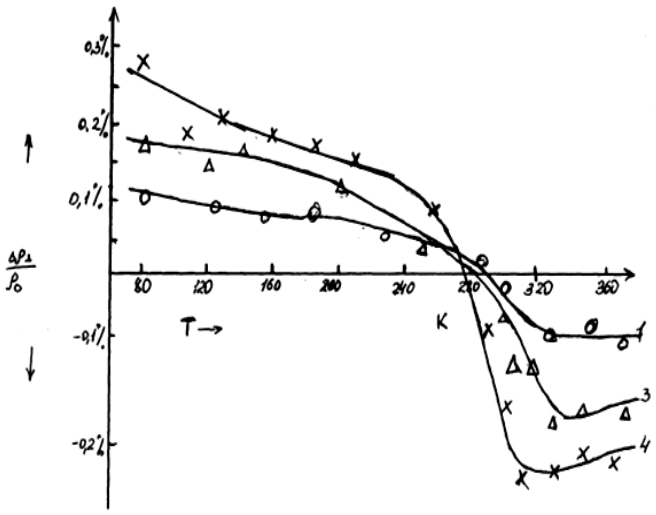

Şəkil 3. $(SnSe)_{1-x}(GdSe)_x$ sistem ərintilərində maqnit müqavimətinin temperaturdan asılılığı:
1-x=0,025 mol %
3-x=1,00 mol %
4-x=2,00 mol %

Cədvəldə T=300^{0}K temperaturunda bəzi parametrlərin tərkib asılılıqları verilmişdir.

	Tərkiblər	ρ, Om·sm	R_n, sm^3/Kl	p, 10^{18} sm^3	μ, sm^2/B·s	α, mkV/dər
1	x=0,25	0,11	10,835	0,577	99	310
2	x=0,50	0,17	11,848	0,528	71	246
3	x=1,06	0,901	18,051	0,346	20	123
4	x=2,00	1,587	22,221	0,281	14	62

Cədvəldən göründüyü kimi tərkiblərdə konsentrasiya Gd atomunun artması ilə mütənasib $0{,}58\cdot10^{18}$-dən $0{,}28\cdot10^{18}$sm^{-3}-ə qədər azalır. Yükdaşıyıcıların Holl yürüklüyü isə U=99-dan 14sm^2/B·s-yə qədər azalır. Bu isə qeyd etdiyimiz kimi maddələrin kompensasiya olunmuş tərkiblər olduğunu bilavasitə göstərir.

Qrafiklərdən göründüyü kimi (şəkil 1 və 2) $\rho=f(T)$ və $R_n=f(T)$ asılılıqları tərkiblərdə Gd atomunun miqdarı artdıqca T=77÷285K temperatur intervalında metallik keçiriciliyi intensivləşir. Digər tərəfdən temperaturun verilmiş qiymətində tərkiblərdə Gd atomunun miqdarının artması ilə keçiricilik artmaq əvəzinə, əksinə azalır. Bu tərs mütənasibliyi $R_n=f(T)$ asılılığı da təsdiq edir. Buna səbəb maqnit təbiətli Gd atomunun miqdarının artmasıdır. Güman edilir ki, kiçik konsentrasiyalarda Gd atomlarının yaratdıqları lokallaşmış maqnit mərkəzləri ayrılıqda "maqnit eksitonları" kimi zəif mərkəzlər yaradır. Bu mərkəzlər keçiricilikdə iştirak etmir. Gd atomunun miqdarının artması ilə ərintilərdə bu mərkəzlərin bir-biri ilə əlaqələri artaraq ferromaqnit mikromərkəzlərə çevrilir. Burada Gd^{3+} ionu hesabına yaranan lokallaşmış mərkəzlər adi yarımkeçiricilərə xas olan fonon cəzb etməsindən başqa əlavə maqnit təbiətli mərkəzlərin cəzb etməsi, "maqnit eksitonu" rolunu oynayır.

Gd^{3+} ionunun verdiyi elektron nisbətən yüksək enerji səviyyəsində yenidən həmin ion tərəfindən (və ya defekt) tərəfindən tutularaq bağlı vəziyyətdə qalır. Tutulmuş elektron Gd^{3+} ionu ilə birlikdə nizamlı maqnit xassəli elektronlara çevrilir.

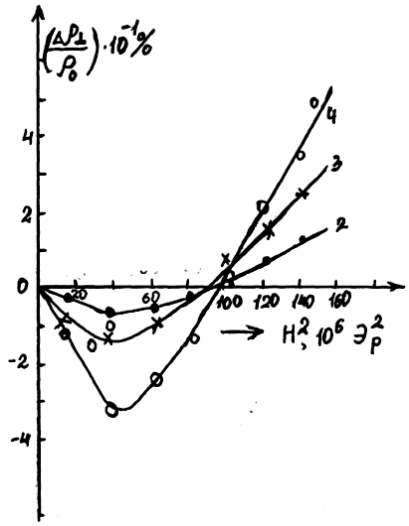

Şəkil 4. $(SnSe)_{1-x}(GdSe)_x$ sistem ərintilərində maqnit müqavimətinin H-maqnit sahəsindən asılılığı.
T=304^{0}K
2-x=0,5 mol %
3-x=1,0 mol %
4-x=2,0 mol %

Nisbətən güclü rabitədə olan bu tip lokallaşmış mikromaqnit mərkəzləri aşağı temperaturlarda keçiricilikdə iştirak etmirlər. Ona görə də aşağı temperaturlarda T-nin artması ilə keçiriciliyin azalması müşahidə olunur. T artdıqca bu mərkəzlərin, o cümlədən kristallik quruluşun həyəcanlanması artaraq T_a-da paramaqnit xassəli

mərkəzlərə çevrilməsi baş verir. Bu isə konsentrasiyanın zəif artmasına (şəkil 2) və əlavə mübadilə enerjisinin qeyri elastiki səpilməsinin güclənməsinə səbəb olur.

Maksimum keçid oblastında (T=300^{0}K) $\frac{\Delta\rho_\perp}{\rho_0}=f\left(H^2\right)$ asılılığı qrafiki analiz edilmişdir (şəkil 4).

Şəkildən göründüyü kimi xarici H-maqnit sahəsinin kiçik qiymətlərində, H-sahə istiqamətində həm sərbəst və həm də lokallaşmış mikromərkəzlərin istiqamətlənmiş spin düzülüşündə enerji sərf olunmur [7]. H-sahəsinin artması ilə spinə görə ortalanmış elektronların sayı artır və H-ın müəyyən qiymətində - $\frac{\Delta\rho_\perp}{\rho_0}$ xətti artır. Bu isə yuxarıda göstərdiyimiz kimi tərkiblərdə olan lokallaşmış mikroferromaqnit mərkəzlərinin paramaqnetizmə keçməsinə uyğundur.

.

[1] *A.P. Qurşumov, B.B. Kuliev, A.M. Axmedov*: İzv. AN SSSR. Neorqan. materialı, 1984, T.20, №7, s.1090-1094.

[2] *A.P. Qurşumov, B.B. Kuliev, A.M. Axmedov i dr*. İzv. AN SSSR. Neorqan. materialı, 1984, T.20, №7, s.367.

[3] *M.İ.Murquzov, A.P.Qurşumov* "Zakonomernosti vzaimodeystviya v sistemax SnSe-LnSe". Tezisı dokl. vsesoyuznoy konferentsii po fizike i ximii redkozemelnıx poluprovodnikov. Saratov, 1990.

[4] *M.İ. Murquzov, Ş.S. İsmayılov, R.F. Məmmədova.* $(SnSe)_{1-x}$-$(LnSe)_x$ (Ln=La, Gd) sistem ərintilərinin bəzi kinetik xassələri. ADPU-nun 2000-ci ildəki konf. mater.

[5] *P.V. Cuze.* Fiziçeskie svoystva xalkogenidov redkozemelnıx elementov, 1973, str.303.

[6] *Z.Metfessel, D.Mattis.* Maqnitnıe poluprovodniki, M., 1972, UFN, 1968.96.21.

[7] *R.M. Mehra, R. Shyam, P.C. Mathyr* "Magnetoresistence in Amorphous semiconductors. Thin Solid Films - 1983. Vol.100. №2.p.81-109.

М.С. Мургузова, М.И. Мургузов, Ш.С. Исмайылов

ГАЛЬВАНОМАГНИТНЫЕ СВОЙСТВА ТВЕРДЫХ РАСТВОРОВ НА ОСНОВЕ SnSe С УЧАСТИЕМ ЭЛЕМЕНТА ГАДОЛИНИУМА

В работе исследованы коэффициент Холла (R_x), электрическое (ρ) и магнитное сопротивления системы сплава $(SnSe)_{1-x}$-$(GdSe)_x$ ($0{,}25\le x\le 2{,}0$мол%) в температурном интервале T=77÷420K. Определено, что в температурном интервале T=285÷310K обсуждаемые параметры меняются аномально. Температурная зависимость сопротивления выявляет в температурном интервале $T<T_a$ (T_a=285÷310K) металические, а и при $T>T_a$ полупроводниковые свойства. Исследована общая закономерность изменения этих свойств.

M.S. Murguzova, M.I. Murguzov, Sh.S. Ismayilov

GALVANOMAGNETIC PROPORTIES OF SOLID SOLUTIONS ON THE BASE OF SnSe WITH TAKING PART OF GADOLINIUM ELEMENT

In this work the Holle coefficient (R_x), electric (ρ) and magnetic resistances of the melting systems on the base GaSe $(SnSe)_{1-x}$-$(GdSe)_x$ ($0{,}25\le x\le 2{,}0$ mol%) in the temperature interval T=77÷420K have been investigated. It was found that, the discussed parameters change anomally in the temperature interval T=285÷310K. Temperature dependence of resistance shows metalic proporties in the temperature interval $T<T_a$ (T_a=285÷310K) and semiconductor proporties when $T>T_a$. A general rules of change of these proporties has been investigated.

Received: 16.04.03

THE INFLUENCE OF THE THERMAL TREATMENT ON THE AIR ON THE DRIFT AND RECOMBINATION BARRIERS IN THE FILMS $Cd_{1-x}Zn_xS$ (x=0÷0,6)

E.N. ZAMANOVA
Institute of Physics, Azerbaijan National Academy of Sciences,
Baku. Az - 1143, H. Javid st. 33

The values of the drift and recombination barriers for the main carriers have been calculated in the films $Cd_{1-x}Zn_xS$ (x=0-0,6), obtained by the deposition from the solution. It has been established, that the height of the recombination barrier is higher, than drift, and it leads to the charge accumulation and remanent conductivity. The role of these barriers reduces effectively as a result of the thermal treatment on the air and the light sensitivity increases.

The films CdS, obtained by the method of the chemical deposition, distinction by the high technological reproduction of parameters and are applicable for the formation on their base a large number of devices. Therefore they are actively investigated for the recent years [1-5]. It is possible to observe the heterogeneities (defects) by the structure and local fluctuation in the impurity spreading with the internal electric fields, taking the part of the potential barriers in the polycrystal films, obtained by the deposition from the solution. Therefore the research of the heterogeneous barrier relief in these films has the practical and scientific interest. The temperature dependence of the dark current, photoconductivity, thermostimulated current and remnant conductivity of films $Cd_{1-x}Zn_xS$, obtained on the sitall substrate by the method of the chemical deposition from the aqueous solution, containing salt of Cd, Zn and thiourea has been investigated. The samples with the remanent conductivity (RC), anomaly conductivity and high photosensitivity have been obtained by the parameters change (such as the deposition time, the film thickness, the reaction mixture content, the thermal treatment (TT) regime). The conditions: the concentration is 0,05m $CdCl_2$, 5÷10ml - NH_4OH, 0,05m $(NH_2)_2CS$, the temperature is 90° C, the deposition time is 20÷30 min. are the optimal to receive the stable film of the highest thickness (8÷12mcm), achieved at the single deposition, adhesion to the substrate and heterogeneities.

The specific dark conductivity of the initial samples makes 10^{-9}÷10^{-10} $(Ohm\cdot cm)^{-1}$, the ratio of the photocurrent to dark is $\gamma = \frac{I_{ph}}{I_d} = 10^2$. RC has been observed both at room and nitrogen temperatures. In the range 90÷140K the anomalies of the activation energy 0,147eV have been observed at the temperature dependence of the dark current (fig.1).

After cut-off the photocurrent reduces to the fixed value (RC) and then it remains practically invariable. The remanent conductivity occurs, when the relaxation time of non-equilibrium carriers τ exceeds the observation interval τ_0. The relaxation time of RC is τ=10^3÷10^6s for the various samples and depends on the duration and intensity of the preliminary illumination.

The sudden maximum has been observed on the curves of the thermostimulated currents (TSC) at the temperature range 240÷270K [5].

Samples, subjected to TT on the air at 500°C during 15min. have high specific resistivity (ρ≈5÷7·10^{-9}Ohm·cm) and are photosensitive with the multiplicity γ=10^7÷10^8. After TT the peak intensity on TSC at 240÷270 K have reduced and anomalies in the temperature dependence of the dark current and RC at the nitrogen temperature have disappeared.

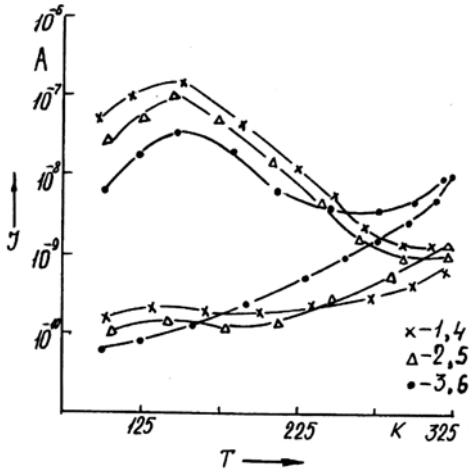

Fig.1. The temperature dependence of the current of the initial films $Cd_{1-x}Zn_xS$ in the darkness (1, 2, 3) and in the state of RC (4, 5, 6) (1,4-x=0; 2,5-x=0,1; 3,6-x=0,6)

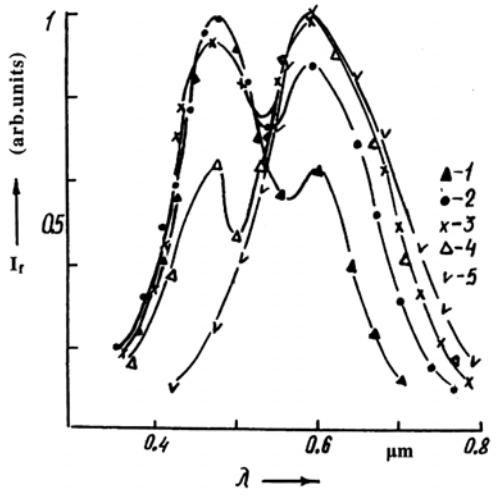

Fig.2. The spectral dependence of the films photoconductivity $Cd_{1-x}Zn_xS$ (x=0,2) versus the thermal treatment time on the air at 500°C (I - t=3 min, 2 - t=5 min, 3 - t=7 min, 4 - t=10 min, 5 - t=15 min.)

The maximum of the spectral characteristic of the samples photocurrent, subjected to TT on the air is in the range 0,47÷0,048mcm (fig.2). It should be noticed, that the maximum bias of the spectral sensitivity of the films $Cd_{1-x}Zn_xS$

to the short-wave side has been observed by the x increase. The samples has the sensitivity in the ultrasound region of the spectrum (0,32÷0,4mcm). One more peak has been observed on the spectral curves at λ=0,57mcm. The appearance of the extra maximum on the spectral curves of the photoconductivity, obviously, is connected with the formation of the cubic phase [6]. The spectrum dependence of the photoconductivity on TT time testifies the statement. The recrystallization of films occurs during the thermal treatment on the air at the temperature 500°C and it leads to the formation on the substrate more perfect by the structure films. In spite of the fact, the specific resistivity reduces, the relative intensity of the extra maximum increases.

The obtained results have the explanation in the framework of the barrier model, connected with the recombination and drift barriers for the main charge carriers. The macroscopic barriers of such type may occur, for example, in consequence of the density fluctuation of the surface state [7]. In framework of the observed model the current ratio through the drift barriers in the RC state (I_{RC}) and in the darkness (I_d) have been determined by the formula:

$$\frac{I_{RC}}{I_d} = exp\left(\frac{\varphi_{ST}}{kT}\right) \qquad (1)$$

Hence it follows, that the height of the dark drift barrier at 80 K makes φ_{ST} = 0,045÷0,06 eV. The typical relaxation time of RC depends on the height of the recombination barrier in the form:

$$\tau = \tau_0 \, exp \frac{\varphi}{kT} \qquad (2)$$

The barrier height, calculated on the base of the formula (2) and experimental data φ=0,11÷0,14eV coincides with the activation energy value of the optimal temperature dependence, i.e the recombination barrier is higher, than drift and therefore the charge accumulation occurs and the anomaly conductivity phenomenon with the following RC at the nitrogen temperature has been observed. The potential barriers reduce the section of the main carriers capture of the recombination center, and it leads to the sudden delay of the relaxation time.

The presence of the peaks on the curves of TSC predicts that there exist traps, surrounded by the powerful potential barriers in the samples. The role of these barriers reduces effectively in the process of TT. It is testified by the increase of the light sensitivity and peak reduction at 240÷270K on the curves of TSC after TT on the air at 500°C.

[1] *P.K. Nair, V.M. Garcia, O. Gomez-Daza and MTS Nair.* Semicond. Sci. Technol. 2001, v.16, № 10, 855-863.

[2] *E.N. Zamanova, M.A. Jafarov, S.M. Bagirova, K.Kh, Eivazova, L.A. Aliyeva.* Izv. AN, Azerbaijan, 2001 № 2, v.XX, Elm., Baku

[3] *E. Bacaksi, V. Novruzov, H. Karal, E. Yanmaz, M. Altunbas and A.I. Kopya.* J.Phys. D: Appl. Phys., 2001, v. 34, № 21, 2109-2112.

[4] *E.N. Zamanova, M.A. Jafarov.* PTS, 1995, v.29, issue 8, 1411-1415.

[5] *E.N. Zamanova, M.A. Jafarov, H.M. Mamedov.* Effect of Heat treatment on electrophysical and photoelectrical properties of *p*-type CdS Polycrystals, Semiconductor Science and Technology. Ins. of Phys. Publishing, Bristol, London, Philodelp., Paris, St. Petersburg, 12 SSt/ABC, 1999, 1234-1239.

[6] *W. Kahle.* Phys. Status Solidi, 1970, 2, № 4, 717-723.

[7] *V.B. Sandomirskiy, A.G. Jolan*. PTS, 1973, v.7, issue 7, p. 1314-1323.

E.N. Zamanova

$Cd_{1-x}Zn_xS$ TƏBƏQƏLƏRİNDƏKİ REKOMBİNASİYA VƏ DREYF BARYERLƏRİNƏ HAVADA TERMOEMALIN TƏSİRİ

Məhluldan çökülmə üsulu ilə alınmış $Cd_{1-x}Zn_xS$ (x=0÷0,6) təbəqələrində əsas yükdaşıyıcılar üçün dreyf və rekombinasiya baryerləri hesablanıb. Təyin olunub ki, rekombinasiya baryerlərinin hündürlüyü dreyfdən yüksəkdir, bu da yüklərin toplanmasına və qalıq keçiriciliyinin yaranmasına səbəb olur. Təbəqələrin havada termoemalı baryerlərin rolunu zəiflədir, işığa həssaslığı artırır.

Э.Н. Заманова

ВЛИЯНИЕ ТЕРМООБРАБОТКИ НА ВОЗДУХЕ НА РЕКОМБИНАЦИОННЫЕ И ДРЕЙФОВЫЕ БАРЬЕРЫ В ПЛЕНКАХ $Cd_{1-x}Zn_xS$ (x=0-0,6)

В пленках $Cd_{1-x}Zn_xS$ (x=0-0,6), полученных осаждением из раствора, вычислены значения дрейфового и рекомбинационного барьера для основных носителей. Установлено, что высота рекомбинационного барьера выше, чем дрейфового, что приводит к накоплению зарядов и остаточной проводимости. В результате термообработки на воздухе роль этих барьеров эффективно снижается, светочувствительность увеличивается.

Received: 12.04.03

SPARTIAL STRUCTURE OF HEXADECAPEPTIDE FRAGMENT OF BAM-20P`MOLECULE

E.M. HASANOV, Z.H. TAGIYEV,
Azerbaijan Medical University,
Baku-22, Bakikhanov str.,23.

G.A. AKHVERDIYEVA, N.A. AKHMEDOV
Baku State University,
Z.Khalilov str., 23, Baku, 370143

Using a method of the theoretical conformational analysis, a spatial structure of the Tyr1-Asp16 hexadecapeptide fragment of BAM-20P molecule (Tyr1-Gly2-Gly3-Phe4-Met5-Arg6-Arg7-Val8-Gly9-Arg10-Pro11-Gly12-Trp13-TRp14-Met15-Asp16-Tyr17-Gln18-Lyz19-Arg20), isolated from adrenal medulla was investigated.

The potential energy of the molecule is given as the sum of the contributions of Van der Vaals, electrostatic, torsional interactions and hydrogen bonds energy. It has been shown that the spatial structure of tyr1-asp16 fragment is represented by ten backbone forms.

The opioid peptide Tyr1Gly2-Gly3-Phe4-Met5-Arg6-Arg7-Val8-Gly9-Arg10-Pro11-Glu12-Trp13-Trp14-Met15-Asp16-Tyr17-Gln18-Lys18-Lys19-Arg20 is isolated from medulla of bovine adrenal, indicated as BAM-20P (bovine adrenal medulla 20 reside peptide). The opiate activity of the BAM-20P in several times higher, than the activity of Met-enkefalin and β-endofine. There are Met-enkefalin (Tyr1-Met5), adrenorfine (Tyr1-Val1), BAM-12P (Tyr1-Glu12), in the succession of BAM-20P, and the molecule BAM-20P itself is the part of composition of peptides *E* and *I* [1, 2]. Therefore the investigation of the spatial structure of the molecule BAM-20P is the big interest as for elucidation of structure-functional organization of the molecule itself, as all the above mentioned peptides.

The study of structure-functional organization of the hormone on the atom-molecule level requests firstly the knowledge of set of low-energy molecule states and consequently the potential physiological active conformation ones.

The spatial structure of the molecule BAM-20P is investigated fragmently. At first the conformation probabilities of fragments Val6-ValP, Arg10-Glu12,Trp13-Asp16, Asp16-Arg20 were studied on base of the low-energy states of according aminoacid residues. The spatial structures of the molecules of Met-enkefalin (Tyr1-Met5) and adrenorfine (tyr1-Val8) were investigated by us earlier, the results are presented in ref [3, 4]. On the second stage the three-dimensional structure of molecule BAM-12P (Tyr1-Glu12) was found on the base of stable conformations Tyr1-Val8, Gly19, Arg10-Glu12.

The conformation probabilities of fragment Tyr1-Asp16 (fig.1) were studied on the following stage on the base of the stable three-dimensional structures of fragments Tyr1-Glu12 and Trp13-Asp15.

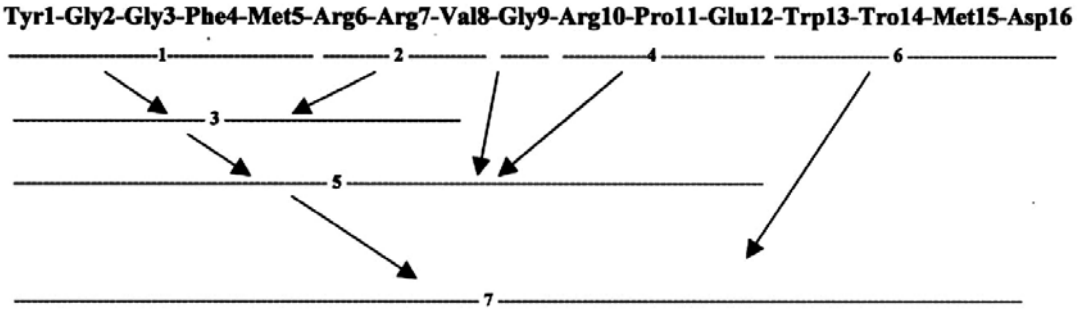

Fig.1. Circuit of the calculation of the hexadecapeptide fragment of the molecule BAM-20P.

In this paper the results of theoretical conformation analysis of the *N*-ended hexapeptide fragment, Tyr1-Gly2-Gly3-Phe4-Met5-Arg6-Arg7-Val8-Gly9-Arg10-Pro11-Glu12=Trp13-Trp14-Met15-Asp16 of the molecule BAM-20P are given. The potential function of the system is taken in the sum form of the nonvalence, electrostatical and torque interactions and the energy of the hydrogene bonds. The calculation of the fragments is made on the base of the theory and method, which are presented in ref [5-8]. The classification of the peptide structure on conformations, forms of the fundamental chain and the shapes of the peptide scelet, proposed in ref [5-8] was used at the presentation of calculation results.

The optimal conformations of the molecule (Tyr1-Glu12) BAM-12P, established as a result of calculation, the energy of which isn't more, than 10kcal/mol are given in the table 1. The four conformations of Met-enkefalin (Tyr1-Met15) and the eleven conformations of adrenorfine (Tyr1-Val8) were between the lowenergy conformations BAM-12P and are presented in the table 1. In geometrical interpretation of adrenorfine fragment, given in this table, the conformations of molecule BAM-12P, which are preferred on the energy, disintegrate on the four groups (*A*-*D*). These 23 conformations are chosen as the initial approximations for the calculation of the *N*-ended hexapeptide fragment Tyr1-Asp16 of the molecule BAM-20P.

Table 1

The relative energy and energy contributions of nonvalence ($U_{nv.}$), electrostatic ($U_{el.}$), torsional interactions of optimum conformations of the molecule BAM-12P.

Gr.	№	Conformation	$U_{nv.}$	$U_{el.}$	$U_{tor.}$	$U_{rel.}$
	1	$B_{211}PRR_{21}B_{332}R_{2222}R_{3222}R_2BL_{22}RR_{32}$	-41.4	8.5	6.4	0
	2	$B_{211}PRR_{21}B_{332}R_{2222}R_{3222}B_2RB_{21}RR_{32}$	-39.6	14.7	8.0	9.7
A	3	$B_{211}PRR_{21}B_{332}R_{2222}R_{3222}R_2PB_{21}RR_{32}$	-44.2	18.0	7.7	8.0
	4	$B_{211}PRR_{21}B_{332}R_{2222}R_{3222}R_2PL_{22}RR_{32}$	-42.7	18.7	5.9	8.5
	5	$B_{211}PRR_{21}B_{332}R_{2222}R_{3222}R_2LL_{22}RR_{32}$	-42.2	18.2	6.4	9.1
	6	$B_{131}BPB_{21}B_{212}B_{1222}B_{2222}R_2BL_{22}RR_{32}$	-41.1	10.3	6.0	1.8
	7	$B_{131}BPB_{21}B_{212}B_{1222}B_{2222}R_2PB_{21}RR_{32}$	-37.4	13.4	7.1	9.7
	8	$B_{131}BPB_{21}B_{212}B_{1222}B_{2222}B_2RB_{21}RR_{32}$	-39.8	11.2	8.0	6.1
	9	$B_{131}BPB_{21}B_{212}B_{1222}B_{2222}B_2BL_{22}RR_{32}$	-39.7	10.9	8.8	6.5
B	10	$B_{131}BPB_{21}B_{212}B_{1222}R_{2222}B_2BL_{22}RR_{32}$	-42.7	15.9	7.0	6.8
	11	$B_{131}BPB_{21}B_{212}B_{1222}R_{2222}B_2RB_{21}RR_{32}$	-41.4	15.3	6.7	7.2
	12	$B_{131}BPB_{21}B_{212}B_{1222}R_{2222}B_2BB_{21}RR_{32}$	-42.2	15.2	7.8	7.4
	13	$B_{131}BPB_{21}B_{212}B_{1222}R_{2222}B_2RL_{22}RR_{32}$	-39.9	16.3	5.3	8.3
	14	$B_{132}RPB_{33}B_{222}B_{1222}B_{2222}R_2BL_{22}RR_{32}$	-40.2	10.1	5.8	2.2
	15	$B_{132}RPB_{33}B_{222}B_{1222}B_{2222}B_2RB_{21}RR_{32}$	-40.0	9.1	9.6	5.3
	16	$B_{132}RPB_{33}B_{222}B_{1222}B_{2222}B_2BL_{22}RR_{32}$	-38.4	11.7	8.4	8.4
	17	$B_{132}RPB_{33}B_{222}B_{1222}R_{2222}B_2BB_{21}RR_{32}$	-41.6	14.8	7.2	7.0
C	18	$B_{132}RPB_{33}B_{222}B_{1222}R_{2222}B_2BL_{22}RR_{32}$	-41.7	15.7	7.3	8.0
	19	$B_{132}RPB_{33}B_{222}B_{1222}R_{2222}B_2RB_{21}RR_{32}$	-40.2	15.8	6.6	8.7
	20	$B_{132}RPB_{33}R_{222}B_{1222}R_{3222}B_2BL_{22}RR_{32}$	-42.8	14.8	9.5	8.1
	21	$B_{132}RPB_{33}R_{222}B_{1222}R_{3222}B_2BB_{21}RR_{32}$	-40.9	15.5	8.2	9.3
	22	$B_{212}BPR_{21}R_{212}B_{1222}B_{2222}R_2BL_{22}RR_{32}$	-43.3	11.8	9.1	4.1
D	23	$B_{212}BPR_{21}R_{212}B_{1222}B_{2222}B_2RB_{21}RR_{32}$	-43.3	11.8	12.9	7.9

Table 2.

Energy distribution of conformations of the fragment Trp-13-Asp16 of the molecule BAM-20P

The fundamental chain form	The number of energy conformations, kcal/mol.					
	0-1	1-2	2-3	3-4	4-5	>5
BBBB	-	-	2	1	7	7
RRRR	3	5	7	2	-	25
RRBR	-	-	-	-	2	7
BRRR	-	-	-	-	1	2
RBBB	-	-	-	2	1	3
BBRR	-	1	1	-	-	4
BRBB	-	-	-	-	1	8
RBRR	-	-	-	-	-	6

The spatial structure of the tetrapeptide fragment Trp13-Trp14-Met15-Asp16 of the molecule BAM-20P is investigated on the base of the lowenergy conformations according aminoacid residues of triptofane, methionine and the calculation was made on the forms of the fundamental chain. Firstly the conformations of the total unwrapped form BBBB and the total curtailed form RRRR. The considered interactions between the aminoacid residues in these forms are taken into consideration in another forms of the fundamental chain too. Therefore the number of the considered conformations for them is less, than in curtailed and unwrapped forms. The energy distribution of the conformations of the fragment Trp13–Asp16 of the molecule BAM 20P is shown in the table 2. At the energy 0-4kcal/mol there are 24 conformations of the four forms of the fundamental chain, but in the energy interval 0-6kcal/mol. there are conformations of the eight forms of the fundamental chain. The relative energy of the lowenergy conformations of each form of the fragment Trp13-Asp16 of the molecule BAM-20P is shown in the table 3. These conformations are chosen for the calculation of the fragment Tyr1–Asp16 of the molecule BAM-20P. Thus, the lowenergy states of the fragments Tyr1–Glu12 and Trp13–Asp16 became the base of the consisting of the zero approximations for the calculation of the three-dimensional structure of the *N*-ended hexapeptide fragment Tyr1–Asp16 of the molecule BAM-20P, the number of which is 184. The results of the calculations are shown, that the sharp energy differentiation appears between the forms of the fundamental chain and between conformations.

Table3

The relative energy of lowenergy conformations of the fragment Trp13-Asp16 of the molecule BAM-20P

The fundamental chain form	$E_{rel.}$
$B_2B_2B_{21}B_1$	2.1
$R_1R_1R_{32}R_1$	0
$R_1R_1B_{21}R_1$	4.9
$B_3R_1R_{32}R_1$	4.6
$R_2B_2B_{21}B_1$	4.0
$B_2B_1R_{21}R_1$	1.4
$B_1R_2B_{21}B_1$	5.0
$R_2R_2R_{32}R_1$	5.7

In the wide energy interval 0-10kcal/mol there are only ten conformations. The forms of the fundamental chain, the energies of nonvalence, electrostatical and torsional interactions, and also the relative energy of these conformations are presented in the table 4. The addition of

the tetrapeptide fragment Trp13-Asp16 leads to the sharp decrease of the number of their lowenergy conformations, entering to the preferred structures Tyr1-Asp16. The group *A* of the molecule Tyr1-Glu12 has the 5 conformations, but the fragment Tyr1-Asp16 has the remaining 3 conformations, the group *B* is presented by *P* conformations, and the remain is 5 conformations, the group *C* is presented by 8 conformations and the remain is 2 ones. Among the lowenergy conformations of the fragment Tyr1-Asp16 the 3 forms of the fundamental chain from the 8 chosen of the *C*-ended tetrapeptide region Trp13-Trp14-Met15-Asp16 are realized. The form of the fundamental chain BRRR is realized in the 5 conformations, RBRR is in the 4, and RBBB is in the only one. The triptofane and methionine have the big and the labile side chain, therefore only in the especial cases they can arrange energetically by propit to the formed structures.

In the stable conformations of the fragment Tyr1-Asp16 the energy of nonvalence interactions changes in the interval 71.3-62.4kcal/mol, the energy of electrostatical interactions changes in the interval 5.9-13.6kcal/mol, the energy of torque interactions changes in the interval 8.1-13.6kcal/mol. As it is seen, the difference between the energies of nonvalence, electrostatical and torsional interactions is equal to 8.9, 7.7 and 5.2kcal/mol among the optimal conformations of the fragment Tyr1-Asp16 BAM-20P correspondingly. It means, that the each from these three forms of interactions playes the important role at the formation of the spatial structure of the fragment Tyr1-Asp16. The global conformation is the most benefit on the nonvalence (-71.3kcal/mol) and electrostatical (5.9kcal/mol) interactions, but the less benefit on the torsional interactions (13.3kcal/mol). This conformation of Met-enkefalin has the relative energy 3.5kcal/mol, of adrenofine one is 4.3kcal/mol, of BAM-12P one is 6.5kcal/mol. This means, that the far-away interactions, playing the essential role in the stabilization of the spatial structure of the investigated fragment with the lengthening of the peptide chain. The pentapeptide region in the structure with relative energy 5.2kcal/mol has the conformation, according to the clobal conformation of the Met-enkefalin. It loses 1.6kcal/mol on the nonvalence, 6.3kcal/mol on the electrostatical, but benefits the 3.7kcal/mol on the torsional interactions in comparison of the global conformation. The relative energy of the rest of three conformations of the group B changes in the interval 9.2-9.8kcal/mol. The group *A* is presented by the three conformations, the relative energy of which changes in the interval 6.4-9.0kcal/mol, but the group *C* is presented by the two conformations with the relative energies 6.7 and 9.2kcal/mol (table 4). The conformations, given in table 4, are the base for the finishing of the investigation of the spatial structure of the whole molecule BAM-20P.

Table 4.

The fundamental Chain forms, energy contributions of non valence ($U_{nv.}$) electrostatic ($U_{el.}$), torsional interactions (U_{tor}) and relative energy ($U_{rel.}$) of lowenergy conformations of fragment Tyr1-Asp16 of molecule BAM-20P

Gr.	№	Conformation	$U_{nv.}$	$U_{el.}$	$U_{tor.}$	$U_{rel.}$
A	1	$B_{211}PRR_{21}B_{322}R_{222}R_{322}R_2BL_{222}RR_{32}B_3R_1R_{322}R_1$	-64.3	9.4	9.2	6.4
	2	$B_{111}PRR_{21}B_{322}R_{222}R_{322}R_2BL_{222}RR_{32}B_3R_1R_{21}R_1$	-64.1	12.0	8.1	8.1
	3	$B_{211}PRR_{21}B_{332}R_{222}R_{222}R_2PL_{222}RR_{32}R_2B_2R_{33}R_1$	-65.2	13.6	8.5	9.0
B	4	$B_{131}BPB_{21}B_{212}B_{122}B_{222}R_2BL_{222}RR_{32}B_3R_1R_{32}R_1$	-64.6	12.8	8.9	9.2
	5	$B_{131}BPB_{21}B_{212}B_{122}B_{222}B_2BL_{222}RR_{32}B_3R_1R_{32}R_1$	-64.6	10.5	11.8	9.8
	6	$B_{131}BPB_{21}B_{212}B_{122}B_{222}B_2BL_{222}RR_{32}R_2B_2B_{21}B_1$	-62.4	9.0	10.8	9.4
	7	$B_{131}BPB_{21}B_{212}B_{122}B_{222}B_2BL_{222}RR_{32}R_2B_2R_{33}R_1$	-71.3	5.9	13.3	0
	8	$B_{131}PRR_{21}B_{212}B_{122}R_{222}B_2BL_{222}RR_{32}R_2B_1R_{33}R_1$	-69.7	12.2	9.6	5.2
C	9	$B_{131}PRB_{33}B_{222}B_{122}B_{322}B_2BL_{222}RR_{32}B_3R_1R_{32}R_1$	-63.6	11.9	8.7	9.2
	10	$B_{132}PRB_{33}B_{222}B_{122}B_{222}B_2BL_{222}RR_{32}R_2B_2R_{33}R_1$	-65.6	7.4	12.9	6.7

[1] *K. Mizumo, N. Minamino, K.Kandowa, H. Matsuo*. Biochem. Biophys. Res. Commun., 1980, v. 95, №4, p.1482-1488.

[2] *G.Kupruszewski*. Wiss. Beitt. M. Luther-Univ. Hulle, Wittenberg, 1988, №32, p.218-240.

[3] *E.M.Popov, N.M.Godjayev, N.A.Akhmedov, E.B Suleymanova.* Bioorgan. Khimiya, 1990, t.16, №4, s. 482-491.

[4] *N.A. Akhmedov, T.A. Makhmudova, E.M. Popov.* Bioorgan. Khimiya, 1993, t.19, №6, s.623-628.

[5] *E.M. Popov*. Int. J. Quant. Chem. 1979, v.16, p.707-737.

[6] *E.M. Popov*. Molekulyarnaya boil., 1985, t.19, s. 1107-1138

[7] *E.M. Popov*. M., Nauka, 1989, s.352

[8] *N.A. Akhmedov, G.A. Akhverdiyeva, N.M. Godjayev, E.M. Popov*. Int. J. Peptide and Protein Res. 1986, v.27. №2, p.95-111.

E.M. Həsənov, Z.H. Tağıyev, Q.Ə. Haqverdiyeva, N.A. Əhmədov

BAM-20P MOLEKULUNUN HEKSADEKAPEPTİD FRAQMENTİNİN FƏZA QURULUŞU

Sümük iliyindən ayrılmış BAM-20P molekulunun (Tyr1-Gly2-Gly3-Phe4-Met5-Arg6-Arg7-Val8-Gly9-Arg10-Pro11-Gly12-Trp13-TRp14-Met15-Asp16-Tyr17-Gln18-Lyz19-Arg20) Tyr1-Asp16 heksadekapeptid fraqmentinin fəza quruluşu nəzəri konformasiya metodu ilə öyrənilmişdir. Molekulun potensial enerjisi Van-der Vaals elektrostatik, torsion qarşılıqlı təsir

enerjilərinin və hidrogen rabitəsi enerjisinin cəmi şəklində seçilmişdir. Göstərilmişdir ki, Tyr1-Asp16 fraqmentinin fəza quruluşu əsas zəncirin on forması ilə tərənnüm olunur.

Э.М. Гасанов, З.Г. Тагиев, Г.А. Ахвердиева, Н.А. Ахмедов

ПРОСТРАНСТВЕННАЯ СТРУКТУРА ГЕКСАДЕКАПЕПТИДНОГО ФРАГМЕНТА ВАМ-20Р

Методом теоретического конформационного анализа изучена пространственная структура гексадекапептидного фрагмента (Tyr1-Gly2-Gly3-Phe4-Met5-Arg6-Arg7-Val8-Gly9-Arg10-Pro11-Gly12-Trp13-TRp14-Met15-Asp16-Tyr17-Gln18-Lyz19-Arg20) молекулы ВАМ-20Р выделенной из костного мозга. Потенциальная энергия молекулы выбрана в виде суммы энергии Ван-дер Ваальсовых, электростатических, торсионных взаимодействий и энергии водородных связей. Показано, что пространственная структура фрагмента Tyr1-Asp16 представлена десятью формами основной цепи.

Received: 14.04.03

METHODS OF DEVELOPMENT OF INTERACTIVE WAP APPLICATIONS.

TEIMUR MUKHTAROV
Institute of Cybernetics of the Azerbaijan National Academy of Sciences
370602, Baku, F. Agayev str. 9, Azerbaijan

In this paper interactive WAP applications working with Oracle database building principles are stated. Characteristics of protocol itself are given, data storage solutions and data representation in database are described. Also program code snippels, allowing creation of database structure and fully functional set of application.

Introduction.

Internet takes the increasing and greater place in our life. With growth of popularity of a world wide web the growing amount of users has complexities with access to their information resources. In most cases it is related to need of possession of transmission device - computer, modem, phone line. Manufacturers of cellular telephones have equipped their devices with modems and browsers (the last now even more often settle down not on the handset itself, but on a phone card) as the decision of the given problem. The special protocol working with a mobile communication facility - WAP (Wireless Application Protocol or Wireless Access Protocol) has been developed.

By development of family of protocols WAP the following principles were used:

- Complete set WAP should provide access to Internet, intranets and information services of mobile operators. Whenever possible, it should be based on existing standards;
- It is necessary, when using WAP not conflict with the basic functions of the handset;
- The architecture of family of protocols should correspond with OSI model; it is necessary to provide scalability and expansion opportunity;
- Protocol should be designed for use in networks with small bandwidth and, probably, the big information transfer delays. It is required to consider also small volume of operative memory and low speed of the central processors of user's terminals;
- It is necessary to take into account, that user's terminals have rather limited opportunities for input of the information by the user;
- In architecture WAP support of various types of wireless networks should be incorporated;
- It is necessary, that the family of protocols WAP provide data protection;
- New application model providing services for data transfer to wireless phones should be developed.

For increase speed of data processing special language WML (Wireless Markup Language) based on known language XML which has in turn taken place from HTML has been developed. Standard HTML has so many different features, that memory of cellular devices cannot contain an existing set of processing rules. And for small displays of mobile phones many HTML features were an obvious excess. In addition to WML language WMLS has been developed - WML Script. WMLS is adapted variant of language JavaScript.

Now the basic inconvenience for WAP users is insufficient amount of information resources. WAP developers meet tasks in maintenance of services for mobile devices owners. The user who has so many services with Internet cannot be content any more with their limited subset. One of the basic moments here is interactivity and "freshness" of the information provided.

In fact there is no sense to use mobile means to access static and "dead" - unchangeable data. Therefore development of WAP site includes not only providing user with the information, but also simplification of routines for the data responsible person on a site, and also integration tools with other various systems which will provide interactivity to a site.

1. Data presentation

For effective work WAP site it is necessary to design mechanisms for maintenance fast, convenient and safe delivery of the data, which further will be given to the end user. For this purpose, first of all, it is necessary to define, where this information will be stored. There are, at least, four variants of the decision of this problem:

- The Information is stored statically on a WAP-site as WML-pages
- The Information is stored in text files
- The Information is stored in operative memory
- The Information is stored in a database

The fourth variant seems to be most convenient for development of interactive systems. It provides, both speed of access, and safety of the stored data. Besides, developers of databases, as a rule, give the interface for DB(database) access, that essentially makes easier work of the programmer. Further in this work as a database we shall understand Oracle product of the version higher than 7.3[1]. In a database the arrived information will be stored in hierarchical treelike structure (fig. 1).

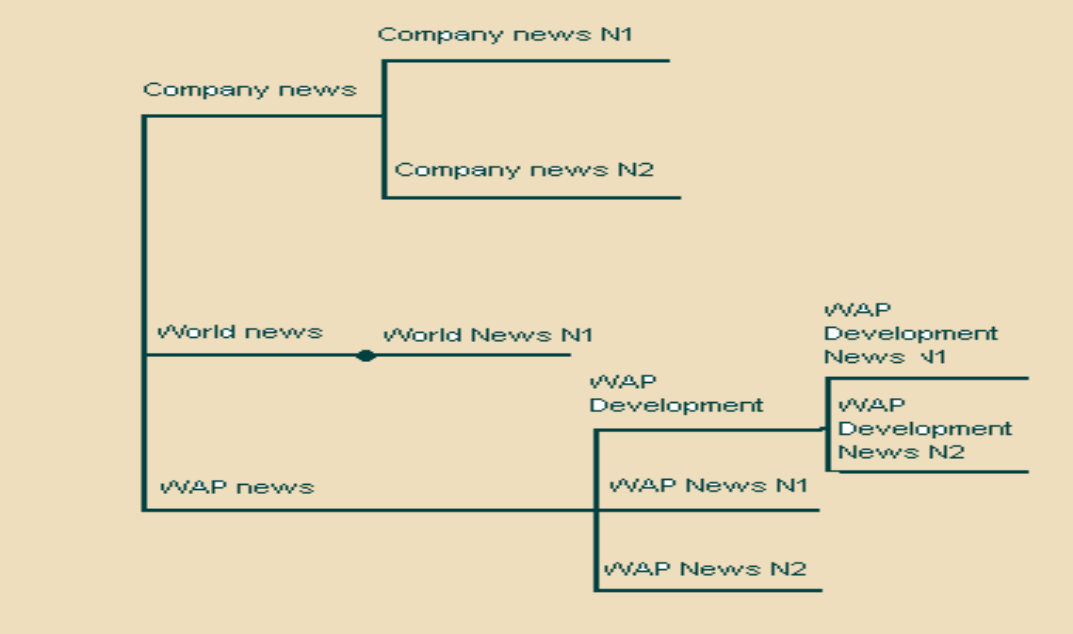

Fig. 1.

Hierarchy is provided by pair of identifiers for each element of a tree: the first - the identifier of the parental element, the second - the serial identifier of the element. At the end-point of the information delivery, uniqueness of last identifier is guaranteed by such built-in Oracle object as sequence. So the static elements submitted on rice 2.1, will have the following identifiers according to the offered scheme:

(0,1) - Company news

(0,2) - World news

(0,3) - WAP news

(3,4) - WAP Development

Further dynamic elements (data given to the WAP-site) at receipt will receive the following identifiers:

(1,5) - Company news N1

(1,6) - Company news N2

(2,7) - World news N3

(4,8) - WAP Development News N1

(4,9) - WAP Development News N2

(3,10) - WAP News N1

(3,11) - WAP Development News N2

Certainly in that case when the data will be received in the corresponding order. Besides, for dynamic elements the additional identifier also is necessary to distinguish them from the static data. The static data may be used in system as well for simplification of applications development.

2. Development of the application

Now we shall pass to development database structure and an initial code of system itself. We shall start with development of organization of database, and then we shall pass to initial modules directly processing the information. At creation of the database structure it is meant, that we have privelegies of the system administrator (SYSADM) in this base. So, the scripts necessary for creation of the table containing data provided to the WAP-site will look as follows[3,4]

```
CREATE TABLE WAP_DATA (
        I_ID            FLOAT,
        P_ID    FLOAT,
        PARAM_1         VARCHAR2 (22),
        PARAM_2         VARCHAR2 (22),
        PARAM_3         VARCHAR2 (22),
        PARAM_4         VARCHAR2 (22),
        PARAM_5         VARCHAR2 (22),
        I_DESC          VARCHAR2 (15),
        I_SELF          VARCHAR2 (2000),
        DATE_1          DATE,
        DATE_2          DATE,
        DATE_3          DATE,
        I_STAT  VARCHAR2 (1));
```

```
CREATE INDEX SYSADM.WAP_DATA_IID_IDX
        ON SYSADM.WAP_DATA (I_ID)
TABLESPACE INDX;

CREATE INDEX SYSADM.WAP_DATA_PID_IDX
        ON SYSADM.WAP_DATA (P_ID)
TABLESPACE IDX;

CREATE INDEX SYSADM.WAP_DATA_D1_IDX
        ON SYSADM. WAP_DATA (DATE_1)
TABLESPACE INDX;

CREATE INDEX SYSADM.WAP_DATA_D2_IDX
        ON SYSADM.WAP_DATA (DATE_2)
TABLESPACE INDX;

CREATE INDEX SYSADM.WAP_DATA_I_STAT_IDX
        ON SYSADM. WAP_DATA (I_STAT)
TABLESPACE INDX;

GRANT SELECT ON WAP_DATA TO PUBLIC;

GRANT DELETE ON WAP_DATA TO WAP_OPER;

GRANT INSERT ON WAP_DATA TO WAP_OPER;

GRANT UPDATE ON WAP_DATA TO WAP_OPER;
```

Fields *I_ID* and *P_ID* form a pair of the hereditary relation about which was spoken above. Fields-parameters *PARAM1, PARAM2, PARAM3, PARAM4, PARAM5* can be used under the discretion of the developer, or are not used in general. In a system - example field *PARAM1* will be used for identification of structural recordings and directly information, and field *PARAM_2* for identification of language of the information. Pair of fields *DATE_1* and *DATE_2* define a time interval during which the information is considered to be valid. It is obvious, that these fields make sense only for records, which contain the data, for providing to the WAP-site, instead of the structural information. Whether field *DATE_3* defines if the information has passed the control of the data by the WAP-operator. And at last the field *I_STAT* is necessary for emergency removal of the data.

A plenty of indexes is caused that, that in view of small bandwidth of a mobile network, time of references to a database should be minimal. In case of a small amount of the data a part, or even all indexes can be omitted. We shall notice only, that indexes are created in separate space of a database (*TABLESPACE INDX).* Such use of indexes is directed on even more to increase speed of data processing in database.

As on the Internet there is a set various manuals and guides, and taking into account rather simple realization we shall not result here detailed consideration of development static wml pages, and at once we shall pass to realization JAVA servlet carrying out exact search of the data in resulted information structure[2]:

```
System.out.println (" <? xml version = \ " 1.0 \ "?> ");
System.out.println (" <! DOCTYPE wml PUBLIC \ "-
                    // WAPFORUM // DTD WML 1.1 // EN \ "
                    \ " http: // www.wapforum.org/DTD/wml_1.1.xml \ "> ");
System.out.println ("<wml>");
System.out.println (" <card id = \ " start \ " title = \ " WAP News \ "> ");
System.out.println (" <do type = \ " accept \ "
                    label = \ " Back \ "> <prev/> </do> ");
System.out.println (" <p align = \ " left \ "> ");
……
    try {
        ResultSet rs = null;
```

```
Statement stmt=conn.createStatement ();
rs=stmt.executeQuery (" select I_SELF, I_ID,
P_ID, PARAM1 from WAP_DATA where
P_ID = " +p_id + " and DATE1 <SYSDATE and
DATE2> SYSDATE and PARAM_2 = ” + lang + ” and
DATE3 is not null ");
while (rs.next ()) {
        qryCnt ++;
        rsString=rs.getString (1);
        isLink = rs.getString (4);
        if ("A" .equals (isLink)) {
                System.out.println (rsString);
                System.out.println (" <br> </br> ");
        }
        System.out.println (" <br> </br> ");
        continue;
        }
}
catch (SQLException sqle)
{
rsString = sqle.toString ();
}
……………………………………………….
System.out.println (" </p> ");
System.out.println (" <p align = \ " center \ "> ");
System.out.println (" <a href = \ " http: // 127.0.0.1/main.wml \ ">
                        WAP News </a> ");
System.out.println (" </p> ");
System.out.println (" </card> ");
System.out.println (" </wml> ");
```

Thus, we provided basic actions needed for development of real interactive WAP service. Though Oracle is considered to be used in our case, generally any database providing multi-user access can be used as well. The system designed on the principles stated above has successfully passed approbation in Azercell Telecom JV. Further work supposes implementation of interactive information services on different mediums.

[1] *T.M. Mukhtarov.* Oracle: Evolution and Perspectives for Database Applications Developers, Thesis’s of VIII international conference “Mathematics, Computer, Education”, Pushino, 2001, p.74

[2] *Christoffer Andersson*, GPRS and 3G Wireless Applications: Professional Developer's Guide

[3] *S. Urman.* Oracle 8. Programmirovaniye na yazike PL/SQL M., ЛОРИ, 1999, p.607.

[4] *S. Bobrovsky* Oracle 8. Arkhitektura. M., ЛОРИ, 1999, p.207.

Teymur Muxtarov

İnteraktiv WAP əlavələrinin işlənməsi metodları

Məqalədə Oracle verilənlər bazasının idarə olunma sistemi əsasında interaktiv WAP əlavələrinin arxitekturasınn quruluşu

prinsipləri təhlil edilmişdir. Bilavasitə protokol xarakteristikaları göstərilmiş, məlumatların saxlanma və onların verilənlər bazasında əks etdirilmə qaydaları təsvir edilmişdir. Eləcə də verilənlər bazasının quruluşunu və əlavələrin tam sistemini yaratmağa imkan verən mənbə kodlarının fraqmentləri təklif edilmişdir.

Теймур Мухтаров

МЕТОДЫ РАЗРАБОТКИ ИНТЕРАКТИВНЫХ WAP ПРИЛОЖЕНИЙ

В статье изложены принципы построения архитектуры интерактивных WAP приложений на базе СУБД Oracle. Приведены характеристики непосредственно протокола, описаны способы хранения данных и представления их в базе данных. Также предлагаются фрагменты исходных кодов, позволяющие создать структуру базы данных и полноценную систему приложений.

Received: 14.03.03

AZƏRBAYCANCA-RUSCA-İNGİLİSCƏ FİZİKİ TERMİNLƏR LÜĞƏTİ

AZERBAIJAN-RUSSIAN-ENGLISH DICTIONARY OF THE PHYSICAL TERMS

АЗЕРБАЙДЖАНО-РУССКО-АНГЛИЙСКИЙ ФИЗИЧЕСКИЙ ТЕРМИНОЛОГИЧЕСКИЙ СЛОВАРЬ

Tərtib edənlər: **AME-nın müxbir üzvü**
A.İ. Muxtarov

SSRİ EA-nın müxbir üzvü,

akademik **H.M. Abdullayev**

Fizika-riyaziyyat elmləri doktoru
T.R. Mehdiyev

Fizika-riyaziyyat elmləri namizədi
E.A. Axundova

N.İ. Acalova

S.İ. Əliyeva

A.İ. Muxtarov

Azərbaycanca-Rusca-İngiliscə fiziki terminlər lüğəti

Azərbaycan Respublikası 10 ildən artıqdır ki, dünyanın bütün dövlətləri tərəfindən tanınmış, sərbəst dövlət kimi mövcuddur. Buna görə də, Azərbaycan dili dövlət statusuna malikdir. Başqa sözlə, Azərbaycan Respublikasının bütün vətəndaşları dövlət dilində tam təhsil almaq, pedaqoji fəal elmi iş aparmaq imkanına malik olmalıdır.

Azərbaycan elmi, dünya elminin və texnikanın əksər sahələrində həmişə özünə layiq yer tutmuşdur. Bu yeri itirməmək üçün respublika alimləri müasir dünya elminin inkişaf istiqamətlərində əldə edilmiş müvəffəqiyyətləri həmişə işləməli və onları elm sahəsində işləyən gənclərə çatdırmalıdırlar.

Bundan başqa, xarici ölkələrdən respublikaya daxil olan elmi ədəbiyyat və dərs vəsaitlərinin əksər hissəsi rus və ingilis dillərində nəşr edilmiş olur. Eləcə də dünya xalqları arasında elmi əlaqələr, əsasən ingilis dilində aparılır. Bütün bunlar respublikada fizika elminin fəal inkişafı üçün daha dolğun və daha mükəmməl azərbaycan-rus-ingilis dillərində fizika terminləri lüğətinin yaradılması məsələsini aktual bir problem kimi qarşıya qoymuş olur. Belə ki, hazırda mövcud olan lüğətlər, məsələn, Azərbaycan MEA-nın Fizika institutunun kollektivi tərəfindən tərtib edilmiş "Fizika terminləri lüğəti"nə fizika elminin müasir inkişaf mərhələsində istifadə olunan fizika terminlərinin əksəriyyəti daxil olmur.

Azərbaycan MEA-nın Fizika institutunun və Bakı Dövlət Universitetinin əməkdaşları birlikdə fizika terminlərini belə bir mükəmməl lüğəti tərtib etməyi qərara almışlar. Təklif olunan terminlər lüğətinə fizika elmi ilə təmasda olan texnikada təsadüf olunan terminləri də daxil etmək nəzərdə tutulur.

Redaksiya heyəti Akademiyanın, universitetlərin və başqa müəssisələrin elmi işçilərinə müraciət edərək xahiş edir ki, onlar bu lüğətin yaradılmasında fəal iştirak etsinlər. İştirakçılara əvvəlcədən təşəkkür edirik.

Azerbaijan-Russian-English dictionary of the physical terms

The Azerbaijan Republic more than ten years exists as the independent state recognized by the world community, thus to the Azerbaijan language the status of a state language has been validated.

It means that all citizens of the Azerbaijan Republic should have an opportunity to receive full education in a state language, actively carrying out on it the scientific and teaching activities.

The Azerbaijan science always took a worthy place in many areas of a world science and techniques. For these positions have not been lost, scientists or the republic are obliged to keep up all modern directions in development of a world science, to bring in due time its tendencies to studying young generation.

At the same time the majority of the scientific and educational literature, coming to republic from abroad, is issued in Russian and English languages. Besides that, the English language is the language of international scientific communication due to the set of historical reasons. All this makes rather actual for active development in republic of a physical science the edition of as much as possible full and perfect the Azerbaijan-Russian-English dictionary of physical terms, because the dictionaries issued earlier, for example «Fizika terminləri luğəti», created by scientists of Institute of Physics of National Academy of Sciences of Azerbaijan, does not contain many terms used in modern physics.

Institute of Physics NAS of Azerbaijan together with the Baku State University have started to work on the Azerbaijan-Russian-English dictionary of the physical terms, more adequate answering to a modern level of development of a physical science. It is supposed to include in the dictionary also a plenty of terms of adjoining with a physical science technical areas.

The editorial board applies to scientists of academy and universities, other scientific institutes of Azerbaijan Republic to participate actively in creation of this dictionary and to send to editors their offers on its contents and updating by missing terminology, which will be accepted with gratitude.

Азербайджано-русско-английский терминологический физический словарь

Азербайджанская Республика более десяти лет существует как самостоятельное государство, общепризнанное мировым сообществом, при этом азербайджанскому языку придан статус государственного языка.

Это означает, что все граждане Азербайджанской Республики должны иметь возможность получить полное образование на государственном языке, активно вести на нем научную и преподавательскую деятельность.

Азербайджанская наука всегда занимала достойное место во многих областях мировой науки и техники. Чтобы эти позиции не были утеряны, ученые республики обязаны следить за всеми современными направлениями в развитии мировой науки, своевременно доводить наметившиеся тенденции до сведения учащейся молодежи.

Вместе с тем, основная масса научной и учебной литературы, поступающей в республику из-за рубежа, издана на русском и английском языках. Кроме того, в научной среде языком межнационального общения в силу ряда исторических причин общепризнан английский язык. Все это делает весьма актуальным для активного развития в республике физической науки издание как можно более полного и совершенного азербайджанско-русско-английского словаря физических терминов, так как изданные ранее словари, например «Fizika terminləri luğəti», созданный коллективом Института Физики НАН Азербайджана, не содержит многих терминов, используемых в современной физике.

Институт Физики НАН Азербайджана совместно с Бакинским Государственным Университетом приступили к работе над азербайджанско-русско-английским словарем физических терминов, более полно отвечающем современному уровню развития физической науки. В словарь предполагается включить также большое количество терминов по соприкасающимся с физической наукой технических областей.

Редакция обращается к научным работникам академии и университетов, других научных учреждений Азербайджанской Республики принять активное участие в создании данного словаря и присылать в редакцию свои предложения по его содержанию и пополнению недостающей терминологией, которые будут приняты с благодарностью.

Abel qrupu	Абелева группа	Abelian group
Abel diferensialı	Абелев дифференциал	Abelian differential
Abel inteqralı	Абелев интеграл	Abelian integral
Abel tənliyi	Абелево уравнение	Abelian equation
Abel funksiyası	Абелева функция	Abelian function
Abel çoxluğu	Абелево многообразие	Abelian variety
Aberasiya	Аберрация	Aberration
Aberasiya ellipsi	Аберрационный эллипс	Aberrational ellipse
Ablyasiya materialı	Абляционный материал	Ablative material
Abraziv materiallar, hamarlamaq, yonmaq, itiləmək üçün işlədilən materiallar	Абразивные материалы	Abrasives
Absorbent: udan maddə	Абсорбент	Absorbent
Absorber: qazı, buxarı tutan cihaz	Абсорбер	Absorber
Absorbsiya	Абсорбция	Absorption
Absorbsiya qabiliyyəti	Абсорбционная способность	Absorptive power
Absorbsiya dalğaölçəni	Абсорбционный волномер	Absorption wavemeter
Absorbsiya cərəyanı	Абсорбционный ток	Absorption current
Absorbsiya işıq filtri	Абсорбционный светофильтр	Absorption filter
Absorbsiya kəsilməsi	Абсорбционное замирание	Absorption fading
Absorbsiya rentgen spektral analiz	Абсорбционный рентгеноспектральный анализ	X-ray absorption analyses
Absorbsiya spektral fotometriyası	Абсорбционная спектрофотометрия	Absorption spectrophotometry
Absorbsiya spektroskopiyası	Абсорбционная спектроскопия	Absorption spectroscopy
Absorbsiya tezlikölçəni	Абсорбционный частотомер	Absorption frequency meter
Absorbsiya faktoru	Абсорбционный фактор	Absorption factor
Absorbsiya faktoru	Абсорбционный спектрометр	Absorption spectrometer
Absorbsiya hiqrometri	Абсорбционный гигрометр	Absorption hygrometer
Absorbsiya əmsalı	Абсорбции показатель	Absorption index
Absorbsiometriya	Абсорбциометрия	Absorptiometry
Abstrak cəbr	Абстрактная алгебра	Abstract algebra
Abstraksiya	Абстракция	Abstraction
Abstrakt qrup	Абстрактная группа	Abstract group
Abstrakt cəbri çoxduq	Абстрактное алгебраическое многообразие	Abstract algebraic variety
Abstrakt inteqral	Абстрактный интеграл	Abstract integral
Abstrakt kompleks (məcmu)	Абстрактный комплекс	Abstract complex
Abstrakt təsvir	Абстрактное представление	Abstract representation
Abstrakt fəza	Абстрактное простанство	Abstract space
Abstrakt Hilbert fəzası	Абстрактное гильбертово пространство	Abstract Hilbert space
Aviaelektronika	Авиаэлектроника	Avionics
Aviasiya meteorologiyası	Авиационная метеорология	Aeronautical meteorology
Avirpnevmatoliz	Автопневматолиз	Autopneumatolysis
Avroral xətt	Авроральная линия	auroral line
Avtoqütblü tetraedr	Автополярный тетраэдр	Self-polar tetrahedron
Avtoqütblü üçbucaq	Автополярный треугольник	Self-polar triangle
Avtodin, yaxın tezlikli dalğaların təsiri işləyən radiocihaz	Автодин	Self-heterodyne, autodyne receiver
Avtoelektron qövsü	Автоэлектронная дуга	High-field emission arc
Avtoelektron emissiya	Автоэлектронная эмиссия	High-field emission
Avtoindeks	Автоиндекс	Autoindex
Avtoion mikroskopu	Автоионный микроскоп	Field-ion microscope
Avtokataliz	Автокатализ	Autocatalysis
Avtokatalitik reaksiya	Автокаталитическая реакция	Autocatalytic reaction
Avtokeçiricilik	Автопроводимость	Autoconduction
Avtoklav, kip bağlanmış qazan	Автоклав	Autoclave
Avtokod	Автокод	Autocode
Avtokollimasiya	Автоколлимация	Autocollimation
Avtokollimatik spektroqraf	Автоколлимационный спектрограф	Autocollimating spectrograph
Avtokollimator	Автоколлиматор	Autocollimator
Avtokonveksiya	Автоконвекция	Autoconvection
Avtokonvektiv qradiyent	Автоконвективный градиент	Autoconvective lapse rate
Avtokorrelyasiya	Автокорреляция	Autocorrelation

Avtokorrelyasion funksiya	Автокорреляционная функция	Autocorrelation function
Avtoliz, özbaşına həllolma	Автолиз	Autolysis
Avtomat	Автомат	Automaton
Avtomatik qazı təhlil edən cihaz	Автоматический газоанализатор	Automatic gas analyzer
Avtomatik qurma, qurulma	Автоматическая настройка	Automatic tuning
Avtomatik dəqiq qurma	Автоматическая точная настройка	Automatic fine tuning
Avtomatik idarə edilmə sistemi	Автоматическая система управления	Automatic control system
Avtomatik kodlaşdırma	Автоматическое кодирование	Automating coding
Avtomatik ossilyator	Автоматический осциллограф	Automatic oscillograph
Avtomatik peyk	Автоматический спутник	Unmanned satellite
Avtomatik potensiometr	Автоматический потенциометр	Automatic potentiometer
Avtomatik proqramlaşdırma	Автоматическое программирование	Automatic programming
Avtomatik təqibləmə	Автоматическое слежение	Automatic tracking
Avtomatik tənzimlənmə	Автоматическая регулировка	Automatic adjustment
Avtomatik tərəzi	Автоматические весы	Automatic scales
Avtomatik fazalı tənzimləmə	Автоматическое фазовое регулирование	Automatic phase control
Avtomatik fokuslama	Автоматическое фокусирование	Automatic focusing
Avtomatika	Автоматика	Automation
Avtomatlaşma	Автоматизация	Automation
Avtometamorfizm	Автометаморфизм	Autometamorphism
Avtomiorfizm	Автоморфизм	Automorphism
Avtomorf forma	Автоморфная форма	Automorphic form
Avtomorf funksiya	Автоморфная функция	Automorphic function
Avtonom yaddaş	Автономная память	Offline memory
Avtoradioqraf	Авторадиограф	Autoradiograph
Avtoradioqrafiya	Авторадиография	Autoradiography
Avtorotasiya	Авторотация	Autorotation
Avtorəqslər	Автоколебание	Self-excited oscillation
Avtotransformasiya	Автотрансформатор	Autotransformer
Avtogeriləmə	Авторегрессия	Autoregression
Avtogeriləmə prosesi	Авторегерессивный процесс	Autoregressive process
Aqlyüsinasiya, sözün kökünü saxlamaqla yeni sözlər düzəltmək	Агглюцинация	Agglutination
Aqlomerasiya	Агломерация	Agglomeration
Aqreqat hal	Агрегатное состояние	State of aggregation
Aqrometeorologiya, yer meteorologiyası	Агрометеорология	Agrocultural meteorology
Aqrofizika, yer fizikası	Агрофизика	Agrophysics
Adaptasiya, uyğunlaşma	Адаптация	Adaptation
Adveksiya	Адвекция	Advection
Advektiv duman	Адвективный туман	Advection fog
Advektiv tufan	Адвективная гроза	Advective tundesthorm
Advsorbsiya tarazlığı	Адсорбционное равновесие	Adsorption equilibrium
Adqeziya	Адгезия	Adhesion
Additiv qrup	Аддитивная группа	Additive group
Additiv operator	Аддитивный оператор	Additive operator
Additiv proses	Аддитивный процесс	Additive process
Additiv toplanma	Аддитивное сложение	Additive addition
Additiv funksiya	Аддивная функция	Additive function
Additiv funksional	Аддитивный функционал	Additive functional
Additiv xassələr	Аддитивные свойства	Additive properties
Additiv ölçü	Аддитивная мера	Additive measure
Additivlik	Аддитивность	Additivity
Adiabata	Адиабата	Adiabatic line
Adiabatik axın	Адиабатическое течение	Adiabatic flow
Adiabatik divar	Адиабатическая стенка	Adiabatic wall
Adiabatik dielektrik nüfuzluğu	Адиабатическая диэлектрическая проницаемость	Adiabatic dielectric constant
Adiabatik invariant	Адиабатический инвариант	Adiabatic invariant
Adiabatik invariantlıq	Адиабатическая инвариантность	Adiabatic invariance
Adiabatik ionlaşma	Адиабатическая ионизация	Adiabatic ionization
Adiabatik yaxınlaşma	Адиабатическое приближение	Adiabatic approximation
Adiabatik kalorimetr	Адиабатический калориметр	Adiabatic calorimeter

Adiabatik maqnitsizləşmə	Адиабатическое размагничивание	Adiabatic demagnetization
Adiabatik potensial	Адиабатический потенциал	Adiabatic potential
Adiabatik proses	Адиабатический процесс	Adiabatic process
Adiabatik reaksiya	Адиабатическая реакция	Adiabatic reaction
Adiabatik soyuma	Адиабатическое охлаждение	Adiabatic cooling
Adiabatik sıxılma	Адиабатическое сжатие	Adiabatic compression
Adiabatik tarazlıq	Адиабатическое равновесие	Adiabatic equilibrium
Adiabatik teorem	Адиабатическая теорема	Adiabatic theorem
Adiabatik fərziyyə	Адиабатическая гипотеза	Adiabatic hypothesis
Adiabatik hal	Адиабатическое состояние	Adiabatic state
Adiabatik həyəcanlanma	Адиабатическое возмущение	Adiabatic perturbation
Adiabatik genişlənmə	Адиабатическое расширение	Adiabatic expansion
Adsorbat, səthdə udulan qaz və ya maye	Адсорбат	Adsorbate
Adsorbent, səthində qaz və ya maye udulan cisim	Адсорбент	Adsorbent
Adsorber	Адсорбер	Adsorber
Adsorbsiya analizi	Адсорбционный анализ	Adsorption analysis
Adsorbsiya qatı	Адсорбционный слой	Adsorption layer
Adsorbsiya qüvvəsi	Адсорбционная сила	Adsorption force
Adsorbsiya dalğası	Адсорбционная волна	Adsorption wave
Adsorbsiya cərəyanı	Адсорбционный ток	Adsorption current
Adsorbsiya izotermləri	Адсорбционные изотермы	Adsorption isotherm
Adsorbsiya inqibitoru	Адсорбционный ингибитор	Adsorption inhibitor
Adsorbsiya indikatoru, təzyiqi ölçən cihaz	Адсорбционный индикатор	Adsorption indicator
Adsorbsiya kinetikası	Адсорбционная кинетика	Adsorption kinetics
Adsorbsiya olunan maddə	Адсорбирующее вещество	Adsorbing substance
Adsorbsiya olunmuş atom	Адсорбированный атом	Adsorbed atom
Adsorbsiya olunmuş qaz	Адсорбированный газ	Adsorbed gas
Adsorbsiya olunmuş molekul	Адсорбированная молекула	Adsorbed molecule
Adsorbsiya təbəqəsi	Адсорбционная пленка	Adsorption film
Adsorbsiya xromatoqrafiyası	Адсорбционная хроматография	Adsorption chromatography
Adsorbsiya, cisimlərin üz təbəqəsində maye və qazların udulması	Адсорбция	Adsorption
Adsorbüionnıy potenüial	Адсорбционный потенциал	Adsorption potential
Adgezi möhkəmlik, bərklik	Адгезионная прочность	Adhesive strength
Azeotrop qarışıq	Азеотропная смесь	Azeotropic mixture, azeotrope
Azeotrop distillə etmə	Азеотропная дистилляция	Azeotropic distillation
Azeotrop nöqtəsi	Азеотропная точка	Azeotropic point
Azeotropiya	Азеотропия	Azeotropy
Azimut	Азимут	Azimuth
Azimutal kvant ədədi	Азимутальное квантовое число	Azimuthal quantum number
Alovun absorbsiya fotometriyası	Абсорбционная фотометрия пламени	Absorption flame photometry
Ardıcıl yaxınlaşma metodu	Метод последовательного приближения	Method of successive approximation
Ardıcıl yerdəyişmək	Чередовать	Interleave, alternate
Ardıcıllıq	Последовательность	Sequence
Atmosfer	Атмосфера	Atmosphere
Bərabərlik	Равенство	Equality
Qayıtma ünvanı	Адрес возврата	Return address
Düyün nöqtəsi	Узловая точка	Nodal point
Düstur	Формула	Formulae
Dönməyən adiabatik proses	Адиабатический необратимый процесс	Adiabatic irreversible process
Dönən adiabatik dəyişilmə	Адиабатическое обратимое изменение	Adiabatic reversible change
Dönən adiabatik proses	Адиабатический обратимый процесс	Adiabatic reversible process
Dəf etmək	Отталкивать	Repel
Evolyusiya (inkişaf)	Эволюция	Evolution
Eynilik	Тождество	Identity
Elementar zərrəcik	Элементарная частица	Elementary particle
Enerji («E») təsviri	Энергетическое («E») представление	Energy representation
Erenfestin adibatik qanunu	Адиабатический закон Эренфеста	Erenfest’s “E” adiabatic law
Cazibə qüvvəsi	Сила притяжения	Attractive force

Cırlaşma	Вырождение	Degeneracy, degeneration
Cırlaşmış hallar	Вырожденное состояние	Degenerate state
Cəzb etmək	Притягивать	Attract
Cəlb etmək	Привлечь	Attract, involve
Cərəyanın fəlakətli qiyməti	Аварийное значение тока	Emergency fault current
Zərrəcik	Частица	Particle
İmpuls («R») təsviri	Импульсное («P») представление	Momentum “P” representation
İonlaşdırıcı aqent	Агент ионизирующий	Ionizing agent
İstilah (termin)	Термин	Term
İşığın aberasiyası	Аберрация света	Aberration of light
İşığın absorbsiyası	Абсорбция света	Optical absorption
Yayılma	Распространение	Propagation
Yerdəyişmək	Перемещать	Translocate
Yerli (lokal) sahə	Локальное поле	Local field
Yön	Ориентир	Reference point
Kainat	Вселенная	Cosmos, universe, space
Kamil elektrometr	Абсолютный электрометр	Absolute electrometer
Kamil eşitmə qabiliyyəti	Абсолютный слух	Absolute pitch
Kamil spirt	Абсолютный спирт	Absolute alcohol
Kanalın ünvan sözü	Адресное слово канала	Channel address word
Keçmiş	Пройденный, прошедший	Past
Komanda ünvanı	Адрес команды	Instruction address
Koordinat («x») təsviri	Координатное («x») представление	Coordinate “x” representation
Kristalların aqreqatı	Агрегат кристаллов	Crystal aggregate
Kütlə absorbsiya əmsalı	Абсорбции массовый коэффициент	Mass-absorption coefficient
Lokallaşma	Локализация	Localization
L-təsviri	L-представление	L-representation
Maqnit aqenti	Агент магнитный	Magnetic agent
Maqnit fırlanma additivliyi	Аддитивность магнитного вращения	Magnetorotation additivity
Mikroaləm	Микромир	Microcosm
Mübadilə	Обмен	Exchange
Mübadilə qüvvəsi	Обменная сила	Exchange force
Mübadilə enerjisi	Обменная энергия	Exchange energy
Mübahisə etmək	Обсуждать	Discuss
Mülahizə	Рассуждение	Reasoning
Mülahizə etmək	Рассуждать	Argue
Mütləq adres (ünvan)	Абсолютный адрес	Absolute address
Mütləq aktivlik, mütləq fəallıq	Абсолютная активность	Absolute activity
Mütləq amper	Абсолютный ампер	Absolute ampere
Mütləq antisimmetrik sintez	Абсолютный асимметрический синтез	Absolute asymmetric synthesis
Mütləq burulğanlıq	Абсолютная завихренность	Absolute vorticity
Mütləq bərk cisim	Абсолютно твердое тело	Perfectly rigid body
Mütləq vakuum	Абсолютный вакуум	Absolute vacuum
Mütləq vahid	Абсолютная единица	Absolute unit
Mütləq vahidlər sistemi	Абсолютная система единиц	Absolute system of units
Mütləq qalvanometr	Абсолютный гальванометр	Absolute galvanometer
Mütləq qara cisim	Абсолютно черное тело	Perfectly black body
Mütləq qeyri-bərabərlik	Абсолютное неравенство	Absolute inequality
Mütləq qeyri-elastiki toqquşma	Абсолютно неупругое столкновение	Absolute perfectly inelastic collision
Mütləq quruluş	Абсолютная структура	Absolute structure
Mütləq dayanıqlıq	Абсолютная устойчивость	Absolute stability
Mütləq dayanıqsızlıq	Абсолютная неустойчивость	Absolute instability
Mütləq diferensial	Абсолютный дифференциал	Absolute differential, absolute differentiation
Mütləq ekstremumlar	Абсолютные экстремумы	Absolute extremums
Mütləq elastiki toqquşma	Абсолютно упругое столкновение	Perfectly elastic collision
Mütləq entropiə	Абсолютная энтропия	Absolute entropy
Mütləq zaman	Абсолютное время	Absolute time
Mütləq invariant	Абсолютный инвариант	Absolute invariant
Mütləq inteqral invariant	Абсолютный интегральный инвариант	Absolute integral invariant
Mütləq inteqrallanan	Абсолютно интегрируемый	Absolutely integrable
Mütləq intensivlik	Абсолютная интенсивность	Absolute intensity

Mütləq yaş	Абсолютный возраст	Absolute age
Mütləq yığılma	Абсолютная сходимость	Absolute convergence
Mütləq kalibrləmə	Абсолютная калибровка	Absolute calibration
Mütləq kovariant	Абсолютный ковариант	Absolute covariant
Mütləq kodlama	Абсолютное кодирование	Absolute coding
Mütləq konfiqurasiya	Абсолютная конфигурация	Absolute configuration
Mütləq kəmiyyət	Абсолютная величина	Absolute value
Mütləq kəsilməz paylanma	Абсолютно непрерывное распределение	Absolutely continuous distribution
Mütləq kəsilməz spektr	Абсолютно непрерывный спектр	Absolutely continuous spectrum
Mütləq kəsilməz funksiya	Абсолютно непревная функция	Absolutely continuous function
Mütləq maqnit nüfuzluğu	Абсолютная магнитная проницаемость	Absolute permeability
Mütləq maqnitölçən	Абсолютный магнитомер	Absolute magnetometer
Mütləq moment	Абсолютный момент	Absolute moment
Mütləq parallaks	Абсолютный параллакс	Absolute parallax
Mütləq potensial	Абсолютный потенциал	Absolute potential
Mütləq retrakt	Абсолютный ретракт	Absolute retract
Mütləq rütubət	Абсолютная влажность	Absolute humidity
Mütləq spektral həssaslıq	Абсолютная спектральная чувствительность	Absolute spectral sensitivity
Mütləq statistik çəki	Абсолютный статистический вес	Absolute statistical weight
Mütləq sürət	Абсолютная скорость	Absolute velocity
Mütləq sındırma əmsalı	Абсолютный показатель преломления	Absolute index of refraction
Mütləq sıfır	Абсолютный нуль	Absolute zero
Mütləq səviyyə	Абсолютный уровень	Absolute level
Mütləq temperatur	Абсолютная температура	Absolute temperature
Mütləq təcil	Абсолютное ускорение	Absolute acceleration
Mütləq təzyiq	Абсолютное давление	Absolute pressure
Mütləq ulduz kəmiyyəti	Абсолютная звездная величина	Absolute magnitude
Mütləq fəza	Абсолютное простанство	Absolute space
Mütləq xəta	Абсолютная ошибка	Absolute error
Mütləq üzüyolalıq	Абсолютная податливость	Absolute compliance
Mütləq şkala	Абсолютная шкала	Absolute scale
Mütləq hündürlüyü ölçən	Абсолютный высотомер	Absolute altimeter
Mütləq hündürlük (yüksəklik, təpə)	Абсолютная высота	Absolute altitude
Mütləq hərəkət	Абсолютное движение	Absolute motion
Mütləq hərəkət miqdarı momenti	Абсолютный момент количества движения	Absolute angular momentum
Mütləq həssaslıq	Абсолютная чувствительность	Absolute sensitivity
Mütləq özlülük	Абсолютная вязкость	Absolute viscosity
Mütləq ölçü	Абсолютное измерение	Absolute measurement
Mütləq ətraf retraktı	Абсолютный окрестностный ретракт	Absolute neighbourhood retract
Məlumatın avtomatik işlənməsi	Автоматическая обработка данных	Automatic data processing
Məxsusi funksiya	Собственная функция	Eigenfunction
Ozon fəzası	Озоносфера	Ozonosphere
Optik fəallığın additivliyi	Аддитивность оптической активности	Additivity of optical activity
Parlaqlığın özbaşına tənzimlənməsi	Автоматическое регулирование яркости	Automatic brightness control
Radioaktiv şüalanma absorbsiyası	Абсорбция радиоактивного излучения	Radioactive radiation absorption
Reliktiv şüalanma	«Реликтовое» излучение	«Relict» radiation
Rentgen şüaları absorbsiyası	Абсорбция рентгеновских лучей	X-ray absorption
Refraksiya additivliyi	Аддитивность рефракции	Refraction additivity
Rənglərin additiv qarışdırılması	Аддитивное смещение цветов	Additive color mixture
Sahənin abel genişlənməsi	Абелево расширение поля	Abelian extension field
Seçilmənin özbaşına tənzimlənməsi	Автоматические регулирование избирательности	Automatic selectivity control
Spontan (özbaşına)	Спонтанный	Spontaneous
Stratosfera	Стратосфера	Stratosphere
Sürətin özbaşına tənzimlənməsi	Автоматическое регулирование скорости	Automatic speed control
Sürətli adiabatik keçid	Адиабатическое быстрое прохождение	Adiabatic rapid passage
Süxur səthlərinin tədricən dağılması	Абляция	Ablation
Sınaq funksiya	Пробная функция	Trial function
Səs gurluğunun avtomatik tənzimlənməsi	Автоматическая регулировка громкости	Automatic volume control

Səsin güclənməsinin tənzimlənməsi	Автоматическая регулировка усиления	Automatic gain control
Səs-küyü avtomatik məhdudlaşdıran cihaz	Автоматический ограничитель шумов	Automatic noise limiter
Səhvlərin avtomatik düzəldilməsi	Автоматическое исправление ошибок	Automatic error correction
Tam sistem	Полная система	Complete system
Tezliyin özbaşına tənzimlənməsi	Автоматическое регулирование частоты	Automatic frequency control
Temperaturun adiabatik qradiyenti	Адиабатический градиент температуры	Adiabatic temperature gradient, adiabatic lapse rate
Tenzor additivliyi	Аддитивность тензорная	Tensor additivity
Tormozlanma	Торможение	Braking
Tənlik	Уравнение	Equation
Təsvir	Представление	Representation
Təsvir nəzəriyyəsi	Теория представлений	Representation theory
Fikir	Мысль	Idea
Fikir çəkmək	Думать о чем (о ком) то	Think
Fikirləşmək	Размышлять	Reflect
Fəza	Пространство	Space
Fəlakət dayanacağı	Аварийная остановка	Emergency shut-down
Fəlakətli soyuma	Аварийное охлаждение	Emergency cooling
Ünvan yolu	Адресная дорожка	Address track
Ünvan sabiti	Адресная константа	Address constant
Ünvan sözü	Адрес слова	Word address
Ünvan hissəsi	Адресная часть	Address part
Ünvanlanma	Адресация	Addressing
Çevirici inteqral	Интегральное преобразование	Integral transformation
Çoxluğun additiv funksiyası	Аддитивная функция множеств	Additive set function
Hesablama cihazı	Абак	Abacus
Hissə	Часть	Part
Hissəcik	Маленькая часть вещества (как атом, молекула)	Microscopic particle
Həyəcanlanma	Возбуждение, возмущение	Excitation, perturbation
Həyəcanlanma nəzəriyyəsi	Теория возмущений	Perturbation theory
Gibbsin adsorbsiya tənliyi	Адсорбционное уравнение Гиббса	Gibbs adsorption equation
Gücün özbaşına tənzimlənməsi	Автоматическое регулирование мощности	Automatic power control
Gələcək	Будущее	Next, future
Gərginliyin avtomatik tənzimçiyi	Автоматический регулятор напряжения	Automatic voltage regulator
Özbaşına ionizasiya	Автоионизация	autoionization
Özbaşına yerdəyişmə	Автоматическое смещение	Auto-bias, self-bias
Özbaşına keçid	Постоянный переход	Constant transition
Özbaşına tənzimləmə	Автоматическое регулирование	Automatic control
Özünə uzlaşan sahə	Самосогласованное поле	Self-consistent field
Ədədlərin additiv nəzəriyyəsi	Аддитивная теория чисел	Additive number theory

Abacus	Hesablama cihazı	Абак
Abelian differential	Abel diferensialı	Абелев дифференциал
Abelian equation	Abel tənliyi	Абелево уравнение
Abelian extension field	Sahənin abel genişlənməsi	Абелево расширение поля
Abelian function	Abel funksiyası	Абелева функция
Abelian group	Abel qrupu	Абелева группа
Abelian integral	Abel inteqralı	Абелев интеграл
Abelian variety	Abel çoxluğu	Абелево многообразие
Aberration	Aberasiya	Аберрация
Aberration of light	İşığın aberasiyası	Аберрация света
Aberrational ellipse	Aberasiya ellipsi	Аберрационный эллипс
Ablation	Süxur səthlərinin tədricən dağılması	Абляция
Ablative material	Ablyasiya materialı	Абляционный материал
Abrasives	Abraziv materiallar, hamarlamaq, yonmaq, itiləmək üçün işlədilən materiallar	Абразивные материалы
Absolute acceleration	Mütləq təcil	Абсолютное ускорение
Absolute activity	Mütləq aktivlik, mütləq fəallıq	Абсолютная активность
Absolute address	Mütləq adres (ünvan)	Абсолютный адрес
Absolute age	Mütləq yaş	Абсолютный возраст
Absolute alcogol	Kamil spirt	Абсолютный спирт
Absolute altimeter	Mütləq hündürlüyü ölçən	Абсолютный высотомер
Absolute altitude	Mütləq hündürlük (yüksəklik, təpə)	Абсолютная высота
Absolute ampere	Mütləq amper	Абсолютный ампер
Absolute angular momentum	Mütləq hərəkət miqdarı momenti	Абсолютный момент количества движения
Absolute asymmetric synthesis	Mütləq antisimmetrik sintez	Абсолютный асимметрический синтез
Absolute calibration	Mütləq kalibrləmə	Абсолютная калибровка
Absolute coding	Mütləq kodlama	Абсолютное кодирование
Absolute compliance	Mütləq üzüyolalıq	Абсолютная податливость
Absolute configuration	Mütləq konfiqurasiya	Абсолютная конфигурация
Absolute convergence	Mütləq yığılma	Абсолютная сходимость
Absolute covariant	Mütləq kovariant	Абсолютный ковариант
Absolute differential, absolute differentiation	Mütləq diferensial	Абсолютный дифференциал
Absolute electrometer	Kamil elektrometr	Абсолютный электрометр
Absolute entropy	Mütləq entropiə	Абсолютная энтропия
Absolute error	Mütləq xəta	Абсолютная ошибка
Absolute extremums	Mütləq ekstremumlar	Абсолютные экстремумы
Absolute galvanometer	Mütləq qalvanometr	Абсолютный гальванометр
Absolute humidity	Mütləq rütubət	Абсолютная влажность
Absolute index of refraction	Mütləq sındırma əmsalı	Абсолютный показатель преломления
Absolute inequality	Mütləq qeyri-bərabərlik	Абсолютное неравенство
Absolute instability	Mütləq dayanıqsızlıq	Абсолютная неустойчивость
Absolute integral invariant	Mütləq inteqral invariant	Абсолютный интегральный инвариант
Absolute intensity	Mütləq intensivlik	Абсолютная интенсивность
Absolute invariant	Mütləq invariant	Абсолютный инвариант
Absolute level	Mütləq səviyyə	Абсолютный уровень
Absolute magnetometer	Mütləq maqnitölçən	Абсолютный магнитомер
Absolute magnitude	Mütləq ulduz kəmiyyəti	Абсолютная звездная величина
Absolute measurement	Mütləq ölçü	Абсолютное измерение
Absolute moment	Mütləq moment	Абсолютный момент
Absolute motion	Mütləq hərəkət	Абсолютное движение
Absolute neighbourhood retract	Mütləq ətraf retraktı	Абсолютный окрестностный ретракт
Absolute parallax	Mütləq parallaks	Абсолютный параллакс
Absolute perfectly inelastic collision	Mütləq qeyri-elastiki toqquşma	Абсолютно неупругое столкновение
Absolute permeability	Mütləq maqnit nüfuzluğu	Абсолютная магнитная проницаемость
Absolute pitch	Kamil eşitmə qabiliyyəti	Абсолютный слух
Absolute potential	Mütləq potensial	Абсолютный потенциал
Absolute pressure	Mütləq təzyiq	Абсолютное давление
Absolute retract	Mütləq retrakt	Абсолютный ретракт
Absolute scale	Mütləq şkala	Абсолютная шкала
Absolute sensitivity	Mütləq həssaslıq	Абсолютная чувствительность

Absolute space	Mütləq fəza	Абсолютное простанство
Absolute spectral sensitivity	Mütləq spektral həssaslıq	Абсолютная спектральная чувствительность
Absolute stability	Mütləq dayanıqlıq	Абсолютная устойчивость
Absolute statistical weight	Mütləq statistik çəki	Абсолютный статистический вес
Absolute structure	Mütləq quruluş	Абсолютная структура
Absolute system of units	Mütləq vahidlər sistemi	Абсолютная система единиц
Absolute temperature	Mütləq temperatur	Абсолютная температура
Absolute time	Mütləq zaman	Абсолютное время
Absolute unit	Mütləq vahid	Абсолютная единица
Absolute vacuum	Mütləq vakuum	Абсолютный вакуум
Absolute value	Mütləq kəmiyyət	Абсолютная величина
Absolute velocity	Mütləq sürət	Абсолютная скорость
Absolute viscosity	Mütləq özlülük	Абсолютная вязкость
Absolute vorticity	Mütləq burulğanlıq	Абсолютная завихренность
Absolute zero	Mütləq sıfır	Абсолютный нуль
Absolutely continuous distribution	Mütləq kəsilməz paylanma	Абсолютно непрерывное распределение
Absolutely continuous function	Mütləq kəsilməz funksiya	Абсолютно непревная функция
Absolutely continuous spectrum	Mütləq kəsilməz spektr	Абсолютно непрерывный спектр
Absolutely integrable	Mütləq inteqrallanan	Абсолютно интегрируемый
Absorbent	Absorbent: udan maddə	Абсорвент
Absorber	Absorber: qazı, buxarı tutan cihaz	Абсорбер
Absorptiometry	Absorbsiometriya	Абсорбциометрия
Absorption	Absorbsiya	Абсорбция
Absorption current	Absorbsiya cərəyanı	Абсорбционный ток
Absorption factor	Absorbsiya faktoru	Абсорбционный фактор
Absorption fading	Absorbsiya kəsilməsi	Абсорбционное замирание
Absorption filter	Absorbsiya işıq filtri	Абсорбционный светофильтр
Absorption flame photometry	Alovun absorbsiya fotometriyası	Абсорбционная фотометрия пламени
Absorption frequency meter	Absorbsiya tezlikölçəni	Абсорбционный частотомер
Absorption hygrometer	Absorbsiya hiqrometri	Абсорбционный гигрометр
Absorption index	Absorbsiya əmsalı	Абсорбции показатель
Absorption spectrometer	Absorbsiya faktoru	Абсорбционный спектрометр
Absorption spectrophotometry	Absorbsiya spektral fotometriyası	Абсорбционная спектрофотометрия
Absorption spectroscopy	Absorbsiya spektroskopiyası	Абсорбционная спектроскопия
Absorption wavemeter	Absorbsiya dalğaölçəni	Абсорбционный волномер
Absorptive power	Absorbsiya qabiliyyəti	Абсорбционная способность
Abstract algebra	Abstrak cəbr	Абстрактная алгебра
Abstract algebraic variety	Abstrakt cəbri çoxduq	Абстрактное алгебраическое многообразие
Abstract complex	Abstrakt kompleks (məcmu)	Абстрактный комплекс
Abstract group	Abstrakt qrup	Абстрактная группа
Abstract Hilbert space	Abstrakt Hilbert fəzası	Абстрактное гильбертово пространство
Abstract integral	Abstrakt inteqral	Абстрактный интеграл
Abstract representation	Abstrakt təsvir	Абстрактное представление
Abstract space	Abstrakt fəza	Абстрактное простанство
Abstraction	Abstraksiya	Абстракция
Adaptation	Adaptasiya, uyğunlaşma	Адаптация
Additive addition	Additiv toplanma	Аддитивное сложение
Additive color mixture	Rənglərin additiv qarışdırılması	Аддитивное смещение цветов
Additive function	Additiv funksiya	Аддивная функция
Additive functional	Additiv funksional	Аддитивный функционал
Additive group	Additiv qrup	Аддитивная группа
Additive measure	Additiv ölçü	Аддитивная мера
Additive number theory	Ədədlərin additiv nəzəriyyəsi	Аддитивная теория чисел
Additive operator	Additiv operator	Аддитивный оператор
Additive process	Additiv proses	Аддитивный процесс
Additive properties	Additiv xassələr	Аддитивные свойства
Additive set function	Çoxluğun additiv funksiyası	Аддитивная функция множеств
Additivity	Additivlik	Аддитивность
Additivity of optical activity	Optik fəallığın additivliyi	Аддитивность оптической активности
Address constant	Ünvan sabiti	Адресная константа
Address part	Ünvan hissəsi	Адресная часть

Address track	Ünvan yolu	Адресная дорожка
Addressing	Ünvanlanma	Адресация
Adhesion	Adqeziya	Адгезия
Adhesive strength	Adgezi möhkəmlik, bərklik	Адгезионная прочность
Adiabatic approximation	Adiabatik yaxınlaşma	Адиабатическое приближение
Adiabatic calorimeter	Adiabatik kalorimetr	Адиабатический калориметр
Adiabatic compression	Adiabatik sıxılma	Адиабатическое сжатие
Adiabatic cooling	Adiabatik soyuma	Адиабатическое охлаждение
Adiabatic demagnetization	Adiabatik maqnitsizləşmə	Адиабатическое размагничивание
Adiabatic dielectric constant	Adiabatik dielektrik nüfuzluğu	Адиабатическая диэлектрическая проницаемость
Adiabatic equilibrium	Adiabatik tarazlıq	Адиабатическое равновесие
Adiabatic expansion	Adiabatik genişlənmə	Адиабатическое расширение
Adiabatic flow	Adiabatik axın	Адиабатическое течение
Adiabatic hypothesis	Adiabatik fərziyyə	Адиабатическая гипотеза
Adiabatic invariance	Adiabatik invariantlıq	Адиабатическая инвариантность
Adiabatic invariant	Adiabatik invariant	Адиабатический инвариант
Adiabatic ionization	Adiabatik ionlaşma	Адиабатическая ионизация
Adiabatic irreversible process	Dönməyən adiabatik proses	Адиабатический необратимый процесс
Adiabatic line	Adiabata	Адиабата
Adiabatic perturbation	Adiabatik həyəcanlanma	Адиабатическое возмущение
Adiabatic potential	Adiabatik potensial	Адиабатический потенциал
Adiabatic process	Adiabatik proses	Адиабатический процесс
Adiabatic rapid passage	Sürətli adiabatik keçid	Адиабатическое быстрое прохождение
Adiabatic reaction	Adiabatik reaksiya	Адиабатическая реакция
Adiabatic reversible change	Dönən adiabatik dəyişilmə	Адиабатическое обратимое изменение
Adiabatic reversible process	Dönən adiabatik proses	Адиабатический обратимый процесс
Adiabatic state	Adiabatik hal	Адиабатическое состояние
Adiabatic temperature gradient, adiabatic lapse rate	Temperaturun adiabatik qradiyenti	Адиабатический градиент температуры
Adiabatic theorem	Adiabatik teorem	Адиабатическая теорема
Adiabatic wall	Adiabatik divar	Адиабатическая стенка
Adsorbate	Adsorbat, səthdə udulan qaz və ya maye	Адсорбат
Adsorbed atom	Adsorbsiya olunmuş atom	Адсорбированный атом
Adsorbed gas	Adsorbsiya olunmuş qaz	Адсорбированный газ
Adsorbed molecule	Adsorbsiya olunmuş molekul	Адсорбированная молекула
Adsorbent	Adsorbent, səthində qaz və ya maye udulan cisim	Адсорбент
Adsorber	Adsorber	Адсорбер
Adsorbing substance	Adsorbsiya olunan maddə	Адсорбирующее вещество
Adsorption	Adsorbsiya, cisimldərin üz təbəqəsində maye və qazların udulması	Адсорбция
Adsorption analysis	Adsorbsiya analizi	Адсорбционный анализ
Adsorption chromatography	Adsorbsiya xromatoqrafiyası	Адсорбционная хроматография
Adsorption current	Adsorbsiya cərəyanı	Адсорбционный ток
Adsorption equilibrium	Advsorbsiya tarazlığı	Адсорбционное равновесие
Adsorption film	Adsorbsiya təbəqəsi	Адсорбционная пленка
Adsorption force	Adsorbsiya qüvvəsi	Адсорбционная сила
Adsorption indicator	Adsorbsiya indikatoru, təzyiqi ölçən cihaz	Адсорбционный индикатор
Adsorption inhibitor	Adsorbsiya inqibitoru	Адсорбционный ингибитор
Adsorption isotherm	Adsorbsiya izotermləri	Адсорбционные изотермы
Adsorption kinetics	Adsorbsiya kinetikası	Адсорбционная кинетика
Adsorption layer	Adsorbsiya qatı	Адсорбционный слой
Adsorption potential	Adsorbüionnıy potenüial	Адсорбционный потенциал
Adsorption wave	Adsorbsiya dalğası	Адсорбционная волна
Advection	Adveksiya	Адвекция
Advection fog	Advektiv duman	Адвективный туман
Advective tundesthorm	Advektiv tufan	Адвективная гроза
Aeronautical meteorology	Aviasiya meteorologiyası	Авиационная метеорология
Agglomeration	Aqlomerasiya	Агломерация
Agglutination	Aqlyüsinasiya, sözün kökünü	Агглюцинация

	saxlamaqla yeni sözlər düzəltmək	
Agrocultural meteorology	Aqrometeorologiya, yer meteorologiyası	Агрометеорология
Agrophysics	Aqrofizika, yer fizikası	Агрофизика
Argue	Mülahizə etmək	Рассуждать
Atmosphere	Atmosfer	Атмосфера
Attract	Cəzb etmək	Притягивать
Attract, involve	Cəlb etmək	Привлечь
Attractive force	Cazibə qüvvəsi	Сила притяжения
auroral line	Avroral xətt	Авроральная линия
Auto-bias, self-bias	Özbaşına yerdəyişmə	Автоматическое смещение
Autocatalysis	Avtokataliz	Автокатализ
Autocatalytic reaction	Avtokatalitik reaksiya	Автокаталитическая реакция
Autoclave	Avtoklav, kip bağlanmış qazan	Автоклав
Autocode	Avtokod	Автокод
Autocollimating spectrograph	Avtokollimatik spektroqraf	Автоколлимационный спектрограф
Autocollimation	Avtokollimasiya	Автоколлимация
Autocollimator	Avtokollimator	Автоколлиматор
Autoconduction	Avtokeçiricilik	Автопроводимость
Autoconvection	Avtokonveksiya	Автоконвекция
Autoconvective lapse rate	Avtokonvektiv qradiyent	Автоконвективный градиент
Autocorrelation	Avtokorrelyasiya	Автокорреляция
Autocorrelation function	Avtokorrelyasion funksiya	Автокорреляционная функция
Autoindex	Avtoindeks	Автоиндекс
autoionization	Özbaşına ionizasiya	Автоионизация
Autolysis	Avtoliz, özbaşına həllolma	Автолиз
Automatic adjustment	Avtomatik tənzimlənmə	Автоматическая регулировка
Automatic brightness control	Parlaqlığın özbaşına tənzimlənməsi	Автоматическое регулирование яркости
Automatic control	Özbaşına tənzimləmə	Автоматическое регулирование
Automatic control system	Avtomatik idarə edilmə sistemi	Автоматическая система управления
Automatic data processing	Məlumatın avtomatik işlənməsi	Автоматическая обработка данных
Automatic error correction	Səhvlərin avtomatik düzəldilməsi	Автоматическое исправление ошибок
Automatic fine tuning	Avtomatik dəqiq qurma	Автоматическая точная настройка
Automatic focusing	Avtomatik fokuslama	Автоматическое фокусирование
Automatic frequency control	Tezliyin özbaşına tənzimlənməsi	Автоматическое регулирование частоты
Automatic gain control	Səsin güclənməsinin tənzimlənməsi	Автоматическая регулировка усиления
Automatic gas analyzer	Avtomatik qazı təhlil edən cihaz	Автоматический газоанализатор
Automatic noise limiter	Səs-küyü avtomatik məhdudlaşdıran cihaz	Автоматический ограничитель шумов
Automatic oscillograph	Avtomatik ossilyator	Автоматический осциллограф
Automatic phase control	Avtomatik fazalı tənzimləmə	Автоматическое фазовое регулирование
Automatic potentiometer	Avtomatik potensiometr	Автоматический потенциометр
Automatic power control	Gücün özbaşına tənzimlənməsi	Автоматическое регулирование мощности
Automatic programming	Avtomatik proqramlaşdırma	Автоматическое программирование
Automatic scales	Avtomatik tərəzi	Автоматические весы
Automatic selectivity control	Seçilmənin özbaşına tənzimlənməsi	Автоматические регулирование избирательности
Automatic speed control	Sürətin özbaşına tənzimlənməsi	Автоматическое регулирование скорости
Automatic tracking	Avtomatik təqibləmə	Автоматическое слежение
Automatic tuning	Avtomatik qurma, qurulma	Автоматическая настройка
Automatic voltage regulator	Gərginliyin avtomatik tənzimçiyi	Автоматический регулятор напряжения
Automatic volume control	Səs gurluğunun avtomatik tənzimlənməsi	Автоматическая регулировка громкости
Automating coding	Avtomatik kodlaşdırma	Автоматическое кодирование
Automation	Avtomatlaşma	Автоматизация
Automation	Avtomatika	Автоматика
Automaton	Avtomat	Автомат
Autometamorphism	Avtometamorfizm	Автометаморфизм
Automorphic form	Avtomorf forma	Автоморфная форма
Automorphic function	Avtomorf funksiya	Автоморфная функция
Automorphism	Avtomiorfizm	Автоморфизм
Autopneumatolysis	Avirpnevmatoliz	Автопневматолиз

Autoradiograph	Avtoradioqraf	Авторадиограф
Autoradiography	Avtoradioqrafiya	Авторадиография
Autoregression	Avtogeriləmə	Авторегрессия
Autoregressive process	Avtogeriləmə prosesi	Авторегерессивный процесс
Autorotation	Avtorotasiya	Авторотация
Autotransformer	Avtotransformasiya	Автотрансформатор
Avionics	Aviaelektronika	Авиаэлектроника
Azeotropic distillation	Azeotrop distillə etmə	Азеотропная дистилляция
Azeotropic mixture, azeotrope	Azeotrop qarışıq	Азеотропная смесь
Azeotropic point	Azeotrop nöqtəsi	Азеотропная точка
Azeotropy	Azeotropiya	Азеотропия
Azimuth	Azimut	Азимут
Azimuthal quantum number	Azimutal kvant ədədi	Азимутальное квантовое число
Braking	Tormozlanma	Торможение
Channel address word	Kanalın ünvan sözü	Адресное слово канала
Complete system	Tam sistem	Полная система
Constant transition	Özbaşına keçid	Постоянный переход
Coordinate representation	Koordinat («x») təsviri	Координатное («x») представление
Cosmos, universe, space	Kainat	Вселенная
Crystal aggregate	Kristalların aqreqatı	Агрегат кристаллов
Degeneracy, degeneration	Cırlaşma	Вырождение
Degenerate state	Cırlaşmış hallar	Вырожденное состояние
Discuss	Mübahisə etmək	Обсуждать
Eigenfunction	Məxsusi funksiya	Собственная функция
Elementary particle	Elementar zərrəcik	Элементарная частица
Emergency cooling	Fəlakətli soyuma	Аварийное охлаждение
Emergency fault current	Cərəyanın fəlakətli qiyməti	Аварийное значение тока
Emergency shut-down	Fəlakət dayanacağı	Аварийная остановка
Energy (“E”) representation	Enerji («E») təsviri	Энергетическое («E») представление
Equality	Bərabərlik	Равенство
Equation	Tənlik	Уравнение
Erenfest’s adiabatic law	Erenfestin adibatik qanunu	Адиабатический закон Эренфеста
Evolution	Evolyusiya (inkişaf)	Эволюция
Exchange	Mübadilə	Обмен
Exchange energy	Mübadilə enerjisi	Обменная энергия
Exchange force	Mübadilə qüvvəsi	Обменная сила
Excitation, perturbation	Həyəcanlanma	Возбуждение, возмущение
Field-ion microscope	Avtoion mikroskopu	Автоионный микроскоп
Formulae	Düstur	Формула
Gibbs adsorption equation	Gibbsin adsorbsiya tənliyi	Адсорбционное уравнение Гиббса
High-field emission	Avtoelektron emissiya	Автоэлектронная эмиссия
High-field emission arc	Avtoelektron qövsü	Автоэлектронная дуга
Idea	Fikir	Мысль
Identity	Eynilik	Тождество
Instruction address	Komanda ünvanı	Адрес команды
Integral transformation	Çevirici inteqral	Интегральное преобразование
Interleave, alternate	Ardıcıl yerdəyişmək	Чередовать
Ionizing agent	İonlaşdırıcı aqent	Агент ионизирующий
L – representation	L-təsviri	L - представление
Local field	Yerli (lokal) sahə	Локальное поле
Localization	Lokallaşma	Локализация
Magnetic agent	Maqnit aqenti	Агент магнитный
Magnetorotation additivity	Maqnit fırlanma additivliyi	Аддитивность магнитного вращения
Mass-absorption coefficient	Kütlə absorbsiya əmsalı	Абсорбции массовый коэффициент
Method of successive approximation	Ardıcıl yaxınlaşma metodu	Метод последовательного приближения
Microcosm	Mikroaləm	Микромир
Microscopic particle	Hissəcik	Маленькая часть вещества (как атом, молекула)
Momentum “P” representation	İmpuls («P») təsviri	Импульсное («P») представление
Next, future	Gələcək	Будущее
Nodal point	Düyün nöqtəsi	Узловая точка
Offline memory	Avtonom yaddaş	Автономная память
Optical absorption	İşığın absorbsiyası	Абсорбция света

Ozonosphere	Ozon fəzası	Озоносфера
Part	Hissə	Часть
Particle	Zərrəcik	Частица
Past	Keçmiş	Пройденный, прошедший
Perfectly black body	Mütləq qara cisim	Абсолютно черное тело
Perfectly elastic collision	Mütləq elastiki toqquşma	Абсолютно упругое столкновение
Perfectly rigid body	Mütləq bərk cisim	Абсолютно твердое тело
Perturbation theory	Həyəcanlanma nəzəriyyəsi	Теория возмущений
Propagation	Yayılma	Распространение
Radioactive radiation absorption	Radioaktiv şüalanma absorbsiyası	Абсорбция радиоактивного излучения
Reasoning	Mülahizə	Рассуждение
Reference point	Yön	Ориентир
Reflect	Fikirləşmək	Размышлять
Refraction additivity	Refraksiya additivliyi	Аддитивность рефракции
Relict radiation	Reliktiv şüalanma	Реликтовое излучение
Repel	Dəf etmək	Отталкивать
Representation	Təsvir	Представление
Representation theory	Təsvir nəzəriyyəsi	Теория представлений
Return address	Qayıtma ünvanı	Адрес возврата
Self-consistent field	Özünə uzlaşan sahə	Самосогласованное поле
Self-excited oscillation	Avtorəqslər	Автоколебание
Self-heterodyne, autodyne receiver	Avtodin, yaxın tezlikli dalğaların təsiri işləyən radiocihaz	Автодин
Self-polar tetrahedron	Avtoqütblü tetraedr	Автополярный тетраэдр
Self-polar triangle	Avtoqütblü üçbucaq	Автополярный треугольник
Sequence	Ardıcıllıq	Последовательность
Space	Fəza	Пространство
Spontaneous	Spontan (özbaşına)	Спонтанный
State of aggregation	Aqreqat hal	Агрегатное состояние
Stratosphere	Stratosfera	Стратосфера
Tensor additivity	Tenzor additivliyi	Аддитивность тензорная
Term	İstilah (termin)	Термин
Think	Fikir çəkmək	Думать о чем (о ком) то
Translocate	Yerdəyişmək	Перемещать
Trial function	Sınaq funksiya	Пробная функция
Unmanned satellite	Avtomatik peyk	Автоматический спутник
Word address	Ünvan sözü	Адрес слова
X-ray absorption	Rentgen şüaları absorbsiyası	Абсорбция рентгеновских лучей
X-ray absorption analyses	Absorbsiya rentgen spektral analiz	Абсорбционный рентгеноспектральный анализ

Абак	Abacus	Hesablama cihazı
Абелев дифференциал	Abelian differential	Abel diferensialı
Абелев интеграл	Abelian integral	Abel inteqralı
Абелева группа	Abelian group	Abel qrupu
Абелева функция	Abelian function	Abel funksiyası
Абелево многообразие	Abelian variety	Abel çoxluğu
Абелево расширение поля	Abelian extension field	Sahənin abel genişlənməsi
Абелево уравнение	Abelian equation	Abel tənliyi
Аберрационный эллипс	Aberrational ellipse	Aberasiya ellipsi
Аберрация	Aberration	Aberasiya
Аберрация света	Aberration of light	İşığın aberasiyası
Абляционный материал	Ablative material	Ablyasiya materialı
Абляция	Ablation	Süxur səthlərinin tədricən dağılması
Абразивные материалы	Abrasives	Abraziv materiallar, hamarlamaq, yonmaq, itiləmək üçün işlədilən materiallar
Абсолютная активность	Absolute activity	Mütləq aktivlik, mütləq fəallıq
Абсолютная величина	Absolute value	Mütləq kəmiyyət
Абсолютная влажность	Absolute humidity	Mütləq rütubət
Абсолютная высота	Absolute altitude	Mütləq hündürlük (yüksəklik, təpə)
Абсолютная вязкость	Absolute viscosity	Mütləq özlülük
Абсолютная единица	Absolute unit	Mütləq vahid
Абсолютная завихренность	Absolute vorticity	Mütləq burulğanlıq
Абсолютная звездная величина	Absolute magnitude	Mütləq ulduz kəmiyyəti
Абсолютная интенсивность	Absolute intensity	Mütləq intensivlik
Абсолютная калибровка	Absolute calibration	Mütləq kalibrləmə
Абсолютная конфигурация	Absolute configuration	Mütləq konfiqurasiya
Абсолютная магнитная проницаемость	Absolute permeability	Mütləq maqnit nüfuzluğu
Абсолютная неустойчивость	Absolute instability	Mütləq dayanıqsızlıq
Абсолютная ошибка	Absolute error	Mütləq xəta
Абсолютная податливость	Absolute compliance	Mütləq üzüyolalıq
Абсолютная система единиц	Absolute system of units	Mütləq vahidlər sistemi
Абсолютная скорость	Absolute velocity	Mütləq sürət
Абсолютная спектральная чувствительность	Absolute spectral sensitivity	Mütləq spektral həssaslıq
Абсолютная структура	Absolute structure	Mütləq quruluş
Абсолютная сходимость	Absolute convergence	Mütləq yığılma
Абсолютная температура	Absolute temperature	Mütləq temperatur
Абсолютная устойчивость	Absolute stability	Mütləq dayanıqlıq
Абсолютная чувствительность	Absolute sensitivity	Mütləq həssaslıq
Абсолютная шкала	Absolute scale	Mütləq şkala
Абсолютная энтропия	Absolute entropy	Mütləq entropiə
Абсолютно интегрируемый	Absolutely integrable	Mütləq inteqrallanan
Абсолютно непревная функция	Absolutely continuous function	Mütləq kəsilməz funksiya
Абсолютно непрерывное распределение	Absolutely continuous distribution	Mütləq kəsilməz paylanma
Абсолютно непрерывный спектр	Absolutely continuous spectrum	Mütləq kəsilməz spektr
Абсолютно неупругое столкновение	Absolute perfectly inelastic collision	Mütləq qeyri-elastiki toqquşma
Абсолютно твердое тело	Perfectly rigid body	Mütləq bərk cisim
Абсолютно упругое столкновение	Perfectly elastic collision	Mütləq elastiki toqquşma
Абсолютно черное тело	Perfectly black body	Mütləq qara cisim
Абсолютное время	Absolute time	Mütləq zaman
Абсолютное давление	Absolute pressure	Mütləq təzyiq
Абсолютное движение	Absolute motion	Mütləq hərəkət
Абсолютное измерение	Absolute measurement	Mütləq ölçü
Абсолютное кодирование	Absolute coding	Mütləq kodlama
Абсолютное неравенство	Absolute inequality	Mütləq qeyri-bərabərlik
Абсолютное простанство	Absolute space	Mütləq fəza
Абсолютное ускорение	Absolute acceleration	Mütləq təcil
Абсолютные экстремумы	Absolute extremums	Mütləq ekstremumlar
Абсолютный адрес	Absolute address	Mütləq adres (ünvan)

Абсолютный ампер	Absolute ampere	Mütləq amper
Абсолютный асимметрический синтез	Absolute asymmetric synthesis	Mütləq antisimmetrik sintez
Абсолютный вакуум	Absolute vacuum	Mütləq vakuum
Абсолютный возраст	Absolute age	Mütləq yaş
Абсолютный высотомер	Absolute altimeter	Mütləq hündürlüyü ölçən
Абсолютный гальванометр	Absolute galvanometer	Mütləq qalvanometr
Абсолютный дифференциал	Absolute differential, absolute differentiation	Mütləq diferensial
Абсолютный инвариант	Absolute invariant	Mütləq invariant
Абсолютный интегральный инвариант	Absolute integral invariant	Mütləq inteqral invariant
Абсолютный ковариант	Absolute covariant	Mütləq kovariant
Абсолютный магнитомер	Absolute magnetometer	Mütləq maqnitölçən
Абсолютный момент	Absolute moment	Mütləq moment
Абсолютный момент количества движения	Absolute angular momentum	Mütləq hərəkət miqdarı momenti
Абсолютный нуль	Absolute zero	Mütləq sıfır
Абсолютный окрестностный ретракт	Absolute neighbourhood retract	Mütləq ətraf retraktı
Абсолютный параллакс	Absolute parallax	Mütləq parallaks
Абсолютный показатель преломления	Absolute index of refraction	Mütləq sındırma əmsalı
Абсолютный потенциал	Absolute potential	Mütləq potensial
Абсолютный ретракт	Absolute retract	Mütləq retrakt
Абсолютный слух	Absolute pitch	Kamil eşitmə qabiliyyəti
Абсолютный спирт	Absolute alcogol	Kamil spirt
Абсолютный статистический вес	Absolute statistical weight	Mütləq statistik çəki
Абсолютный уровень	Absolute level	Mütləq səviyyə
Абсолютный электрометр	Absolute electrometer	Kamil elektrometr
Абсорбер	Absorber	Absorber: qazı, buxarı tutan cihaz
Абсорбции массовый коэффициент	Mass-absorption coefficient	Kütlə absorbsiya əmsalı
Абсорбции показатель	Absorption index	Absorbsiya əmsalı
Абсорбциометрия	Absorptiometry	Absorbsiometriya
Абсорбционная спектроскопия	Absorption spectroscopy	Absorbsiya spektroskopiyası
Абсорбционная спектрофотометрия	Absorption spectrophotometry	Absorbsiya spektral fotometriyası
Абсорбционная способность	Absorptive power	Absorbsiya qabiliyyəti
Абсорбционная фотометрия пламени	Absorption flame photometry	Alovun absorbsiya fotometriyası
Абсорбционное замирание	Absorption fading	Absorbsiya kəsilməsi
Абсорбционный волномер	Absorption wavemeter	Absorbsiya dalğaölçəni
Абсорбционный гигрометр	Absorption hygrometer	Absorbsiya hiqrometri
Абсорбционный рентгеноспектральный анализ	X-ray absorption analyses	Absorbsiya rentgen spektral analiz
Абсорбционный светофильтр	Absorption filter	Absorbsiya işıq filtri
Абсорбционный спектрометр	Absorption spectrometer	Absorbsiya faktoru
Абсорбционный ток	Absorption current	Absorbsiya cərəyanı
Абсорбционный фактор	Absorption factor	Absorbsiya faktoru
Абсорбционный частотомер	Absorption frequency meter	Absorbsiya tezlikölçəni
Абсорбция	Absorption	Absorbsiya
Абсорбция радиоактивного излучения	Radioactive radiation absorption	Radioaktiv şüalanma absorbsiyası
Абсорбция рентгеновских лучей	X-ray absorption	Rentgen şüaları absorbsiyası
Абсорбция света	Optical absorption	İşığın absorbsiyası
Абсорвент	Absorbent	Absorbent: udan maddə
Абстрактная алгебра	Abstract algebra	Abstrak cəbr
Абстрактная группа	Abstract group	Abstrakt qrup
Абстрактное алгебраическое многообразие	Abstract algebraic variety	Abstrakt cəbri çoxduq
Абстрактное гильбертово пространство	Abstract Hilbert space	Abstrakt Hilbert fəzası

Абстрактное представление	Abstract representation	Abstrakt təsvir
Абстрактное простанство	Abstract space	Abstrakt fəza
Абстрактный интеграл	Abstract integral	Abstrakt inteqral
Абстрактный комплекс	Abstract complex	Abstrakt kompleks (məcmu)
Абстракция	Abstraction	Abstraksiya
Аварийная остановка	Emergency shut-down	Fəlakət dayanacağı
Аварийное значение тока	Emergency fault current	Cərəyanın fəlakətli qiyməti
Аварийное охлаждение	Emergency cooling	Fəlakətli soyuma
Авиационная метеорология	Aeronautical meteorology	Aviasiya meteorologiyası
Авиаэлектроника	Avionics	Aviaelektronika
Авроральная линия	auroral line	Avroral xətt
Автодин	Self-heterodyne, autodyne receiver	Avtodin, yaxın tezlikli dalğaların təsiri işləyən radiocihaz
Автоиндекс	Autoindex	Avtoindeks
Автоионизация	autoionization	Özbaşına ionizasiya
Автоионный микроскоп	Field-ion microscope	Avtoion mikroskopu
Автокатализ	Autocatalysis	Avtokataliz
Автокаталитическая реакция	Autocatalytic reaction	Avtokatalitik reaksiya
Автоклав	Autoclave	Avtoklav, kip bağlanmış qazan
Автокод	Autocode	Avtokod
Автоколебание	Self-excited oscillation	Avtorəqslər
Автоколлиматор	Autocollimator	Avtokollimator
Автоколлимационный спектрограф	Autocollimating spectrograph	Avtokollimatik spektroqraf
Автоколлимация	Autocollimation	Avtokollimasiya
Автоконвективный градиент	Autoconvective lapse rate	Avtokonvektiv qradiyent
Автоконвекция	Autoconvection	Avtokonveksiya
Автокорреляционная функция	Autocorrelation function	Avtokorrelyasion funksiya
Автокорреляция	Autocorrelation	Avtokorrelyasiya
Автолиз	Autolysis	Avtoliz, özbaşına həllolma
Автомат	Automaton	Avtomat
Автоматизация	Automation	Avtomatlaşma
Автоматика	Automation	Avtomatika
Автоматическая настройка	Automatic tuning	Avtomatik qurma, qurulma
Автоматическая обработка данных	Automatic data processing	Məlumatın avtomatik işlənməsi
Автоматическая регулировка	Automatic adjustment	Avtomatik tənzimlənmə
Автоматическая регулировка громкости	Automatic volume control	Səs gurluğunun avtomatik tənzimlənməsi
Автоматическая регулировка усиления	Automatic gain control	Səsin güclənməsinin tənzimlənməsi
Автоматическая система управления	Automatic control system	Avtomatik idarə edilmə sistemi
Автоматическая точная настройка	Automatic fine tuning	Avtomatik dəqiq qurma
Автоматические весы	Automatic scales	Avtomatik tərəzi
Автоматические регулирование избирательности	Automatic selectivity control	Seçilmənin özbaşına tənzimlənməsi
Автоматический газоанализатор	Automatic gas analyzer	Avtomatik qazı təhlil edən cihaz
Автоматический ограничитель шумов	Automatic noise limiter	Səs-küyü avtomatik məhdudlaşdıran cihaz
Автоматический осциллограф	Automatic oscillograph	Avtomatik ossilyator
Автоматический потенциометр	Automatic potentiometer	Avtomatik potensiometr
Автоматический регулятор напряжения	Automatic voltage regulator	Gərginliyin avtomatik tənzimçiyi
Автоматический спутник	Unmanned satellite	Avtomatik peyk
Автоматическое исправление ошибок	Automatic error correction	Səhvlərin avtomatik düzəldilməsi
Автоматическое кодирование	Automating coding	Avtomatik kodlaşdırma
Автоматическое программирование	Automatic programming	Avtomatik proqramlaşdırma
Автоматическое регулирование	Automatic control	Özbaşına tənzimləmə
Автоматическое регулирование мощности	Automatic power control	Gücün özbaşına tənzimlənməsi
Автоматическое регулирование	Automatic speed control	Sürətin özbaşına tənzimlənməsi

скорости		
Автоматическое регулирование частоты	Automatic frequency control	Tezliyin özbaşına tənzimlənməsi
Автоматическое регулирование яркости	Automatic brightness control	Parlaqlığın özbaşına tənzimlənməsi
Автоматическое слежение	Automatic tracking	Avtomatik təqibləmə
Автоматическое смещение	Auto-bias, self-bias	Özbaşına yerdəyişmə
Автоматическое фазовое регулирование	Automatic phase control	Avtomatik fazalı tənzimləmə
Автоматическое фокусирование	Automatic focusing	Avtomatik fokuslama
Автометаморфизм	Autometamorphism	Avtometamorfizm
Автоморфизм	Automorphism	Avtomiorfizm
Автоморфная форма	Automorphic form	Avtomorf forma
Автоморфная функция	Automorphic function	Avtomorf funksiya
Автономная память	Offline memory	Avtonom yaddaş
Автопневматолиз	Autopneumatolysis	Avirpnevmatoliz
Автополярный тетраэдр	Self-polar tetrahedron	Avtoqütblü tetraedr
Автополярный треугольник	Self-polar triangle	Avtoqütblü üçbucaq
Автопроводимость	Autoconduction	Avtokeçiricilik
Авторадиограф	Autoradiograph	Avtoradioqraf
Авторадиография	Autoradiography	Avtoradioqrafiya
Авторегегрессивный процесс	Autoregressive process	Avtogeriləmə prosesi
Авторегрессия	Autoregression	Avtogeriləmə
Авторотация	Autorotation	Avtorotasiya
Автотрансформатор	Autotransformer	Avtotransformasiya
Автоэлектронная дуга	High-field emission arc	Avtoelektron qövsü
Автоэлектронная эмиссия	High-field emission	Avtoelektron emissiya
Агглюцинация	Agglutination	Aqlyüsinasiya, sözün kökünü saxlamaqla yeni sözlər düzəltmək
Агент ионизирующий	Ionizing agent	İonlaşdırıcı aqent
Агент магнитный	Magnetic agent	Maqnit aqenti
Агломерация	Agglomeration	Aqlomerasiya
Агрегат кристаллов	Crystal aggregate	Kristalların aqreqatı
Агрегатное состояние	State of aggregation	Aqreqat hal
Агрометеорология	Agrocultural meteorology	Aqrometeorologiya, yer meteorologiyası
Агрофизика	Agrophysics	Aqrofizika, yer fizikası
Адаптация	Adaptation	Adaptasiya, uyğunlaşma
Адвективная гроза	Advective tundesthorm	Advektiv tufan
Адвективный туман	Advection fog	Advektiv duman
Адвекция	Advection	Adveksiya
Адгезионная прочность	Adhesive strength	Adgezi möhkəmlik, bərklik
Адгезия	Adhesion	Adqeziya
Аддивная функция	Additive function	Additiv funksiya
Аддитивная группа	Additive group	Additiv qrup
Аддитивная мера	Additive measure	Additiv ölçü
Аддитивная теория чисел	Additive number theory	Ədədlərin additiv nəzəriyyəsi
Аддитивная функция множеств	Additive set function	Çoxluğun additiv funksiyası
Аддитивное сложение	Additive addition	Additiv toplanma
Аддитивное смещение цветов	Additive color mixture	Rənglərin additiv qarışdırılması
Аддитивность	Additivity	Additivlik
Аддитивность магнитного вращения	Magnetorotation additivity	Maqnit fırlanma additivliyi
Аддитивность оптической активности	Additivity of optical activity	Optik fəallığın additivliyi
Аддитивность рефракции	Refraction additivity	Refraksiya additivliyi
Аддитивность тензорная	Tensor additivity	Tenzor additivliyi
Аддитивные свойства	Additive properties	Additiv xassələr
Аддитивный оператор	Additive operator	Additiv operator
Аддитивный процесс	Additive process	Additiv proses
Аддитивный функционал	Additive functional	Additiv funksional
Адиабата	Adiabatic line	Adiabata
Адиабатическая гипотеза	Adiabatic hypothesis	Adiabatik fərziyyə

Адиабатическая диэлектрическая проницаемость	Adiabatic dielectric constant	Adiabatik dielektrik nüfuzluğu
Адиабатическая инвариантность	Adiabatic invariance	Adiabatik invariantlıq
Адиабатическая ионизация	Adiabatic ionization	Adiabatik ionlaşma
Адиабатическая реакция	Adiabatic reaction	Adiabatik reaksiya
Адиабатическая стенка	Adiabatic wall	Adiabatik divar
Адиабатическая теорема	Adiabatic theorem	Adiabatik teorem
Адиабатический градиент температуры	Adiabatic temperature gradient, adiabatic lapse rate	Temperaturun adiabatik qradiyenti
Адиабатический закон Эренфеста	Erenfest's adiabatic law	Erenfestin adibatik qanunu
Адиабатический инвариант	Adiabatic invariant	Adiabatik invariant
Адиабатический калориметр	Adiabatic calorimeter	Adiabatik kalorimetr
Адиабатический необратимый процесс	Adiabatic irreversible process	Dönməyən adiabatik proses
Адиабатический обратимый процесс	Adiabatic reversible process	Dönən adiabatik proses
Адиабатический потенциал	Adiabatic potential	Adiabatik potensial
Адиабатический процесс	Adiabatic process	Adiabatik proses
Адиабатическое быстрое прохождение	Adiabatic rapid passage	Sürətli adiabatik keçid
Адиабатическое возмущение	Adiabatic perturbation	Adiabatik həyəcanlanma
Адиабатическое обратимое изменение	Adiabatic reversible change	Dönən adiabatik dəyişilmə
Адиабатическое охлаждение	Adiabatic cooling	Adiabatik soyuma
Адиабатическое приближение	Adiabatic approximation	Adiabatik yaxınlaşma
Адиабатическое равновесие	Adiabatic equilibrium	Adiabatik tarazlıq
Адиабатическое размагничивание	Adiabatic demagnetization	Adiabatik maqnitsizləşmə
Адиабатическое расширение	Adiabatic expansion	Adiabatik genişlənmə
Адиабатическое сжатие	Adiabatic compression	Adiabatik sıxılma
Адиабатическое состояние	Adiabatic state	Adiabatik hal
Адиабатическое течение	Adiabatic flow	Adiabatik axın
Адрес возврата	Return address	Qayıtma ünvanı
Адрес команды	Instruction address	Komanda ünvanı
Адрес слова	Word address	Ünvan sözü
Адресация	Addressing	Ünvanlanma
Адресная дорожка	Address track	Ünvan yolu
Адресная константа	Address constant	Ünvan sabiti
Адресная часть	Address part	Ünvan hissəsi
Адресное слово канала	Channel address word	Kanalın ünvan sözü
Адсорбат	Adsorbate	Adsorbat, səthdə udulan qaz və ya maye
Адсорбент	Adsorbent	Adsorbent, səthində qaz və ya maye udulan cisim
Адсорбер	Adsorber	Adsorber
Адсорбированная молекула	Adsorbed molecule	Adsorbsiya olunmuş molekul
Адсорбированный атом	Adsorbed atom	Adsorbsiya olunmuş atom
Адсорбированный газ	Adsorbed gas	Adsorbsiya olunmuş qaz
Адсорбирующее вещество	Adsorbing substance	Adsorbsiya olunan maddə
Адсорбционная волна	Adsorption wave	Adsorbsiya dalğası
Адсорбционная кинетика	Adsorption kinetics	Adsorbsiya kinetikası
Адсорбционная пленка	Adsorption film	Adsorbsiya təbəqəsi
Адсорбционная сила	Adsorption force	Adsorbsiya qüvvəsi
Адсорбционная хроматография	Adsorption chromatography	Adsorbsiya xromatoqrafiyası
Адсорбционное равновесие	Adsorption equilibrium	Advsorbsiya tarazlığı
Адсорбционное уравнение Гиббса	Gibbs adsorption equation	Gibbsin adsorbsiya tənliyi
Адсорбционные изотермы	Adsorption isotherm	Adsorbsiya izotermləri
Адсорбционный анализ	Adsorption analysis	Adsorbsiya analizi
Адсорбционный ингибитор	Adsorption inhibitor	Adsorbsiya inqibitoru
Адсорбционный индикатор	Adsorption indicator	Adsorbsiya indikatoru, təzyiqi ölçən cihaz
Адсорбционный потенциал	Adsorption potential	Adsorbüionnıy potenüial
Адсорбционный слой	Adsorption layer	Adsorbsiya qatı
Адсорбционный ток	Adsorption current	Adsorbsiya cərəyanı

Адсорбция	Adsorption	Adsorbsiya, cisimldərin üz təbəqəsində maye və qazların udulması
Азеотропия	Azeotropy	Azeotropiya
Азеотропная дистилляция	Azeotropic distillation	Azeotrop distillə etmə
Азеотропная смесь	Azeotropic mixture, azeotrope	Azeotrop qarışıq
Азеотропная точка	Azeotropic point	Azeotrop nöqtəsi
Азимут	Azimuth	Azimut
Азимутальное квантовое число	Azimuthal quantum number	Azimutal kvant ədədi
Атмосфера	Atmosphere	Atmosfer
Будущее	Next, future	Gələcək
Возбуждение, возмущение	Excitation, perturbation	Həyəcanlanma
Вселенная	Cosmos, universe, space	Kainat
Вырождение	Degeneracy, degeneration	Cırlaşma
Вырожденное состояние	Degenerate state	Cırlaşmış hallar
Думать о чем (о ком) то	Think	Fikir çəkmək
Импульсное («P») представление	Momentum “P” representation	İmpuls («P») təsviri
Интегральное преобразование	Integral transformation	Çevirici inteqral
Координатное («x») представление	Coordinate (“x”) representation	Koordinat («x») təsviri
L - представление	L – representation	L-təsviri
Локализация	Localization	Lokallaşma
Локальное поле	Local field	Yerli (lokal) sahə
Маленькая часть вещества (как атом, молекула)	Microscopic particle	Hissəcik
Метод последовательного приближения	Method of successive approximation	Ardıcıl yaxınlaşma metodu
Микромир	Microcosm	Mikroaləm
Мысль	Idea	Fikir
Наименьшая часть вещества		Zərrə
Обмен	Exchange	Mübadilə
Обменная сила	Exchange force	Mübadilə qüvvəsi
Обменная энергия	Exchange energy	Mübadilə enerjisi
Обсуждать	Discuss	Mübahisə etmək
Озоносфера	Ozonosphere	Ozon fəzası
Ориентир	Reference point	Yön
Отталкивать	Repel	Dəf etmək
Перемещать	Translocate	Yerdəyişmək
Полная система	Complete system	Tam sistem
Последовательность	Sequence	Ardıcıllıq
Постоянный переход	Constant transition	Özbaşına keçid
Представление	Representation	Təsvir
Привлечь	Attract, involve	Cəlb etmək
Притягивать	Attract	Cəzb etmək
Пробная функция	Trial function	Sınaq funksiya
Пройденный, прошедший	Past……..	Keçmiş
Пространство	Space	Fəza
Равенство	Equality	Bərabərlik
Размышлять	Reflect	Fikirləşmək
Распространение	Propagation	Yayılma
Рассуждать	Argue	Mülahizə etmək
Рассуждение	Reasoning	Mülahizə
Реликтовое излучение	Relict radiation	Reliktiv şüalanma
Самосогласованное поле	Self-consistent field	Özünə uzlaşan sahə
Сила притяжения	Attractive force	Cazibə qüvvəsi
Собственная функция	Eigenfunction	Məxsusi funksiya
Спонтанный	Spontaneous	Spontan (özbaşına)
Стратосфера	Stratosphere	Stratosfera
Теория возмущений	Perturbation theory	Həyəcanlanma nəzəriyyəsi
Теория представлений	Representation theory	Təsvir nəzəriyyəsi
Термин	Term	İstilah (termin)
Тождество	Identity	Eynilik
Торможение	Braking	Tormozlanma

Узловая точка	Nodal point	Düyün nöqtəsi
Уравнение	Equation	Tənlik
Формула	Formulae	Düstur
Частица	Particle	Zərrəcik
Часть	Part	Hissə
Чередовать	Interleave, alternate	Ardıcıl yerdəyişmək
Эволюция	Evolution	Evolyusiya (inkişaf)
Элементарная частица	Elementary particle	Elementar zərrəcik
Энергетическое («Е») представление	Energy (E") representation	Enerji («E») təsviri